博士論文

Study on novel electrostatic precipitators for fine particle removal in industry-exhaust gases and indoor air

(産業排出ガス中並びに室内空気中の微粒子除去用電気集塵装置の研究)

Hak-Joon Kim

金 學 埈

Chapter I

Introduction

1.1 Electrostatic precipitator (ESP) and its functions

Particulates cause air pollution in most industries, as well as in homes, businesses, and other buildings. It is crucial to improve indoor air quality (IAQ), particularly because many people spend as much as 80% of their lives indoors. Figure 1 shows the size-dependent spectrums of particulate-control technologies. This figure is modified from that of Parker (1997), who presented the spectrums from an industrial point of view and did not consider high-efficiency filters for IAQ. As shown in Figure 1 and Figure 2, particulates larger than 10 μm can be very efficiently removed by relatively simple mechanical methods, such as cyclones that remove the coarse particles by gravitational and inertial forces, or washers and scrubbers that spray water droplets through polluted gases. In the most common mechanical method, filters made of fabrics, ceramics, and metallic materials remove particles in an entire particle-size range, based on the principle that a porous medium or net-type membrane will filter out particles in a particle-laden gas stream, allowing only clean gas to pass through. In particular, high-efficiency filters, such as high-efficiency particulate air (HEPA, 99.97% removal of 0.3 μm particles) or ultra-low-penetration air (ULPA, 99.999% removal of 0.12 μm particles) filters, are most frequently used for IAQ and cleanrooms in IT manufacturing industries. Although such filters offer superior particle-removal performance, and can theoretically achieve 100% particle removal, problems remain such as the pressure-drop problem which causes short-term maintenance or high cost when filtration devices are exposed to high particle loading or operated at high-volume flow rate.

On the other hand, electrostatic precipitators (ESPs), one of the most frequently used methods for particle cleaning, rely on electrostatic forces to collect charged particles. These forces act only on the particles and can be much stronger than corresponding gravitational or inertial forces. As shown in Figure 3, an ESP has three processes. First, particles are charged by unipolar ions moving toward the collection plate by field or diffusion charging. The two charging mechanisms are described in Chapter 2. Second, when a unipolar-charged particle reaches the grounded collection electrode, the charge on the particle is only partially discharged, and the charge is slowly leaked to

the grounded collection plates. A portion of the charge is retained and contributes to the intermolecular adhesive and cohesive forces that hold the particles onto the plates. Adhesive forces cause the particles to physically hold on to each other because of their dissimilar surfaces. Newly arrived particles are held to the collected particles by cohesive forces. Particles are attracted and held to each other molecularly, and form a dust layer which is allowed to build up on the plate to a desired thickness. Finally, dust that has accumulated to a certain thickness on the collection electrode is removed by one of two processes depending on the type of collection electrode. The collection electrodes in precipitators can be either plates or tubes, with plates being more common. Tubes are usually cleaned by water sprays, whereas plates can be cleaned either by water sprays or a process called rapping (Hinds, 1997; Parker, 1997). In Figure 4, ESPs are classified by the number of stages used to charge and remove particles from a gas stream. In the single-stage precipitator, the corona wires are in the precipitation section, and the same electric field that creates the corona for particle charging also causes particle collection within the same chamber on collection surfaces of the opposite charge. Otherwise, two-stage ESPs have separate sections for charging and collection, with particles charged by low voltage in the first stage and then collected by oppositely charged surfaces in the second stage. This two-stage ESP is primarily designed for air purification in conjunction with IAQ systems, and also for the control of fine mists and particles for industries (Electrostatic Precipitator Knowledge Base, 2013).

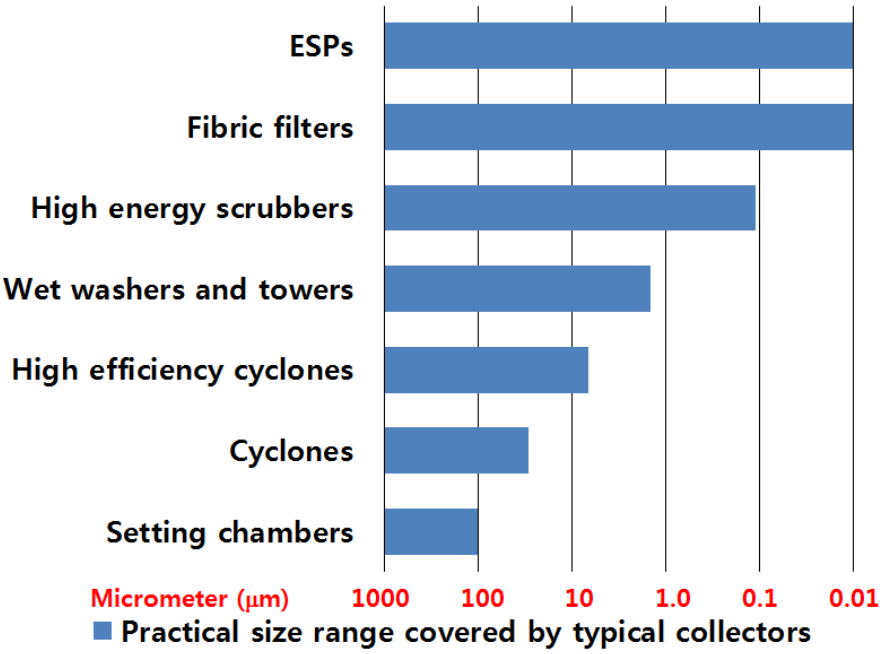

Figure 1. Size-dependent particle-collection mechanisms

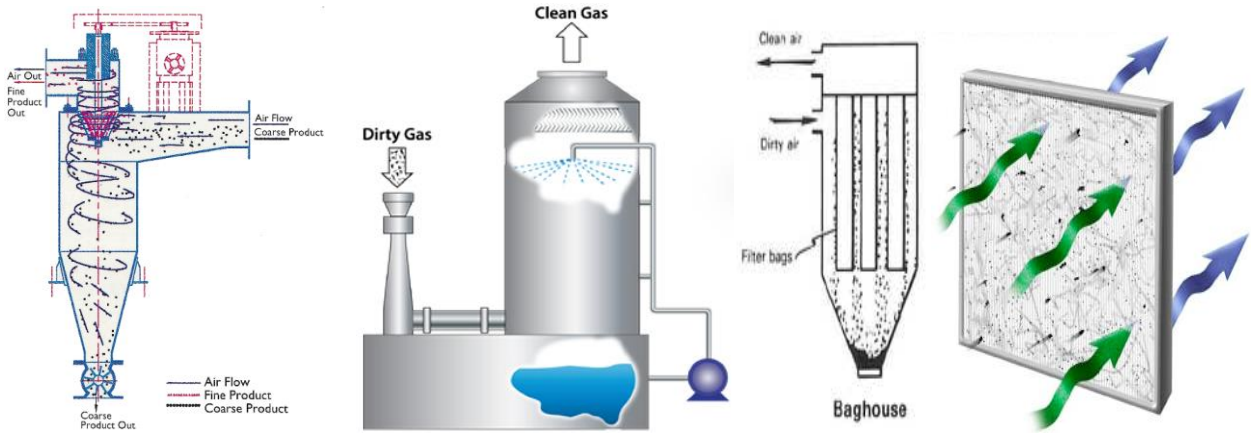

a) cyclone b) wet washer and scrubber b) filter

Figure 2. Mechanical methods for particle removal

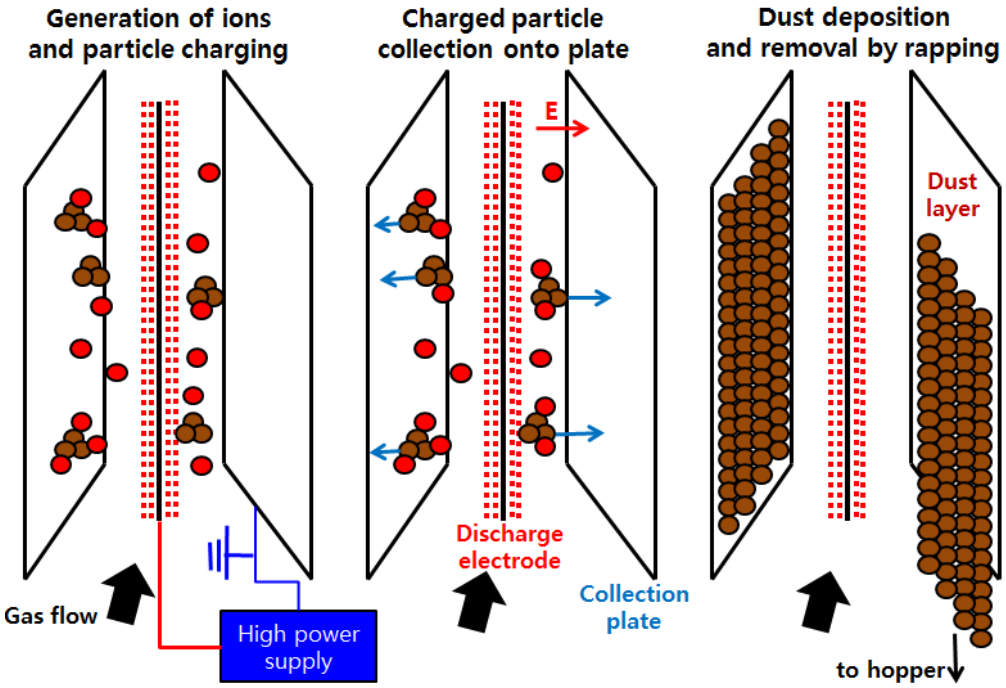

Figure 3. Particle removal mechanism of ESPs

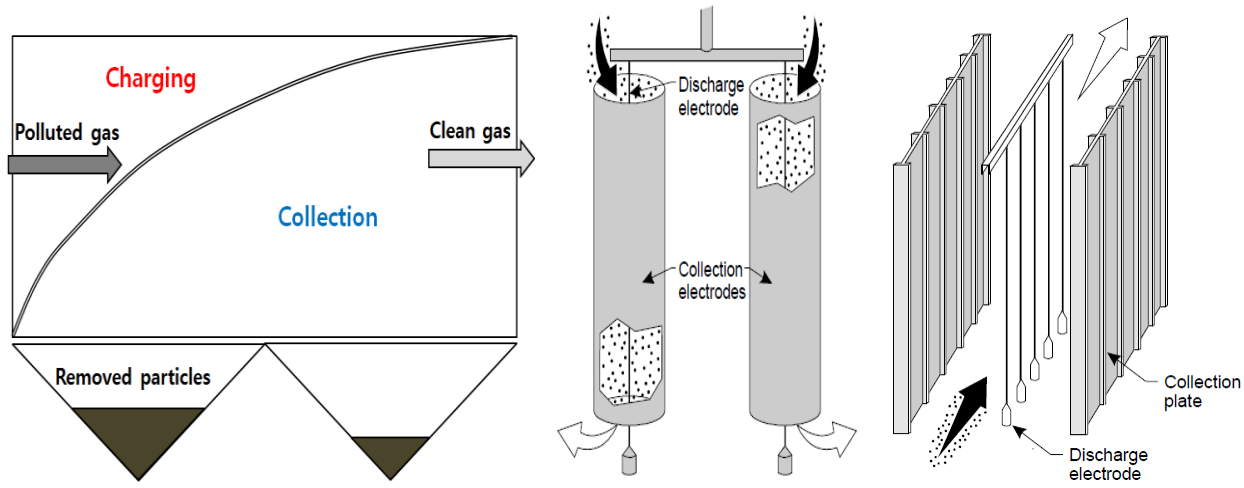

a) Single-stage ESP and schematic example

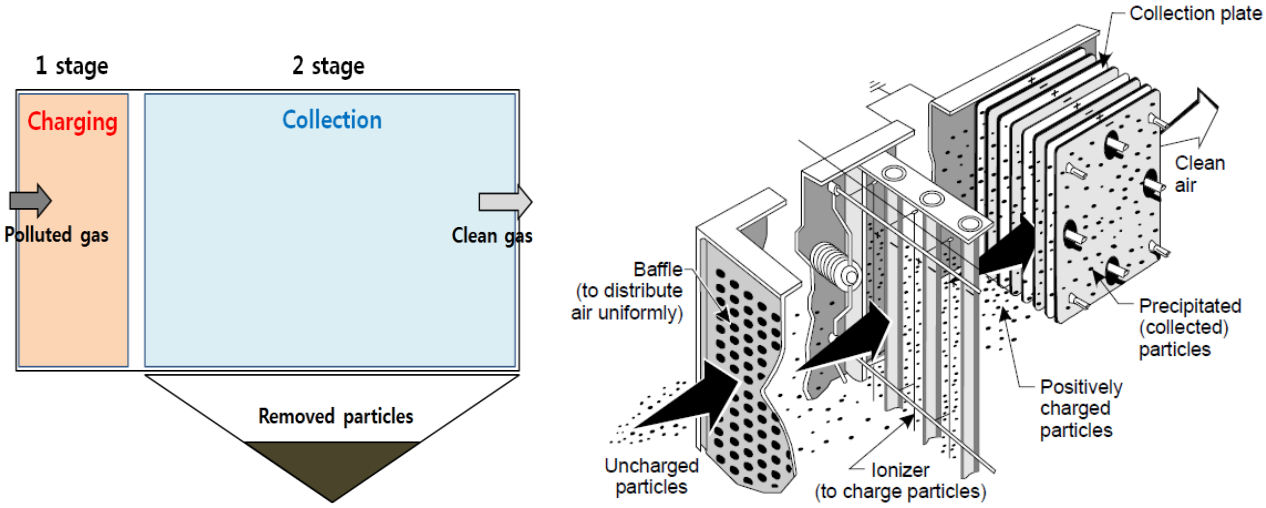

b) Two-stage ESP and schematic example

Figure 4. Types of ESPs and schematic examples (Electrostatic Precipitator Knowledge Base, 2013)

1.2 Historical background of ESPs

Table 1 lists historical milestones in ESP technology, which have been summarized by previous studies (White, 1963; Oglesby and Nichols, 1978; Parker, 1997). The historical steps can be divided into three parts. The ESP was first developed in 1907 when Dr. Frederick Cottrell successfully collected sulfuric acid fumes in his laboratory at the University of California by

introducing high-voltage rectified alternating current to supply electrical energy to an ESP. Pioneering studies on the theory of collection of small particles on an electrically charged surface were made by Deutsch (1922). Until the 1980s, ESPs played a crucial role in the removal of dusts, fumes, and mists for various industries and researches focused on advancing the theoretical background and electrical equipment. Researchers then began to focus on increasing the removal efficiency of high-resistivity particles using chemical conditioning and novel electric high-power sources, such as pulses and intermittent energization, and on decreasing the costs of ESPs and their operation by wide spacing and computer control. Entering the 21st century, dry ESP technologies have fully matured such that low-temperature and wet ESPs can be applied to very low-temperature exhaust gases less than 100℃ that contain fine particles and acidic mists.

According to a report on the future of ESPs published in the environmental magazine Pollution Engineering (Mcllvane et al., 2006), China will spend $1,129 million USD on purchasing dry ESPs, more than the next four largest countries in terms of spending combined. The U.S. purchase of wet ESPs ($340.93 million USD) will be a distant second. Fabric filters rather than dry ESPs would be used for the initial particulate capture. However, a wet ESP would be installed as the last pollution control device following a scrubber in a scheme proposed by the Taylor energy complex in Florida (Mcllvane et al., 2006). From this point of view, research on technologies, materials, and electric equipment related to wet ESPs will be crucial in the future.

Table 1 Scientific, application, and electrical milestones in ESP development

Initial	1900~1910	Theories of corona generation (Townsend; Thomson) **Removing acid mist in a contact sulfuric acid plant (First successful use); removing zinc and lead fumes from smelter gas;** *Introduction of high-energy rectified current to precipitator (Cottrell)*
	1910~1920	Studies of sparkover (Wolcott); experimental discovery of exponential law of electrostatic precipitation (Anderson) **Fine wire electrode (Schmidt); controlling dust from cement kiln; removing lead fume from copper converter gas; gas conditioning; fractional precipitation; absorption of chlorine by powdered lime followed by ESP; recovery of alkali salts in pulp mill** *Use of vacuum-tube rectifiers*
	1920~1930	Theoretical derivation of exponential equation (Deutsch); development of field-charging equation (Rohmann); development of diffusion equation (Arendt and Kallman) **Collection of fly ash from electric power plant boilers; cleaning blast furnace gas** *Motor-driven automatic control*
	1930~1940	Development of field-charging equation (Pauthenier); spark discharge in air-dust mixtures (Franck); effect of particle charge on electric field (Mierdel and Seeliger); fundamental studies of coronas (Loeb) *Use of double half-wave rectifier circuit*

	1940~1950	Effect of resistivity and back corona on precipitation (White) **Continuous rapping (Richardson)** *Use of selenium rectifiers; electronic automatic control*
	1950~1960	Deutsch equation derived from probability theory (White); development of refined diffusion charging equation (White); forces on particles in dust layers (Lowe and Lucas); dust removal from collection plates (Ruckelshausen); experimental studies of diffusion charging (Hewitt); combined field and diffusion charging equation (Penney and Murphy); effect of bipolar ions on charging (Pauthenier) **Cleaning gas from open hearth furnaces; cleaning gas from basic oxygen furnaces; shielded electrodes (White and Baxter)** *Use of silicon rectifiers*
Developing	1960~1970	Back corona studies (Pauthenier); sparkover and breakdown of dust layers (Penny and Craig); contact potentials and adhesion of dust (Penney and Klingler); refined equation for combined field and diffusion charging (Liu and Yeh) **Rapping studies (Dalmon and Lowe); rapping studies (Sproull); hot precipitator on power plant boilers** *Thyristor control*
	1970~1985	Computer model for theoretical analysis of precipitator operation (Oglesby and Nicols); effect of turbulence on collection efficiency (Copperman); ionic conduction in fly ash (Bickelhaupt); adhesive and cohesive forces in dust layers (Tassicker; Dalmon and Tidy); charging theory (Smith and McDonald) **Removing fluorides in Soderberg aluminum reduction; wide spacing (Mastuda); moving electrode (Hitachi Co., Ltd.)** *Micro-second pulse application (Smith; Mastuda); microprocessor; intermittent energization (Reyes)*
Matured	1986~	**Combined with plasma chemistry and fabric filtration; low-low temperature ESP (Hitachi Co., Ltd); wet ESP (e.g., Veltran, Mitsubishi, Hitachi)** *Supervisory computer control.*

Black: Science and theory; **Red: Major applications**; *Blue: Electrical equipment*

1.3 The size-dependent definition of particles

Defining different size categories for particles is necessary because particles of different sizes behave differently in the atmosphere, indoors, and in the respiratory system. In this chapter, the definitions for particles follow those of the Hinds's book (Hinds, 1999). Figure 5 shows the Hinds's terminology along with the corresponding particle sizes, and the size range for fine particles is from 4 nm to 2.5 μm. Shown in Figure 6 of the three-dimensional visual comparison of the sizes of coarse, fine, and ultrafine particles, a substantial difference in size among the particles is understanded. As shown in Figure 7, the size distributions of the particles (Kittelson, 1998) vary significantly depending on weighting conditions such as number or mass. Therefore, particle categories (size, number, or mass) are very important because particulate matters are regulated and tested under these categories.

Currently, much attention is being focused on the effects of fine and ultrafine particles on human health. The U.S. EPA proposed fine particle standards based on studies that link fine particles

with adverse health effects. Many of these studies have shown that there is a stronger correlation between adverse health effects and atmospheric particle concentrations when using the fine-particle concentration (particles 2.5 μm or less: $PM_{2.5}$) than when using the concentration of coarser particles (particles 10 μm or less: PM_{10}) (Dockery et al., 1993; Pope et al., 1995).

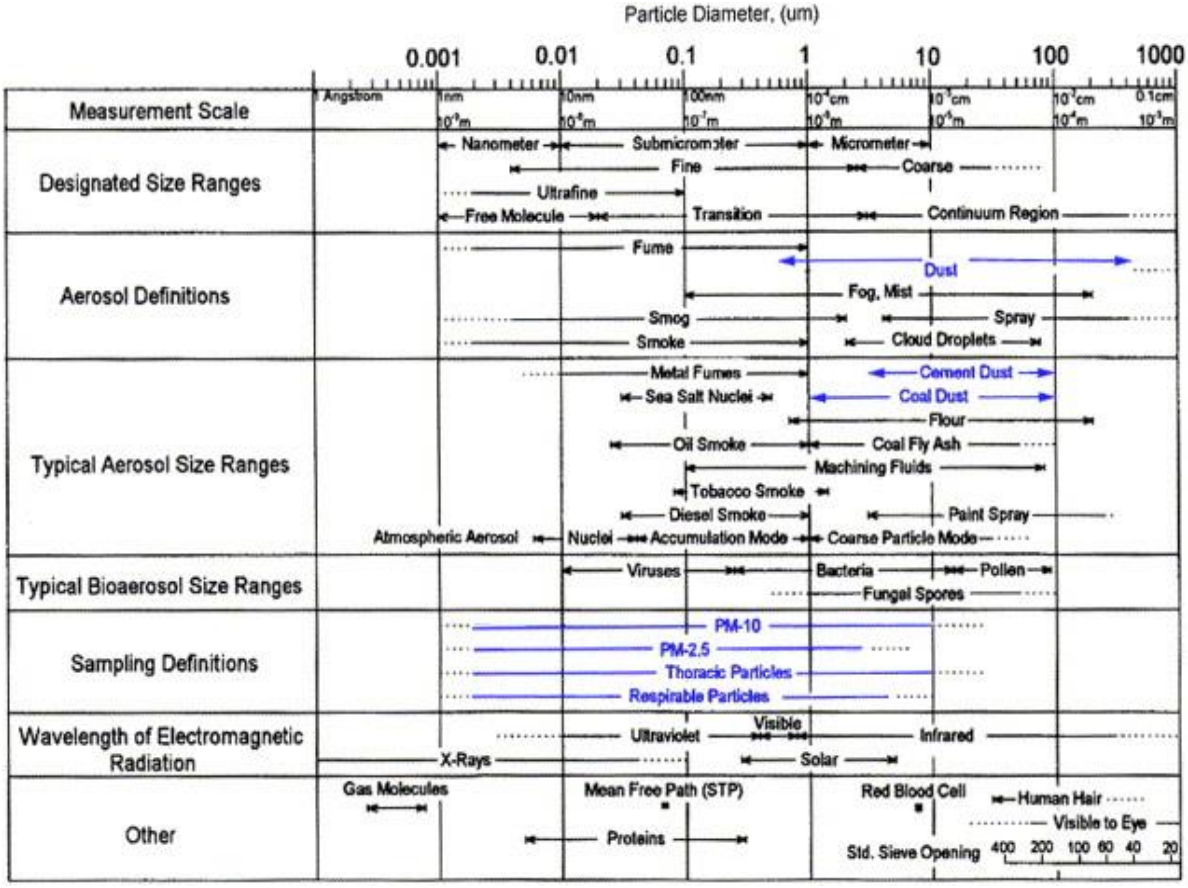

Figure 5. Particle size ranges and difinitions for particles (Hinds, 1999)

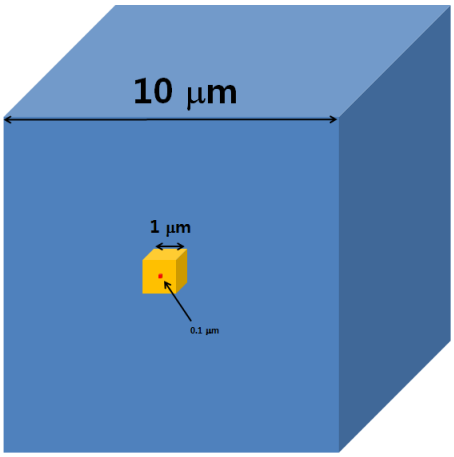

Figure 6. Visual comparison of the sizes of fine particles (0.1 and 1 μm) and a coarse particle (10 μm)

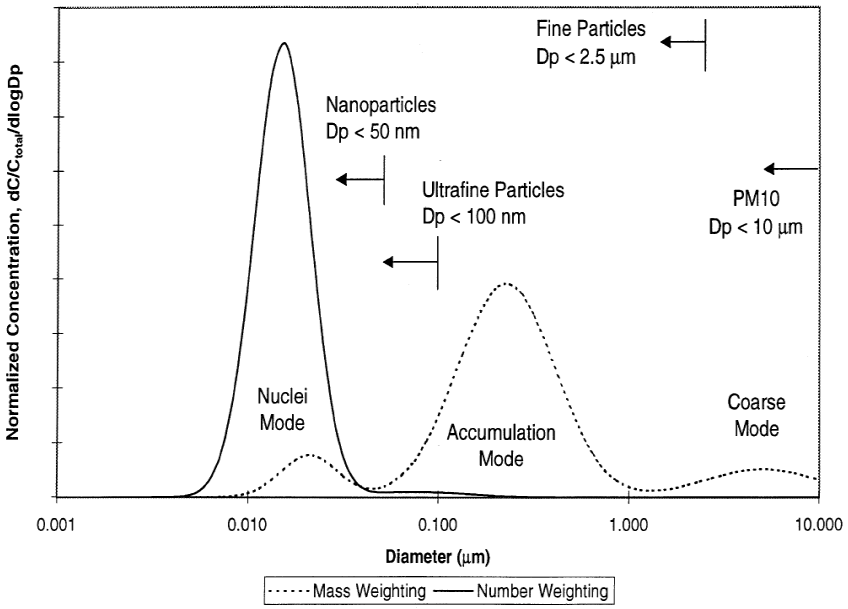

Figure 7. Typical engine-exhaust particle size distribution in terms of both mass and number weightings

1.4 Scientific and social issues regarding fine particles

Adverse health effects seem to be linked with smaller particles, probably largely because of the increase in the number of particles and particle surface area per unit mass with decreasing particle size, among various factors (Kittelson, 1998). Figure 8 shows the efficiency of deposition in the human respiratory tract by particle size (ICRP, 1994). The toxicity of particles of various sizes can have different effects in different parts of the lungs, and this may be particularly important in children with developing lungs or in persons with asthma, which mainly affects the larger airways. Ultrafine particle-deposition density per airway surface area may often exceed that of the gas-exchange region because of the 100-fold larger alveolar surface area when compared to that of airways. In general, ultrafine particles are very capable of reaching the fragile structures of the alveoli (Kreyling et al., 2006). Because of the relationships of adverse health effects and fine particles, current pollution standards are mass-based such that as particles become finer, regulation by number or area will increase.

Table 2 presents US, Japanese, and Korean ambient air quality standards for particle matters based on mass. As awareness of the dangers of fine particles has grown, PM standards based on PM_{10} have become more stringent. Regulations expanded to include $PM_{2.5}$ in the US in 2006 and in Japan

in 2009 and will be implemented in 2015 in Korea.

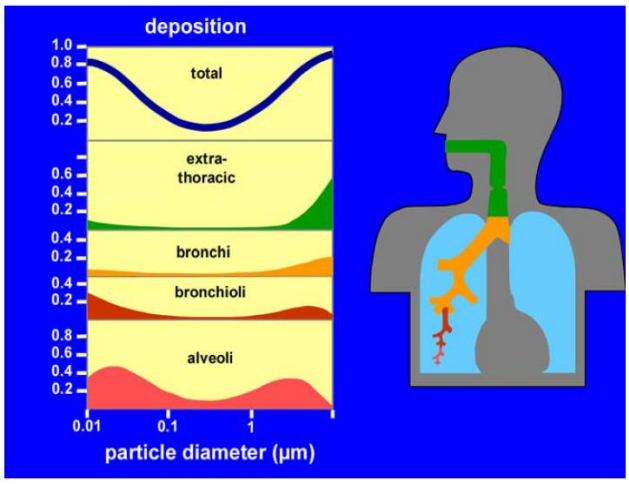

Figure 8. Regional deposition of particles in the human respiratory tract (ICRP, 1994).

In addition, as shown in Figure 9 the PM emission regulations on diesel engines for on- and off-road vehicles have become much more stringent than those for ambient air quality. For instance, the PM emission limit for heavy duty diesel engines in the US and Europe decreased to 0.01 g/HP-hr (EPA, 2010) from 0.1 g/HP-hr (EPA, 1994). Furthermore, the number standard which weights fine and ultrafine particle emission is to be defined as soon as possible and at the latest by the start of the next tier of EU standards, Euro 6, in 2014 (Eur-lex, 2011). Considering these small-particle regulation trends, current particle collection methods should be upgraded and newly developed to achieve extremely high-removal efficiency for particles.

Table 2. Comparison of national ambient air quality standards for particulate matters

Category	Condition	US	Japan	Korea
PM_{10} ($\mu g/m^3$)	1 hour		200	
	24 hours	150	100	100
	year			50
$PM_{2.5}$ ($\mu g/m^3$)	24	35	35	50[2)]
	year	12/15[1)]	15	25[2)]

[1)] primary/secondary, [2)] It will start at 2015

*These data were from the US EPA (http://www.epa.gov/ttn/naaqs/standards/pm/s_pm_history.html), the Ministry of the Environment, Government of Japan (http://www.env.go.jp/kijun/taiki.html), and the Ministry of Environment, Government of Korea (http://www.me.go.kr)

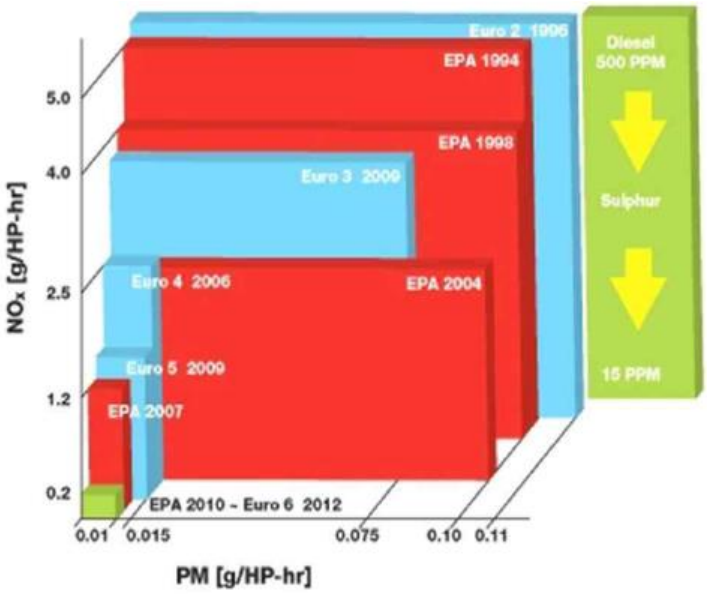

a) On-road

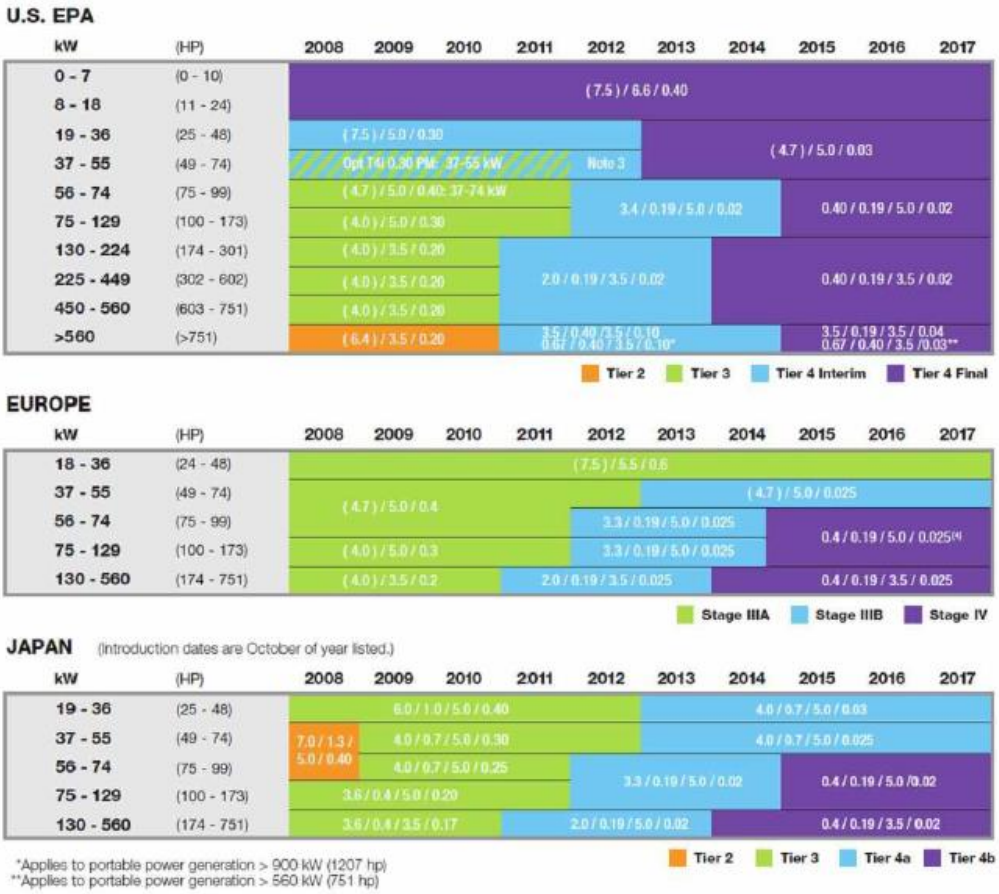

b) Off-road

Figure 9. Comparison of regulations on particulate matters from diesel engines for on- and off-road vehicles in the US, Europe, and Japan

1.5 Research objectives

Table 3 briefly summarizes the main topics addressed in chapters III to VII and also explains specific technologies, fields, and theories related to ESPs. Among various air-cleaning methods such as filters, cyclones, and scrubbers, ESPs are the only electrical method. As noted in the technical and historical background above, dry ESP technology has been already well-developed for conventional industries. Thus, in this study I focused mostly on new application fields such as IT manufacturing, new thermal power generation, diesel engines, and IAQ that currently concern about high efficiency against fine particles. Also, I used novel ESP technologies such as a non-metallic ESP, a thin water film ESP and a combined ESP with metallic filters etc., and compared the research results with theoretical analyses basically using the Deutsch's collection efficiency equation and the field charging theory (Cochet's charging theory), however specially using diffusion charging theories for particles smaller than 0.1 μm which have been rarely used for industrial scale ESP analyses.

Table 3. Major topics examined in this study

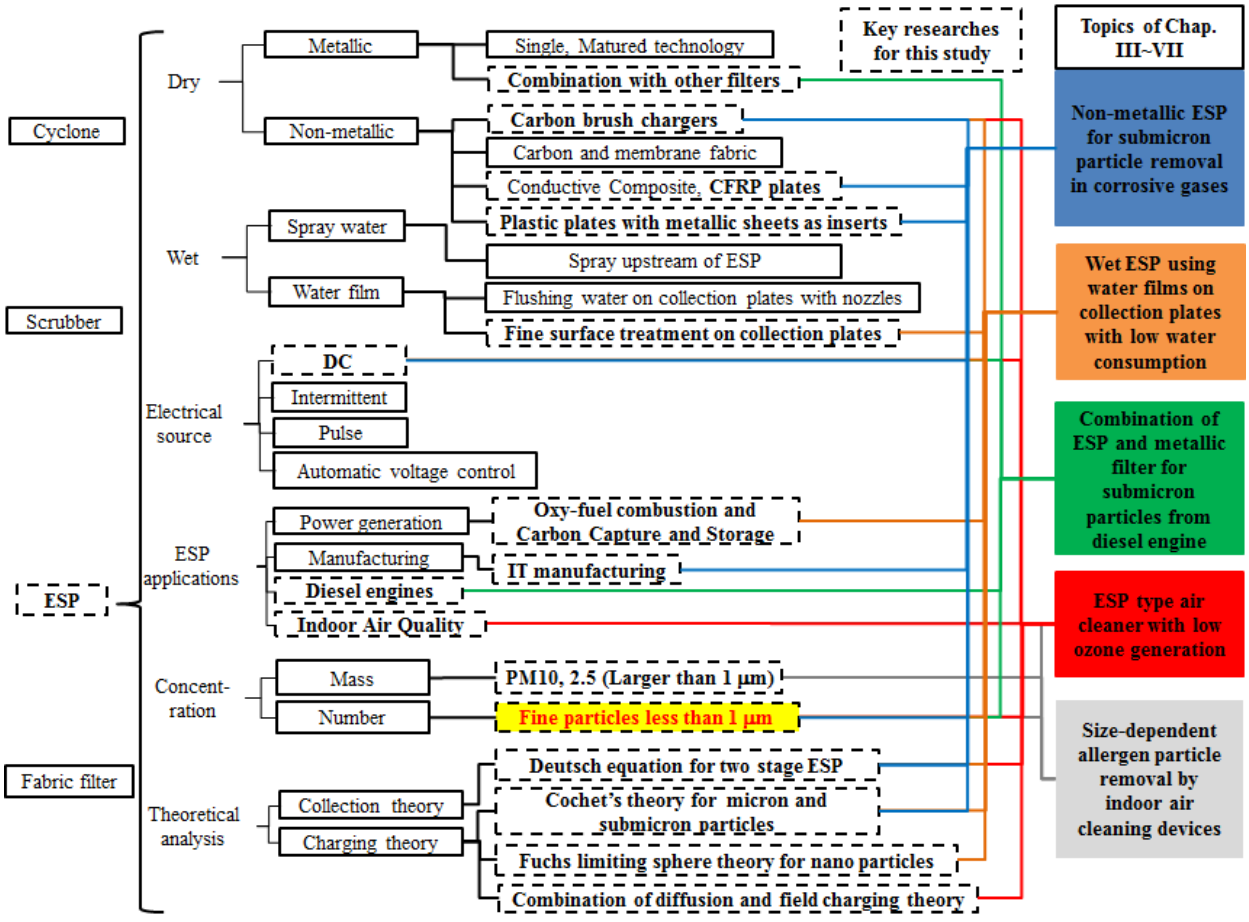

First, I researched non-metallic ESPs, which are composed of only non-metallic materials such as carbon, plastic, and resin for particle removal in corrosive gases from industries, especially in manufacturing IT devices such as semiconductors and LCDs. A number of researchers have investigated non-metallic collection plates for the ESPs. Bayless et al. (2004; 2005) developed a wet ESP that collected fine particles on the membrane-based collection plates with spraying water, and Allan et al. (2011) investigated corrosion resistance and conductive properties of carbon-composite conductive materials used for collection plates for a wet ESP. For IAQ application, Sung et al. (2009) investigated the performance of an ESP using carbon fabric as collection plates, and some electric companies (e.g., Electrolux, Matsushita Electric Works) developed ESP-type air cleaners that use conductive collection plates made of plastic and metal composite materials. However, the above studies focused only on non-metallic collection plates, and the commercialized conductive composite collection plates also had technical limits such as limits to perfect electrical insulation during water washing on the collection plates. I investigated the fine particle removal and electrical performance of a perfect non-metallic ESP using a charger made by carbon-based materials and plastic collection plates with metallic sheets as inserts. The results are summarized in Chapter III. This study began with laboratory tests. A final evaluation was then conducted with a pilot demonstration test using real corrosive exhaust gases on the rooftop of an IT manufacturing factory in Korea.

Second, with the goal of achieving near-zero emission from industries, I researched a wet-type ESP using thin water film on collection plates using low water consumption. Since approximately 2000, when PM regulations started to consider fine particles such as $PM_{2.5}$, SOx, and Hg mists, wet ESPs have been developed and used in many applications including coke ovens, blast furnaces, wood dryers, power boilers, and sewage sludge and hazardous waste incinerators. They are mainly designed to collect the fine particles because re-entrainment of particles (see Figure 10) during rapping on collection plates with hammers is virtually non-existent in wet ESPs.

There are basically two approaches for removing dust in wet ESPs. As shown in Figure 11, one approach is to spray water upstream of the ESP or above the collection and discharge electrodes in an ESP. Each spray has a covering capability and throughput of some 200 L/min/m^2 at a distance of 1.5 m below the spray. Because of the large quantity of water passing through the electric field, it is necessary to reduce power or to electrically separate the section being washed down (Parker, 1997). The wet ESPs using this approach have been commercialized for submicron particles, heavy metal, dioxin, and mist removal by several companies such as TurboSonic Technologies, Inc., and Beltran Technologies, Inc..

The other approach is to form water films on collection plates using full spray irrigation or a weir system in wet ESPs, as shown in Figure 12. This method, which has been used by major Japanese heavy industry companies, does not require the isolation of the section being washed and power reduction control during washing, and typically uses 4 L/min/m of collector to ensure full water coverage on collection plates (Parker, 1997)

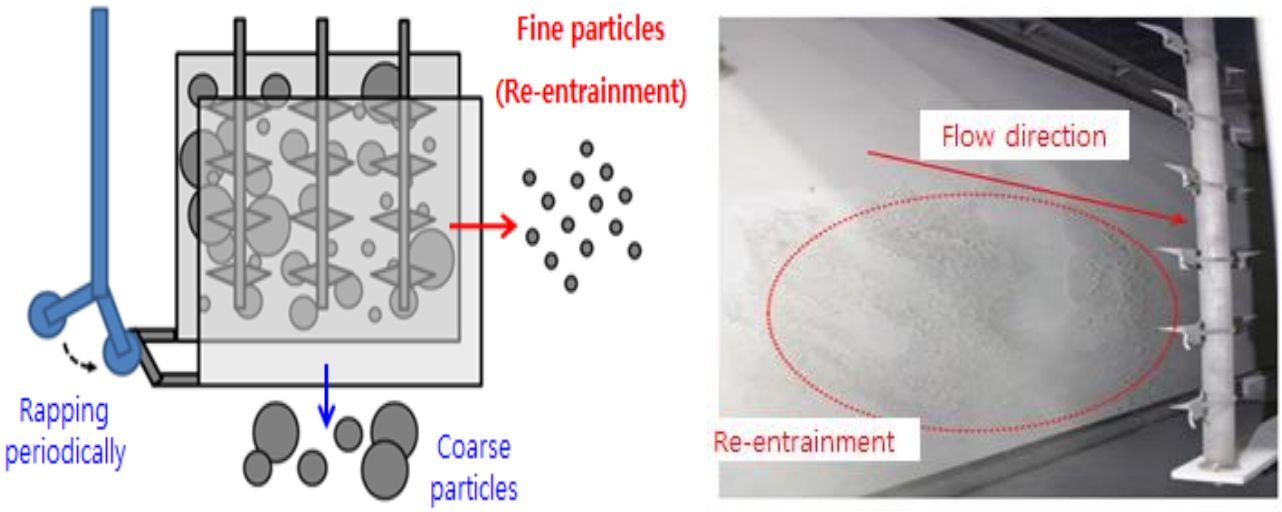

Figure 10. Re-entrainment of fine particles in a dry ESP during rappings

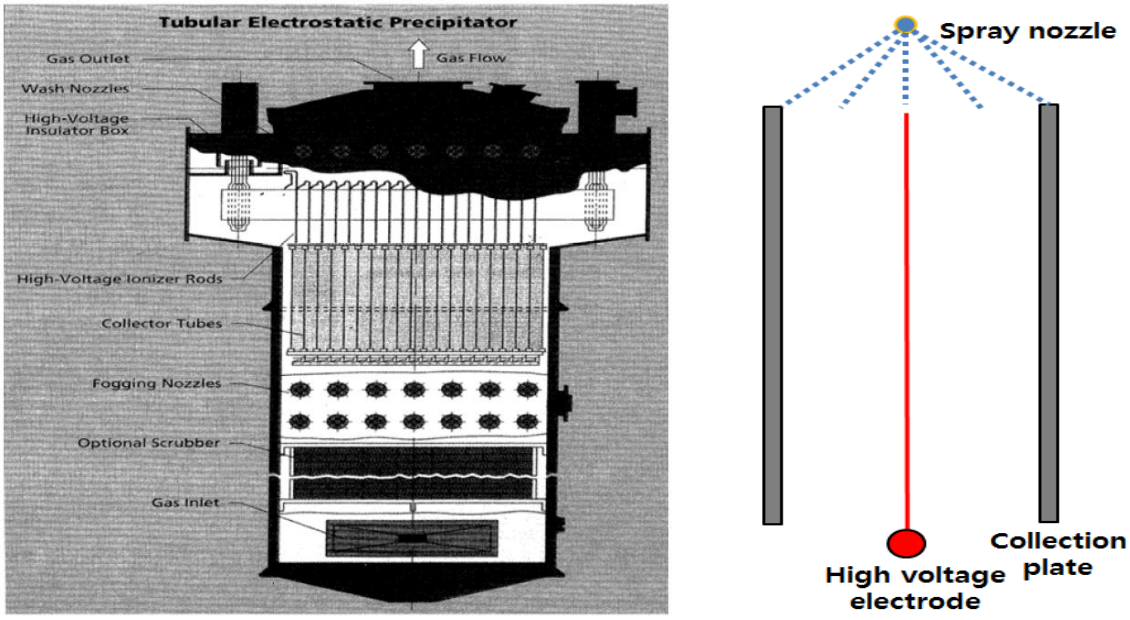

Figure 11. A wash-down type wet ESP and its particle removal principle

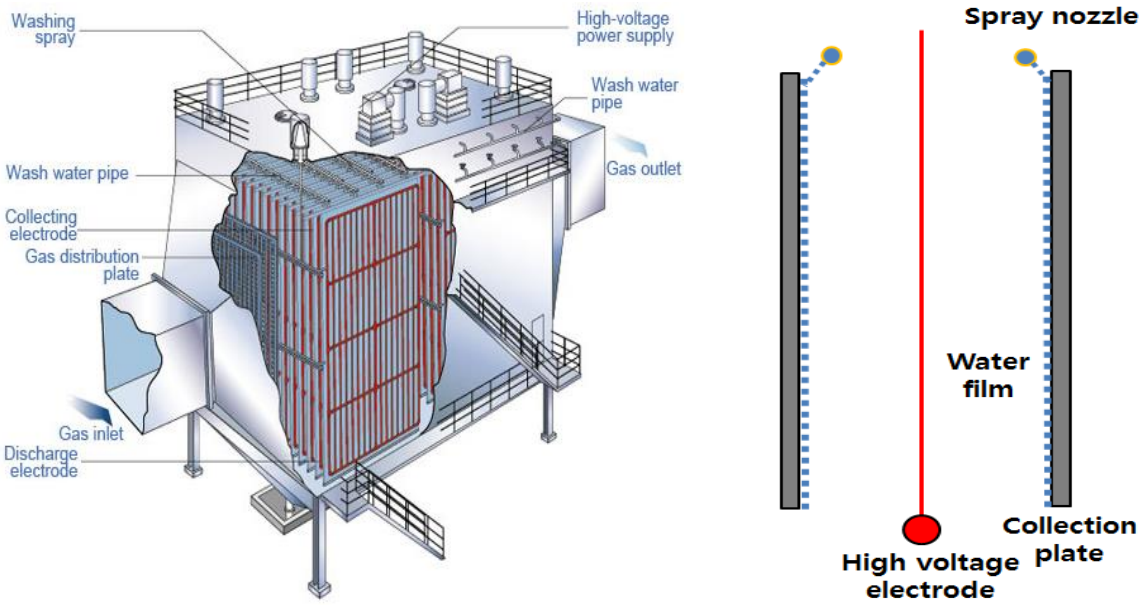

Figure 12. Water-film-type wet ESP and its particle removal principle (Hitachi, Mitsubishi Heavy Industries, Ltd.)

The most important technological challenge is to minimize water consumption to clean the wet ESPs because water consumption is directly related to the cost of operation and additional water treatment devices. Water consumption must be increased if the flushing liquid is not uniformly distributed over the surface. Beading can lead to channeling and formation of "dry spots" of collected particles, and the resulting buildup of collected material causes the precipitator electrical performance to degrade (Bayless, 2005; Pasic, 2006). I researched a water film ESP which consumed significantly less water than those reported previously, which was achieved due to fine surface treatment on the collection plates without nozzle sprays. This ESP was then applied to fine particle removal in pilot tests involving oxy-pulverized coal combustion and carbon capture and storage.

Third, I researched submicron particle removal from diesel engines which is one of the most intensively researched areas today. Ceramic diesel particulate filters (DPFs) with a fully enclosed structure, the only promising filtration technology, are already commercialized for diesel vehicles around to world to meet the most stringent particle regulations of Euro V and VI. However, the sharp increase in pressure drops caused by high particle loading and the high volumetric flow rate are the crucial drawbacks of the ceramic DFPs for high-volume diesel engines. For this reason, other filtration methods, such as metallic filters and ESPs with significant lower pressure drop than DPFs, have been attracting research attention. Yamamoto et al. (2010) investigated particle removal performance of an ESP with specific particle collection and disposal geometry for marine diesel

engines, considering that low-resistivity carbon particles easily escape from conventional ESPs. A standalone ESP could not be applied to clean a whole volume of diesel exhaust under high flow velocity. Thus, research on combining ESPs with other filtration methods has been conducted. Hayashi et al. (2009) combined an ESP with a ceramic DPF, and Park et al. (2007) did the same with a metallic foam filter. In this study, I combined electrostatic precipitation with a metallic flow-through filter (FTF), which has an open structure to reduce the pressure drop. I then performed a European standard mode test based on particle numbers.

The fourth and fifth topics that I studied were related to IAQ and the development of home appliances to improve air quality such as air conditioners, air cleaners, and ventilation devices. I developed an ESP-type air cleaner with high clean air delivery rate (CADR) and significantly low ozone emission. In spite of high collection efficiency over 90% for submicron indoor particles with negligible pressure drop, few ESP-type air cleaners have been commercialized in Korea since 2005 when ozone emission issues from the air cleaners, which use wire or spike electrodes as a particle charger, were spotlighted in the mass media in Korea. Also, in order to achieve a high CADR, which means that an air cleaner purifies a room within a very short time, the increase in applied voltage and corona current to conventional-type chargers may increase ozone emissions from the air cleaner. To develop a cleaner with a high CADR against fine particles and low ozone emission, I used a carbon-brush ionizer with positive polarity, which had been successfully applied for industrial usage as a non-metallic charger. I also evaluated the performance of the cleaner on the basis of ESP and CADR theories.

For my final topic, I investigated an efficient method to test the ability of air cleaning devices to remove airborne fine and coarse allergen particles. I developed a very simple evaluation method for the size-dependent particle-removal performance of air cleaners using a real-time optical particle counter. This method contrasts with previous methods that were both time-consuming and costly.

In summary, as shown in Table 3, all the topics examined in this study are focused on fine particle removal to achieve near-zero emission from ESPs for industries and to improve IAQ. The research explores novel ESP methods, especially a non-metallic ESP, water film ESP, and combination of the ESP with another filtration method. With this study, I would like to emphasize the possibility and importance of electrostatic precipitation technology for cleaner and better atmospheric and indoor environments.

1.6 References

Parker, K.R. In Applied electrostatic precipitation.1st ed; Blackie academic & professional: London, 1997.

Hinds, W.C. Aerosol Technology: Properties, behavior, and measurement of airborne particles. 2nd ed; A wiley-interscience publication: New York, 1999.

Electrostatic precipitator knowledgebase. (2013). Electrostatic precipitator operation. (http://www.neundorfer.com/FileUploads/CMSFiles/ESP%20Operation[0].pdf)

White, H.J. Industrial electrosatic precipitation. 1st ed; Addison-wesley publishing company, Inc.: Massachusetts, 1963.

Oglesby, S. And Nichols, G.B. Electrostatic precipitation. 1sted; Marcel Dekker, Inc.:New Your an Basel, 1978.

Mcllvane, R. (2006). The future of electrostatic precipitators. Pollution Enginnering, November, 18.

US Environmental Protection Agency (2010). Module 3: Characteristics of Particles - Particle Size Categories. (http://www.epa.gov/eogapti1/bces/module3/category/category.htm)

Kittelson, D.B. (1998). Engines and nanoparticles: a review. *J. Aerosol. Sci.* 29(5/6), 575-588.

Dockery, D. W., Pope III, A., Xu, X., Spengler, J. D., Ware, J. H., Fay, M. E., Ferris, Jr. B. G. and Speizer, F. E. (1993). An association between air pollution and mortality in six U.S. cities. *J. Medicine* 329, 1753-1759.

Pope III, C. A., Thun, M. J., Namboodiri, M. M., Dockery, D. W., Evans, J. S., Speizer, F. E. and Heath, Jr. C. W. (1995) Particulate air pollution as a predictor of mortality in a prospective study of U.S. adults. *Am. J. Respir. Crit. Care Med.* 151, 669-674.

ICRP Publication 66 (1994). Human respiratory tract model for radiological protection. A report of a Task Group of the International Commission on Radiological Protection. Ann. ICRP 24(1–3), 1–482.

Kreyling, W.G., Semmler-Behnke, M, and Möller, M. (2006). Health implications of nanoparticles. Journal of Nanoparticle Research 8, 543-562.

EUR-Lex (2011). Regulation (EC) No 715/2007 of the European Parliament and of the Council of 20 June 2007 on type approval of motor vehicles with respect to emissions from light passenger and commercial vehicles (Euro 5 and Euro 6) and on access to vehicle repair and maintenance information. Eur-lex.europa.eu. Retrieved 2011-02-02.

Bayless, D.J., Alam, M.K., Radcliff, R., and Caine, J. (2004). Membrane-based wet electrostatic

precipitation. Fuel Processing Technology 85, 781-798.

Bayless, D.J., Shi, L., Kremer, G., Stuart, B.J., Reynolds, J., and Caine, J. (2005). Membrane-Based Wet Electrostatic Precipitation. Journal of the Air & Waste Management Association 55(6), 784-791.

Allan, R., Jayaram, S., EI-Hag, A., and McGrath, P. (2011). A conductive composite material for wet ESP applications. Presented at 12th International Conference on Electrostatic Precipitation, May 9-13, 2011, Nuremberg, Germany.

Sung, B.J., Naito, T., Aly, A., Lee, S.H., Takashima, K., Katsura, S., and Mizuno, A. (2009). Simultaneous removal of gaseous acetaldehyde and fine particles using corona discharge with wet electrostatic flocking electrode. International Journal of Plasma Environmental Science and Technology 3(1), 61-66.

Beltran, M.R. (2008). Wet ESP for the collection of submicron particles, mist and air toxics. Presented at 11th International Conference on Electrostatic Precipitation, Oct 20-24, 2008, Hangzhou, China.

Allan, R.A. (2001), The wet electrostatic precipitator and the pulp and paper industry: A proven technology for submicron particulate control. Presented at the 87th Annual Meeting of PAPTAC Pulp & Paper Association of Canada, Montreal, 2001.

Fujishima, H. and Nagata, C. (2004). Experiences of wet type electrostatic precipitator successfully applied for SO_3 mist removal in boilers using high sulfur content fuel. Presented at IX International Conference on Electrostatic Precipitation. May 17-21, 2004, Pretoria, So. Africa.

Pasic, H. (2006). Membrane tubular wet electrostatic precipitators. Filtration+Seperation. November 2006.

Yamamoto, T., Mimura, T., Otsuka, N., Ito, Y., Ehara, Y., and Zueran, A. (2010). Diesel PM collection for marine and automobile emissions using EHD electrostatic precipitators. IEEE Transactions on Industry applications. 46 (4), 1606-1612.

Hayashi, H., Kimura, M., Kawahara, K., Takasaki, Y., Takashima, K., and Mizuno. A. Collection of diesel exhaust particle using electrostatic charging prior to mechanical filtration. Presented at the Joint ESA/IEEE-IAS/IEJ/SFE/IEA Conference, Boston, 2009.

Park, S., Lee, D., Cho, G., and Kim, H. A new diesel particulate filter using a metal foam filter combined with electrostatic precipitation mechanism," SAE Technical Paper 2007-01-1267, 2007.

Chapter II

Theoretical backgrounds for particle removal performance of ESPs

2.1 Particle collection and charging theories for ESPs

2.1.1 Particle collection theory

Collection efficiency of the ESP is the most important consideration for ESP researhers. The collection efficiency can be estimated using several equations, and these equations give a theoretical prediction of the size-dependent and whole collection efficiency of an ESP which is operated under ideal conditions. Among various collection theories, the most popular and esiest one to gain insight into the precess of ESP is Deutsch equation.

Shown in Figure 1, the Deutsch model is a well-known fundamental model used to calculate the collection efficiency of a dry ESP (Parker, 1997; Park and Chen, 2002; Xiangron et al., 2002). The Deutsch model assumes that there is complete mixing transverse to the flow direction due to turbulent dispersion; no axial dispersion is considered (Deutsch, 1922; Gutiérrez Ortiz et al., 2010). As a result of this assumption, a uniform particle concentration profile is maintained, and thus the concentration decays exponentially in the flow direction. This leads to the Deutsch efficiency formula as follows:

$$\eta = 1 - \exp\left\{-\frac{W_m(d_p, E_C)\cdot L}{v \cdot s}\right\} \qquad (1)$$

where η is the collection efficiency, W_m is the migration velocity to the collection plate caused by the electric field for the collection (E_C), v is the mean air flow velocity, L is the length of the collection plate, and s is the distance between the high voltage electrode and the collection plate of the ESP. Assuming that Stokes' drag law is valid, the theoretical migration velocity of particles at a steady state resulting from a balance of the drag and electrical forces on the particles is as follows:

$$W_m(d_p, E_c) = \frac{Q_p \cdot E_C \cdot Cu}{3\pi\mu d_p} \quad (2)$$

Where μ is the viscosity of air and Q_p is the particle charge, which is given by the equation (Cochet, 1961; Bai et al., 1995)

$$Q_p^{\infty} = \left\{\left(1 + 2\lambda/d_p\right)^2 + \left(\frac{2}{1+2\lambda/d_p}\right) \cdot \left(\frac{\varepsilon_r - 1}{\varepsilon_r + 2}\right)\right\} \cdot \pi\varepsilon_0 d_p^2 E_p \quad (3)$$

where E_p is the electrical field for the particle charging, λ is the mean free path of the gas molecules, and ε_r and ε_0 are the relative electrical permittivity of gas and of a vacuum, respectively. The Cunningham correction factor, C_u, as a slip correction factor applied whenever the particle sizes approach molecular sizes, is also given as follows (Flagan and Seinfeld, 1988) :

$$Cu = 1 + 1.246 \cdot \frac{2\lambda}{d_p} + 0.42 \cdot \frac{2\lambda}{d_p} \cdot \exp\left(-0.87 \cdot \frac{d_p}{2\lambda}\right) \quad (4)$$

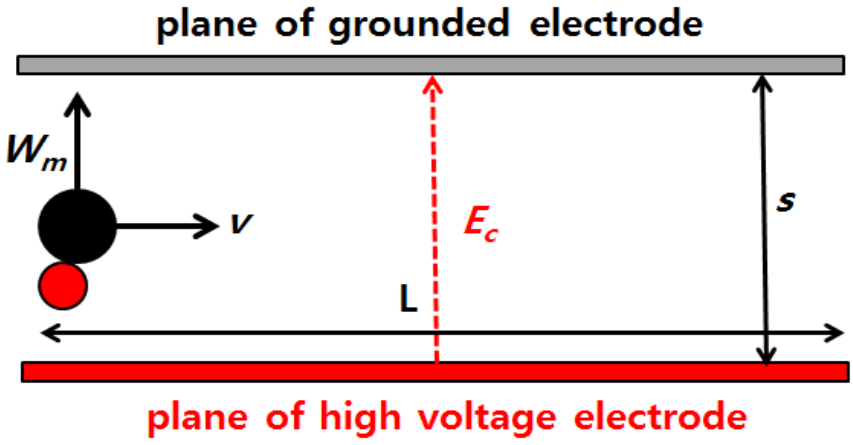

Figure 1. Illustration of the Deutsch model. (Parker, 1997)

2.1.2 Particle charging theories

In order to get a reasonable estimation of collection efficiency for an ESP, the choice of charging a theory is the most important process. Particle charging mechanisms in an ESP include the field charging and diffusion charging. When an ion collides with a particle, it sticks, and the particle acquires its charge. Particles mixed with unipolar ions become charged by random collisions between

the ions and the particles. This process is called "diffusion charging" because the collisions result from the Brownian motion of the ions and particles. This mechanism does not need an external electrical field and does not depended on the particle materials. On the other hand, the "Field charging" is charging by unipolar ions in the presence of a strong electric field. When an uncharged particle is placed in a uniform electric field, the rapid motion of ions in an electric field results in frequent collisions between the ions and the particles. Usually the charging processes is divided into the diffusion charging for particles smaller than than 1 μm, and a field charging for those larger than 1 μm. Many researchers have developed charging theories for the field charging and diffusion charging. Besides, some researchers have developed theories combining both of the mechanisms because various sized particles are present in an ESP. These particle charging theories have different accuracies requiring different computational times and need further evaluation using some experimental results. Among the various charging theories, for the most of the my ESP researches related to particle size ranges from submicrometer to micrometer, I used the Cochet's analytic equation (equation (3)) because it allows an easy calculation and correlation to actual ESP conditions which is quite reasonable in the critical submicromenter size ranges (Parker, 1997).

In this study, a diffusion charging theory based on the Fuchs' limiting sphere theory is also used for the particles which are specially smaller than 0.1 μm because the diffusion charging is predominantly used for nanoparticle charging, and nanoparticle collection in ESPs depends primarily on particle charging efficiency within an ESP and therefore on particle size (Suriyawon et al., 2008). The diffusion charging of aerosol particles induced by unipolar ions can be expressed as follows (Adachi et al., 1985):

$$\frac{dn_0}{dt} = -\beta_0^s n_0 N_i^s \qquad (5)$$

where n is the number concentration of particles, N_i is the ion concentration, and β is the attachment coefficient of an ion with a particle. The subscript 0 indicates the neutral state and the superscript s denotes the polarity of the ions. Equation (5) represents the time-dependent change in number concentration for uncharged particles. If the initial particles are all uncharged, from the equation (5) the following analytical solution can be obtained.

$$\frac{n_0}{n_t} = \exp(-\beta_0^s N_i^s t) \qquad (6)$$

For the value of β, Fuchs' limiting sphere theory is used (Fuchs, 1963). The Fuchs' theory is most commonly used for the diffusion charging of particles in the transient regime, and the equation for combination coefficient, β of ion with particle, based on Fuchs' theory is as follows:

$$\beta_p = \frac{\pi C_i \alpha \sigma^2 \exp\left\{-\frac{\emptyset(\sigma)}{kT}\right\}}{1+\exp\left\{-\frac{\emptyset(\sigma)}{kT}\right\}\frac{C_i \alpha \sigma^2}{4 D_i a}\int_0^{\frac{a}{\sigma}} \exp\left\{\frac{\emptyset(r)}{kT}\right\} d\left(\frac{a}{r}\right)} \quad (7)$$

where

$$\emptyset(r) = \frac{pe^2}{4\pi\varepsilon_0 r} - \frac{\varepsilon_1 - 1}{\varepsilon_1 + 1}\frac{e^2}{8\pi\varepsilon_0}\frac{a^3}{r^2(r^2-a^2)} \quad (8)$$

$$\sigma = \frac{a^3}{\lambda_i^2}\left\{\frac{1}{5}\left(1+\frac{\lambda_i}{a}\right)^5 - \frac{1}{3}\left(1+\frac{\lambda_i^2}{a^2}\right)\left(1+\frac{\lambda_i}{a}\right)^3 + \frac{2}{15}\left(1+\frac{\lambda_i^2}{a^2}\right)^{\frac{5}{2}}\right\} \quad (9)$$

$$\alpha = \frac{b_m}{\sigma} \quad (10)$$

$$b_m^{\,2} = \left[1 + \frac{\{\emptyset(\sigma) - \emptyset(L_m)\}}{1/2 m_i C_i^{\,2}}\right] \quad (11)$$

The subscript p indicates the number of the elementary charges and their polarity. C_i, D_i, and m_i are the thermal velocity, diffusion coefficient and mass of an ion, respectively. k, T, and a are the Boltzman constant, absolute temperature, and particle radius, respectively. ϕ and r represent the electrostatic potential of the ion and particle, and the radius of the limiting sphere (inside this sphere ions move as free molecules in a vacuum, and outside this sphere ions move by diffusion in a continuum), respectively. ε_0 and ε_1 are the vacuum permittivity and the dielectric constant of the particle, respectively.

σ is the radius of the limiting sphere, and is a function of the mean free path of the ion, λ_i. α is the fraction of ions entering the limiting sphere that reach the particle surface, expressed as the ratio of minimum impact parameter, b_m and the radius of the limiting sphere, σ. L_m is the minimum apsoidal distance. β_p depends significantly on the ion properties such as C_i, D_i, and λ_i, which can be derived using the mass, m_i and electrical mobility, Z_i of ions as follows:

$$D_i = \frac{kTZ_i}{e} \quad (12)$$

$$\mathbf{C_i} = \sqrt{\frac{\mathbf{8kT}}{\pi \mathbf{m_i}}} \tag{13}$$

$$\boldsymbol{\lambda_i} = \frac{\mathbf{16\sqrt{2}}}{\mathbf{3\pi}} \frac{\mathbf{D_i}}{\mathbf{C_i}} \left(\frac{\mathbf{M}}{\mathbf{M+m_i}}\right)^{\frac{1}{2}} \tag{14}$$

where M is the molecular weight of the carrier gas. Therefore, at least mass and electrical mobility of ions have to be known to calculate β_p.

Also, in the research for an indoor air cleaner with an ESP method, I assumed that the particle charge (n_p) is a function of time calculated by summing diffusion charging (n_1) and field charging (n_2) theory results because the particle size range that I chose in this study was only from 0.25 to 0.35 μm in which both of the two mechanisms are operating and the charging phenomenon is much more complicated. In particular, particle charges using this summation assumption among various charging theories showed a fairly good agreement with experimental results for size-dependent particle charges in the previous study (Long and Yao, 2010).

The approximate value for the number of charges, $n_1(t)$, acquired by a particle by diffusion charging during time, t, is

$$\boldsymbol{n_1(t)} = \frac{\boldsymbol{d_p \kappa T}}{\boldsymbol{2K_E e^2}} \boldsymbol{ln}\left[\mathbf{1} + \frac{\boldsymbol{\pi K_E d_p \bar{c}_i e^2 N_i t}}{\boldsymbol{2\kappa T}}\right] \tag{15}$$

where d_p is the diameter of a particle (μm), κ is Boltzmann's constant (=1.38 x 10^{-23} J/K), T is temperature (K), K_E is a constant (9.0 x 10^9 Nm^2/C^2), $\bar{C}_i$ is the mean thermal speed of the ions (240 m/s) under standard conditions, N_i is the concentration of ions (ions/m^3), e is the charge on an electron (1.6 x 10^{-19}C), and t is the charging time (sec).

The analytic expression for the number of charges, $n_2(t)$, acquired by a particle during a time, t , in an electric field E with an ion number concentration N_i is

$$\boldsymbol{n_2(t)} = \left(\frac{\boldsymbol{3\varepsilon}}{\boldsymbol{\varepsilon+2}}\right)\left(\frac{\boldsymbol{E{d_p}^2}}{\boldsymbol{4K_E e}}\right)\left(\frac{\boldsymbol{\pi K_E e Z_i N_i t}}{\boldsymbol{1+\pi K_E e Z_i N_i t}}\right) \tag{16}$$

Where ε is the relative permittivity of a particle, E is the electric field (V/m), and Z_i is the mobility of the ions (approximately 0.00015 $m^2/V{\cdot}s$).

Table 1 shows the summary of theoretical analysis methods used in this study. Considering the particle size range of test particles that I used in each chapter, I chose adequate charging and collection theories to obtain the most analogous results with experimental ones.

Table 1. Summary of theoretical analysis methods used in this study.

Chapter No.	Research topic	Particle size range	Charging	Collection
III	Non-metallic ESPs	0.05~10 μm	Cochet's model eq. (3), (4)	Deutsch theory eq. (1), (2)
IV	Wet ESP with thin water films	0.01~0.05 μm	Fuchs' limiting sphere theory eq. (5)~(14)	-
		0.05~1 μm	Cochet's model eq. (3), (4)	Deutsch theory eq. (1), (2)
	ESP for Oxy-PC	0.3~10 μm	Cochet's model eq. (3), (4)	Deutsch theory eq. (1), (2)
VI	ESP air cleaner	0.3 μm	Diffusion & Field charging model eq. (15), (16)	Deutsch theory eq. (1), (2)

2.1.3 References

Parker, K.R. In Applied electrostatic precipitation.1sted; Blackie academic & professional: London, 1997; pp 52-67.

Park, J.H.; Chen, C.H. An improved modeling for prediction of grade efficiency of electrostatic precipitators with negative corona; J. Aerosol. Sci. 2002, 33, 673-694.

Xiangron, Z.; Lianze, W.; Keqin, Z. An analysis of a wire-plate electrostatic precipitator; J. Aerosol. Sci. 2002, 33, 1595-1600.

Deutsch, W. Bewegung und ladung der elektrizitätsträger im zylinderkondensator; Ann. Phys. 1922, 68, 335-344.

Gutiérrez Ortiz, F.J.; Navarrete, B.; Cañada, L. Dimensional analysis for assessing the performance of electrostatic precipitators; Fuel Process. Technol. 2010, 91(12), 1783-1793.

Cochet, R; Lois charge des fines particules (Submicroniques) Etudes théoriques - Controles récents spectre de particules. Colloque International la Physique des Forces Electrostatiques et Leurs Application 1961, Centre National de la Recherche Scientifique, Paris; 102: 331-338.

Bai, H.; Lu, C.; Chang, C.L. A model to predict the system performance of an electrostatic

precipitator for collecting polydisperse particles; Air & Waste Manage. Assoc. 1995, 45, 908-916.

Flagan, R.C.; Seinfeld, J.H. In Fundamentals of air pollution engineering; Prentice-Hall, Inc: New Jersey, 1988.

Suriyawong, A.; J. Hogan Jr, C.; Jiang, J.; Biswas, P. Charged fraction and electrostatic collection of ultrafine and submicrometer particles formed during O_2-CO_2 coal combustion; Fuel. 2008, 87, 673-682.

Adachi, M.; Kousaka, Y.; Okuyama, K. Unipolar and bipolar diffusion charging of ultrafine aerosol particles; J. Aerosol Sci. 1985, 16, 109–123.

Fuchs, N. A. On the stationary charge distribution on aerosol particles in a bipolar ionic atmosphere; Geofis. Pura Appl. 1963, 56, 185–193.

Long, Z. and Yao, Q. (2010). Evaluation of various particle charging models for simulating particle dynamics in electrostatic precipitators, J. Aerosol. Sci., 41, 702-718.

Chapter III

Non-metallic ESP for Submicron Particle Removal in Corrosive gases

3.1 Characteristics of an ESP for submicron particles using non-metallic electrodes and collection plates

3.1.1 Introduction

The semiconductor market, which includes discrete semiconductors, optoelectronics, and integrated circuits, is expected to exceed $331 billion US dollars in 2012 with a 3-year compound annual growth rate of 13.6% from 2009 to 2012. To meet demands, semiconductor companies in Korea, which are some of the major manufacturers worldwide, are planning to increase manufacturing lines, and the emissions of gaseous and solid pollutants are also expected to increase. Large quantities of corrosive pollutants such as basic (NH_3)-waste gases and inorganic acids, including hydrofluoric acid, hydrochloric acid, nitric acid, phosphoric acid, and sulfuric acid, are commonly used in semiconductor and optoelectronic industries for cleaning and etching processes (Eom et al., 2006; Huang et al., 2005; Lu et al., 2011; Tsai et al., 2004). Until now, wet scrubbers have been widely used for gas-phase pollutant removal in the semiconductor manufacturing industries (Chein et al., 2005). In a wet scrubber, methods used to bring the polluted gas stream into contact with the scrubbing liquid include spraying the gas with the liquid or forcing it through a pool of liquid (Gamisans et al., 2002; Korell et al., 2009). Because of the simple physical mechanism of the scrubber, the fine particles generated in the manufacturing process are not usually treated efficiently and pass through the wet scrubbers, finally becoming sources of white smoke, which forms through the homogeneous and heterogeneous nucleation of gaseous compounds and water vapor followed by condensation (Hayes and Woods, 1996; Tsai et al., 1997). The particles in this size range are the sources of the visible plumes that are emitted into the atmosphere (Chang and Tsai, 1996; Tsai et al., 1997). These plumes raise public concerns about the effects of particulates on human health and atmospheric visibility and prompted the US Environmental Protection Agency to regulate the opacity of plumes to <20% (Du et al., 2007; Srivastava et al., 2004). Although

gravitational wet scrubbers have high removal efficiency for soluble corrosive gases, they also have technical limitations, such as requirements for high power and large installation space due to the high pressure drop needed to remove ultrafine particles (Allen and Santen, 1996; Huang et al., 2007; Tsai et al., 2005; Zhao and Zheng, 2008). To increase the low efficiency of the scrubber for ultrafine particles, researchers have examined the use of an electrostatic precipitator (ESP) that collects particles from moving air using the force of an induced electrostatic charge onto a wet scrubber. The resulting removal efficiency was found to be >90% in terms of either the number or mass concentration (Bologa et al., 2009; Hwang et al., 2004; Jaworek et al., 2006; Tsai et al., 1997; Zhao and Zheng, 2008). Despite these successes, the use of general ESPs to remove particles in corrosive exhaust gases has relied on expensive anticorrosive metallic materials, such as Inconel and Hastelloy C alloys, to maintain their performance (Bayless et al., 2004; Kim et al., 2008). Therefore, a less expensive ESP which uses different anticorrosive materials is worth developing.

In addition, ESPs require a relatively high electrical power, generally in the range 59 ~ 295 W per 1,000 m^3/h, in order to meet the regulatory limits for particulate emissions, because the performance of the ESPs is very sensitive to power consumption when charging and collecting particulates (Electrostatic precipitator knowledgebase, 2007; Wang et al., 2004). Furthermore, the ozone that is normally generated as a byproduct of corona discharge in an ESP can cause serious damage to respiratory organs, and causes deterioration in many materials, and thus the daily 8-hour maximum ozone concentration is regulated to less than 60 ~ 80 ppb by the WHO, EPA, and EC, among others (Yehia et al. 2000a, 2000b; Liu et al., 2000; Bell et al., 2006).

In response to the economic and technical demands of efficient ESPs for IT industries such as semiconductor, LCD, photoelectric cell manufacturing companies, a novel anticorrosive ESP has been developed whose charger is made of carbon fibers and whose collection plates are made of polyvinyl chloride (PVC) sheets containing metallic films as inserts. The carbon fiber ionizers are made of an anticorrosive material, carbon graphite, which may be utilized easily and inexpensively by applying a voltage of a few kV to a bundle of carbon fibers in order to generate ions. These can produce stable unipolar ions at sufficiently high concentrations, whilst generating negligible concentrations of ozone (Han et al., 2008a, 2008b, 2009a, 2009b). Furthermore, the PVC sheets that coat the thin metallic films are made of a thermoplastic polymer that is known to be resistant to the effects of acidic and other corrosive gases. I am unaware of any previous attempts to use a carbon brush charger and PVC collection plates with a metallic film in ESPs for an industrial purpose.

In the study reported herein, the performance characteristics of the newly developed ESP were

investigated by changing several of the parameters in the charger and collection plates, and the ozone concentration and the pressure drop were also measured under the maximum operating conditions of the ESP. The tests of dust-loading and water cleaning of collection plates were also performed in order to assess the long term performance of the ESP.

3.1.2 Experimental set up

Figure 1 shows the charger and collection plates of the ESP that was used in the study. The carbon brush precharger was made of several carbon brush ionizers that consisted of a bundle of approximately 300 carbon fibers whose diameter was of the order of a few micrometers. The ionizers were connected to a high-voltage power supply and were located at the center of the channels. In order to increase the charging rates of the submicron particles in the charger, the number of channels used was varied as 4, 9, and 16, while their width, height, and length for the sum all the channels were maintained as 400, 400, and 800 mm, respectively. The collection plate was made of a 0.1 mm aluminum thin film coated by a polyvinyl chloride (PVC) sheet that had a thickness of 0.2 mm. The width and length of the metallic film were 400 and 185 mm, respectively, with a hole positioned at its edge, into which an electrode was inserted. Several tens of collection plates in a 400 x 400 mm PVC duct were aligned in parallel, and the plates were connected to the high-voltage power supply and to ground by turns. The gap between each plate was varied as 7, 10, and 15 mm in order to increase the strength of the electric field between the collection plates.

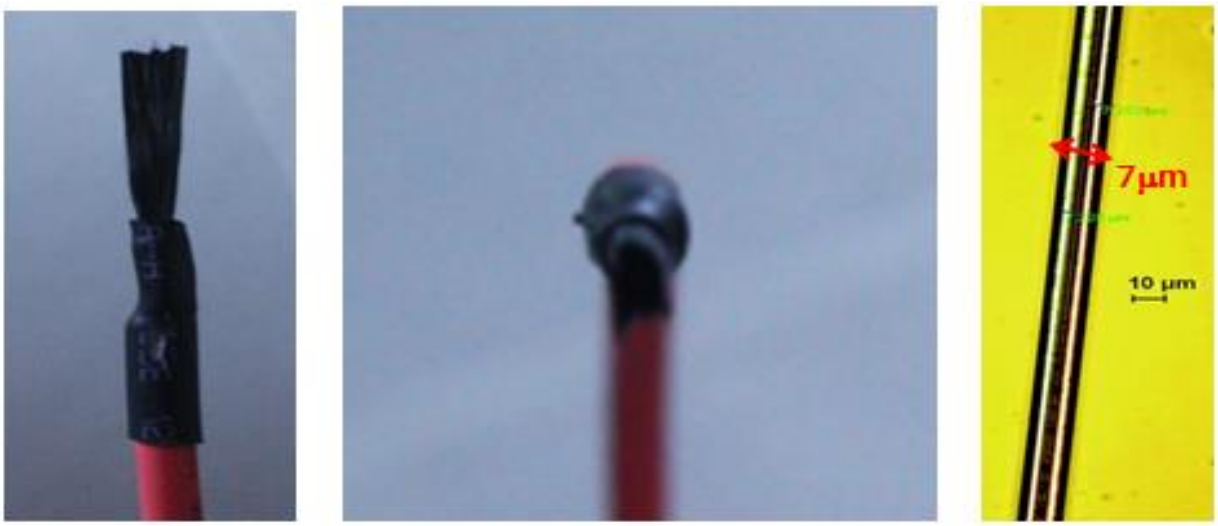

(a) Carbon fiber brushes

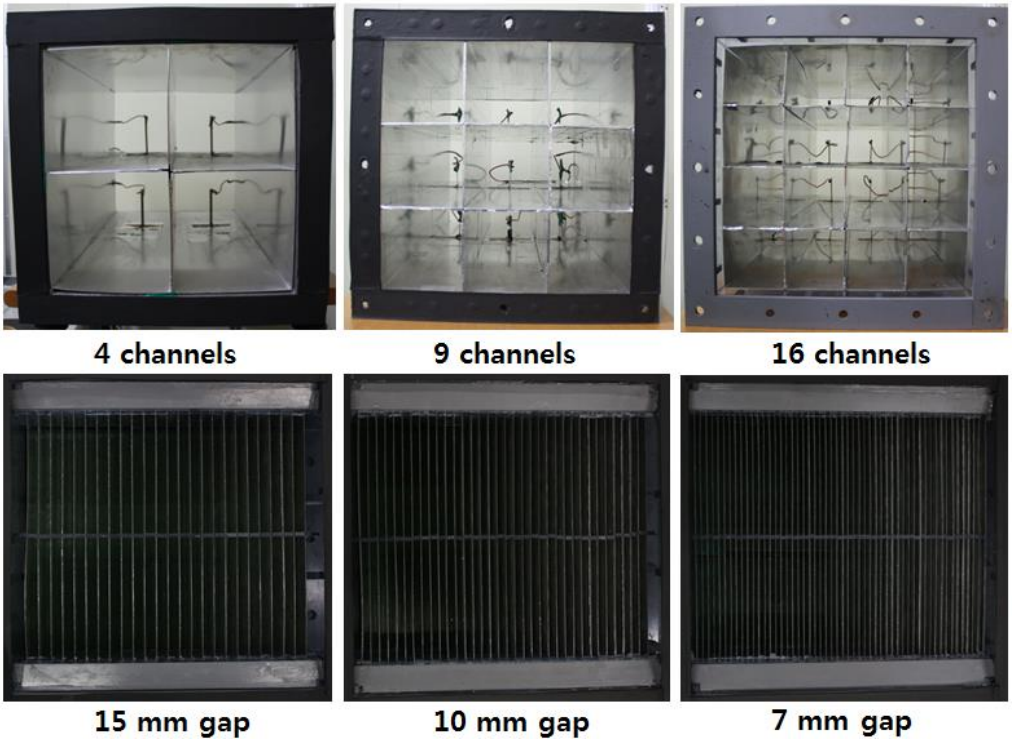

(b) precharging and colleciton stages

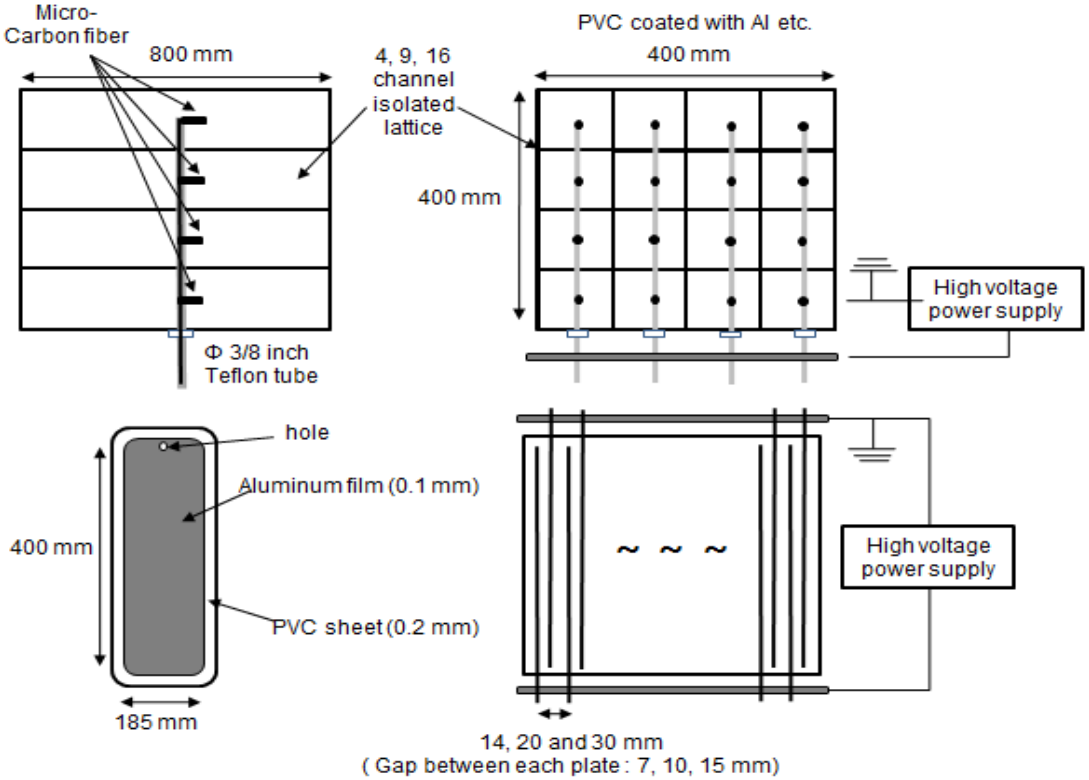

(c) Schematics of the ESP in this study

Figure 1. The unipolar precharger using the carbon fiber ionizers and collection plates of the ESP developed during the study.

Figure 2 shows the experimental setup used in the study. Potassium chloride (KCl) aerosol particles with diameters in the range 0.01 ~ 0.5 μm were generated by nebulizing a solution of KCl (w/w 0.1% in water) using an atomizer with a constant output (Model 3076, TSI Inc., US) and passing them through a Kr-85 neutralizer and a diffusion dryer. The mean diameter, number concentration, and geometric standard deviation of the particles generated were approximately 0.1 μm, 6.0 x 10^6 particles/cm^3, and 1.7, respectively. The charged fractions of the test particles were removed using a plate condenser (to which a high voltage of 10 kV was applied), and uncharged particles were then introduced into the test duct (cross section 400 x 400 mm^2) upstream of the carbon brush precharger.

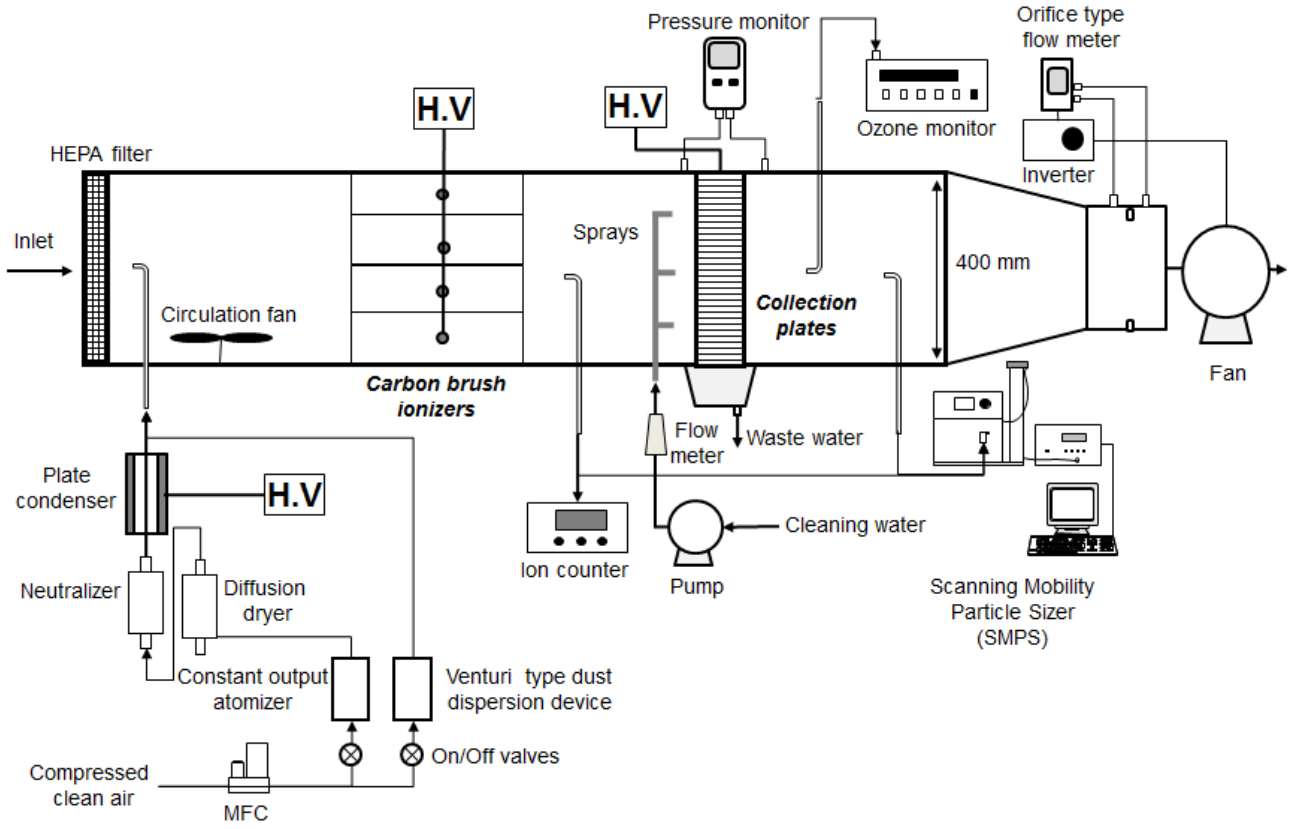

Figure 2. Schematic of experimental set up for the ESP with non-metallic electrodes

High efficiency particulate arrestance (HEPA, 99.97% of airborne particles 0.3 μm in diameter)-filtered clean air was mixed with these particles and the mixture was then passed through the carbon brush precharger and collection plates. The gas flow rate in the duct was controlled using an orifice-type flow meter and inverter that was connected to a fan located at the end of the duct. The size distributions of the test particles upstream and downstream of the collection plates were measured

using a scanning mobility particle sizer (SMPS, Model 3081, TSI Inc., US) system, together with a condensation particle counter (CPC, Model 3076, TSI Inc., US) for particles smaller than 0.3 μm and an optical particle counter (Model 1.109, GRIMM, Germany) for particles larger than 0.3 μm. The loss of the particles in the ESP without applying voltage to it was negligible. The ionic concentration, the average charge and the ozone concentration emitted from the precharger were measured using an ion counter (Model Ionometer IM 806, U.H. Gmbh, Germany), an aerosol electrometer (Model 3068B, TSI Inc., US) combined with a condensation particle counter (CPC, Model 3022A, TSI Inc., US), and an ozone monitor (Model API 400E, Teledyne Technologies Inc., US), whilst varying both the number of ionizers and the voltage applied to them. Differences in pressure between points immediately before and after the collection plates were also measured using a pressure monitor (Model 350-M/XL-454, TESTO AG, Germany) as the distance between the collection plates and the air velocity were varied.

Table. 1 Experimental conditions for the performance tests of the ESP developed in this study

Parameters	Conditions	Measurements
Air face velocity	1.0, 1.5, 2.0 m/s	Collection efficiency (%)
Number of channels (Distance between a carbon brush ionizer and a ground)	4, 9, 16 EA (100, 67, 50 mm)	Collection efficiency (%)
Voltage applied to ionizers	5, 7, 10 kV	Collection efficiency (%) Average charge (-) Ion concentration (ions/cm^3) Ozone concentration (ppb)
Gap between collection plates	7, 10, 15 mm	Collection efficiency (%) Pressure drop (Pa)
Voltage applied to collection plates	7, 10, 15 kV	Collection efficiency (%)

During the experiments, the properties of the precharger and collection plates were varied in order to investigate their effect on the performance of the ESP. The experimental conditions used are listed in Table 1. The performance of the ESP used in this study was expressed in terms of the particle collection efficiency (η), which may be obtained by using the following equation:

$$\eta = \left(1 - \frac{C_{down}}{C_{up}}\right) \times 100 \quad (1)$$

where η is the collection efficiency, C_{down} is the number concentration of the particles downstream of the collection plates, and C_{up} is the number concentration of the particles upstream of them. The particle loss in the precharger with applying voltages to it was less than 10% in this study.

The collection performance during dust loading and water cleaning performance of the ESP was evaluated using a standard dust (Class 8, mean diameter 1.6 ~ 2.3 μm, JIS standard dust, Japan) for the dust loading of the collection plates, and submicron KCl particles for measuring the transient collection efficiency of the ESP during dust loading and after water cleaning. A venture-type dust dispersion device was used to spread the dusts throughout the upstream test duct (Figure 2) and a circulation fan was used in order to distribute the dusts uniformly upstream of the precharger and collection plates. The mass concentration of the loading dust that flowed into the ESP was maintained at approximately 100 mg/m^3. Prior to dust loading, the initial collection efficiency of the ESP was measured, and the transient collection efficiency was then measured every 25 minutes after dust loading, by means of KCl particles. After the transient collection efficiency of the ESP had reached 50% of the initial efficiency, a pump supplied clean water to the sprayers, which were located in front of the collection plates. The pump was operated for 2 minutes per run, with cleaning being continued until the collection efficiency had returned to its initial value. The flow rate of the cleaning water through the pump was 25 L/min. The polluted water was removed periodically from the drain chamber.

3.1.3 Results and discussion

(1) Electrical characteristics of a carbon brush precharger

Figure 3 shows the variation in current against voltage applied to the ionizers of the carbon brush precharger using 4, 9, and 16 channels. The flow velocity of the air at the inlet to the precharger was 2 m/s. The curves were moved to the left and the current increased in proportion to the number of channels used for a given applied voltage. In particular, ‘sparkover’ in the precharger, which indicates the start of the unstable discharge, was observed at a lower applied voltage when more channels were used.

Figure 4 shows the average charge of the particles in the carbon brush precharger as the applied voltage and the number of the channels was varied. The average charge was linearly increased by increasing the applied voltage to the charger and it was also increased by increasing the

number of the channels of the precharger.

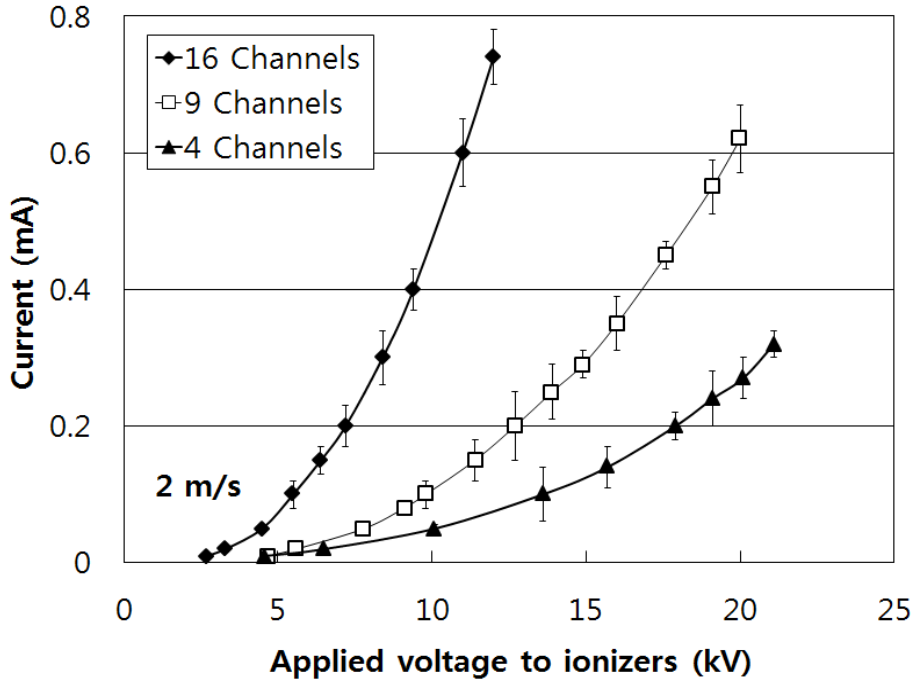

Figure 3. Current against the applied voltage of the precharger using 4, 9, and 16 channels

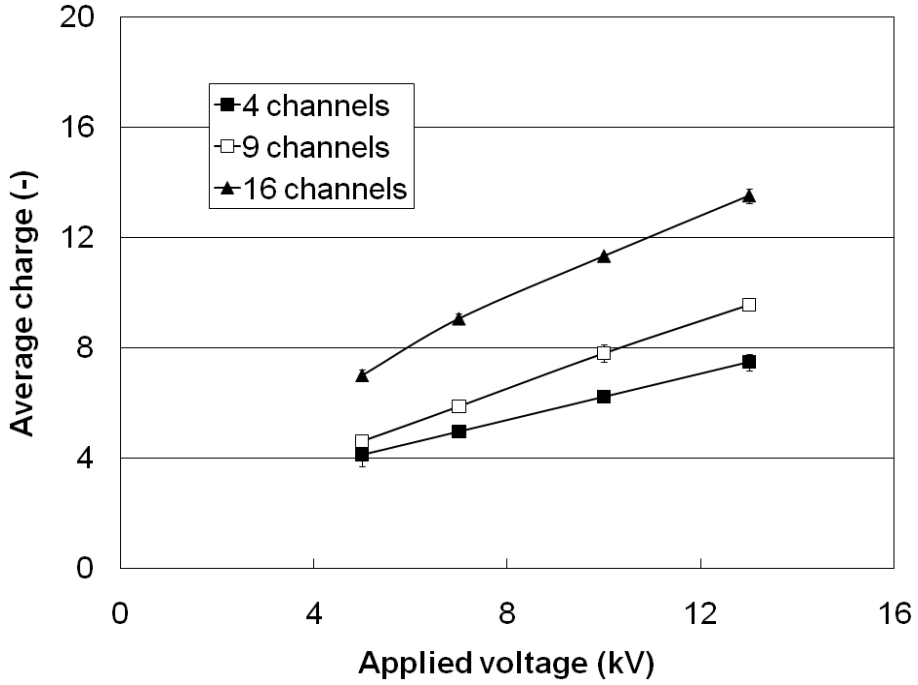

Figure 4. Average charge of the particles against the applied voltages to the carbon brush precharger using 4, 9, and 16 channels.

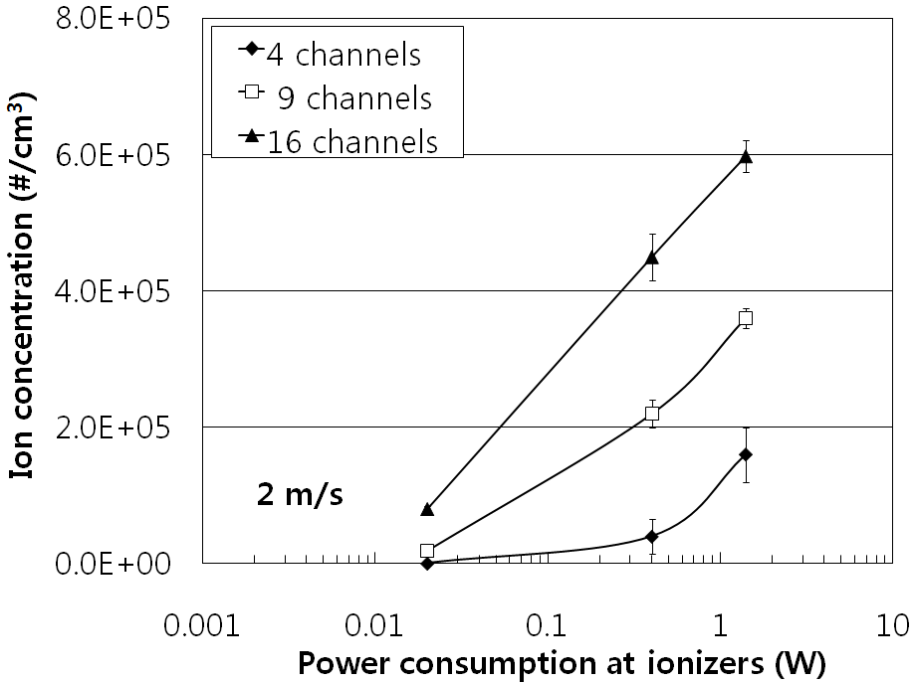

Figure 5. Ionic concentration against the power consumption at the carbon brush precharger using 4, 9, and 16 channels.

Figure 5 shows the unipolar ion concentration generated by the carbon brush precharger plotted against the power consumed by the charger, which was calculated for 4, 9, and 16 channels by multiplying the applied voltage by the corona current. Similarly to Figure 4, the ionic concentration was increased by increasing the applied voltage in all cases, and it was also increased by increasing the number of channels used for a given applied voltage (Han et al., 2008, 2009). These findings are mainly due to the increased number of carbon brush ionizers and the shorter distance between the carbon brush ionizer and the ground of the charger, thus increasing the electrical field, as well as a higher current density in the charger, for a larger number of channels (White, 1963; Parker, 1997).

Figure 6 shows the variation in the concentration of ozone emitted from the carbon brush precharger, plotted against the power consumed by the precharger. In order to measure the maximum concentration of ozone emitted from the charger, 16 channels were used, because this setup was shown to generate the most ions from the charger, and the air velocity was maintained at 2 m/s. The average ozone concentration was proportional to the power consumption of the ionizers. This finding was in quite good agreement with the results of previous studies (Yehia et al., 2000a, 2000b). In particular, when the maximum 10 kV, was applied to the ionizers in 16 channels, the ozone

concentration was less than 2 ppb, which was significantly lower than the 60 ~ 80 ppb limit set out in the EPA and WHO regulations. The maximum result was 40,000 ppb·L/min for a power consumption of approximately 5 W (i.e. 2 ppb x 20,000 L/min), which is much lower than the value of 500,000 ppb·L/min previously reported for the same power consumption (Yehia et al., 2000). This indicates that the use of a carbon brush precharger that does not produce ozone as a byproduct could be a more promising environmentally friendly method of charging than that used in existing corona dischargers, particularly those used in industrial ESPs, as well those used indoors.

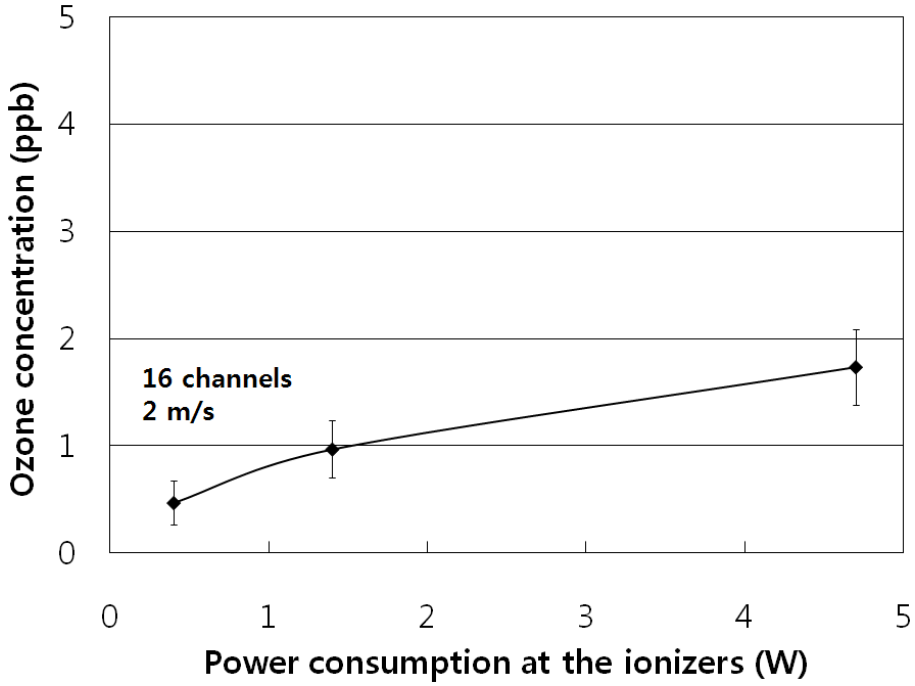

Figure 6. Ozone concentration at the outlet of the carbon brush precharger aginst applied voltage.

(2) Collection performances for submicron particles by parameter in the precharger

Figure 7 shows the collection efficiency of 0.3 μm particles in the ESP plotted against the voltage applied to the ionizers using 4, 9, and 16 channels. The voltage that was applied to the collection plates and the air velocity were maintained at 15 kV and 2 m/s, respectively. Increasing the voltage that was applied to the ionizers resulted in an increase in collection efficiency for the submicron particles, due to the increased charging rates of the particles, which were caused by an increase in both the number of negative ions in the ionizers and the electrical field strength (White, 1963). The collection efficiency of particles in the ESP using 16 channels was much higher than that using 4 or 9 channels for a given voltage applied to the ionizers. In particular, for the case of only 10 kV of applied voltage and 0.47 mA of corona current, which corresponded to a power consumption

of approximately 5 W, the collection efficiency of the 0.3 μm particles was more than 95 % for an air velocity of 2 m/s. It may be expected that the decrease in collection efficiency that results when the flow rate of the polluted air is increased could be avoided by increasing the number of channels and by applying a higher voltage to the ionizers in the charger.

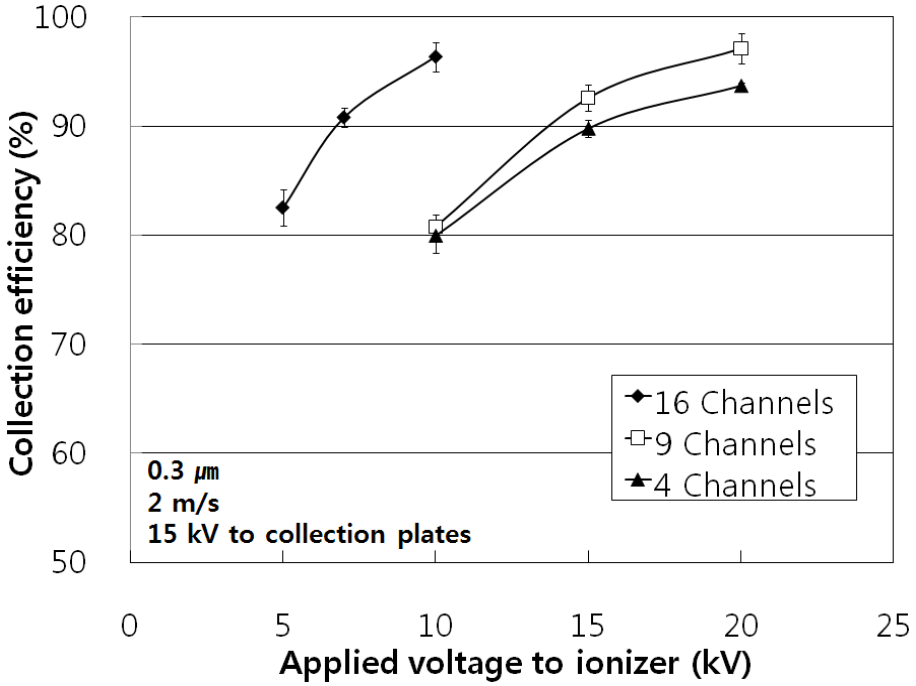

Figure 7. Collection efficiency of the ESP against the voltage applied to the ionizers Using 4, 9, and 16 channels.

Figure 8 shows the variation in the size distributions of the submicron particles, before and after passing them through the ESP, for an applied voltage to the ionizers of 5, 7, and 10 kV. 16 channels were used and the voltage applied to the collection plates was 15 kV, with the air velocity being maintained at 2 m/s. The number of the particles in the entire submicron range was reduced dramatically when the voltage applied to the ionizers was increased from 5 to 10 kV. When the voltage applied to the ionizers was greater than 7 kV, the concentrations of particles in all the size ranges fell to below 1 x 10^3 particles/cm^3.

Figure 9 shows the variation in collection efficiency plotted against particle diameter for different voltages applied to the ionizers. Apart from the voltage applied to the ionizers, the experimental conditions were kept constant at 16 channels, a flow rate of 2 m/s, and a voltage of 15 kV applied to the collection plates. When the voltage applied to the ionizers was between 5 and 10 kV, the collection efficiency of the particles exceeded 80% in all cases, regardless of particle size.

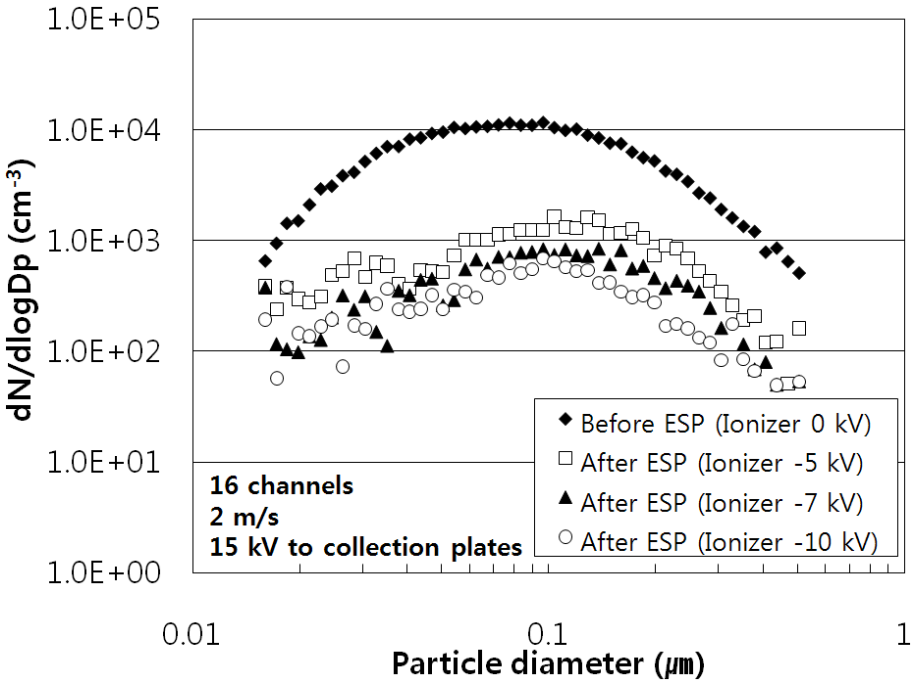

Figure 8. Changes in particle size distribution, before and after the ESP for various applied voltages to the ionizers for a constant voltage applied to the collection plates.

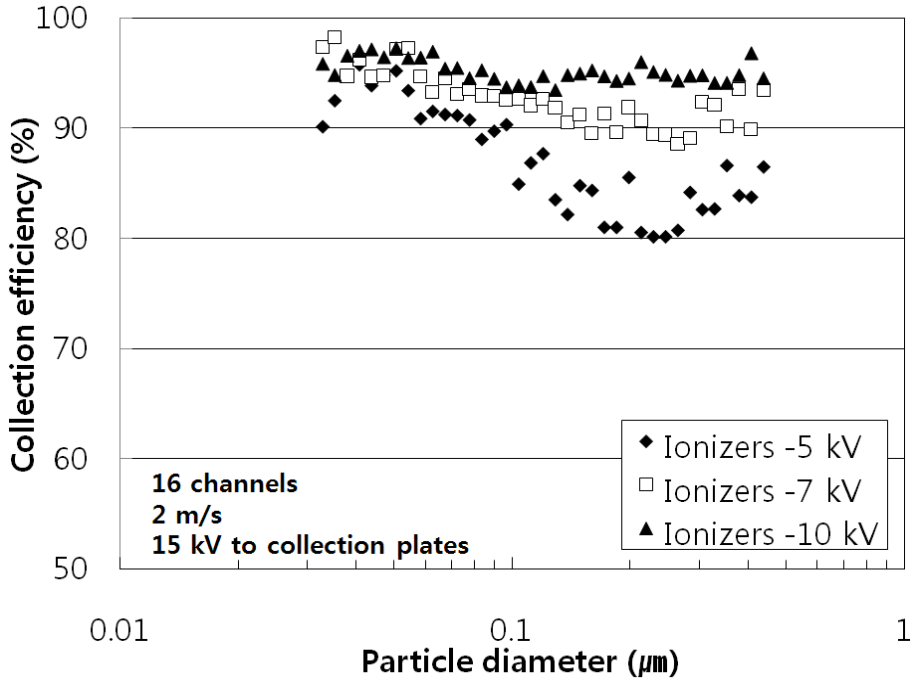

Figure 9. Collection efficiency of the ESP against the particle diameter for various voltages to the ionizers.

Furthermore, the collection efficiency of the particles in the range 0.1 ~ 0.3 μm was approximately 5 ~ 10% less than that of larger and smaller particles. This phenomenon may be attributed to the fact

that the charging rates of particles smaller than 0.1 μm and larger than 0.3 μm were higher than those of particles between 0.1 and 0.3 μm, due to the diffusion charging and field charging effects, respectively (Hinds, 1999). However, when the voltage applied to the ionizers reached 10 kV, the collection efficiency was more than 95% for all particles.

Figure 10 shows the variation in collection efficiency of 0.3 μm particles plotted against power consumption in the 16-channel precharger of the ESP for a range of different air velocities, while keeping the voltages applied to the collection plates constant at 10 kV or 15 kV. The collection efficiency of the particles increased in proportion to the power consumption, due to the increased concentration of unipolar ions. The collection efficiency showed a significant decrease of 15 ~ 35% for a voltage of 10 kV applied to the collection plates when the air velocity was increased from 1 to 2 m/s, and also showed a decrease of 5 ~ 10% for a voltage of 15 kV applied to the collection plates when the air velocity was increased from 1.5 to 2 m/s. However, the collection efficiency of the submicron particles reached more than 95% for a small electrical power of less than 5 W at an air flow rate of 1200 m^3/h (corresponding to a velocity of 2 m/s), compared with the much higher value of about 50 ~ 300 W that is generally required by ESPs to clean flue gases at a flow rate of about 1000 m^3/h (Wang et al., 2004).

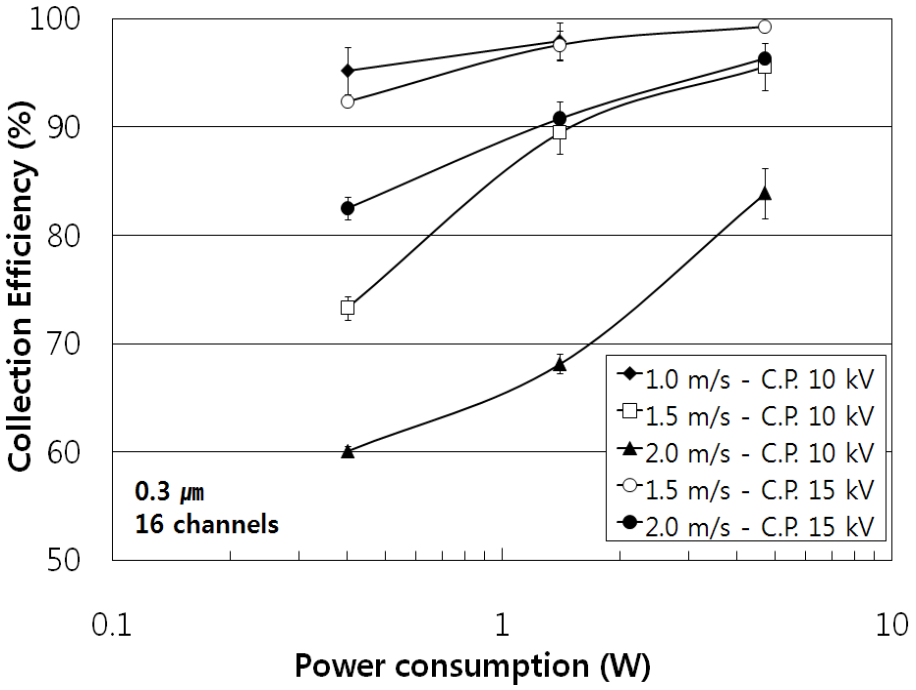

Figure 10. Collection efficiency of the ESP aginst the power consumption for various combinations of air velocity and voltage applied to the collection plates.

(3) Collection performances for submicron particles by parameter in the collection plates

Figure 11 shows the variation in collection efficiency of the ESP plotted against the width of the gap between the collection plates for a range of particle sizes in the submicron range. 16 channels were used in the precharger and the voltages applied to the ionizers and collection plates were 10 and 15 kV, respectively. A decrease in the gap between the plates resulted in an increase in the collection efficiency, due to a greater electric field strength between the collection plates for a given applied voltage, and a larger surface area at the collection plates. Particles less than 0.1 μm in size were collected more efficiently than larger ones due to the diffusion effect, which is an effect similar to that shown in Figure 9. However, the collection efficiency of the ESP was greater than 97% with a 7 mm gap between the collection plates, almost regardless of particle size.

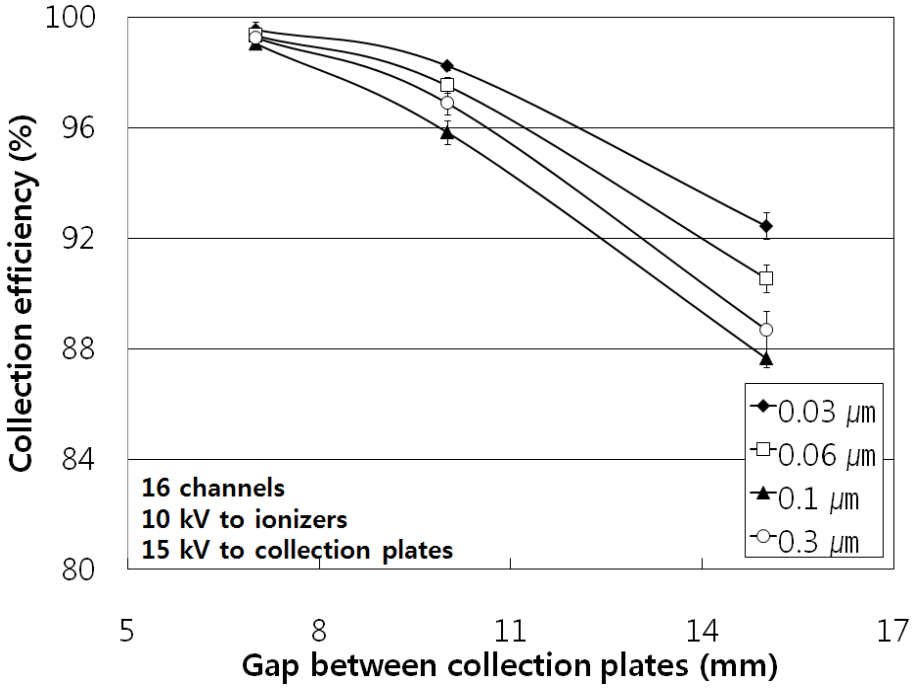

Figure 11. Collection efficiency of the ESP aginst the gap between the collction plates for various particle sizes

Figure 12 shows the variation in collection efficiency of 0.3 μm particles using 16 channels plotted against the voltage applied to the collection plates for a range of different air velocities, while keeping the voltage applied to the ionizers constant at 7 or 10 kV. The collection efficiency increased with increasing voltage applied to the collection plates, due to the increased electric field strength between them. The collection efficiency showed a significant decrease of 20 ~ 40% for a voltage of 7 kV applied to the ionizers when the air velocity was increased from 1 to 2 m/s and showed a decrease

of 5 ~ 13% for a voltage of 10 kV applied to the ionizers when the air velocity was increased from 1.5 to 2 m/s. However, the collection efficiency of the submicron particles reached more than 95% when 15 kV was applied to the collection plates and 10 kV was applied to the ionizers, even for an air velocity of 2 m/s. As shown in Figure 11, by reducing the gap between the collection plates it is possible to increase the collection efficiency of the ESP considerably at high air flow rates. However, it is also possible that the higher pressure drop caused the shorter gap may damage some of the other facilities (e.g. blowers) and thus increase maintenance costs. There is therefore a trade-off to be considered in the design of the gap between the collection plates. In the study described herein, the difference in pressure between points just before and after the collection plates was measured using a pressure monitor (shown in Figure 13). The pressure drops across the collection plates obtained using gaps of 7, 10, and 15 mm were all below 5 Pa for air velocities in the range of 1 ~ 2 m/s. In particular, the drops in pressure that were obtained when using collection plates with a 10 mm gap, which was used for all the experiments as a parameter of the precharger in Figures 12 to 14, were less than 3 Pa. Such a drop in pressure may be considered to be much lower in comparison with those of the most commonly used particulate removal systems in acid exhaust gases from industries such as spray towers and scrubbers, which show a pressure drop of 500 ~ 8,800 Pa corresponding to 50 ~ 880 mmAq at general operation conditions (Vallero, 2008).

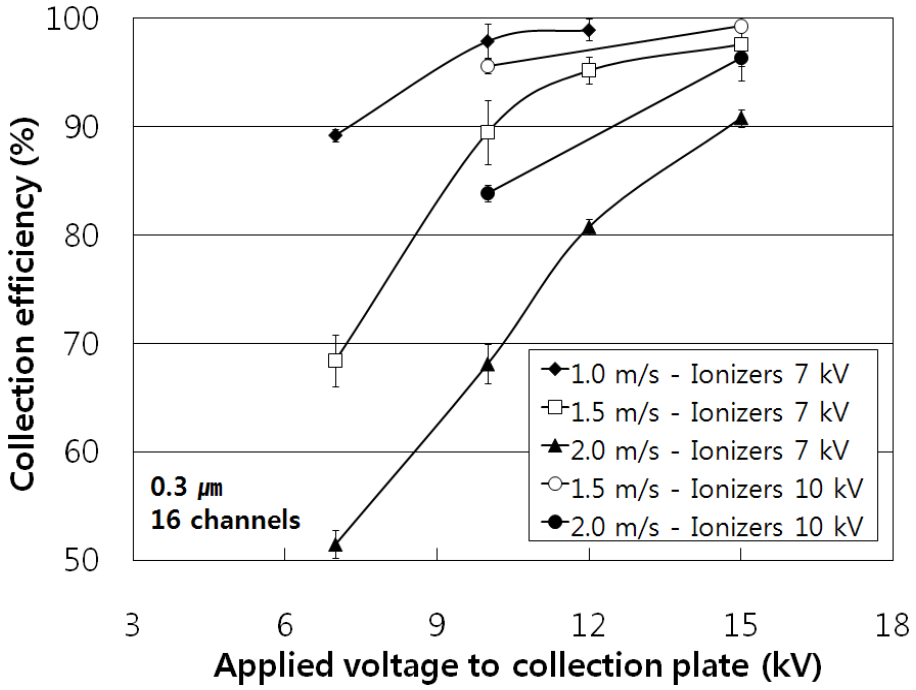

Figure 12. Collection efficiency of the ESP against the voltage applied to the collection plates for various combinations of air velocity and voltage applied to the ionizers

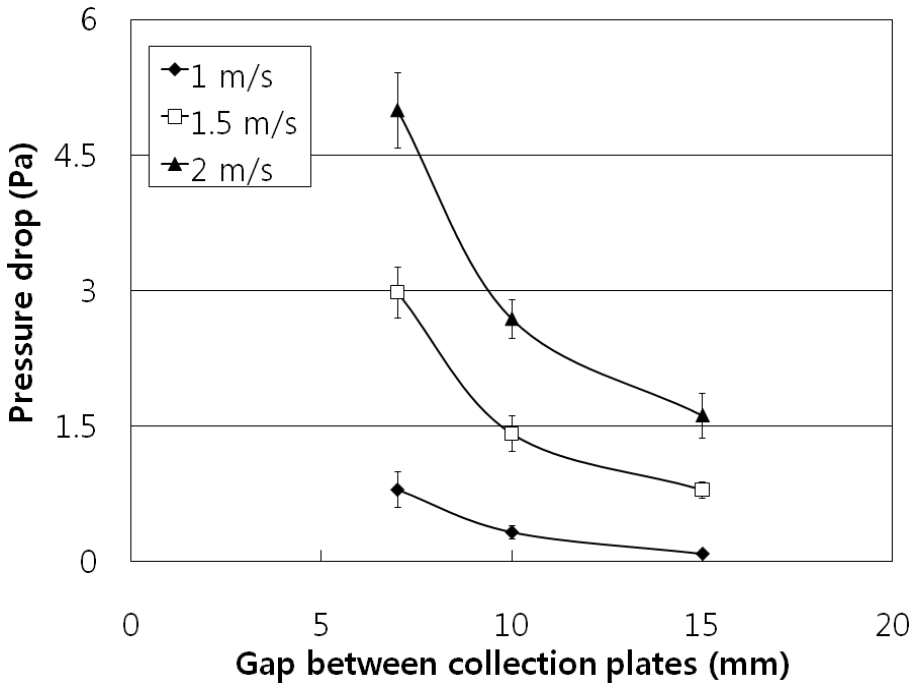

Figure 13. Pressure drop at the ESP against gap between the collection plates for various air velocities

In our own system, it may be expected that the decrease in collection efficiency when the flow rate of polluted air is increased could be minimized by shortening the gap between the collection plates and by increasing the voltage applied to the collection plates, with the advantages of causing very little increase in pressure drop at the collection plates.

(4) Particle loading and water cleaning tests

Figure 14 shows the variation in collection efficiency of the ESP plotted against particle size for different particle loading and cleaning conditions at the collection plates. The collection plates with a 10 mm gap were polluted intentionally using dust loading for 1 and 2 h using a mass concentration of approximately 100 mg/m^3, and regenerated by spraying it with water for 2 and 4 minutes at a flow rate of 25 L/min. 16 channels were used, and the voltages that were applied to the ionizers and collection plates were 10 and 15 kV, respectively, which represented the condition of maximum collection efficiency. The collection efficiency for submicron particles was more than 95% for the clean collection plates at the beginning of the experiment over the whole size range 0.01 to 0.5 μm.

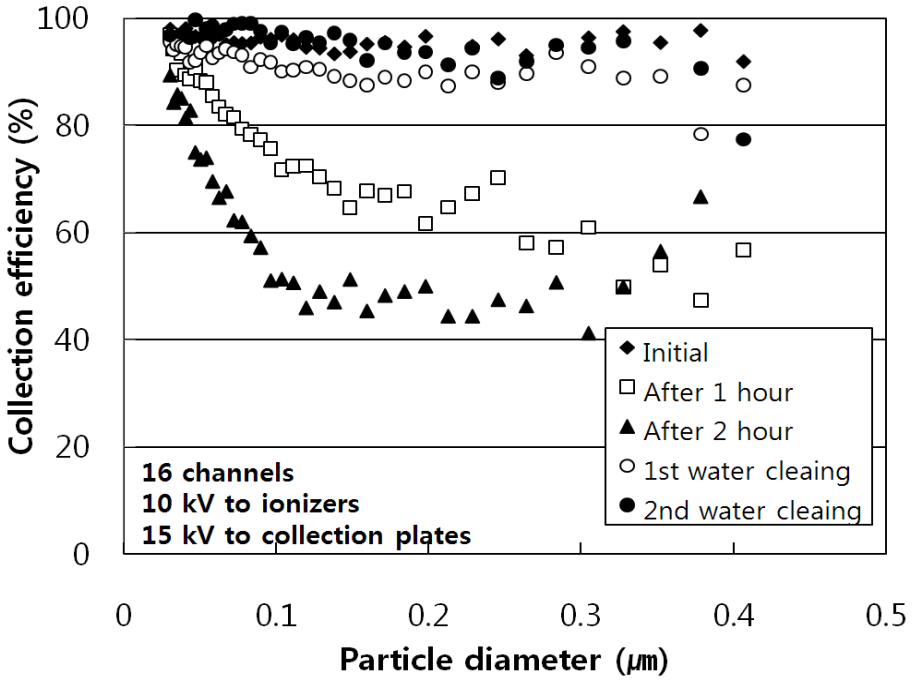

Figure 14. Collection efficiency of the ESP against the particle diameter for the initial state, after dust loading and water cleaning

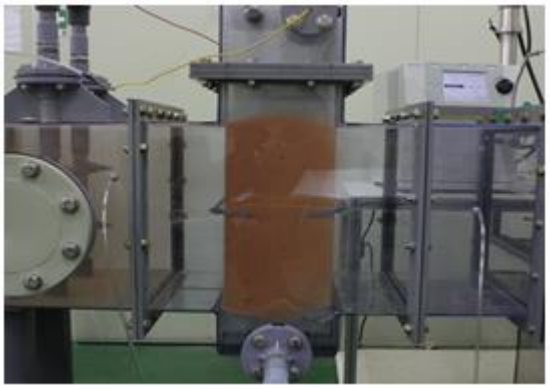

(a) Before water cleaning

(b) After water cleanig

Figure 15. Collection plates before and after water cleaning

The dust loading had almost no effect on 0.01 ~ 0.03 μm, showing that diffusion may be important for these particles. However, the collection efficiency of the ESP fell from 95 ~ 100% to 60 ~ 95% after 1 h of dust loading and to 40 ~ 90% after 2 h. In particular, the collection efficiency of the ESP for particles in the range 0.1 ~ 0.3 μm was decreased significantly, from 95% to 45%, after 2 h of dust loading. This finding was the result of the reduction in electric field strength in the ESP due to the accumulation of JIS dusts on the collection plates (Lin et al., 2010). However, the collection efficiency of the ESP for all particle sizes recovered to approximately 95% of the initial collection efficiency of the ESP following water cleaning for 2 minutes, and completely recovered to its initial state after cleaning for 4 minutes, as shown in Figure 15. This finding shows that a long-term performance of particle collection with a high level of efficiency could be achieved by cleaning the collection plates periodically with water.

The conventional dry-type ESPs use hammer or vibrator rapping systems for removing deposit on collection plates and recovering initial collection efficiency of the ESPs, but at the same time they produce re-entrained particles downstream of the ESPs and thus the collection efficiency is reduced less than the initial efficiency, depending on the rapping conditions of the ESPs (Kim and Lee, 1999; Ferge, 2004). Also, commonly used wet-type ESPs use water cleaning, but they require drying after the wet cleaning of the collection plates in order to apply high voltages to them. However, our novel ESP may be used directly after water cleaning for 2 or 4 minutes, due to the perfect electrical insulation that obtained between the collection plates through the use of the PVC coating. It was even possible to operate our ESP during cleaning.

3.1.4 Conclusions

A novel ESP was developed that uses a carbon brush precharger and a plastic collection plates with metallic films as inserts. The performance of the ESP was evaluated experimentally for ultrafine particles in the range 0.01 ~ 0.5 μm by varying the voltages that were applied to the charger and the collection plates, the number of channels in the charger, the gap between the collection plates, and the rate of air flow. The long-term performance and the water cleaning characteristics of the ESP were also studied using a standard JIS dust with a size range measured in micrometers.

The experimental results show that a novel ESP that uses anticorrosive materials can (a) generate a large number of unipolar ions whilst producing only a negligible concentration of ozone, and (b) achieve a strong collection performance of more than 95% for ultrafine particles while only consuming a power of 5 W and generating a pressure drop of 5 Pa per 1,200 m^3/h. It was also found

that a high collection efficiency of the ESP could be achieved by increasing the voltages that were applied to the precharger and the collection plates, by increasing the number of channels in the charger, and by decreasing the gap between the collection plates. In addition, it was found that the decreased collection efficiency that occurred during dust loading (at approximately 100 mg/m^3 for 2 h) was completely reversed to its initial value of over 95% by spraying with water at a flow rate of 25 L/min for 4 minutes.

The ESP described herein is thus a promising post-treatment system for the removal of ultrafine particles, especially in the manufacture of semiconductors where small particulates are emitted in acidic and corrosive gases that could degrade the performance of conventional post-treatment systems.

3.1.5 References

Allen, R.W.K. and Van Santen, A. (1996). Designing for pressure drop in venture scrubbers: the importance of dry pressure drop. *The Chemical Engineering Journal*, 61, 203-211.

Bell, M.L., Peng, R.D. and Dominici, F. (2006). The exposure-response curve for ozone and risk of mortality and the adequacy of current ozone regulations. *Environmental Health Perspectives*, 114(4), 532-536.

Bayless, D.J., Alam, M. K., Radcliff, R. and Caine, J. (2004). Membrane-based wet electrostatic precipitation. *Fuel Processing Technology*, 85: 781-798.

Bologa, A., Paur, H.-R, Seifert, H., Wascher, Th. and Woletz, K. (2009). Novel wet electrostatic precipitator for collection of fine aerosol. *Journal of Electrostatics*, 67, 150-153.

Chang, S.T. and Tsai, C.J. (1996). Feasibility study of white smoke control in semiconductor manufacturing industries. *Journal of Aerosol Science*, 27(4), 109-123.

Chein, H.M., Aggarwal, S.G., Wu, H.H., Chen, T.M. and Huang, C.C. (2005). Field enhancements of packed-bed performance for low-concentration acidic and basic-waste gases from semiconductor manufacturing process. *J. Air & Waste Manage. Assoc.*, 55: 647-657.

Du, K., Rood, M.J., Kim, B.J., Kemme, M.R., Franek, B.J., Mattison, K. and Cook, J. (2007). Field evaluation of digital optical method to quantify the visual opacity of plumes. *Journal of the Air & Waste Management Association*, 57, 836-844.

Eom, Y.S., Hong, J.H., Lee, S.J., Lee, E.J., Cha, J.S., Lee, D.G. and Bang, S.A. (2006). Emission factors of air toxics from semiconductor manufacturing in Korea. *J. Air & Waste Manage. Assoc.*, 56: 1518-1524.

Ferge, T., Maguhn, J., Felber, H. and Zimmermann, R. (2004). Particle collection efficiency and particle re-entrainment of an electrostatic precipitator in a sewage sludge incineration plant, *Environmental Science & Technology*, 38, 1545-1553.

Gamisans, X., Sarra, M. and Lafuente, F.J. (2002). Gas pollutants removal in a single- and two-stage ejector-venturi scrubber. *Jouranl of Hazardous Materials*, B90, 251-266.

Han, B., Hudda, N., Ning, Z., Kim, H.J., Kim, Y.J. and Sioutas, C. (2009). A novel bipolar charger for submicron aerosol particles using carbon fiber ionizers. *Journal of Aerosol Science*, 40, 285-294.

Han, B., Hudda, N., Ning, Z., Kim, Y.J. and Sioutas, C. (2009). Efficient collection of atmospheric aerosols with a particle concentrator-electrostatic precipitator sampler. *Aerosol Science and Technology*, 43, 757-766.

Han, B., Hudda, N., Ning, Z., Kim, Y.J. and Sioutas, C. (2008). Enhanced unipolar charging of concentration-enriched particles using water-based condensational growth. *Journal of Aerosol Science*, 39, 770-784.

Han, B., Kim, H.J., Kim Y.J. and Sioutas C. (2008). Unipolar charging of fine and ultra-fine particles using carbon fiber ionizers. *Aerosol Science and Technology*, 42, 793-800.

Hinds, W. C. (1999). Aerosol Technology: properties, behavior, and measurement of airborne particles. John Wiley & Sons, New York , p.323-331.

Huang, C.H., Ho, Y.T. and Tsai, C.J. (2005). Measurement of inorganic acidic gases and particles from the stack of semiconductor and optoelectronic industries. *Separation Science and Technology*, 39(9): 2223-2234.

Huang, C.H., Tsai, C.J. and Wang, Y.M. (2007). Control efficiency of submicron particles by an efficient venture scrubber system. *Journal of Environmental Engineering-ASCE*, 133(4), 454-461.

Hwang, S.C., Han, B. and Kim, Y.J. (2004). A study on the removal for white smoke and fine aerosols using dielectric coagulation system. Proceeding of the 38th meeting of KOSAE, 1, 461-462.

Hayes, M., and Woods, K. (1996). Treating semiconductor emissions with point-of-use abatement systems. *Solid State Technol.*, 39(10): 141-148.

Jaworek, A., Balachandran, W., Krupa, A., Kulon, J. and Lackowski, M. (2006). Wet electroscrubbers for state of the art gas cleaning. *Environmental Science & Technology*, 31(12), 1824-1837.

Kim, H.J., Han, B., Kim, Y.J., Yoon, J.P. and Han, K.S. (2008). Performance tests on ESP with indirect discharge and dielectric collector. Proceeding of the 47th meeting of KOSAE, 1, 453-454.

Kim, S.H. and Lee, K.W. (1999). Experimental study of electrostatic precipitator performance and comparison with existing theoretical prediction models. *Journal of Electrostatics*, 48, 3-25.

Korell, J., Paur, H.-R., Seifert, H. and Andersson, S. (2009). Simultaneous removal of mercury, PCDD/F, and fine particles from flue gas. *Environmental Science & Technology*, 43, 8308-8314.

Lin, G.Y., Tsai, C.J., Chen, S.C., Chen, T.M. and Li, S.N. (2010). An efficient single-stage wet electrostatic precipitator for fine and nanosized particle control. *Aerosol Science and Technololy*, 44, 38-45.

Liu, L., Guo, J., Li, J. and Sheng, L. (2000). The effect of wire heating and configuration on ozone emission in a negative ion generator. *Journal of Electrostatics*, 48, 81-91.

Lu, M.F., Huang, M.C. and Lin, J.J. (2011). Emission distribution of volatile organic compounds of semiconductor and photovoltaic (TFT-LCD) industries. The paper presented at the 2011 International Conference on Consumer Electronics, Communication and Networks (CECNET), Xianning, China, April 16-18, 2011.

Parker, K.R. (1997). Applied electrostatic precipitation. Blackie academic & professional, London, p. 29-51.

Srivastava R.K., Miller, C.A., Erickson, C. and Jambhekar, R. (2004). Emissions of sulfur trioxide from coal-fired power plants. *Journal of the Air & Waste Management Association*, 54, 750-762.

Tsai, C.J., Miao, C.C. and Lu, H.C. (1997). White smoke emission from a semiconductor manufacturing plant. *Environment International*, 23(4), 489-496.

Tsai, C.J., Chang, C.T., Liu, T.W., Huang, C.C., Chien, C.L., and Chein, H.M. (2004). Emission characteristics and control efficiency of acidic and basic gases and aerosols from packed towers. *Atmospheric Environment*, 38: 643-646.

Tsai, C.J., Lin, C.H., Wang, Y.M., Huang, C.H., Li, S.N., Wu, Z.X. and Wang, F.C. (2005). An efficient venturi scrubber system to remove submicron particles in exhaust gas. *J. Air & Waste Manage. Assoc.*, 55: 319-325.

Vallero, D. A. (2008). Fundamentals of air pollution. Elsevier, Inc., Amsterdam, p. 805-810.

Wang, L.K., Pereira, N.C. and Hung, Y.T. (2004). Air pollution control engineering. Humana Press,

Inc., New Jersey, p. 181-184.

White, H.J. (1963). Industrial electrostatic precipitation. Addison-Wesley publication company, Inc., Massachusetts, p. 74-83.

Yehia, A., Abdel-Salam, M. and Mizuno, A. (2000). On assessment of ozone generation in dc coronas. *Journal of Physics D: Applied Physics*, 33, 831-835.

Yehia, A., Mizuno, A. and Takashima, K. (2000). On the characteristics of the corona discharge in a wire-duct reactor. *Journal of Physics D: Applied Physics*, 33, 2807-2807.

Zhao, H. and Zheng, C. (2008). Modeling of gravitational wet scrubbers with electrostatic enhancement. *Chemical Engineering & Technology*, 31(12), 1824-1837.

Electrostatic precipitator knowledgebase. (2007). ESP Design review. Neundorfer, Inc., Chapter 4, p. 1-6.

[online] http://www.neundorfer.com/FileUploads/CMSFiles/ESP%20DesignReview[0].pdf

3.2 Integration of a non-metallic ESP and a wet scrubber for improved removal of particles and corrosive gas cleaning in semiconductor manufacturing industries

3.2.1 Introduction

For particle removal in corrosive gases from various industries, the novel ESP that uses an anticorrosive carbon brush precharger and plastic collection plates into which metallic films are inserted was successfully developed, and evaluated using ultrafine KCl particles and JIS class #8 dusts, varing applied voltages to the charger and collection plates, the number of channels in the charger, the gap between the collection plates, and flow rates. The experimental results showed that the precharger (400 x 400 x 800 mm) generated a lot of unipolar ions whilst producing negligible concentrations of ozone (<5 ppb), and that when the ESP was operated with 16 channels of ionizers and a 10 mm gap between the collection plates (400 x 400 x 185 mm), it removed more than 95% of the ultrafine particles with a power consumption of only 5 W and a pressure drop of 5 Pa per 1,200 m^3/h at 2 m/s (Kim et al., 2010).

However, the ESP in the previous study is needed to improve for a perfect non-metallic ESP because the carbon brush chargers were surrounded by metallic stainless steel channels which were electrically grounded, and the metallic ground plates tend to easily corrode and degrade under severe corrosive conditions with strongly acidic and basic gases generally emitted from IT device manufacturing industries. For the non-metallic two-stage ESP, the particle charging stage is composed of non-metallic carbon brush chargers, a carbon forced resin plate (CFRP) grounded channel, and a particle collection stage of plastic sheets. In this study, the ground plates for particle charging were made of CFRP, which is a blend of carbon fibers and thermosetting resins known to be non-metallic conductive hybrid composite materials (Allan et al., 2011). The particle collection stage for this study comprised collection plates made by anticorrosive polyvinyl chloride (PVC) sheets containing metallic films as inserts, developed by us (Kim et al., 2010).

In addition, to increase collection performance and to reduce the cost of the ESP, the evaluation of the collection performance of the ESP by other parameters such as lengths of the ionization channels and collection plates is inevitable under realistic environments such as silica particles and mists in corossive gases such as HCl, HF, NH_3, and PFCs etc. Here I report the

performance characteristics of the newly improved ESP, which were investigated by changing several of the design parameters of the charger and collection plates, such as sizes of the charger and collection plates and materials, and by changing the operation parameters, such as applied voltage and flow rate. The enhancement effect of the addition of the ESP to an acidic scrubber was also evaluated using silica (SiO_2) dusts and hydrochloric acid (HCl). Finally, a demonstration test of the ESP was conducted for 1 month with exhaust gas from perfluorinated compounds (PFC) and acidic gas scrubbers at the rooftop of a semiconductor manufacturing plant in Korea.

3.2.2 Experimental set up

Figure 1(a) shows the separate particle charging and collection stages of the non-metallic ESP that was used in the study. The geometry of the ESP was the same as the geometry of the one developed in our previous study (Kim et al., 2010). The ionizing stage (400 [W] x 400 [H] mm) comprised 16 channels made of CFRPs of a non-metallic, anti-corrosive material (Allan et al, 2011). At the center of the 16 channels, non-metallic carbon brush chargers composed of a bundle of approximately 300 carbon fibers with a diameter on the order of a few micrometers were inserted. The chargers were connected to a negative high-voltage source (maximum -30 kV/10 mA; Korea Switching Inc., Korea), and the channels were grounded electrically. To minimize pollutant deposition on the carbon chargers, the chargers were continuously shielded by compressed clean air at dozens of liters per minute. The collection stage was made of a 0.1-mm aluminum thin film coated by a non-metallic PVC sheet with a thickness of 0.2 mm. The length of the metallic film was 400 mm, and the length was varied to increase the collection area. Several tens of collection plates in a 400- x 400-mm PVC duct were aligned in parallel, and the plates were connected to the high-voltage source and to the ground in turn. The gap between each plate was maintained at 10 mm. Figure 1(b) shows a schematic of the wet scrubbing system with packing balls used in this study. The scrubber was supplied by GD Ecotech Inc. (Hwasung-shi, Gyunggi-do, Korea), which is one of the suppliers of wet scrubbers for the semiconductor industry in Korea, and was used to simulate the gas condition of acidic exhaust gas from the semiconductor manufacturing industry. In this study, properties of the packing balls and operation parameters such as the flow rate and liquid-to-gas ratio were varied to determine the high removal efficiency of the wet scrubber of >95% at 2 m/s of gas velocity, which is a general operation condition for wet scrubbers used to clean exhaust gases from the semiconductor manufacturing industry in Korea. The scrubber was composed of spray nozzles, a main body with packing balls, a demister, and a liquid reservoir with a pH controller and circulation pump.

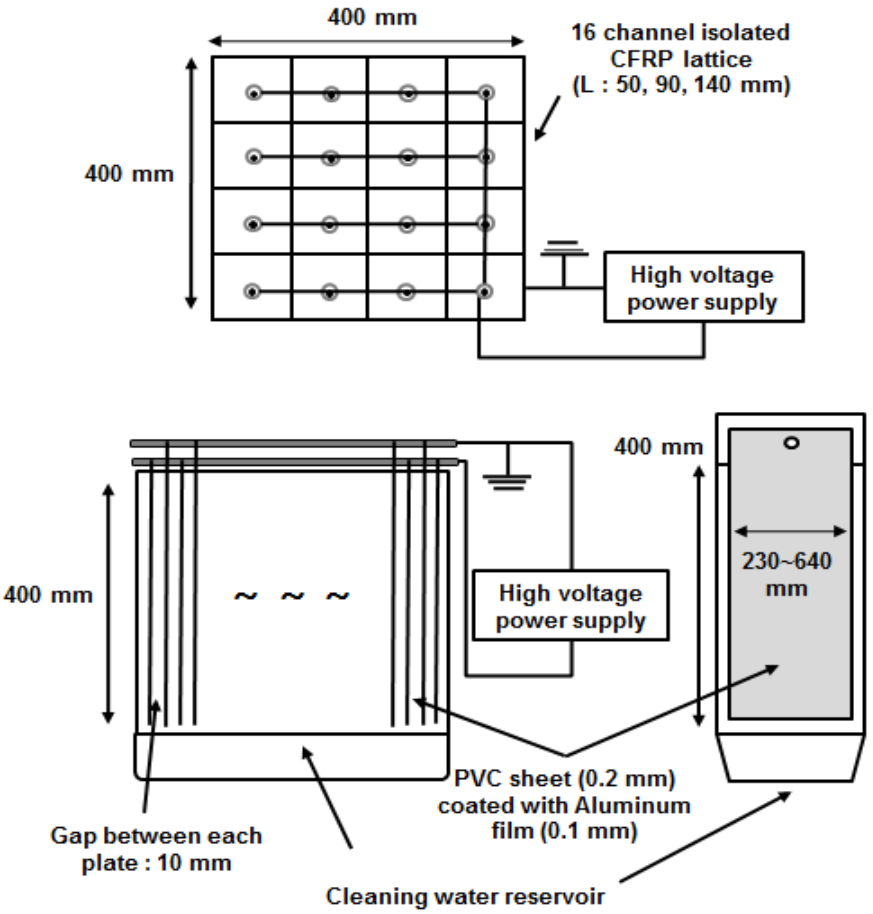

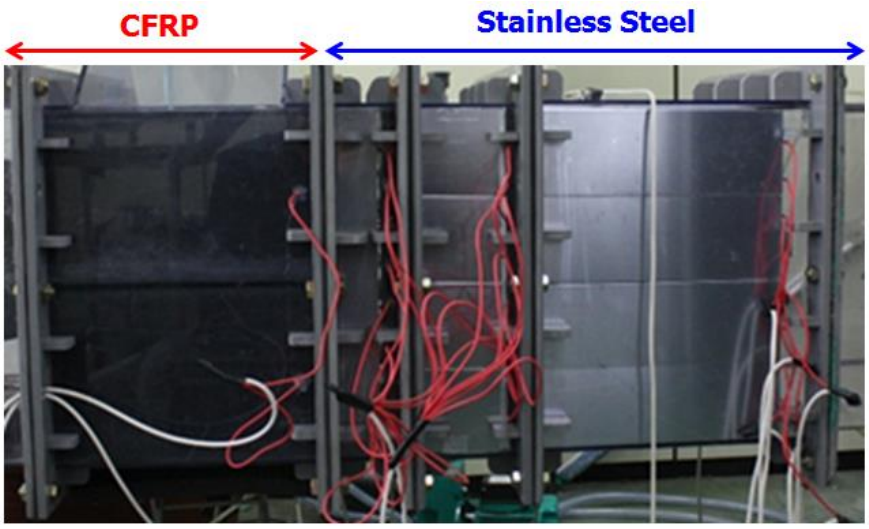

(a) Non-metallic ESP

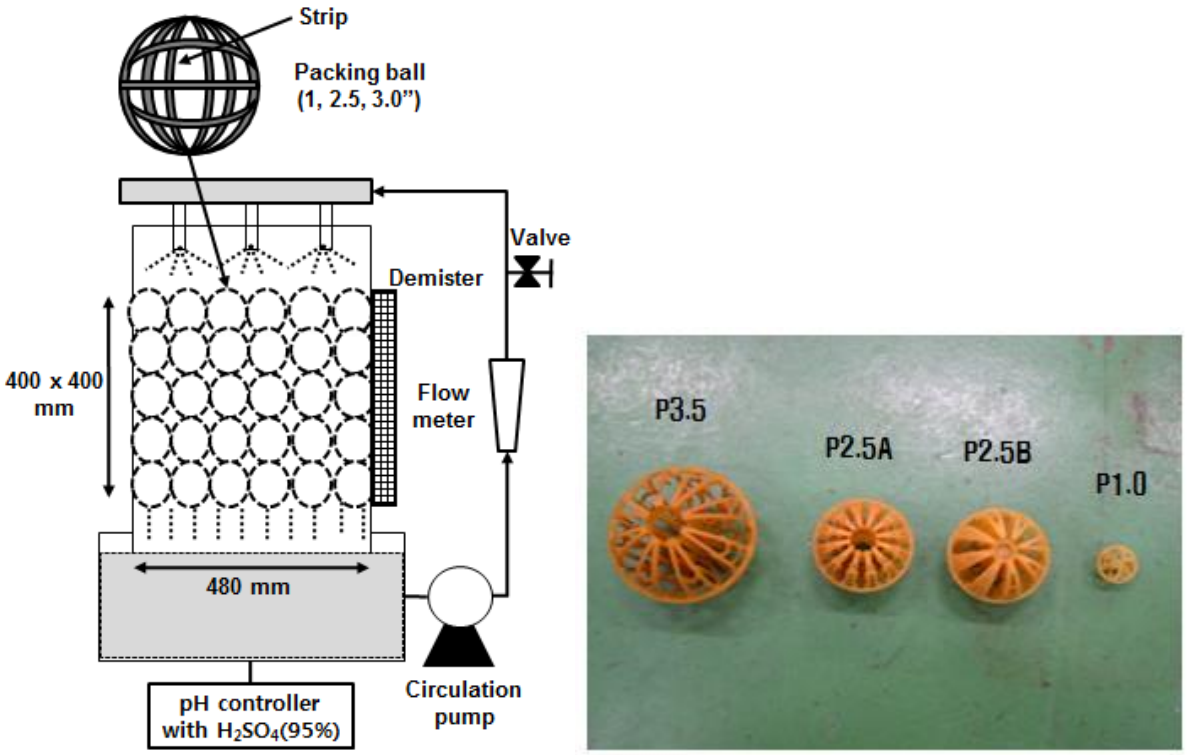

(b) wet scrubber with packing balls

Figure 1. Schematics of the experimental apparatuses used in this study.

In this study, three different packing balls with the same geometry (P1.0, P2.5A, and P3.5) were used to understand the effect of size on the performance of the scrubber, and two packing balls (P2.5A and P2.5B) with 8 and 12 vertical strips, respectively, were used to investigate the effect of surface area on performance. Six nozzles (two rows of three nozzles) were located on the top of the packing zone, and a mesh-type demister was inserted at the exhaust gas outlet of the scrubber.

Table 1. Physical parameters of four different packing balls used in this study.

Packing	Diameter (mm)	Specific surface area (m^2/m^3)	Number of strips
P1.0	2.54	279	8
P2.5A	6.35	150	8
P2.5B	6.35	224	12
P3.5	8.89	125	8

The dimensions (L x W x H) of the packing section were 480 x 400 x 400 mm, and the sizes of the packing balls, which were made of polypropylene, were 2.54, 6.35, and 8.89 mm (1, 2.5, and 3.5 inches, respectively). The physical properties of four different packing balls are shown in Table 1.

Figure 2 shows the experimental setup used in the study. For the submicron particle collection performance tests of the non-metallic ESP with differing basic design and operation parameters, potassium chloride (KCl) aerosol particles with diameters of 0.01 to 0.5 μm were created by nebulizing a solution of KCl (w/w 0.1% in water) with an atomizer at a constant output (Model 3076; TSI Inc., US) and passing the particles through a Kr-85 neutralizer and a diffusion dryer. The charged fractions of the KCl particles were removed using a plate condenser (to which a high voltage of 10 kV was applied), and uncharged particles were then introduced into the test duct (cross section 400 x 400 mm). High-efficiency particulate arrestance (HEPA; 99.97% of airborne particles 0.3 μm in diameter)-filtered clean air was mixed with these particles, and the mixture was then passed through the particle charging and collection stages.

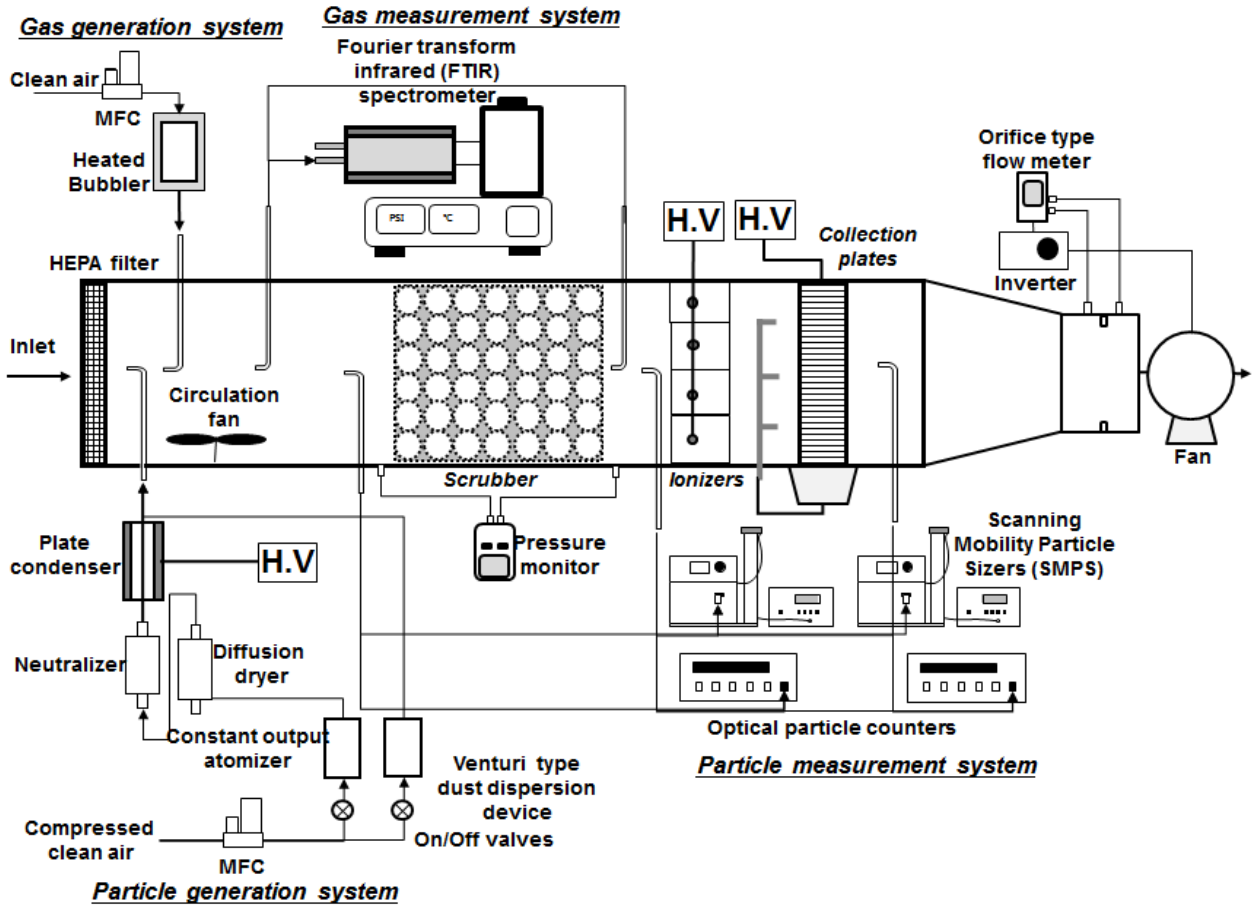

Figure 2. Experimental setup for the performance tests of the two-stage wet ESP and wet scrubber.

The gas flow rate in the duct was controlled using an orifice-type flow meter and inverter that was connected to a fan located at the end of the duct. The size distributions of the test particles upstream and downstream of the ESP were measured with a scanning mobility particle sizer system (SMPS, Model 3081; TSI Inc., US) together with a condensation particle counter (CPC, Model 3076; TSI Inc., US). The loss of particles due to diffusion in the ESP was negligible. During the ESP experiments, the design and operation parameters of the particle charging and collection stages were varied to investigate their effects on the performance of the ESP. As shown in Figure 2, HCl gas was generated by bubbling a solution of HCl (w/w 95% in water) in a thermostat that was controlled at 30 to 40℃, and the gas was then introduced into the test duct upstream of the wet scrubber. The initial concentration was maintained at approximately 40 to 60 ppm. The concentration of the test gas upstream and downstream of the scrubber was measured using a real-time measurement system, Fourier transform infrared spectroscopy (FTIR, Model I-4001; Midac Corporation, US), which is used to measure the concentration of many kinds of gases in situ (EPA, 1998; NIOSH, 2002). During the scrubber experiments, the properties of the packing balls, velocity, and liquid-to-gas ratio were varied to achieve a removal efficiency of >95% at 2 m/s and to investigate their effects on the performance of the scrubber.

The performance of the ESP and scrubber used in this study was expressed in terms of the particle collection and gas removal efficiency (η), which may be obtained using the following equation:

$$\boldsymbol{\eta = \left(1 - \frac{C_{down}}{C_{up}}\right) \times 100}$$

where η is the collection and removal efficiency, C_{down} is the concentration of the pollutants downstream of the ESP, and C_{up} is the concentration of the pollutants upstream of the ESP.

Before a demonstration test at a real industrial site, the collection performance of the combination system with the packing scrubber and non-metallic ESP was evaluated using silica dusts (SiO_2), which are known to be major components in particulates from semiconductor manufacturing processes (Tsai et al., 1997). A venturi-type dust dispersion device was used to spread dusts of 9 g for 9 minutes per one dust loading throughout the upstream test duct, and a gas bubbler was used to generate HCl gas with a concentration of 40 to 60 ppm. A circulation fan distributed the dusts and gas uniformly upstream of the scrubber. The mass concentrations of the silica dusts and mists upstream and downstream of the whole system with and without the operation of the ESP were measured simultaneously using two scanning mobility particle sizer systems (SMPS, Model 3081;

TSI Inc., US) together with two condensation particle counters (CPC, Models 3076 and 3022A; TSI Inc., US) for particles of <0.3 μm and two optical particle counters (Model 1.109; GRIMM, Germany) for particles of >0.3 μm. The performance of the total system was evaluated with and without operation of the non-metallic ESP while changing parameters for collection enhancement, such as applied voltages to the ESP and length of the collection plates. The performance of the ESP after cleaning the collection plates with water was also evaluated after 13 hours of continuous dust loading.

Finally, the non-metallic ESP was installed at one of the exhaust lines of an acidic and PFC gas scrubber of a semiconductor manufacturing plant located at Kyunggi-do in Korea to demonstrate the ESP developed in this study. Exhaust gas of approximately 1,200 m^3/hr was bypassed from the main exhaust duct of the acidic and PFC gas scrubbers at the rooftop of the company and was flowed through the non-metallic ESP. For this real-site study, two charging stages of 16 channels (400 [W] x 400 [H] x 100 [L] mm) and three collection stages (400 x 400 x 230 mm) with a 10-mm gap were used. The experimental conditions in this study were summarized in Table 2.

Table 2: Experimental conditions for the performance tests of the ESP developed in this study.

Tests	Dimension		Voltage		Air velocity	Particle and gas condition	Measurements
	Ionization (WxHxL)	Collection (WxHxL)	Ionization	Collection			
Lab	400 x 400 x 50, 90, 140 mm	400 x 400 x 230, 460, 640 mm	3, 4, 6, 8 kV	10, 12, 14 kV	1,1.5, 2 m/s	KCl	V-I curve and Collection eff.
	400 x 400 x 50 mm	400 x 400 x 460, 540 mm	8, 10, 12 kV	12, 14 kV	2 m/s	SiO_2, Mists L/G 3.6 L/m^3 HCl 40-60 ppm	Collection eff.
Long term (12.5 hr)	400 x 400 x 50 mm	400 x 400 x 540 mm	10 kV	12 kV	2 m/s	SiO_2, Mists L/G 3.6 L/m^3 HCl 40-60 ppm	Collection eff. Water cleaning eff.
Demonst -ration (1month)	400 x 400 x 100 mm x 2 units	400 x 400 x 230 mm x 3 units	13 kV	14 kV	1.6-2 m/s	Dusts and Mists from a semiconductor manufacturing factory	Collection eff.

* eff. : efficiency

3.2.3 Results and discussion

(1) Voltage and Current Characteristics of Non-metallic Particle Chargers

Figure 3 shows the variation in current against voltage applied to the carbon brush chargers using different lengths of the 16 grounded channels (50, 90, and 140 mm) and using the 140-mm channel

with and without air insulation of 30 and 50 L/min.

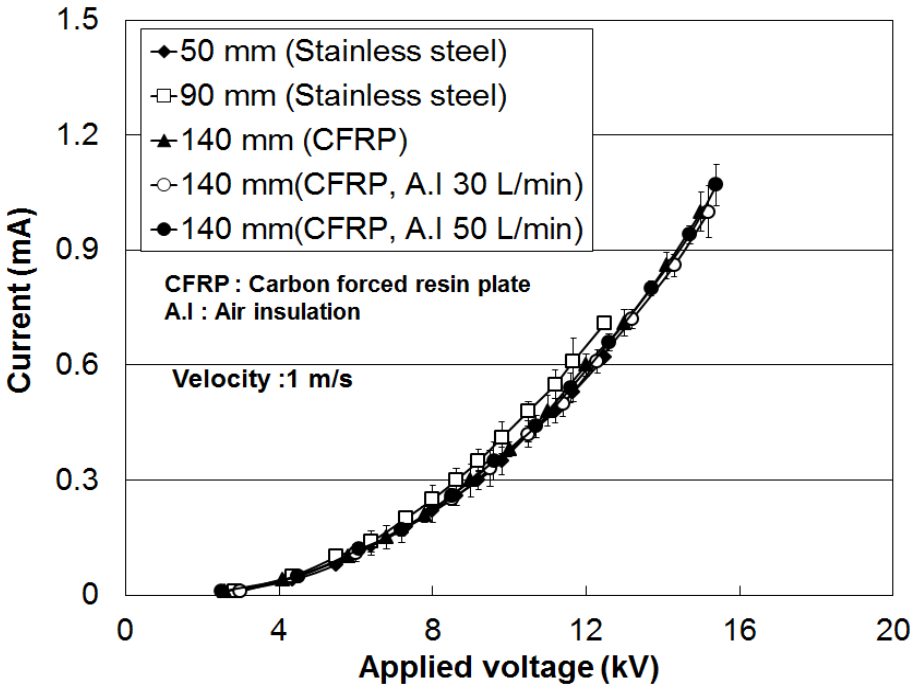

Figure 3. Voltage-current curves of the carbon brush charger for different lengths and materials with and without insulation air.

The each carbon brush charger was covered with a PVC tube, and compressed filtered air was introduced into the PVC tube for the electrical insulation. The flow velocity of the air at the inlet to the charging stage was maintained at 1 m/s. The currents with different lengths and different materials for a given applied voltage were almost identical. This result indicates that reducing the length of the channels to decrease the size of the charging stage is possible to 50 mm and that the use of a non-metallic CFRP as a grounded electrode is also possible. In addition, the curves with and without air insulation of 30 and 50 L/min were not changed. This shows that the corona discharge was not disturbed by the air insulation shielding the carbon brush chargers to prevent pollutant loading.

(2) Removal Efficiency of Submicron Particles by the Non-metallic ESP

Figure 4 shows the migration velocity of 0.3-μm particles in the ESP plotted against the specific corona power applied to the charging stage using channels with length of 50, 90, and 140 mm. The voltage applied to the collection plates and the air velocity were maintained at 12 kV and 1

m/s, respectively. Increasing the specific corona power applied to the charger from 4 x 10^{-5} to 5 x 10^{-3} W/m^3/hr resulted in an increase in migration velocity for the submicron particles from 0.04 to 0.18 m/s (corresponding to 70 to 95% of collection efficiency) because of the increased charging rates of the particles, which were caused by an increase in both the number of negative ions in the charger and the electrical field strength (Han et al., 2010; Kim et al, 2010).

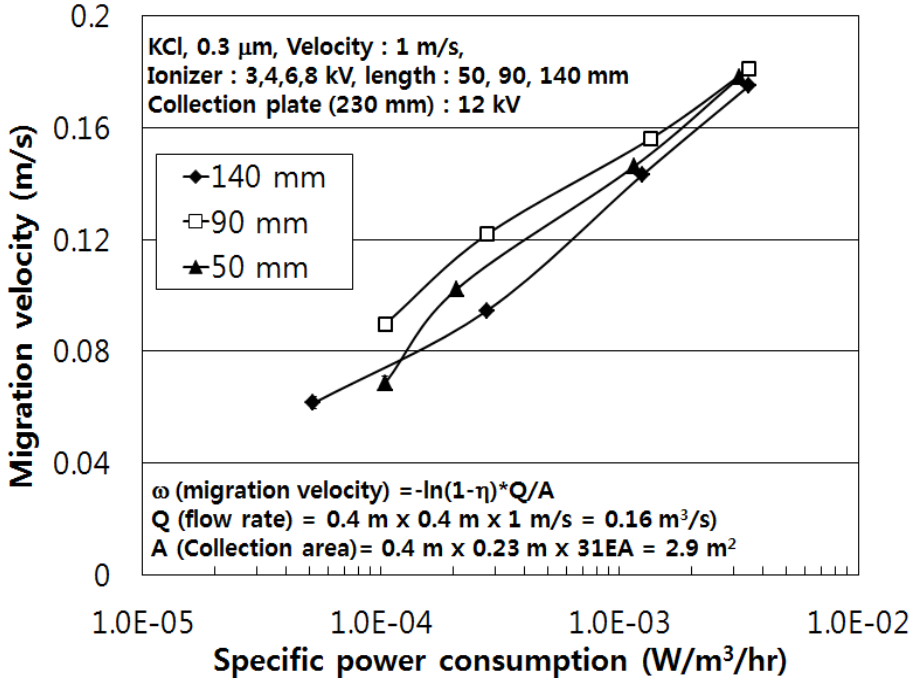

Figure 4. Particle migration velocity of the ESP against the specific power consumption applied to the charger using 16 channels with lengths of 50, 90, and 140 mm.

Increasing the length of the channels did not significantly change the migration velocity of particles in the ESP for a given specific corona power applied to the charger. In particular, in the case of high specific corona power (>10^{-3} W/m^3/hr), the migration velocity of 0.3-μm particles with different channels was >0.16 m/s (corresponding to 90% of collection efficiency) and was not differentiated for an air velocity of 1 m/s. As shown in Figure 3, despite different channel sizes of 50, 90, and 140 mm, the applied corona currents were not changed for a given voltage, and thus the charging rates for the submicron particles with different channels could be similar. It may be expected that the decrease in the particle charging stage size to 50 mm would not significantly affect the particle collection performance of the ESP in this study, and decreases in the collection efficiency when the flow rate of the polluted air is increased could be avoided by applying a higher corona power to the ESP.

Figure 5 shows the variation in collection efficiency of 0.3-μm particles using the 16

channels with a size of 50 mm plotted against the air velocity for the different voltages applied to the collection plates while keeping the voltage applied to the charger constant at 6 kV. The collection efficiency showed a significant linear decrease of 30% to 40% for a voltage of 6 kV applied to the charger when the air velocity was increased from 1 to 2 m/s. However, the collection efficiency increased by 13% at 2 m/s when the voltage applied to the collection plates increased from 10 to 14 kV because of the increased electric field strength between them (Parker et al., 1997).

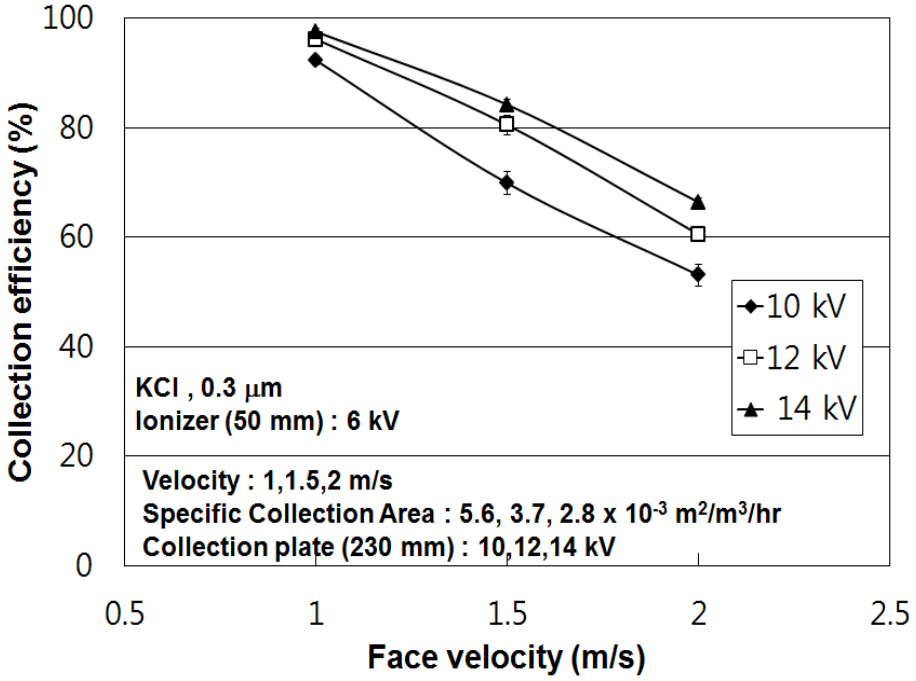

Figure 5. Particle collection efficiency of the ESP against the polluted gas velocity for different applied voltages to the collection plates.

Figure 6 shows the variation in collection efficiency of 0.3-μm particles using the 16 channels plotted against the length of the collection plates with different voltages applied to particle charging stage and different air velocities while keeping the voltage applied to the collection plates constant at 12 kV. The collection efficiency with collection plates of 230 mm showed a significant decrease from 96% to 81% for a voltage of 6 kV applied to the charger when the air velocity was increased from 1 to 2 m/s. However, the efficiency showed a linear increase of 20% when the applied voltage to the charger was increased from 6 to 8 kV. In particular, the collection efficiency of the submicron particles reached >98% when the length of the collection plates was increased from 230 to 640 mm with applied voltages to the charger and collection plates of 8 and 12 kV, respectively,

even for an air velocity of 2 m/s. It is expect that the decrease in collection efficiency with an increase in the flow rate of polluted air could be avoided by applying a higher voltage to the ESP charger and collection plates and by increasing the length of the non-metallic collection plates.

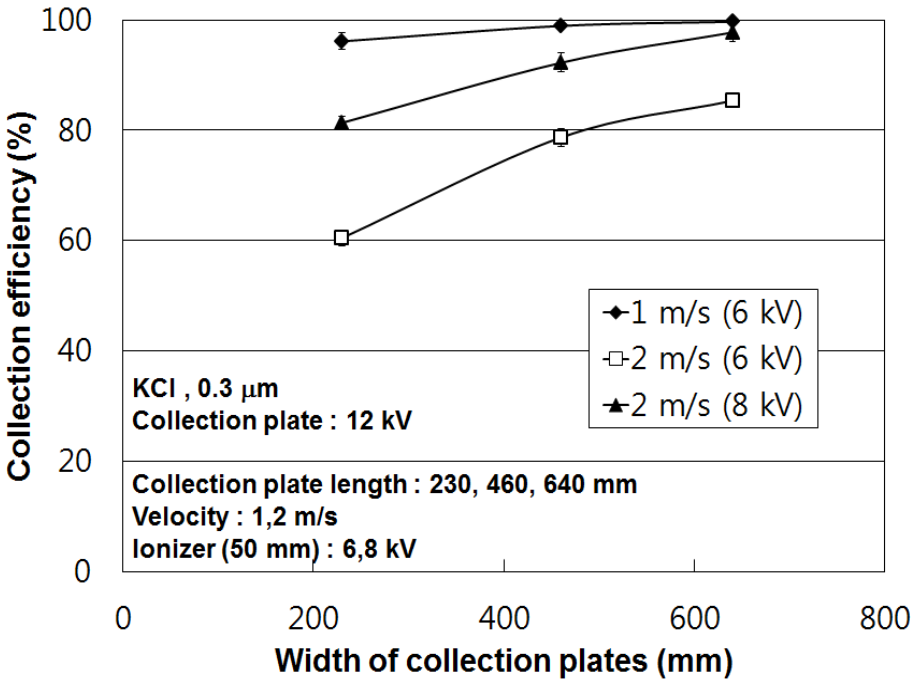

Figure 6. Particle collection efficiency of the ESP against the width of collection plates for different polluted air velocities and applied voltages to the charger.

(3) Removal Efficiency of an Acidic Gas by the Scrubber

In order to test the non-metallic ESP with particles in a similar gas condition from acidic gas scrubbers of semiconductor manufacturing industries, it is necessary to determine the operation parameters of a wet scrubber in this study. The properties of operation parameters such as the size and design of the packing balls, the flow rate and liquid-to-gas ratio were varied to determine the high removal efficiency of the wet scrubber of >95% at 2 m/s of gas velocity, which is a general operation condition for wet scrubbers used to clean exhaust gases from the semiconductor manufacturing industry in Korea. Figure 7 shows the variation in gas removal efficiency of HCl gas using the wet scrubber plotted against the air velocity for the different sizes of packing balls while keeping the liquid-to-gas ratio and pH constant at 2 L/m^3 and 11, respectively. Although the liquid-to-gas ratio was maintained at 2 L/m^3 when the air velocity was increased from 1 to 3 m/s, the removal efficiency showed a linear decrease regardless of the size of the packing balls because the

gas-liquid contact time decreased from 0.48 to 0.16 seconds (Shi et al., 1996). However, the removal efficiency with the 3.5-inch balls was increased from 82.4% to 94.6% when the size of the packing balls was decreased to 1 inch. In addition, although the size of these balls was the same, the removal efficiency with the 2.5”B balls was 2% to 3.5% higher than that with the 2.5”A balls because the specific surface area of 2.5”B was 1.5 times larger than that of 2.5”A (150 m^2/m^3), as shown in Table 2. This result indicates that a larger surface area of the packing balls in a wet scrubber could increase the amount of liquid film on the balls, which may enhance the amount of gas absorbance (Han et al., 2007).

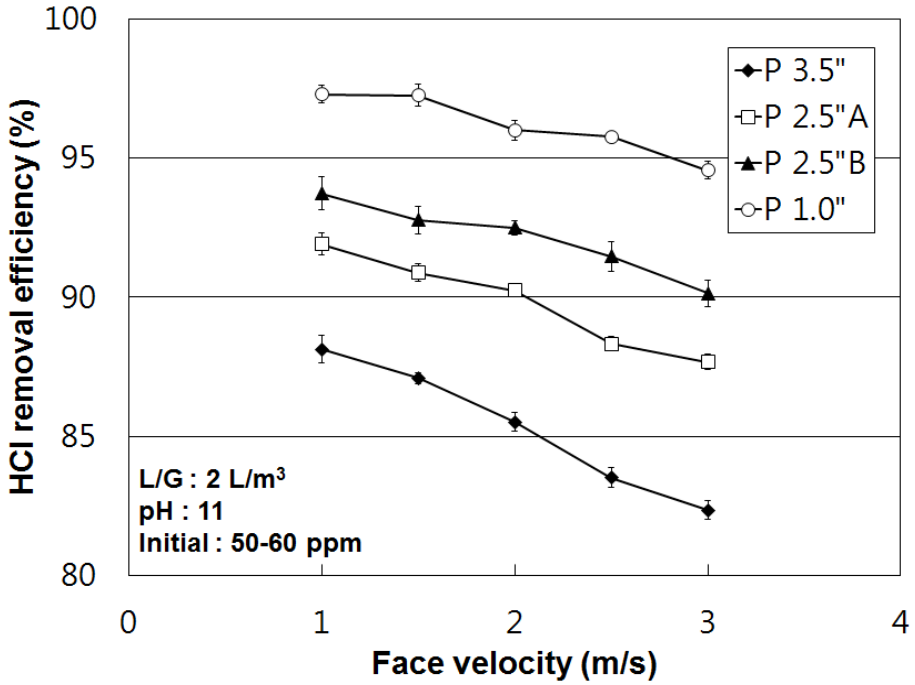

Figure 7. Gas removal efficiency of the wet scrubber against the polluted gas velocity for different sizes of packing balls.

Figure 8 shows the variation in removal efficiency of HCl gas using the wet scrubber plotted against the liquid-to-gas ratio for the different sizes of packing balls while keeping the face velocity and pH constant at 2 m/s and 11, respectively. The removal efficiency showed a linear increase regardless of the size of the packing balls because the higher liquid-to-gas ratio means an increase in the gas-liquid contacting surface area (Chein and Chu, 2000). The removal efficiency with the 3.5-inch balls was increased from 82.8% to 97.5% when the size of the packing balls was decreased to 1 inch and the liquid-to-gas ratio was increased to 3 L/m^3.

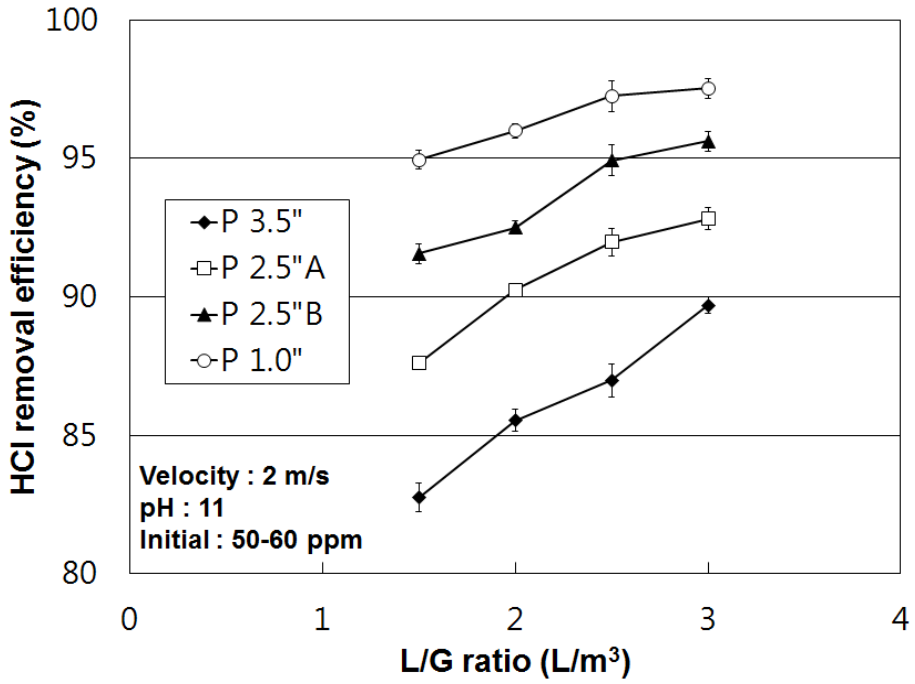

Figure 8. Gas removal efficiency of the wet scrubber against the liquid-to-gas ratio for different sizes of packing balls.

(4) Removal Efficiency of Particles and Mists in Acid Gases by the Combination System with the Scrubber and Non-metallic ESP

Figure 9 shows the variation in the mass distributions of the submicron and micron SiO_2 dusts and mists before and after passing them through the combination system without and with operation of the ESP. Loadings of 9 g of SiO_2 dusts for 9 minutes and 40- to 60-ppm HCl gases were supplied to a test air stream of 10 m^3/min at the upstream of the test duct. The operation conditions of wet scrubber, packing size, liquid-to-gas ratio, and pH were chosen as P2.5A, >3 L/m^3, and 11, respectively, which showed high gas removal performance of >95% at 2 m/s, as described in Figure 8.

With operation of the ESP, a voltage of 12 kV was applied to the charger to adequately charge the highly loaded dusts and mists; this voltage was higher than that needed for the KCl submicron particles in the previous experiments. In addition, 12 kV was applied to the collection plates with the air velocity, pH, and liquid-to-gas ratio maintained at 2 m/s, 11, and 3.6 L/m^3, respectively.

The mass concentration of the particles was bi-modal, and the peak diameters of the particles were located at approximately 0.3 and 3 μm. The mass concentration of the SiO_2 dusts and mists in the

size range of >1 μm was largely decreased, while that in the size range of <1 μm was very slightly decreased. However, the mass concentration of the particles in the entire size range was significantly reduced when high voltages of 12 kV were applied to the charger and collection plates.

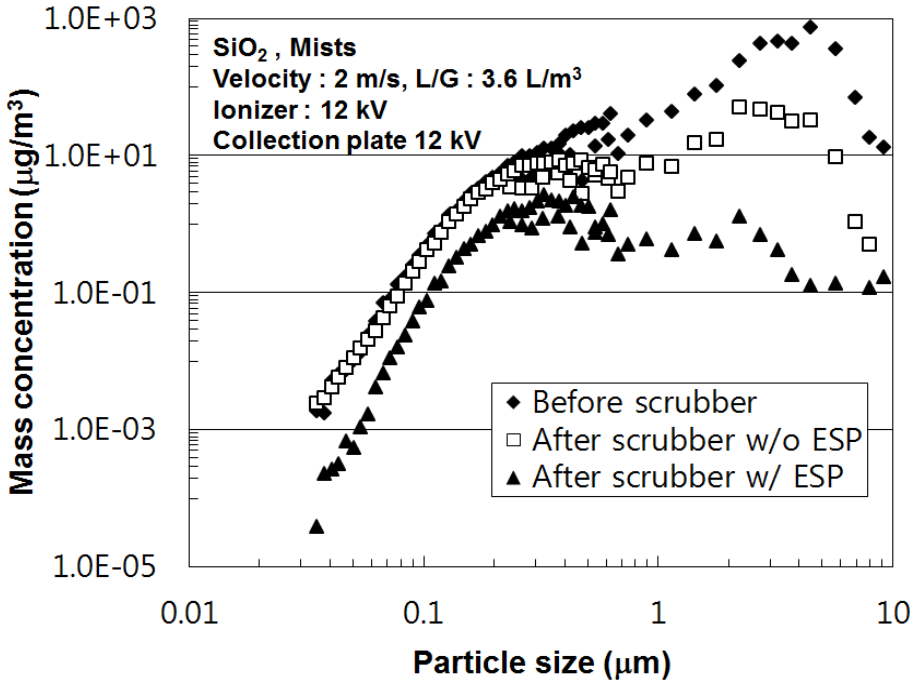

Figure 9. Changes in particle size distribution before and after the combination system with the non-metallic ESP and wet scrubber with and without the ESP operation.

Figure 10 shows the variation in collection efficiency plotted against particle diameter for different voltages applied to the chargers. Apart from the voltage applied to the chargers, the experimental conditions were kept constant at a flow rate of 2 m/s, a liquid-to-gas ratio of 3.6 L/m^3, and a voltage of 12 kV applied to the collection plates (460 mm). The collection efficiency with only the scrubber operation was approximately 80% to 95% at 1 to 10 μm; however, the efficiency was dramatically decreased to 20% at 0.1 to 0.3 μm because particles of <0.01 μm and >5 μm are effectively captured by droplets due to Brownian diffusion and inertial impaction, respectively; most wet scrubbers have low efficiency for intermediately sized particles in the range of 0.1 to 1 μm (Zhao and Zheng, 2008). However, when voltages of 8 and 12 kV were applied to the charger and collection plates, respectively, the collection efficiency was increased from 20% to 65% in the size range showing the lowest efficiency with the scrubber, and the efficiency for particles larger and smaller than this size range was increased to >80%, even to almost 100%, for particles of >1 μm. In

addition, when the voltage applied to the charger was 12 kV, the collection efficiency of the particles exceeded 80% regardless of particle size.

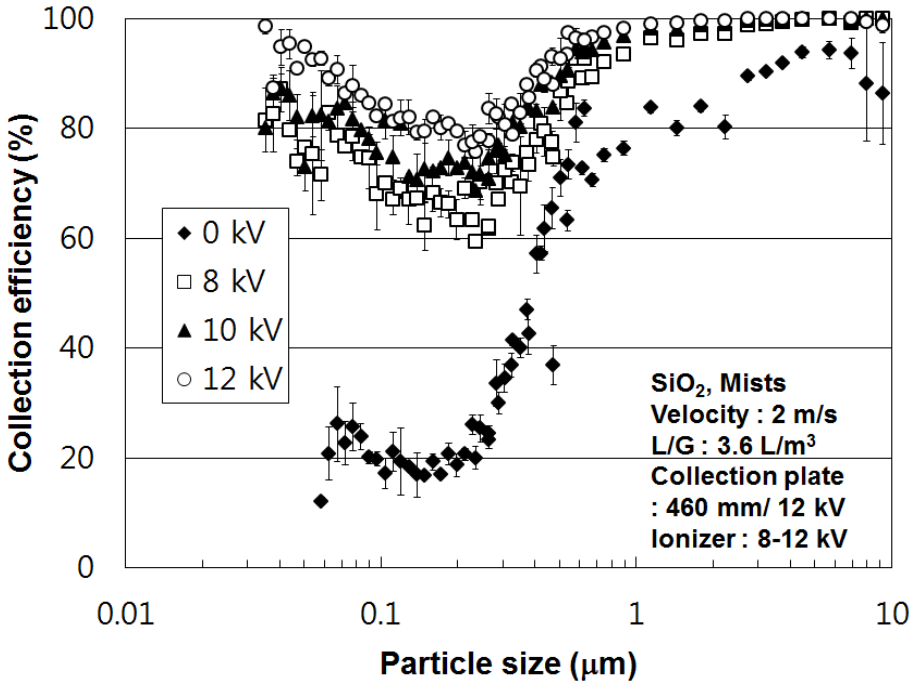

Figure 10. Particle collection efficiency of the ESP plotted against particle size for different applied voltages to the charger.

Figure 11 shows the variation in collection efficiency plotted against particle diameter for different applied voltages and length of collection plates. Apart from these parameters, the experimental conditions were kept constant at a flow rate of 2 m/s, a liquid-to-gas ratio of 3.6 L/m^3, and a voltage of 10 kV applied to the chargers (50 mm). Similar to the results shown in Figure 10, the lowest collection efficiency was located at 0.1 to 0.3 μm. This phenomenon may have resulted from the fact that charging for particles larger and smaller than the size range is higher than that for particles of 0.1 to 0.3 μm because of the diffusion and field charging effects (Hinds, 1999). The collection efficiency of the combination system was increased from 70% to 80% in the size range of lowest efficiency when the voltage to collection plates (460 mm) was enhanced from 12 to 14 kV. Moreover, the collection efficiency of the system for the entire particle size range of the SiO_2 dusts and mists reached >90% at 2 m/s velocity and 3.6 L/m^3 liquid-to-gas ratio when the size of the collection plates was wider (460 to 540 mm), even with an applied voltage to collection plates of only 12 kV. These results indicate that particles of submicron size are not removed efficiently by only applying scrubbing water to the packing balls; an additional collection device such as an ESP is

needed for these small particles. Moreover, enhancement of the low collection efficiency at a high velocity of polluted gas could be obtained by changing the operation parameters of voltages applied to the ESP and the design parameter of the collection plate size.

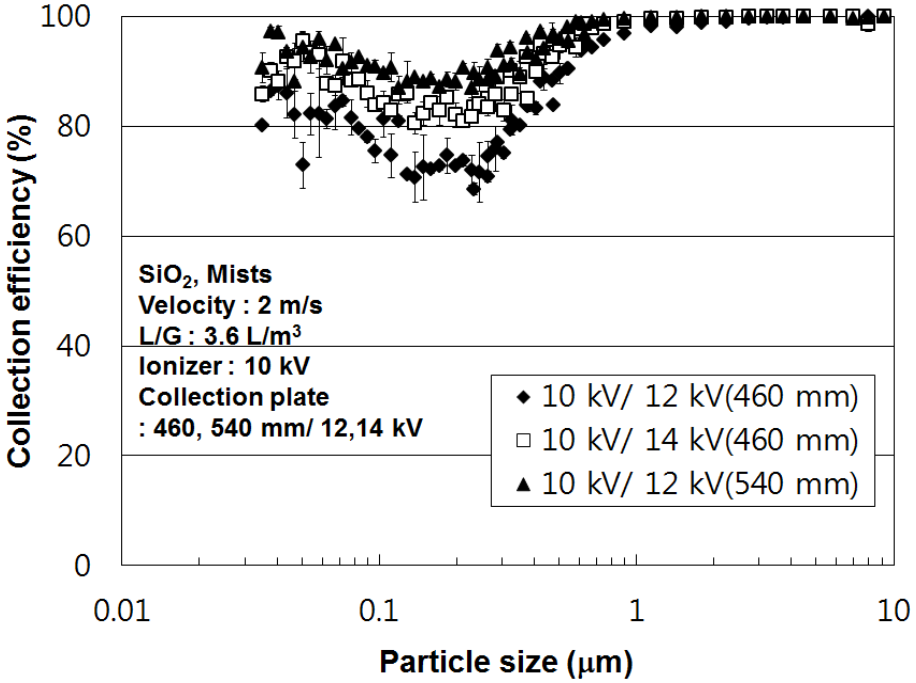

Figure 11. Particle collection efficiency of the ESP plotted against particle size for different voltages applied to and lengths of the collection plates.

Figure 12 shows the variation in collection efficiency of the combination system plotted against particle size for different particle loading and cleaning conditions at the collection plates. The collection plate was polluted intentionally with dust loading for 12.5 hours using SiO_2 dust and mists with the same conditions shown in Figures 9 to 11. The plate was then regenerated by spraying it with water for 5 minutes at a flow rate of 70 L/min. The voltages that were applied to the charger (50 mm) and collection plates (540 mm) were 10 and 12 kV, respectively, which represented the condition of maximum collection efficiency. The collection efficiency for the entire particle size range was >90% for the clean collection plates at the beginning of the experiment. The efficiency of the system for particles outside the size ranges of <0.05 μm and >3 μm was decreased differently depending on size; in particular, the efficiency at 0.1 to 0.3 μm was dramatically decreased from 90% to 50%. This reduction resulted from a decrease in the strength of the electric field between the ESP collection plates due to the accumulation of particles on the collection plates (Lin et al., 2010). However, the collection efficiency of the system for all particle sizes was recovered to nearly the

initial collection efficiency by the water cleaning. This result indicates that long-term performance of particle collection with a high level of efficiency could be achieved by periodically cleaning the collection plates with water.

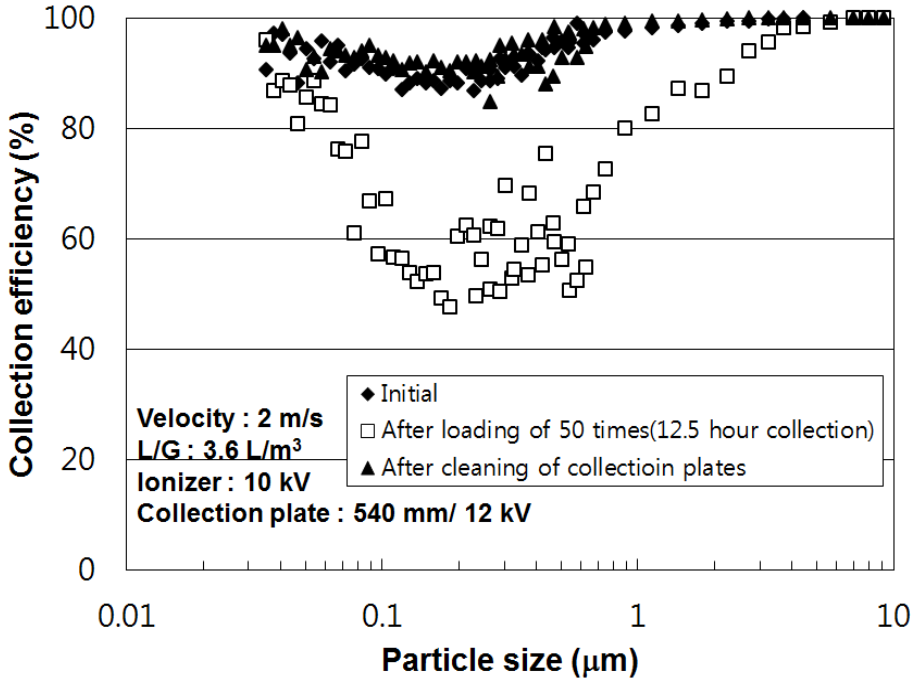

Figure 12. Particle collection efficiency of the ESP plotted against particle size for the initial state, after dust and mist loadings, and after water cleaning.

(5) Comparison of Removal Efficiency of Particles by the Non-metallic ESP Based on Theory and Experiment

The Cochet's charging model is mainly used because it allowed an easy calculation and corrlation to actual ESP conditions is quite reasonable for particles micrometer to the critical size of 0.1 μm. The Deutsh model is a well-known fundamental model which is used to calculate the collection efficiency of dry ESP (Park and Chen, 2002; Parker, 1997; Xiangron et al., 2002). In particular, Yoo et al. (1997) used the Deutsch model to calculate the collection efficiency of a two-stage ESP, based on various charging theories. I also used the Deutsch's collection theory, and the Cochet's charging model to calcuate the efficiency. The equations and brife explanations are summarized in equation (1) to (4) in Chanper II. Figure 13 shows the comparison of collection efficiency as a function of particle size, as found in this study and the efficiency which was predicted by the theories. For the theoretical calculation of the collection efficiency, the voltage applied to the chargers (E_c), the air velocity (v) and the gap (s) between the high voltage and ground collection

plates were constant at 10 kV, 2 m/s and 10 mm, while the voltage (E_p) and length (L) of collection plates were varied as 12, 14 kV and 460, 540 mm. For both cases, the lowest collection efficiency was located at 0.2 μm, and the experimental efficiencies of the non-metallic ESP were similar to those from the Deutsch ESP collection theory, based on the Cochet's charging model since the average differences between the efficiencies from experiment and theory were 4.32, 3.44, and 4.57 % for the three cases, respectively. However, the experimental efficiencies for particles between 0.1 and 1 μm were a little higher than those from the theory. This could be attributable to the fact that the particles could be collected not only by electrostatic precipitation but also by other possible collection mechanisms such as impactions and diffusions etc in the ESP. In addition, the experimental efficiencies for the particles ranged less than 0.5 μm were 13.7, 7.11, and 4.1 % lower than those from the theory because the particles in the size rage significantly related to diffusion charging, not field charging, and they are poorly charged by diffusion and the lower ion attachment coefficients (Kulkarni et al., 2002; Adachi et al, 1985; Zhuang et al., 2000; Lin and Tsai et al., 2010). This result indicates that the particle collection performance of the non-metallic ESP could be expected by a simple calculation with the same design and operation parameters of the ESP such as flow rate, applied voltages, and geometries, using the Deutsch theory which is used generally in industries.

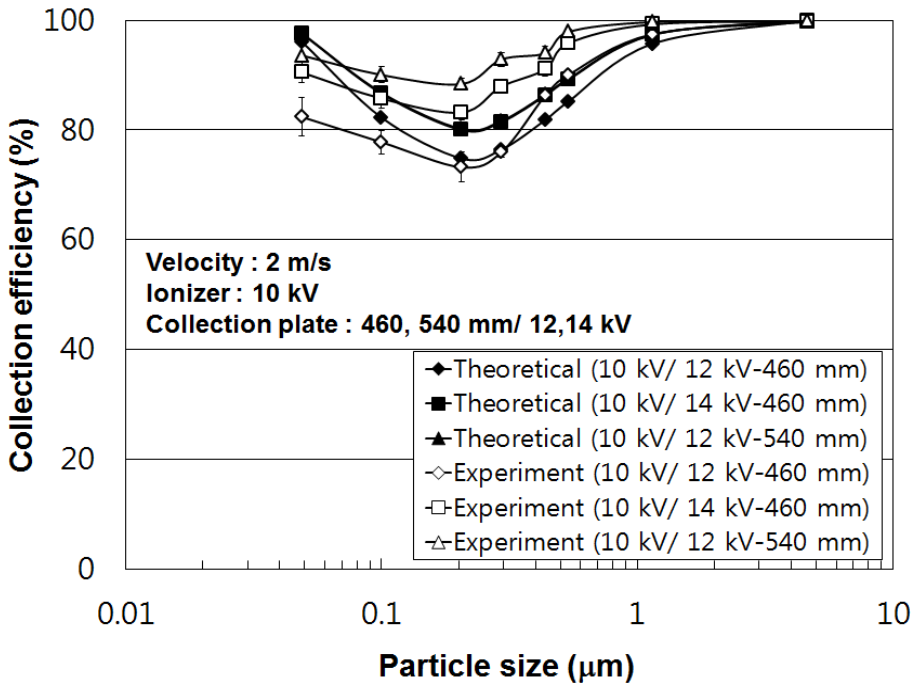

Figure 13. Comparison of collection efficiency as function of particle size, as found in this study and theoretically predicted for different voltages and lengths of collection plates.

(6) Removal efficiency of Particles and Mists in Exhaust Gases from a Semiconductor Manufacturing Company by the Non-metallic ESP

Figure 14 shows collection efficiencies of the non-metallic ESP operated for about 1 month at the rooftop of a semiconductor manufacturing plant in Gyeonggi-do, Korea. The demonstration test with an exhaust gas from perfluorinated compounds (PFC) and acidic gas scrubbers of the company was performed from 5 October to 10 November 2011. During the demonstration period, five measurements were conducted with our own two optical particle counters (Model 1.109; Grimm, Germany), and three measurements with EPA Method 5 were conducted based on mass concentration (EPA, 2000) by a third-party measurement institute that was chosen by the semiconductor manufacturing company. Measurements based on particle number concentration were done at 18th, 19th of Oct. and 2nd, 3rd, 10th of Nov., and those based on mass were done at 5th of Oct. and 3rd, 10th of Nov. The ESP used in this test was composed of two nonmetallic particle charging stages (400 x 400 x 100 mm, 16 channels, 2 units), three nonmetallic collection stages (400 x 400 x 230 mm, 10-mm gap, 3 units), and a water cleaning system for the collection plates. The ESP was intentionally regenerated with water spray every day during the test period to keep the collection plate clean. High voltages of 13 and 14 kV were applied to the charger and collection plates, respectively, and the face velocity through the ESP was maintained at 1.6 to 2.0 m/s.

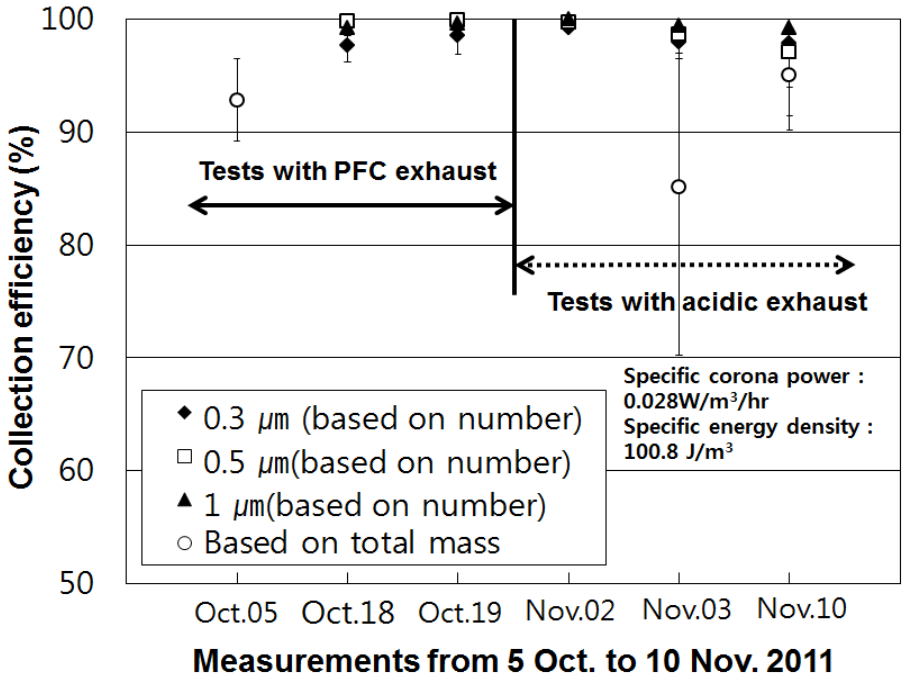

Figure 14. Particle collection efficiencies of the ESP operated for 1 month with acidic and PFC exhaust gases from a real semiconductor manufacturing plant in Korea, measured based

on number concentration of different size particles and total mass.

As shown in Figure 13, the collection efficiencies of the ESP based on concentrations of 0.3-, 0.5-, and 1-μm particles were >97%, while those based on total mass were 93%, 85%, and 95%. These collection efficiencies were achieved with a much smaller specific corona power of 0.028 W/m^3/hr (specific energy density of 100.8 J/m^3) compared with the 0.05 to 0.3 W/m^3/hr that is commonly required by ESPs to clean industrial flue gases (Wang et al., 2004). This result indicates that the gas cleaning system combined with the non-metallic ESP, composed of carbon brush chargers in CFRP channels and PVC collection plates with inserted aluminum sheets, could be a promising technology for removing particles and gases in corrosive gases produced by the semiconductor and optoelectronics industries.

3.2.4 Conclusion

Wet scrubbers and ESPs are commonly used to remove particulates in the acidic and corrosive gases generated by the semiconductor manufacturing industries. However, these devices suffer from problems such as low collection performance for ultrafine particles and corrosion caused by the gases involved. I have developed a novel non-metallic, two-stage ESP composed of separate nonmetallic charging and collection stages. This ESP uses carbon brush chargers at the center of the grounded channels of carbon fiber-reinforced polymer for the particle charging stage and PVC collection plates into which metallic films are inserted for the particle collection stage. The collection efficiency of the ESP was measured using KCl particles, SiO_2 dusts, and mists (0.01–10 μm) by varying operation parameters, such as the voltages applied to both the charger and the collection plates and test gas velocity, and design parameters, such as the length of channels in the charger and size of the collection plates using SMPS systems for ultrafine particles and optical particle counters for fine particles. Tests of long-term performance for 13 hours and regeneration performance with water washing of 70 L/min were also conducted using SiO_2 dusts and mist particles when a scrubber with a 400- x 400- x 480-mm^3 volume was operated with maximum performance conditions of 2-inch packing balls, a 3.6-L/m^3 liquid-to-gas ratio at a 40- to 60-ppm HCl concentration, and a 2-m/s polluted gas velocity. Finally, the ESP (400 x 400 m^2) was demonstrated with a bypassed gas of 1,200 m^3/hr from the exhaust line of acidic and PFC gas scrubbers of a semiconductor manufacturer in Korea.

The experimental results showed that electrical and collection performances of the carbon brush charger (400 x 400 mm^2) were not changed with different materials (stainless steel, CFRP) that were

used for 16 ground channels and with reduction of the channel lengths to 140, 90, and 50 mm. Furthermore, by increasing the voltage applied to the charger and the collection plates and by increasing the length of the collection plates, an improvement in the collection efficiency of the ESP could be achieved for a high air flow velocity of 2 m/s. In particular, when the ESP with the carbon brush charger (400 x 400 m^2, CFRP, 16 channels with 100 mm length) and collection plates (400 x 400 m^2, 400 x 540 mm^2 with 10-mm gap) was operated with 10 and 12 kV applied voltages to the charger and collection plates, respectively, it removed >90% of the ultrafine SiO_2 particles and mists at 2 m/s of gas velocity and 3.6 L/m^3 of liquid-to-gas ratio. In addition, the collection efficiency for particles in the range 0.1 to 0.3 μm fell from approximately 90% to 50% after 13 hours of continuous operation, but then recovered perfectly to the efficiency of the clean initial state after the collection plates were sprayed with water at 70 L/min for 5 min. The experimental efficiencies of the non-metallic ESP were compared with those from the Deutch collection theory, based on the Cochet charging model, and the efficiencies from the experiments could be predicted with the same design and operation parameters of the ESP. Finally, during 1 month of operation at the demonstration site, the ESP had average collection efficiencies of 97% based on particle numbers of 0.3, 0.5, and 1 μm and 92% based on total particle mass; these collection efficiencies were achieved with a much smaller specific corona power of 0.028 $W/m^3/hr$ compared with the 0.05 to 0.3 $W/m^3/hr$ of conventional ESPs.

These results indicate that the non-metallic ESP with carbon brush chargers in CFRP channels and PVC collection plates with inserted aluminum sheets could be a promising technology to remove particles and mists in corrosive gases generated by the semiconductor and optoelectronics industries.

3.2.5 References

Adachi, M., Y. Kousaka, and K. Okuyama. 1985. Unipolar and bipolar diffusion charging of ultrafine aerosol particles. J. Aerosol. Sci. 16(2): 109-123. doi:10.1016/0021-8502(85)90079-5.

Allan, R., S. Jayaram, A. El-Hag, and P. McGrath. A conductive composite material for wet ESP applications. Paper presented at the XII International Conference on Electrostatic Precipitation, Nuernberg, Germany, May 9-13, 2011.

Chein, T.W., and H. Chu. 2000. Removal of SO_2 and NO from flue gas by wet scrubbing using an aqueous $NaClO_2$ solution. Journal of Hazardous Materials B80: 43-57. doi:10.1016/S0304-3894(00)00274-0.

Han, B., H.J. Kim, Y.J. Kim. 2010. Fine particle collection of an electrostatic precipitator in CO_2-rich

gas conditions for oxy-fuel combustion. Science of the Total Environment 408: 5158-5164. doi: 10.1016/j.scitotenv.2010.07.028.

Han, B., H.J. Kim, Y.J. Kim, and K.S. Han. 2007. Removal characteristics of gaseous contaminants by a wet scrubber with different packing materials. J. KOSAE. 23(6): 744-751.

Hinds, W.C. 1999. Aerosol technology: properties, behavior, and measurement of airborne particles. New York: John Wiley & Sons, Inc.

Kim, H.J., B. Han, Y.J. Kim, and S.J. Yoa. 2010. Characteristics of an electrostatic precipitator for submicron particles using non-metallic electrodes and collection plates. J. Aerosol. Sci. 41: 987-997. doi: 10.1016/j.jaerosci.2010.08.001.

Kulkarni, P., N. Namiki, Y. Otani, and P. Biswas. 2002. Charging of particles in unipolar coronas irradiated by in-situ soft X-rays: enhancement of capture efficiency of ultrafine particles. J. Aerosol. Sci. 33(9):1279-1296. doi: 10.1016/S0021-8502(02)00067-8.

Lin, G.Y., C.J. Tsai, S.C. Chen, T.M. Chen, and S.N. Li. 2010. An efficient single-stage wet electrostatic precipitator for fine and nanosized particle control. Aerosol Sci Technol. 44: 38-45. doi:10.1080/02786820903338298.

Lin, G.Y., and C.J. Tsai. 2010. Numerical modeling of nanoparticle collection efficiency of single-stage wire-in-plate electrostatic precipitators. Aerosol. Sci. Tech. 44(12): 1122-1130. doi: 10.1080/02786826.2010.512320.

National Institute for Occupational Safety and Health. Organic and inorganic gases by extractive FTIR spectrometry; NIOSH Method 3800, NIOSH Manual of Analytical Methods 2002; 4th Ed: 1-47.

Park, J.H., and C.H. Chen. 2002. An improved modeling for prediction of grade efficiency of electrostatic precipitators with negative corona. J. Aerosol. Sci. 33: 673-694. doi:10.1016/S0021-8502(01)00205-1.

Parker, K.R. 1997. Applied electrostatic precipitation. London: Blackie Academic & Professional.

Shi, Y.S., D. Littlejohn, P.B. Kettler, and S.G. Chang. 1996. Removal of nitric oxide from flue gas with iron thiochelate aqueous solution in a turbulent contact absorber. Environmental Progress. 15(3): 153-158. doi: 10.1002/ep.670150313.

Tsai, C.J., C.C. Miao, and H.C. Lu. 1997. White smoke emission from a semiconductor manufacturing plant. Environment International 23(4): 489-496. doi: 10.1016/S0160-4120(97)00036-6.

U.S. Environmental Protection Agency. Determination of particulate matter emissions from

stationary sources; EPA Method 5, 2000.

U.S. Environmental Protection Agency. Measurement of vapor phase organic and inorganic emissions by extractive Fourier transform infrared (FTIR) spectroscopy; EPA Test Method 320, 1998.

Wang, L.K., N.C. Pereira, and Y.T. Hung. 2004. Air pollution control engineering. New Jersey: Humana Press, Inc.

Xiangron, Z., W. Kianze, and Z. Keqin. 2002. An analysis of a wire-plate electrostatic precipitator. J. Aerosol. Sci. 33(11), 1595-1600. doi:10.1016/S0021-8502(02)00104-0.

Yoo, K.H., J.S. Lee, and M.D. Oh. 1997. Charging and Collection of Submicron Particles in Two-Stage Parallel-Plate Electrostatic Precipitators. Aerosol. Sci. Tech. 27(3): 308-323, doi:10.1080/02786829708965476.

Zhao, H., and C. Zheng. 2008. Modeling of gravitational wet scrubbers with electrostatic enhancement. Chem. Eng. Technol. 31(12), 1824-1837. doi: 10.1002/ceat.200800360.

Zhuang, Y., Y.J. Kim, T.G. Lee, and P. Biswas. 2000. Experimental and theoretical studies of ultra-fine particle behavior in electrostatic precipitators. J. Electrostat. 48(3-4): 245-260. doi: 10.1016/S0304-3886(99)00072-8.

Chapter IV

Wet ESP using thin water films on collection plates with low water consumption

4.1 Fine particle removal performance of a two-stage wet ESP using a nonmetallic pre-charger

4.1.1 Introduction

Two-stage electrostatic precipitators (ESPs) have been widely applied to remove fine particles from industrial pollutants and also to enhance indoor air quality (Yoo et al., 1997; Zukeran et al., 1999; Grinshpun et al., 2005). This type of ESP differs from single-stage ESPs, which use high voltage to charge particles and subsequently collect them within the same chamber on surfaces of opposite charge. Two-stage ESPs consist of a charging stage, utilizing thin wires equally spaced from the parallel or cylindrical grounded plates or tubes, and a collection stage involving separate parallel metal plates that collect negatively (positively) charged particles at positively (negatively) charged plates (Li et al., 2006; Electrostatic Precipitator Knowledgebase, 2011). Yoo et al. (1997), Li and Christofides (2006), and Talaie et al. (2001) conducted theoretical and experimental research on particle collection performance of general two-stage ESPs with a wire plate-type pre-charger and parallel plate-type collection cell. Jayaram et al. (1996) and Zukeran et al. (1997) applied a cooled pre-charger before using an ESP and enhanced the collection efficiency of the standalone ESP via stabilization of the corona discharge by water cooling and pulse energization. Zukeran et al. (1999) examined the re-entrainment phenomenon under diesel flue gas using a two-stage ESP. They noted that, even with the two-stage ESP, the collection efficiency decreased due to re-entrainment of particles with low resistivity. Zhu et al. (2010) developed an ESP with a bipolar pre-charger and achieved a collection efficiency exceeding 95% for micrometer and submicrometer particles, attributable to particle agglomeration by the bipolar pre-charger. However, previous studies for two-stage ESPs used metallic wires or spikes as high voltage electrodes. These wires or spikes could exhibit corrosion problems when treating particles in corrosive and acidic gaseous materials such as SO_3, HF, and HCl. In addition, the polarity of the voltage applied to the pre-charger in two-stage ESPs is generally positive; however, a pre-charger with negative polarity could produce high ozone

concentrations at the voltage levels necessary to increase the collection efficiency of very small particles (Electrostatic Precipitator Knowledgebase, 2011).

The ozone that is normally generated as a by-product of corona discharge in an ESP can damage respiratory organs and degrade many materials. Consequently, the daily 8-hour maximum ozone concentration is set to less than 60~80 ppb by environmental regulatory agencies such as the World Health Organization, Environmental Protection Agency, and European Commission (Liu et al., 2000; Yehia et al., 2000; Bell et al., 2006). The ozone production by particle charging in the metallic corona pre-charger of general ESPs depends on a number of factors, including flow rate, relative humidity, materials, and the diameter or thickness of high voltage electrode as well as the operational voltage, current and the polarity of the corona discharge (Yehia et al., 2000; Cardello et al., 2002; Goheen et al., 1984; Kelkarni et al., 2002). In particular, the thickness of the corona discharge electrode at the same discharge current results in reduction of ozone generation from the charger because ionization and dissociation areas of oxygen decreases with decreasing the thickness of discharge electrode in the pre-charger (Yasumoto et al., 2008).

Wet ESPs are used for industrial applications in cases of high potential for explosion or very sticky, corrosive, or highly resistive dust. A water flow is applied continuously or intermittently to wash particles from the collection electrodes into a reservoir used to collect liquid. Wet ESPs have the advantage of avoiding problems with rapping re-entrainment and back corona. These features make wet ESPs more effective for controlling ultrafine particles (Jaasund, 1981; Musdalslien et al., 1991; Altman et al., 2001) and efficiently removing corrosive liquid phase particulates such as SO_3, PAH, and HCl compared to dry ESPs (Lee et al., 1998; Staehle et al., 2003; Saiyasitpanich et al., 2008; Snyer et al., 2008; Bologa et al., 2009). However, wet ESPs might experience disruptions caused by spraying (misting) of water, the formation of dry spots due to effects of water surface tension (channeling), and corrosion of the collector surfaces. These factors limit the applicability of current wet precipitators (Bayless et al., 2004).

Bayless et al. (2004) and Pasic et al. (2001) developed a novel hydrophilic membrane-based wet ESP to minimize dry spot formation on collection plates which could be attacked by corrosive gases, and achieved more than 95% removal efficiency based on particle mass. For the same purpose, Lin et al. (2010) developed a novel wet ESP with a thin water film on its collection plates to control fine and nanosized particles and achieved over 95% collection efficiency for corn oil mists at a residence time of 0.39 s. However, these wet ESPs also used metallic spikes and wires as the high voltage electrodes of the positive charger.

Carbon fiber ionizers are made of graphite, an anticorrosive material that can be utilized easily and inexpensively by applying a voltage of a few kilovolts to a bundle of approximately 300 carbon fibers, a few micrometers in diameter, to generate ions (Peterson et al., 2005). These ionizers can produce stable unipolar ions at sufficiently high concentrations while emitting low ozone (Chen et al., 2006; Han et al., 2008a, 2008b; Han et al., 2009a, 2009b, Kim et al., 2010).

I am unaware of any previous attempts to combine a carbon brush charger with wet collection plates cleaned by a thin water film for a two-stage wet ESP for an industrial purpose. In this study, the electrical and particle collection performance characteristics of the newly developed two-stage wet ESP were investigated by changing the applied voltage and its polarity. The particle collection result was compared with theoretical results obtained from theoretical models for ESPs. The concentration of ozone produced as a by-product of ESP usage was measured by changing the voltage and its polarity applied to the pre-charger, and was compared to those from general pre-charges which were made of different materials for high voltage electrode or were made of carbon electrodes with different diameters. This was done in order to understand the reason why carbon brush pre-charger emits low ozone, which has not been researched until now. Finally, dust loading tests with Japanese Industrial Standards (JIS) dust was also performed to assess the long-term performance of the ESP with and without a water film.

4.1.2 Experimental set up

Figure 1 shows a schematic diagram of the two-stage wet ESP consisting of the carbon brush charger and collection cell that were developed in this study. As shown in Figure 1 (a), the carbon brush pre-charger was composed of a bundle of approximately 300 carbon fibers with a diameter of a few micrometers; the bundle of brushes was 6 mm long. The brush was connected to a stainless steel rod, which was in turn connected to a high voltage power supply. The high voltage electrode was inserted into the center of a 1-inch stainless steel tube (S/S tube), and the tip of the carbon brushes was located 104 mm from the left side of the tube. To prevent particle deposition on the carbon brushes, the high voltage electrode was insulated by a cylindrical Teflon housing and shielded from a 10 L/min airflow streaming into the 1 mm slit between the housing and the electrode. As shown in Figure 1 (b), the wet-type collection cell consisted of upper and lower water reservoirs, which both connected to a water circulation pump (Model PW-S3545MA, WILO SE, Germany), water film collection plates, and a plate-type high voltage electrode. The upper water reservoir (54 x 160 x 13

mm^3) was attached to the back side of the collection plate, and the make-up water from the circulation pump was supplied at the bottom of the reservoir. The water from the reservoir flowed through 2-mm-diameter holes (separated by a distance of 5 mm) in the collection plates. To enhance the hydrophilicity of the collection plates, which increases the water film uniformity and minimizes water consumption, the collection surfaces of the plates were first sand-blasted and then coated with an alcohol solution (Model P&T-100HX, Nanopac Co., LTD, Korea) in which approximately 5~10 nm TiO_2 nanoparticles were dispersed. The plates were then dried and calcined with an electrical dryer at 500 ℃ for 30 min to strengthen the bonding of the TiO_2 particles onto the collection plates. The process of making the hydrophilic collection surfaces was based on the method described by Lin et al. and Tsai et al. (Lin et al., 2010; Tsai et al., 2008). The effect of surface treatment on the collection plates was shown in Figure 2.

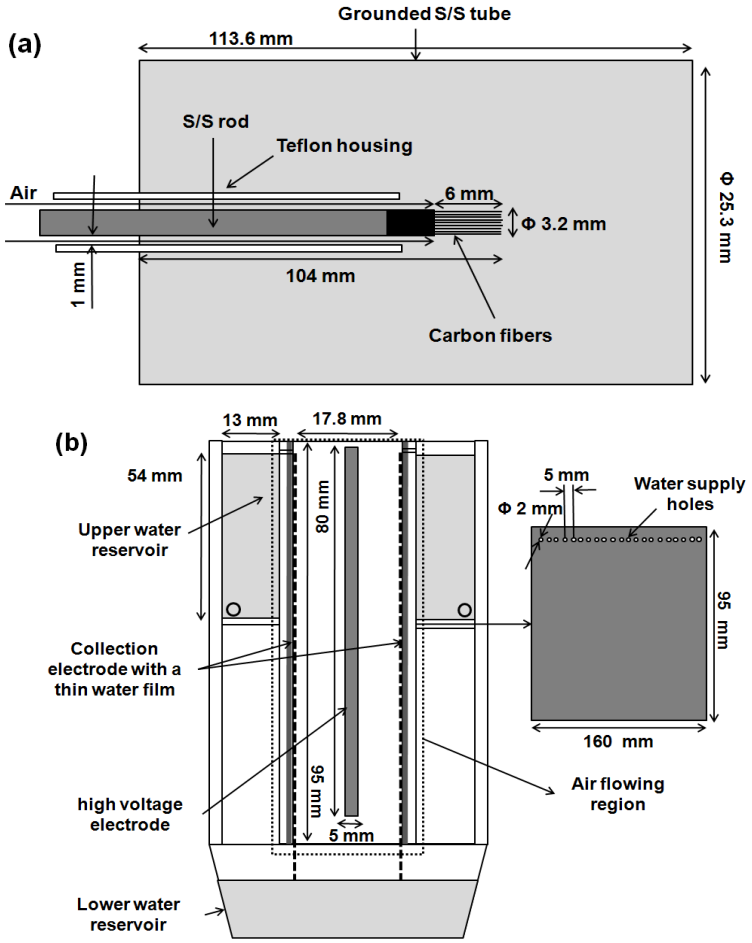

Figure. 1 Schematics of the two-stage wet ESP developed in this study. The stages consist of the carbon brush pre-charger (a) and the collection cell (b).

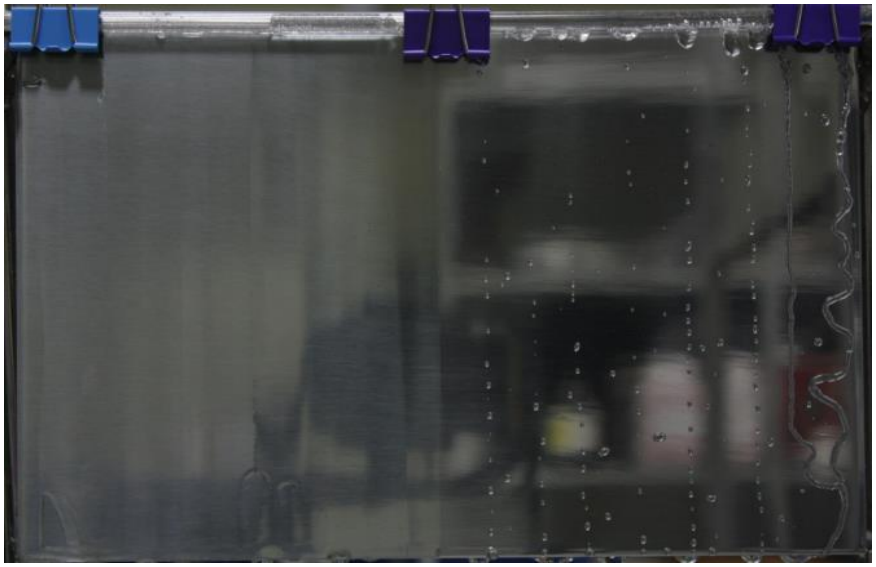

(a) Formation of water film w/ nano particle coating (left) and w/o the coating (right)

(b) Formation of water film w/ particle coating and sand-blasting (left) and w/ the blasting only (right)

Figure. 2 Comparison of water films on collection plates with different surface treatments

To generate strong electrostatic fields for the collection plates, the polished S/S plate (80 x 160 x 5t mm^3) was inserted at the center of the collection cell and was connected to a high voltage power supply. The gap between the high voltage power supply and the collection plates was 6.4 mm, and test air was streamed through the central area (17.8 x 98 mm^2).

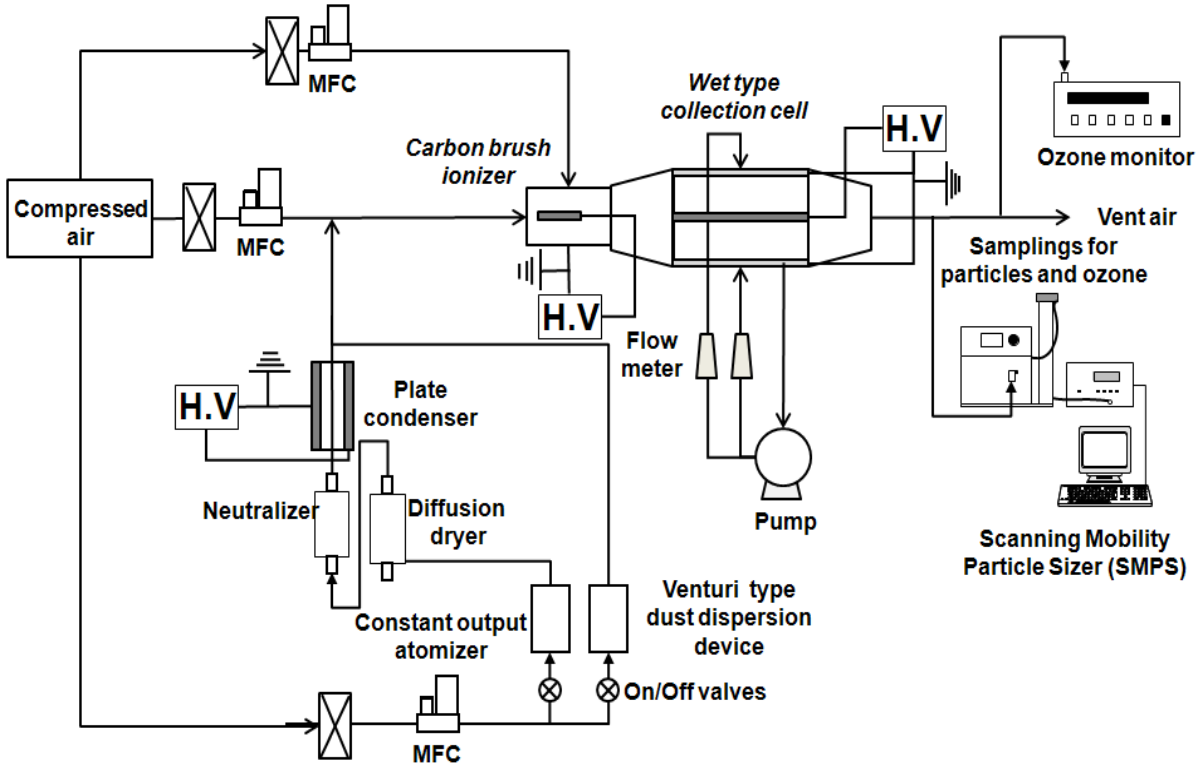

Figure. 3 Experimental setup for the performance tests of the two-stage wet ESP.

Figure 3 shows the experimental setup used in this study. Potassium chloride (KCl) aerosol particles with diameters in the range of 0.01~0.5 μm were generated by nebulizing a 0.05% KCl-water solution using a constant-output atomizer (Model 3076, TSI Inc., U.S.) and passing this through a Kr-85 neutralizer and a diffusion dryer. The number mean diameter, number concentration, and geometric standard deviation of the particles generated were approximately 0.045 μm, 2.5 x 10^5 particles/cm^3, and 1.7, respectively. The charged fractions of the test particles were removed using a plate condenser (to which a voltage of -10 kV was applied), and uncharged particles were then introduced into the upstream portion of the carbon brush pre-charger. Clean compressed air was mixed with these particles and the mixture subsequently passed through the carbon brush pre-charger and collection cell. The total air flow rate through the wet-type ESP was maintained at 95 L/min using mass flow controllers (MFCs, Model Tylan® FC-2920 Series-100 slpm, Mykrolis Corporation, U.S.); this flow rate corresponded to flow speeds of 4 m/s through the carbon brush pre-charger and 1.0 m/s through the collection cell. High voltage power supplies (Max +/- 30 kV/ 10 mA, Korea Switching, Korea) were connected to the pre-charger and the collection cell. The applied voltages and corona currents were measured by using digital multi-meters (Model 286, Fluke Corporation, Japan). The voltage to the pre-charger was allowed to vary from 2 to 8 kV, and from 4 to 8 kV, to

understand the effect of the applied voltages on the performances of the charger and the whole ESP. The polarity of the voltage applied to the pre-charger was also changed to understand the effect of polarity changes on the pre-charger and ESP performances. For wetting the collection plates, the water flow rate per collection surface area was 6.5 L/min/m^2 (0.16 x 0.095 m^2). The size distributions of the test particles downstream of the collection cell were measured using a scanning mobility particle sizer (SMPS, Model 3081, TSI Inc., U.S.) system, as well as a condensation particle counter (CPC, Model 3076, TSI Inc.)

The performance of the ESP used in this study was expressed in terms of the particle collection efficiency (η), which may be obtained by using the following equation:

$$\boldsymbol{\eta = \left(1 - \frac{C_2}{C_1}\right) \times 100} \qquad (1)$$

where η is the particle collection efficiency, C_1 is the number concentration of the particles downstream from the ESP without any applied voltage, and C_2 is the number concentration of the particles downstream from the ESP with voltages applied to its charger or collection cell.

The long-term collection performances of dry- and wet-type ESPs during dust loading were compared using JIS standard dust (Class 8, mass mean diameter 1.6~2.3 μm, JIS standard dust, Japan) for the dust loading of the collection plates, and submicrometer KCl particles for measuring the transient collection efficiency of the ESP during the test. A venture-type dust dispersion device was used to generate and supply the dusts upstream to the pre-charger (Figure 2). The mass concentration of the loading dust that flowed into the ESP was maintained at approximately 50 mg/m^3. Prior to dust loading, the collection efficiency of the ESP without any dust collected on the collection plates was measured. The transient collection efficiency was then measured every 15 min after each dust loading of 1 g, by means of KCl particles. The polluted water was removed periodically from the lower water reservoir. During the experiments, the operational parameters of the pre-charger and collection cell were varied to investigate their effect on the performance of the wet-type ESP. Table 1 summarizes the experimental conditions.

In this study, ozone emission from a carbon brush pre-charger was measured using an ozone monitor (Model API 400E, Teledyne Technologies Inc., U.S.), while varying the voltage applied to the pre-charger and its polarity. The ozone emission was compared to those from general pre-chargers with sharp-edge electrodes which were made by various materials such as aluminum, copper, silver, tungsten and carbon (graphite), and also to those from pre-chargers with carbon-based high voltage electrodes with different diameters of electrodes such as 0.3, and 0.9 mm. This was

performed to evaluate the material and diameter effect on the low ozone emission of the carbon brush pre-charger.

Table 1. Parameters and test conditions used to study wet ESP performance.

Set No	Velocity in charger (m/s)	Velocity in collection cell (m/s)	Voltage to pre-charger (kV)	Voltage to collection plates (kV)	Polarity	Type	Test particle	Measurement
1	4	1	2, 4, 6, 8	0	P/N	-	KCl	Particle loss/ voltage and current/ ozone
2	4	1	2, 4	4, 6, 8	P	Wet	KCl	Collection efficiency
3	4	1	2, 4	4, 6, 8	N	Wet	KCl	Collection efficiency
4	4	1	4	8	N	Wet/ Dry	KCl/JIS (loading)	Collection efficiency

4.1.3 Results and discussion

(1) Electrical performance and ozone emission of the carbon brush pre-charger

Figure 4 shows current variation against the voltages applied to the carbon brush pre-charger. The test airflow rate was maintained at 95 L/min, which corresponded to a flow velocity of 4 m/s through the carbon brush pre-charger. A negative corona led to higher corona currents than a positive corona for the same applied voltage because of higher electrical mobility of negative ions due to lower clustering of the molecules (Cabane and Playe, 1980) and the photoelectric effects from the surface of the discharging electrodes at the negative corona (Trichel, 1938). Figure 5 shows the variation in the concentration of ozone emitted from the carbon brush pre-charger, plotted against the voltage applied to the pre-charger for different polarities at a constant air velocity of 4 m/s. The average ozone concentration was proportional to the voltage applied to the pre-charger, and ozone generation was much higher with a negative high voltage than with a positive high voltage (Yehia et al., 2000; Nomoto et al., 1995). In particular, when the voltage applied to the charger was less than 4 kV, the ozone concentration was less than 30 ppb, which was significantly lower than the 60~120 ppb limit set out in the Federal Aviation Administration-recommended level and the U.S. Environmental Protection Agency's National Ambient Air Quality Standard (Spengler et al., 2004).

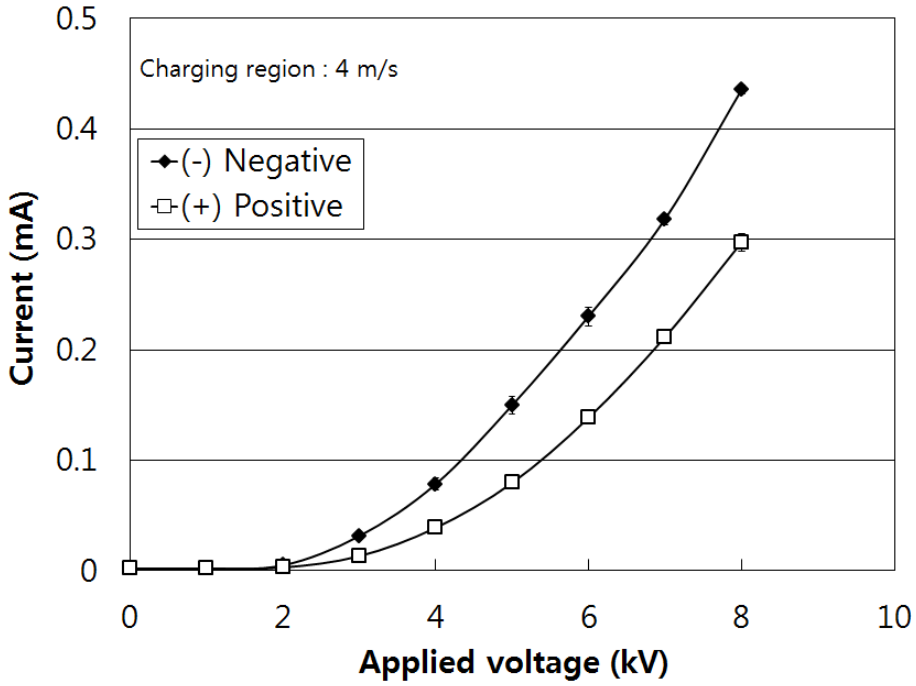

Figure. 4 Voltage-current curves of the carbon brush pre-charger for negative and positive polarities.

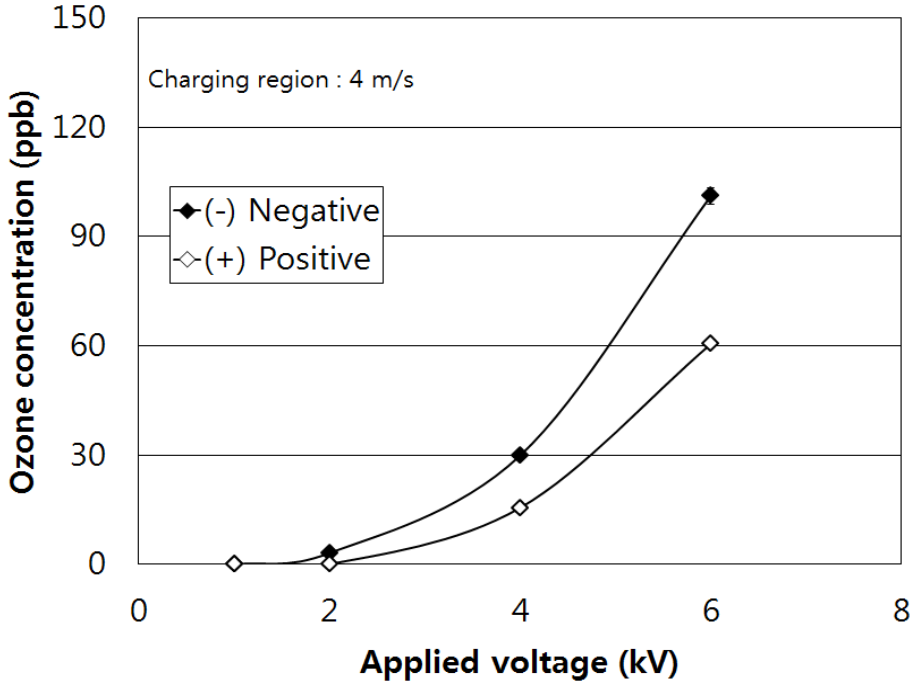

Figure. 5 Ozone emission as a function of the voltage applied to the pre-charger for negative and positive polarities.

The reason why the carbon brush pre-charger emits low ozone has been not clearly understood. There are two possibilities to explain the reason, and one is the electrode material effect on ozone emission because carbon is known to be an efficient chemical absorption material (Hart et al., 1967),

and the other is the thin diameter effect because the ionization and dissociation areas of oxygen decreases with decreasing the thickness of discharge electrodes in the pre-charger (Chen and Davidson, 2002; Yasumoto et al., 2008; Bo et al., 2010).

Figure 6 shows the pictures which were taken using an optical microscope at the tips of the high voltage electrodes with different materials such as aluminum, copper, silver, tungsten, and carbon. The diameters at 200 μm from the tip of electrodes (the sharpness of electrodes) with different materials, approximately 100 to 200 μm, were kept similarly in order to minimize effect of sharpness at the tips on ozone emission from the pre-chargers.

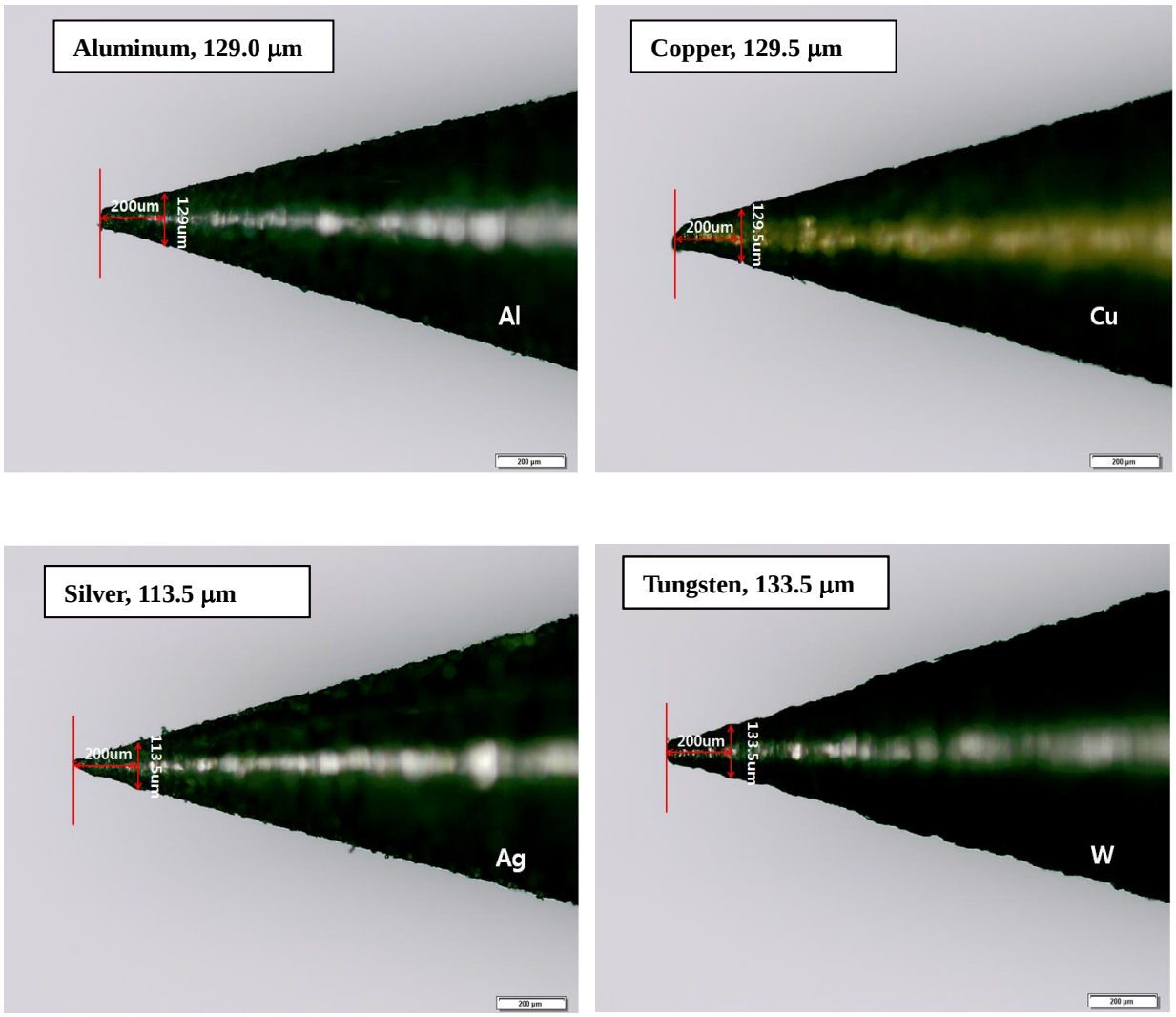

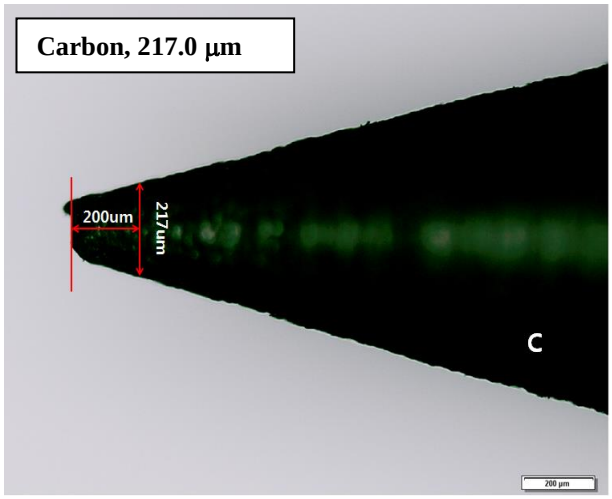

Figure. 6 Pictures at the tips of high voltage electrodes used in this study which were made aluminum, copper, silver, tungsten, and carbon.

Figure 7 shows current variation against the voltages applied to various pre-chargers with sharp-edge electrodes made by different materials such as aluminum, copper, silver, tungsten, and carbon. The current-voltage characteristics were not clearly discriminated with the electrode materials in dry air, which was also observed the previous research (Yehia and Mizuno, 2008).

Figure 8 shows the ozone emission from pre-chargers with sharp-edge high voltage electrodes made by different materials, as a function of corona current. Similarly to results in Figure 7, the ozone emissions for the metallic electrodes and carbon electrode were not clearly discriminated. This result is not explained with the previous results that for positive discharges ozone generation is linked to electrode material by the rate of formation of an oxide film quantified by the maximum standard heat (or enthalpy) of formation of an oxide per oxygen atom for exothermic reactions ($-\Delta H_o$) (Boelter and Davidson, 1997) because the enthalpies of carbon for oxidation (-26 kcal/mol for CO and -94 kcal/mol for CO_2) is quite different to those of the other materials which are clearly varied from -10 to -70 kcal/mol by types of materials (Boelter and Davidson, 1997; Vijh, 1974). With the results with Figures 6 to 8, it is expected that the ozone emission in this study is not significantly affected by the type of materials.

Figure 9 shows voltage-current curves of the pre-charger for different electrode diameters and of the carbon brush pre-charger. To compare the sharpness effect of the high voltage electrodes, graphite rods with diameters of 0.3 and 0.9 mm were used. The corona current for the carbon brush was much higher than those for 0.3 and 0.9 mm at the same applied voltages due to the thin edges of carbon brush. Corona discharge by the graphite electrode with the diameter of 0.9 mm was not

occurred because applied voltage in this study was too low to generate corona.

Figure 10 shows ozone emission as a function of the corona currents to the pre-chargers for different electrode diameters and to the carbon brush pre-charger. Even though the corona current of the carbon brush at the same applied voltage as the 0.3 mm electrode was much higher, the ozone emission at the same corona current was significantly lower than that with 0.3 mm. The lower ozone emission from the carbon brush pre-charger is resulted from the thinner diameter of the carbon fibers, only about several micrometers which is significantly thinner than the diameters of graphite electrodes, and these results about diameter effect on low ozone emission with metallic electrodes were observed in previous studies (Boelter and Davidson, 1997; Chen and Davidson, 2002; Yasumoto et al., 2008; Islamov and Krishtafovich, 2013).

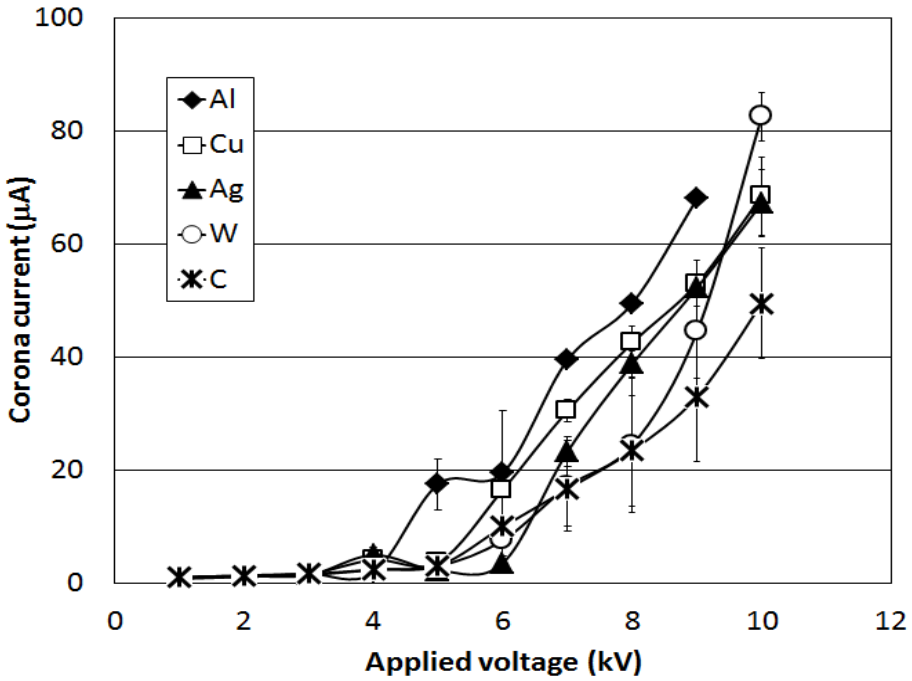

Figure. 7 current variations against the voltages applied to various pre-chargers with sharp-edge electrodes made by different materials such as aluminum, copper, silver, tungsten, and carbon.

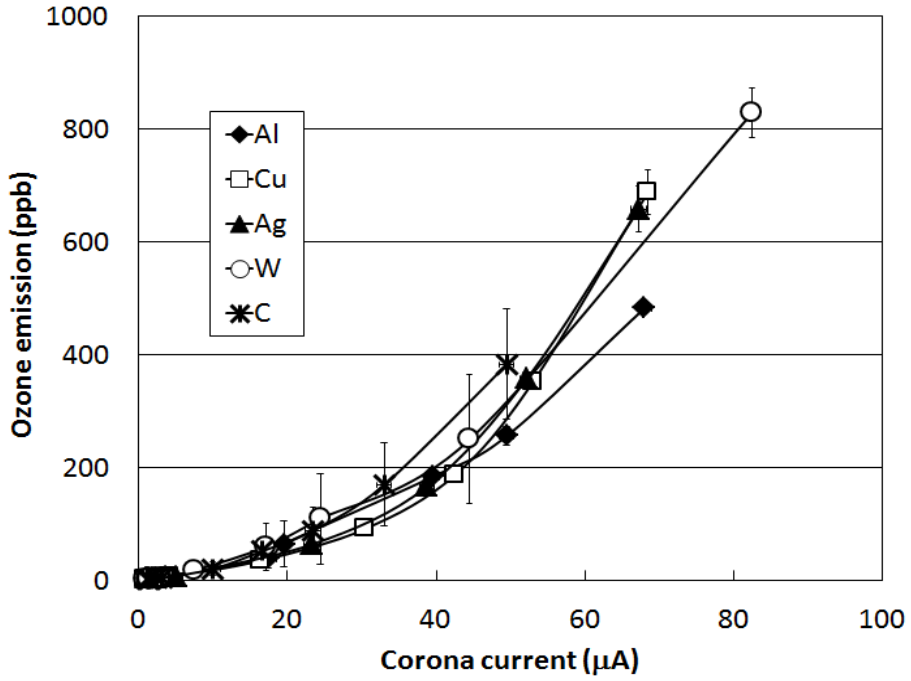

Figure. 8 Ozone emission by changes of corona current from pre-chargers with sharp-edge high voltage electrodes made by different materials.

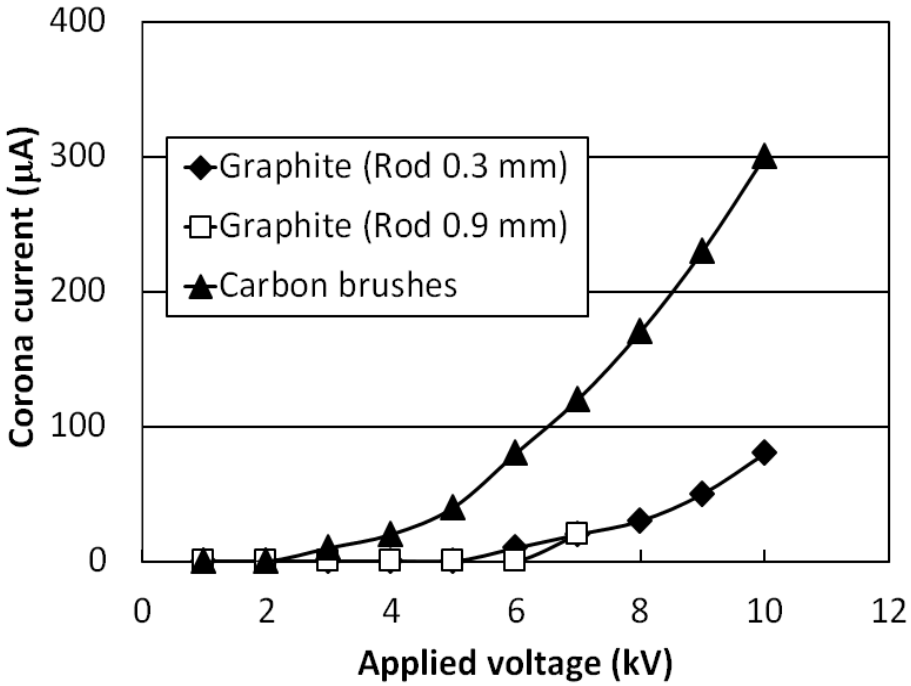

Figure. 9 Current variations against the voltages applied to pre-chargers with sharp-edge electrodes made by different diameters and to the carbon brush pre-charger.

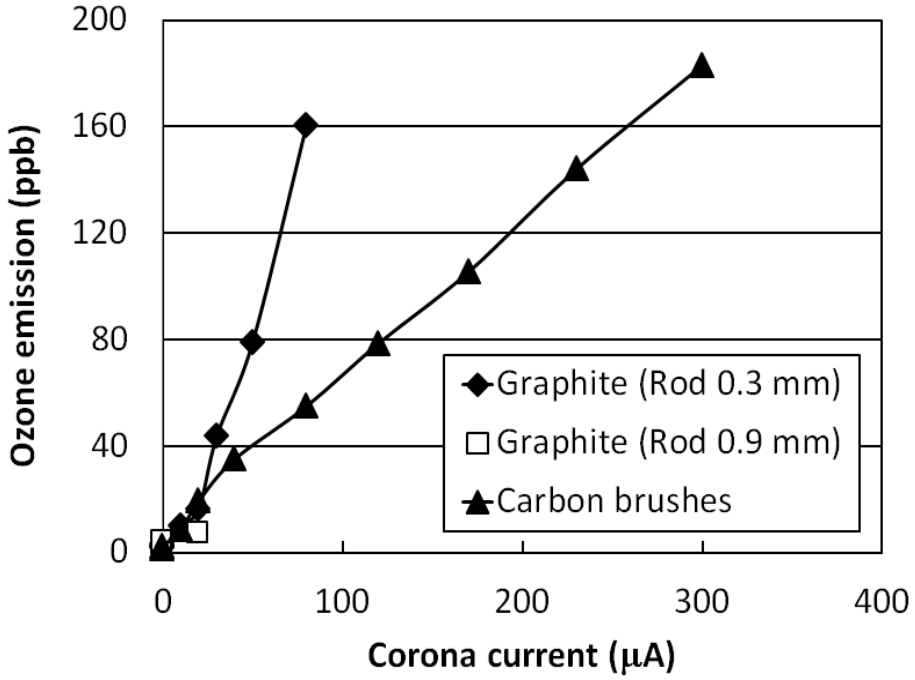

Figure. 10 Ozone emission by changes of corona current from pre-chargers with sharp-edge high voltage electrodes made by different diameters, and from the carbon brush pre-charger.

(2) Particle capture in the carbon brush pre-charging zone

In general, for the industrial purpose it is necessary to minimize particle capture in the pre-charging zone of two stage ESPs because particle contamination on the ground tube by the particle capture in the zone for a long operation time could decrease the electrical field in the pre-charging zone, and thus reduce the particle charging efficiency in the charging zone.

The particle capture only in the pre-charging zone was measured with particle size distributions at upstream and downstream of the pre-charging zone with and without an applied voltage to find out a range of applied voltage to the pre-charger to minimize the particle contamination in the zone.

Figure 11 shows the relationship between the particle capture efficiency of submicrometer particles in the pre-charger and the voltage applied to it. The polarity of the applied voltage was negative, and air velocity was 4 m/s. As the applied voltage increased, the particle capture efficiency increased across the whole range of particle sizes. It should be noted that increased particle capture could result in a reduction of the electrical field for particle charging due to particle contamination on the grounded tube. The smallest particle capture in the pre-charger was observed for particles between 100 and 200 nm in mobility diameter, regardless of the applied voltage. In particular, particle capture of less than 10% within the entire size range was acquired with the applied voltages

of 2 and 4 kV for a negative polarity.

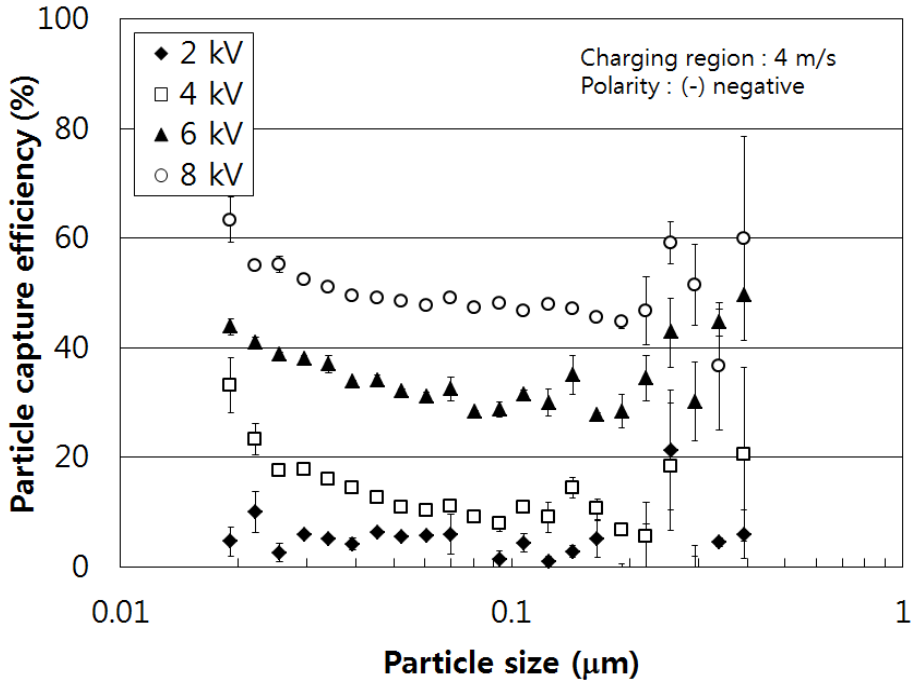

Figure. 11 Collection efficiency of submicrometer particles against particle size with different voltages applied to the pre-charger.

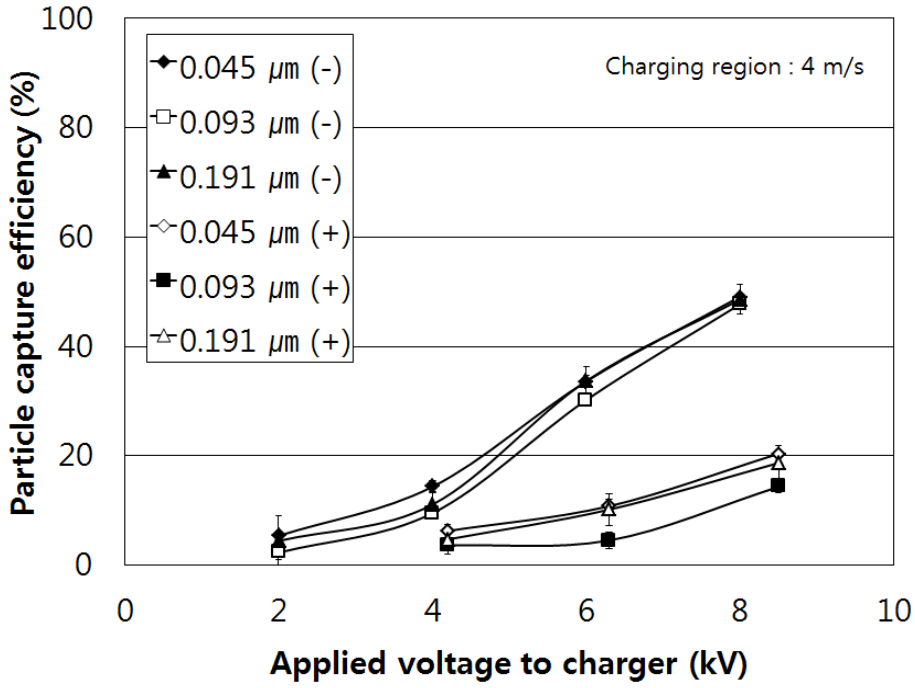

Figure. 12 Collection efficiency of submicrometer particles against voltage applied at different high voltage polarities for particle sizes of 0.045, 0.093, and 0.191 μm.

Figure 12 shows the variation in submicrometer particle capture efficiency with applied voltage at different corona polarities for particle sizes of 0.045, 0.093, and 0.191 μm. The particle capture for both polarities was proportional to the voltage applied to the pre-charger. For a given applied voltage, particle capture was higher with a negative corona than with a positive corona due to the higher ionic mobility of negative ions (Cabane and Playe, 1980). However, for both polarities, less than 10% particle capture was obtained with an applied voltage of less than 4 kV. To minimize ozone generation to less than 30 ppb and particle capture in the pre-charger to less than 10%, the voltage applied to the pre-charger was kept at 2 or 4 kV during testing the particle collection performance of the ESP developed in this study.

(3) Collection performances for submicrometer particles of the two-stage wet ESP

Figure 13 shows the relationship between the collection efficiency of submicrometer particles in the ESP and the voltage applied to the collection plates. Positive polarity voltages were applied to the pre-charger and the high voltage between ground plates in the middle of the collection cell; voltages of 2 and 4 kV were applied to the pre-charger.

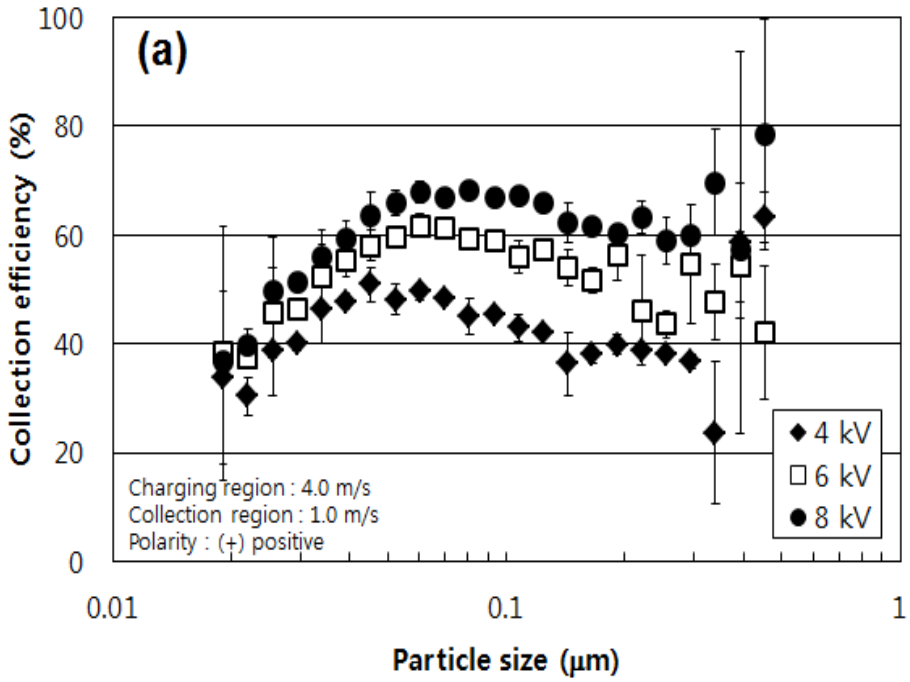

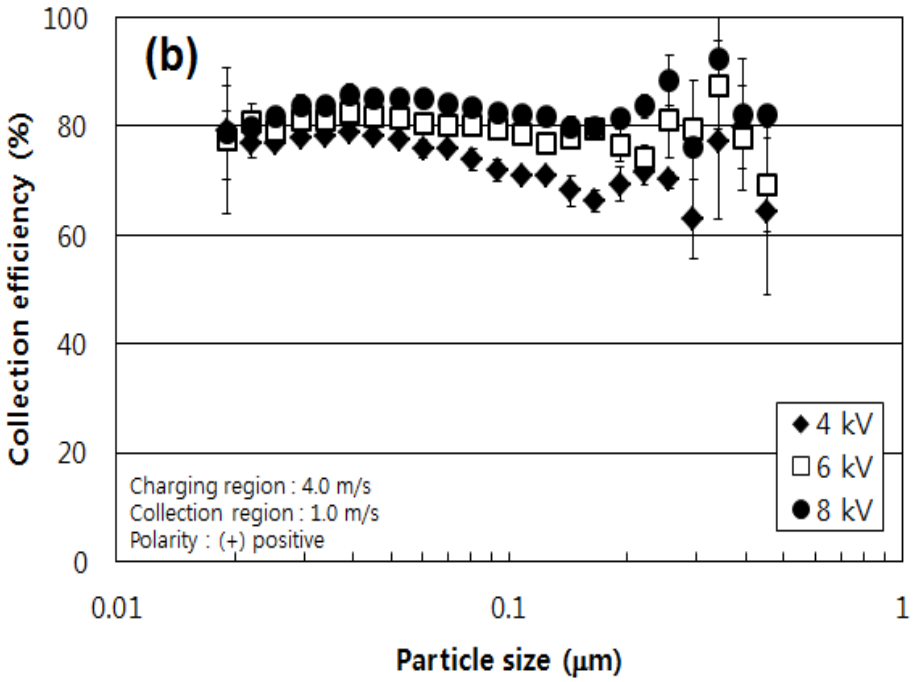

Figure. 13 Collection efficiency of submicrometer particles as a function of particle size for different positive voltages applied to the collection plates. (a) 2 kV and (b) 4 kV applied to the carbon brush pre-charger.

The test airflow rate was 95 L/min, again corresponding to flow velocities of 4 and 1.0 m/s through the charger and collection cell, respectively. The water supply onto the collection plates was maintained at 6.5 L/min/m^2, and the particle capture in the pre-charger without any voltage applied to the collection cell was less than approximately 10%. Increasing the voltage applied to collection plates increased the collection efficiency for almost all particles because the higher electrostatic intensity increased the migration velocity of the particles to the plates, as shown in Figure 13 (a) (White, 1963). However, for particles smaller than 0.05~0.06 μm in diameter, as particle size decreased, collection efficiency decreased at all applied voltages due to the partial charging effect in this size range; this finding agreed with the results of previous studies (Yoo et al., 1997; Li and Christofides, 2006; Zhuang et al., 2000; Huang and Chen, 2002). In particular, for particles smaller than 0.03 μm, the increase in electrostatic intensity between the collection plates had almost no effect on the collection efficiency. Particle collection was restricted by the charging fraction of particle size ranges in the charger (Li and Christofides, 2006). This phenomenon can be regarded as a non-ideal effect, which cannot be explained by the Deutsch theory. As shown in Figure 13 (b), the collection efficiency was also enhanced by increasing the voltage applied to the collection plates. The

collection efficiency in the peak sizes with 4 kV voltage applied to the pre-charger averaged 85% and was enhanced by 10~30%. In particular, compared with results for 2 kV applied to the pre-charger, with 4 kV, the collection efficiency for particles smaller than 0.03 μm in diameter increased significantly (by 20~40%), with the peak efficiency being shifted to smaller particles. This increased collection efficiency in the smaller size range could result from the collection efficiency becoming significantly high when there was a large enough number of ions, as particles are almost fully charged by acquiring just one ion. Particles in the ultrafine size range usually have a very high electrostatic migration velocity. However, as the number of ions is decreased, the efficiency for very small particles drops dramatically as a result of the decreased charging fraction (Li and Christofides, 2006).

Figure 14 shows the relationship between the collection efficiency of submicrometer particles in the ESP and the voltage applied to the collection plates within the ESP. The polarity of the voltage applied to the pre-charger and collection plates was negative. Voltages of 2 and 4 kV were applied to the pre-charger, and the test airflow rate was 95 L/min, again corresponding to flow velocities of 4 m/s through the charger and 1.0 m/s through the collection cell. The water supply onto the collection plates was maintained at 6.5 L/min/m^2. Particle capture in the pre-charger was approximately 10% with both 2 and 4 kV.

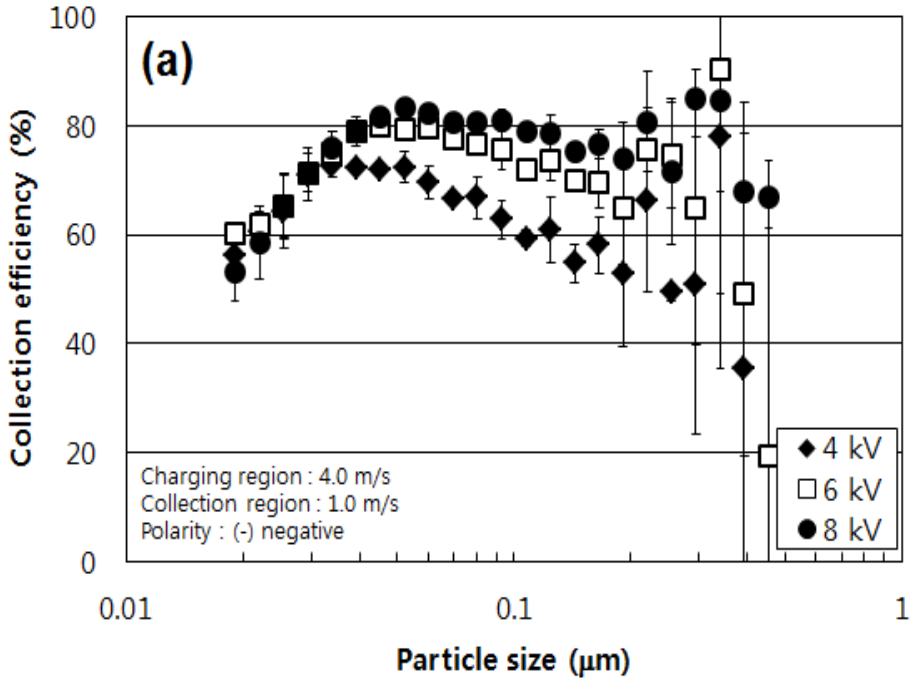

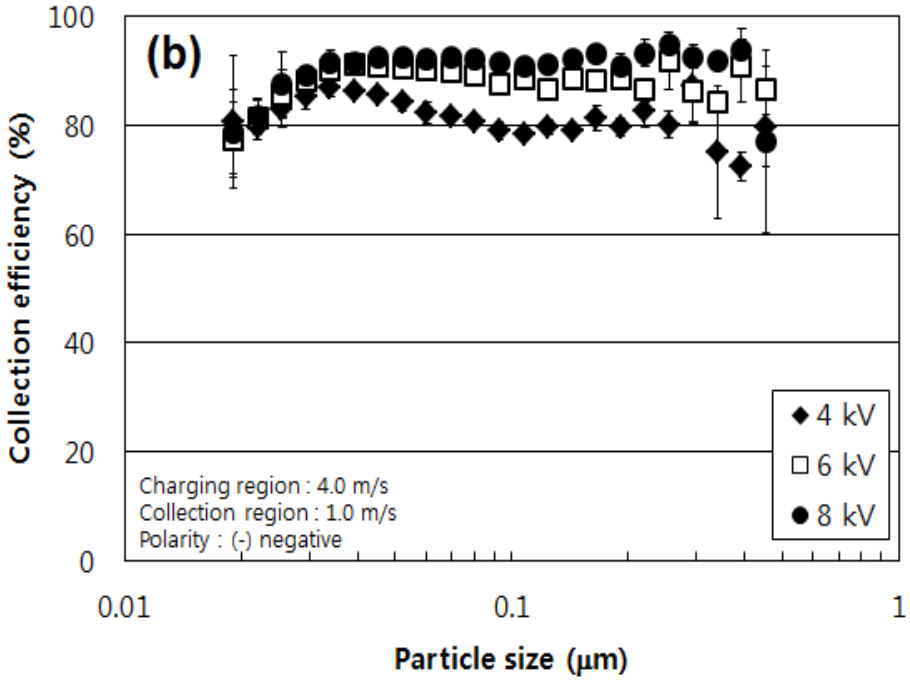

Figure. 14 Collection efficiency of submicrometer particles as a function of particle size for different negative voltages applied to the collection plates. (a) -2 kV and (b) -4 kV applied to the carbon brush pre-charger.

As shown in Figure 14, the size-dependent and electrostatic field-dependent collection efficiencies agreed well with those from the experiments with positive voltage. However, the entire collection efficiencies were enhanced by approximately 20% and 10% for voltage levels of 2 and 4 kV, respectively, applied to the pre-charger, in comparison to those for the same applied voltage levels for positive polarity. In particular, the average particle collection efficiency exceeded 90% for submicrometer particles when negative voltages of 4 and 8 kV were applied to the pre-charger and collection plates, respectively.

In this study, the Cochet's charging model was mainly used because it allowed an easy calculation and the correlation to actual ESP conditions is quite reasonable in the critical size range from 0.1 to 1 μm. The Deutsch model was also used to calculate the collection efficiency of the ESP in this study. The calculation methods were expressed in equation (1) to (4) in Chapter II. However, the diffusion charging theory based on the Fuchs' limiting sphere theory was also used for the particles smaller than 0.1 μm because the diffusion charging is predominantly used for nano particle charging, and nanoparticle collection in ESP depends primarily on particle charging efficiency within an ESP and therefore on particle size (Suriyawong et al., 2008). The detail explanation about Fuchs' theory was written in Chapter II with equation (5) to (14). Figure 15 shows the comparison of

collection efficiency as a function of particle size, as found in this study and the efficiency which was predicted by different theories. Voltages applied to the pre-charger and the collection plates were 4 kV and 4, 6, and 8 kV, respectively, and the air velocities through the pre-charger and collection plates were 4 m/s and 1.0 m/s, respectively. For particles larger than 0.05 μm, the experimental collection efficiencies were similar to those predicted by Deutsch ESP collection theory, based on the Cochet's charging theory. However, the differences between the results and those predicted by the Cochet's theory increased as particle sizes decreased to smaller than 0.05 μm because the charging for the particles in the size range is significantly related to diffusion charging. Therefore, the theoretical collection efficiency for the particles smaller than 0.05 μm, based on the Fuchs' diffusion charging theory (equations (5) to (14)), was calculated with the product of ion number concentration, N_i, and charging time, t, which was approximately 6.0 x 10^{12} sec/m^3 with the test conditions of this study. For the collection efficiency, it was assumed that charged particles in the charging section were completely collected in the collection zone, regardless of the increase in applied voltage to collection plates. Shown in Figure 15, for the particles smaller than approximately 0.05 μm, the efficiency was also fairly similar to those predicted by the theoretical calculation. The efficiency was decreased as particle size decreased below 0.05 μm, and these results were also observed in previous studies because of the poor diffusion charging and the lower ion attachment coefficients for the particles (Kulkarni et al., 2002; Adachi et al., 1985; Huang and Chen, 2002; Zhuang et al., 2000).

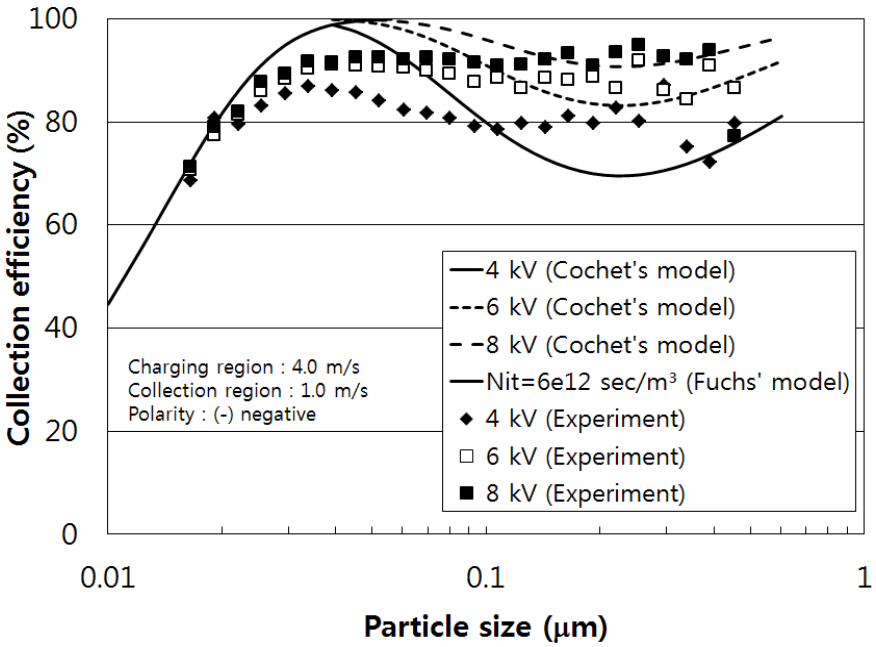

Figure. 15 Comparison of collection efficiency as a function of particle size, as found in this study and theoretically predicted for different voltages applied to the collection plates.

(4) Long-term collection performances of two-stage dry- and wet-type ESPs during dust loading

Figure 16 shows variation in collection efficiency of the ESPs plotted against particle size for different particle loadings with and without water films on the plates. The collection plates were intentionally polluted using dust loading with a mass concentration of approximately 50 mg/m^3. Applied voltages to the pre-charger and collection plates were 4 and 8 kV, respectively, and air velocities through the pre-charger and collection plates were 4 and 1.0 m/s.

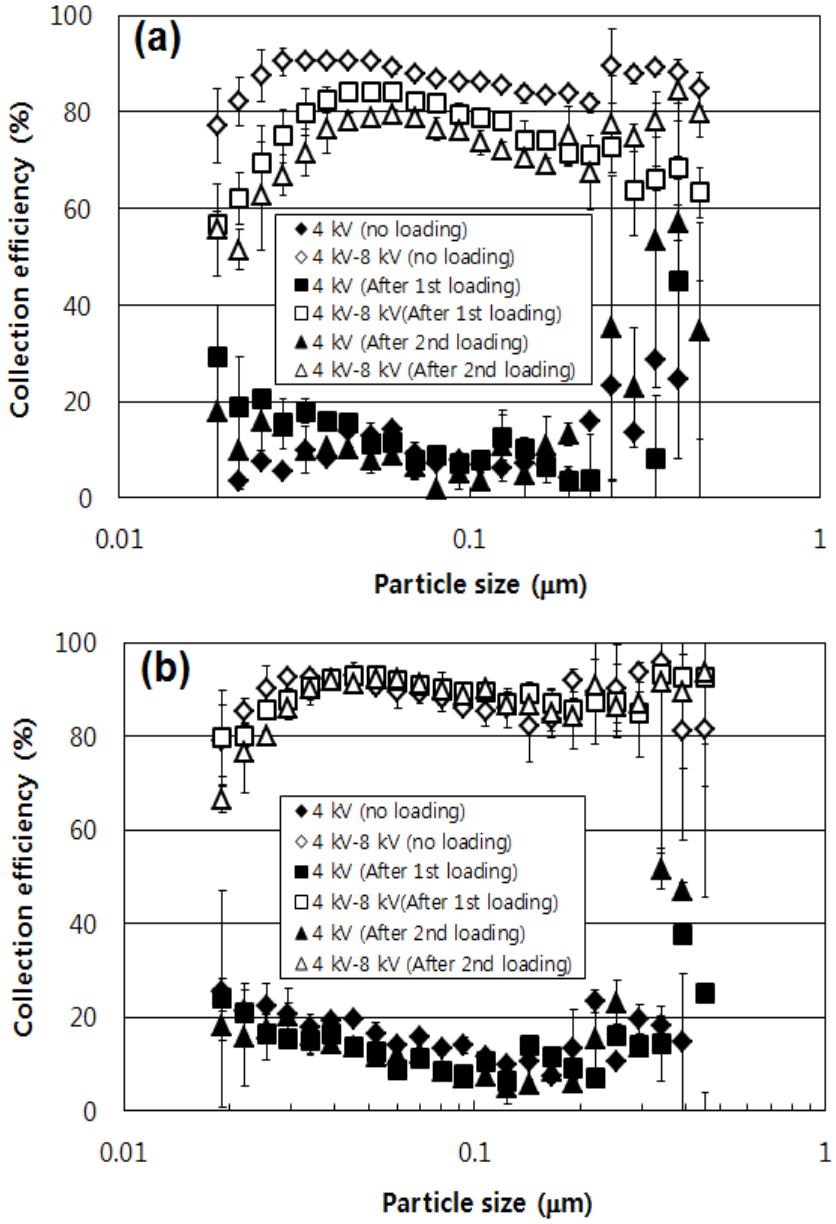

Figure. 16 Collection efficiency of the ESP plotted against particle size for different particle loadings with and without a water film on the plates. (a) Without the water film; (b) with the water film flowing at a rate of 6.5 L/min/m^2.

As shown in Figure 16 (a), the collection efficiency for submicrometer particles was approximately 90% for the clean collection plates at the beginning of the experiment over the entire size range. The average collection efficiency of the ESP fell from 90% to 75% after the first dust loading and to 70% after the second, while particle capture in the pre-charging zone without any voltage to the collection cell was maintained at approximately 10%. This result is explained by reduced electric field strength in the collection cell due to dust accumulation on the collection plates, while no significant particle deposition occurred in the pre-charger. However, as shown in Figure 16 (b), for the wet ESP, in which collection plates were continuously cleaned by water, collection efficiency was maintained at approximately 90% of the collection efficiency of the initial clean ESP after the two dust loadings.

This finding shows that high-efficiency collection performance could be achieved over a long term by continuously cleaning the collection plates with a thin water film. In contrast, conventional dry ESPs require rapping and water spraying of the collection plates to maintain their collection efficiency. The dry devices also generate particle re-entrainment, which results in a low collection efficiency for submicrometer particles.

4.1.4 Conclusion

I have developed a novel two-stage wet ESP that uses a carbon brush pre-charger and collection plates with a thin water film. The performance of the ESP was evaluated experimentally for ultrafine particles in the size range of 0.01~0.5 μm by varying the voltage levels and polarity that were applied to the pre-charger and the collection plates. The results were compared with the theoretical predictions for ESPs. The long-term performance of the ESP with and without water films was also investigated using a standard JIS dust with a size range measured in micrometers.

The experiments showed that the two-stage wet ESP with the carbon brush pre-charger resulted in approximately 10% particle capture, while producing ozone concentrations of less than 20~30 ppb at voltages up to 4 kV, regardless of polarity, which is significantly lower than the current limits set by international agencies. The low ozone emission with the carbon brush pre-charger was resulted from not effect of the material but the thin diameter of the high voltage electrode which was approximately several micorometers.

In particular, the ESP achieved a high collection performance, averaging 90% with negative voltage and 80% with positive voltage, for ultrafine particles based on number concentration. The experimental results were similar to those from the theoretical calculation with the same parameters. Furthermore, a high ESP collection efficiency could be achieved by increasing the voltages applied

to the pre-charger and collection plates. In addition, the decreased collection efficiency that occurred during dust loading without water films was completely eliminated by forming a thin water film at a water flow rate of 6.5 L/min/m^2.

The ESP described herein is thus a promising post-treatment system for removing ultrafine particles, especially in industries where small particulates are emitted in acidic and corrosive gases that could degrade the performance of conventional dry ESPs. Using positive polarity, this process could also be applied to air-cleaning devices to achieve high removal efficiency of over 80% for indoor ultrafine particles with negligible ozone production.

4.1.5 References

Adachi, M.; Kousaka, Y.; Okuyama, K. Unipolar and bipolar diffusion charging of ultrafine aerosol particles; J. Aerosol Sci. 1985, 16, 109–123.

Altman, R.; Offen, G.; Buckley, W.; Ray, I. Wet electrostatic precipitation demonstrating promise for fine particulate control – Part I; Power. Engineer. 2001, 105(1), 37-39.

Bayless, D.J.; Alam, M.K.; Radcliff, R.; Caine, J. Membrane-based wet electrostatic Precipitation; Fuel. Process. Technol. 2004, 85, 781-798.

Bell, M.L.; Peng, R.D.; Dominici, F. The exposure-response curve for ozone and risk of mortality and the adequacy of current ozone regulations; Environ. Health. Persp. 2006, 114(4), 532-536.

Bologa, A.; Paur, H.; Seifert, H.; Wascher, T.; Woletz, K. Novel wet electrostatic precipitator for collection of fine aerosol; J. Electrostat. 2009, 67, 150-153.

Bo, Z.; Yu, K., Lu, G., Mao, S.; Chen, J.; Fan, F.G. Nanoscale discharge electrode for minimizing ozone emission from indoor corona devices; Environ. Sci. Tehcnol. 2010, 44, 6337-6342.

Boelter, K. J.; Davidson, J.H. Ozone generation by indoor electrostatic air cleaners; Aerosol Science and Technology. 1997, 27(6), 689-708.

Cabane, M.; Playe, P. Mass spectra of negative ions in air-like gas mixtures at atmospheric pressure; J. Aerosol. Sci. 1980, 11, 475-482.

Cardello, N.; Volckens, J.; Tolocka, M. P.;Wiener, R.; Buckley, T. J. Performance of a Personal Electrostatic Precipitator Particle Sampler; Aerosol Sci. Technol. 2002, 36, 162-165.

Chen, C.; Huang, B.; Lin, T.; Chen, I. Hsu, C. A new negative ion generator using ZnO nanowire array; J. Electrochem. Soc. 2006, 153(10), G894-G896.

Chen, J.; Davidson, J.H. Ozone production in the positive DC corona discharge: Model and comparison to experiments; Plasma Chemistry and Plasma Processing. 2002, 22(4), 495-522.

Electrostatic Precipitator Knowledgebase. ESP Operation. Neundorfer, Inc. 2011, 1, 10-11. [online] http://www.neundorfer.com/FileUploads/CMSFiles/ESP%20Operation[0].pdf

Grinshpun, S.A.; Mainelis, G.; Trunov, M.; Adhikari, A.; Reponen, T.; Willeke, K. Evaluation of ionic air purifiers for reducing aerosol exposure in confined indoor spaces; Indoor Air 2005, 15, 235-245.

Goheen, S. C.; Larkin, E. C.; Bissell, M. G. Ozone produced by corona discharge in the presence of water; Int. J. Biometeorol. 1984, 28, 157–161.

Han, B.; Hudda, N.; Ning, Z.; Kim Y.J. Sioutas, C. Enhanced unipolar charging of concentration-enriched particles using water-based condensational growth; J. Aerosol. Sci. 2008, 39, 770-784.

Han, B.; Kim, H.J.; Kim, Y.J.; Sioutas, C. Unipolar charging of fine and ultra-fine particles using carbon fiber ionizers; Aerosol. Sci. Tech. 2008, 42, 793-800.

Han, B.; Hudda, N.; Ning, Z.; Kim, H.J.; Kim, Y.J.; Sioutas, C. A novel bipolar charger for submicron aerosol particles using carbon fiber ionizers; J. Aerosol. Sci. 2009, 40, 285-294.

Han, B.; Hudda, N.; Ning, Z.; Kim, Y.J.; Sioutas, C. Efficient collection of atmospheric aerosols with a particle concentrator-electrostatic precipitator sampler; Aerosol. Sci. Tech. 2009, 43, 757-766.

Hart, P.J.; Vastola, F.J., Walker, Jr., P.L. Oxygen chemisorption on well cleaned carbon surfaces; Carbon. 1967, 5, 363-371.

Huang, S.H.; Chen, C.C. Ultrafine aerosol penetration through electrostatic precipitators; Environ. Sci. Technol. 2002, 36, 4625-4632.

Jayaram, S.; Castle, G.S.P.; Chang, J-S.; Berezin, A.A.; Looy, P.C.; Mangal, R.; Mozes, M.S. Semi pilot plant pulse energized cold-pre-charger electrostatic precipitator tests for collection of moderately high resistivity flyash particles; IEEE T. Ind. Appl. 1996, 323(4), 851-857.

Jaasund, S.S. Control of fine particle emissions with wet electrostatic precipitation; Environ. Int. 1981, 6, 233-238.

Kulkarni, P.; Namiki, N.; Otani, Y.; Biswas, P. Charging of the Particles in Unipolar Coronas Irradiated by in-situ Soft X-ray: Enhancement of Capture Efficiency of Ultrafine Particles; J. Aerosol Sci. 2002, 33,1279-1296.

Lin, G.; Tsai, C.; Chen, S.; Chen, T.; Li, S. An efficient single-stage wet electrostatic precipitator for fine and nanosized particle control; Aerosol. Sci. Tech. 2010, 44, 38-45.

Lee, W-J.; Chen, S.J.; Liow, M.C.; Wang, L.C.; Huang, K.L. Removal efficiencies of PAHs by the electrostatic precipitator and wet scrubber; J. Aerosol. Sci. 1998; 29(Suppl. 1), S1081-S1082.

Li, M.; D. Christofides, P. Collection efficiency of nanosize particles in a two-stage electrostatic precipitator; Ind. Eng. Chem. Res. 2006, 45, 8484-8491.

Liu, L.; Guo, J.; Li, J.; Sheng, L. The effect of wire heating and configuration on ozone emission in a negative ion generator; J. Electrostat. 2000, 48, 81-91.

Musdalslien, U.I.; Standal, N.A.; Johansen, J.G.; Oehme M. Pilot plant tests with a wet electrostatic precipitator for reducing PCDD/PCDF in corrosive off-gas from magnesium production; Chemosphere 1991, 23(Nos.8-10), 1097-1108.

Nomoto, Y; Ohkubo, T.; Kanazawa, S.; Adachi, T. Improvement of ozone yield by a silent-surface hybrid discharger ozonizer; IEEE T. Ind. Appl. 1995, 31(6), 1458-1462.

Pasic, H.; Alam, M.K.; Bayless, D.J. Membrane Electrostatic Precipitator; U.S. Patent 2001, 6, 231, 643, B1.

Peterson, M.S.; Zhang, W.; Fisher, T.S.; Garimella, S.V. Low-voltage ionization of air with carbon-based materials; Plasma Sources Sci. Technol. 2005, 14, 654-660.

Staehle, R.C.; Triscori, R.J.; Ross, G.; Kumar, K.S.; Pasternak, E. The past, present and future of wet electrostatic precipitators in power plant applications. In Proceedings of the power plant air pollutant control "Mega" symposium 2003: Washington, DC, BR-1742.

Saiyasitpanich, P.; Keener, T.C.; Lu, M.; Liang, F. Control of diesel gaseous and particulate emissions with a tube-type wet electrostatic precipitator; Air & Waste manage. Assoc. 2008,58, 1311-1317.

Snyer, R.E.; Moretti, A.L.; Tonn, D.P.; Silva, A.A.; Kumar, S.; Lau, A. SO_3 and fine particulate mitigation at AES deepwater. In Proceedings of the power plant air pollutant control "Mega" symposium 2008: Baltimore, MD, BR-1814.

Spengler, J.D.; Ludwig, S.; Weker, R.A. Ozone exposures during trans-continental and trans-Pacific flights; Indoor Air 2004, 14 (Suppl 7), 67-73.

Sh. Islamov, R.; A. Krishtafovich, Y. Erosion and lifetime of tungsten, gold, and nichrome wire anodes in an ultracorona in air; IEEE Transactions on plasma science. 2013, 41(7), 1787-1793.

Suriyawong, A.; J. Hogan Jr, C.; Jiang, J.; Biswas, P. Charged fraction and electrostatic collection of ultrafine and submicrometer particles formed during O_2-CO_2 coal combustion; Fuel. 2008, 87, 673-682.

Talaie, M.R.; Fathikaljahi, J; Taheri, M.; Bahri, P. Mathematical modelling of double-stage electrostatic precipitators based on a modified Eulerian approach; Aerosol. Sci. Tech. 2001, 34(6), 512-519.

Tsai, C.J.; Lin, G.Y.; Chen, S.C. A parallel plate wet denuder for acidic gas measurement. AICHE J. 2008, 54, 2198-2205.

Trichel, G.W. The mechanism of the negative point to plane corona near onset; Phys. Rev. 1938, 54, 1078-1084.

Vijh, A. Relationship between activation energies for the thermal oxidation of metals and the semiconductivity of the oxides; Journal of materials science. 1974, 9, 985-988.

White, H.J. In Industrial electrostatic precipitation. 1st ed; Addison-Wesley Publication Company, Inc: Massachusetts, 1963.

Yehia, A.; Mizuno, A. Suppression of the ozone generation in the positive and negative dc corona discharges; International Journal of Plasma Environmental Science and Technology. 2008, 2, 44-49.

Yehia, A.; Abdel-Salam, M.; Mizuno, A. On assessment of ozone generation in dc Coronas; J. Phys. D. Appl. Phys. 2000, 33, 831-835.

Yehia, A.; Mizuno, A.; Takashima, K. On the characteristics of the corona discharge in a wire-duct reactor; J. Phys. D. Appl. Phys. 2000, 33, 2807-2807.

Yasumoto, K.; Zukeran, A.; Takagi, Y.; Ehara, Y.; Takahashi, T.; Yamamoto, T. Effect of electode thickness for reducing ozone generation in electrostatic precipitator; Denkkai Ronbunshi. 2008, 128-A(7), 689-694.

Yoo, K.H.; Lee, J.S.; Oh, M.D. Charging and collection of submicron particles in two-stage parallel-plate electrostatic precipitators; Aerosol. Sci. Tech. 1997, 27(3), 308-323.

Zhuang, Y.; Kim, Y.J.; Lee, T.G.; Biswas, P. Experimental and theoretical studies of ultra-fine particle behavior in electrostatic precipitators; J. Electrostat. 2000, 48, 245-260.

Zukeran, A.; Ikeda, Y.; Ehara, Y.; Matsuyama, M.; Ito, T.; Takahashi, T.; Kawakami, H.; Takamatsu, T. Two-stage-type electrostatic precipitator re-entrainment phenomena under diesel flue gases; IEEE. T. Ind. Appl. 1999, 35(2), 346-351.

Zukeran, A.; Looy P.C.; Berezin, A.A.; Chang, J-S.; Ito, T. Enhancement of electrostatic precipitator ultrafine particle collection efficiency by pre-chargers; J. Aerosol. Sci. 1997, 28(suppl. 1), S281-s282.

Zhu, J.; Zhang, X.; Chen, W.; Shi, Y.; Yan, K. Electrostatic precipitator of fine particles with a bipolar pre-charger; J. Electrostat. 2010, 68, 174-178.

4.2 Particle removal near to 1 mg/Nm^3 by ESPs for oxygen-pulverlized coal combustion

4.2.1 Introduction

Energy supply is currently an issue of great importance. Fossil fuels are currently the world's most important energy sources, and will continue to be dominant for many decades because alternative clean energy technologies such as solar, wind, and fuel cells are still not cost effective. Due to this technical and economic situation, coal, the most abundant fossil reserve according to the US Energy Information Administration and the International Energy Agency, will play a significant role in global power generation for the foreseeable future. However, burning coal in air also presents many challenges, including the control of particulate matter, mercury, trace metals, and carbon dioxide (CO_2) emissions. In particular, emissions of CO_2, an important greenhouse gas, should be reduced in order that coal can continue to be used in a CO_2-constrained future (Wall, 2007).

As a means of capturing CO_2 gas during combustion, the technology of oxy-fuel combustion has recently received considerable interest (McCauley et al., 2009; Czakiert et al., 2010). The basic concept of oxy-fuel combustion is to replace the combustion air with a mixture of oxygen and recycled flue gas; the resulting flue gas consists of primarily CO_2 and H_2O vapor with some N_2, O_2, and pollutants such as SOx particulates. The flue gas can be processed relatively easily to enrich the CO_2 content to over 90% in the product gas, which can be simply dried and compressed for storage (Levasseur et al., 2009).

For successful and stable CO_2 compression and purification by a CO_2 compression and purification unit (CPU), a state-of-the art flue gas cleaning system for oxy-fuel combustion is necessary to clean the flue gas to a high standard so that the CPU can work effectively over extended periods of time (Stanger and Wall, 2011; Bäck et al., 2011).

Electrostatic precipitators (ESPs) have been widely used for the collection of particles from air-pulverized coal combustion. However, due to the technical limitations of conventional dry ESPs, including particle re-entrainment during the periodic rapping of electrodes and collection plates, it is difficult for the dry ESPs to achieve the low particle emissions that are required (approximately 1 mg/m^3) for carbon capture and storage (CCS) (Burchhardt, 2009). Additionally, changes in the design and operational parameters of conventional ESPs for oxygen-pulverized coal (Oxy-PC) combustion are inevitable because the gas composition of the flue gas from the Oxy-PC combustion is significantly different from the flue gas produced by air combustion.

Several studies of the use of ESPs in oxy-fuel combustion have been conducted (Suriyawong et al., 2008; Han et al., 2010; Bäck et al., 2011). Suriyawong et al. (2008) studied the collection characteristics of submicron particles in a cylinder-wire ESP following the combustion of coal in oxy-fuels with various O_2–CO_2 and N_2–CO_2 compositions and found that particle penetration in an O_2–CO_2 fuel was one to two orders of magnitude higher than that in an O_2–N_2 fuel. Han et al. (2010) also investigated the collection efficiency of submicron particles for a laboratory scale ESP in a CO_2-enriched environment with a changing gas mixture and found that the low electrical mobility of ions resulted in a low corona current under CO_2-enriched conditions. However, these studies have been conducted with a laboratory-scale ESP and used submicron particles that are not representative of the particles emitted from industrial combustion plants; thus, they offer limited information about the design and operation of a full-scale ESP for use with oxy-fuel combustion and CCS. The Alstorm ESP research group has studied the characteristics of a dry ESP, which was operated for a 30 MWth oxyfuel pilot plant that incorporated flue gas desulfurization (FGD) and a flue gas condenser (FGC) as gas cleaning technology. However, the study focused on the particle collection performance of a dry ESP and has not evaluated changes in the collection efficiency of the ESP under different combustion conditions, such as air and oxygen firing.

In this study, we used a novel wet-type ESP with thin water films on the collection plates (water consumption <2 L/min/m^3) and located it downstream of a dry ESP and FGC that removed the particles produced from oxy-PC combustion to ensure a level of approximately 1 mg/m^3. We also investigated changes in the performance of the ESPs when the combustion conditions were varied and in the operational parameters of the ESPs using a 0.7 MW oxy-PC combustion pilot plant. The plant also included desulfurization technology in the form of an in-furnace deSOx system that sprayed limestone directly into the oxy-PC combustor.

4.2.2 Experimental set up

Figure 1 shows the overall process of the 0.7 MW oxy-PC pilot plant with CCS used in this study. The pilot plant was constructed at the Korea Electric Power Research Institute (KEPRI), Daejeon, Korea. The plant was composed of a 0.7 MW oxy-PC boiler with an in-furnace deSOx unit, an air separation unit (ASU), a gas cleaning system composed of a dry ESP, a FGC, a wet ESP with water films, and a CPU. Unlike the conventional desulphurization systems used in coal combustion power plants, an in-furnace deSOx method was employed that sprayed wet limestone directly into the boiler (Chen and Zhao, 2006; Chen et al., 2011).

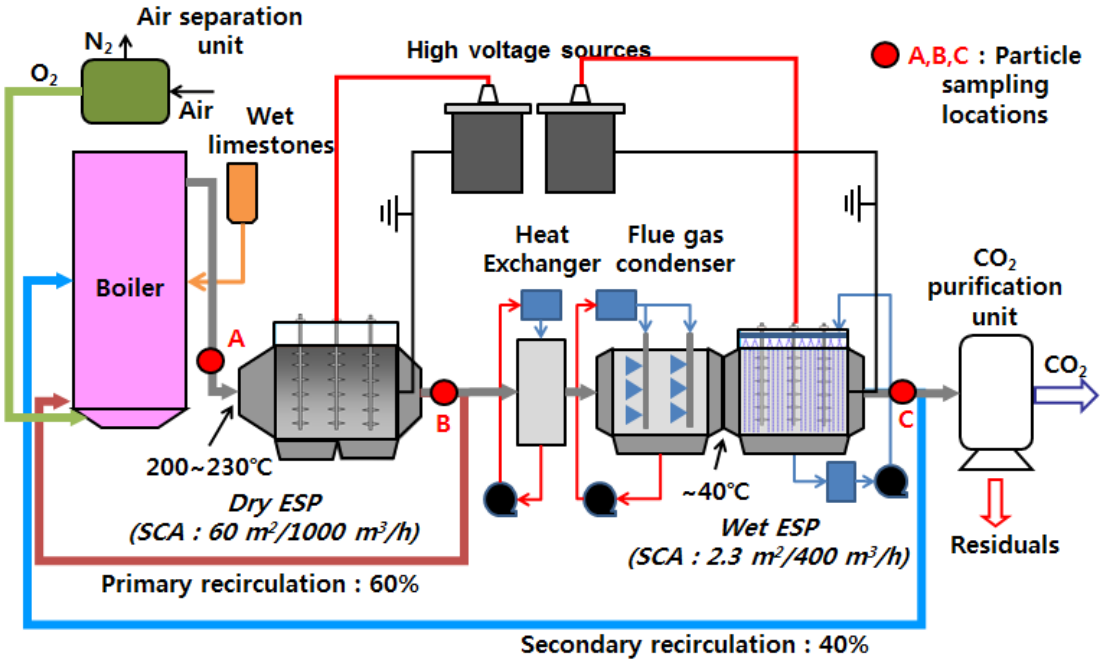

Figure 1. Schematic of the experimental set-up used in this study

As shown in Figure 1, two recirculations occurred downstream of the dry and wet ESPs. A single-field ESP with 300-mm plate spacing and a specific collection area (SCA) of 60 m^2/1,200 m^3/h was used to remove the majority of the particulates in a flue gas of 200–230℃. A heat exchanger and FGC were used to remove water by decreasing the temperature to 40–50℃. The FGC operated by wet scrubbing using water at neutral pH to remove SOx in the flue gas prior to the CPU. Fine particles are difficult to remove using a conventional dry ESP. Here, they were removed using a single-field wet ESP with 300-mm plate spacing and an SCA of 2.3 m^2/400 m^3/h, with a thin water film on the surface of the collection plates. To minimize water consumption, we used patented collection plates and nozzles (Patent No. KR101173496) described in a previous study (Kim et al., 2011). The water used to form the thin water film on the collection plates was supplied by gravitational force through 2-mm holes (separated by 5 mm) and was contained in a water reservoir that was attached to the upper back side of the collection plate. To enhance the hydrophilicity of the collection plates, which increases the water film uniformity and minimizes water consumption, the collection surfaces of the plates were first ball-blasted and then coated with an alcohol solution (Model P&T-100HX, Nanopac Co., Ltd., Korea) in which approximately 5–10 nm TiO_2 nanoparticles were dispersed. The plates were then dried with an electrical dryer at 500℃ for 30 min to strengthen the bonding of the TiO_2 particles to the collection plates. Due to the patented design, which included the surface treatment with the nano particle coating and ball blasting on the

collection plates, the water consumption was only 1.7 L/min/m^2, which was much lower than the minimum water consumption of 2.3 L/min/m^2, which had previously been reported for a wet-ESP (Lin et al., 2010). Maximum high-voltage power supplies of 70 kV/ 400 mA for the dry ESP and 60 kV/ 40 mA for the wet ESP were provided by NWL Pacific, Inc.

Table 1. Brief summary of the test campaigns in this study

Campaign	Period	Measurements		Combustion	Measurement method for pollutant emissions
1st	28th to 29th, Feb.	PM removal efficiency for Dry and Wet ESPs	PM size distribution, Coal analysis, Fly ash analysis	Air/Oxygen firing	EPA 5
2nd	3rd to 4th, May.		Voltage and current characteristics for dry and wet ESP	Air/Oxygen firing	EPA 5
3rd	30th, May to 1st, Jun.		Gas removal for wet ESP	Air/Oxygen firing	EPA 5, 8
4th	18th to 19th, Sep.		Size dependent particle removal for wet ESP	Air/Oxygen firing	Optical particle counter

From February to September 2012, four test campaigns to determine the ESP performance were conducted, and the resulting data is summarized in Table 1. Particle concentrations were measured at three different points (A, B, and C in Figure 1) upstream and downstream of the dry ESP, and downstream of the wet ESP. Seventeen gravimetric measurements based on the EPA Method 5 (EPA, 1996) were conducted by Han Kook Environment & Consultant Co., Ltd. Particle concentration measurements during the third test campaign were also conducted using our own optical particle counter (Model 1.109, Grimm, Germany) with an ejector-type dilutor (DEED, Dekati, Finland) to minimize the effect of water vapor on the measurements. To compare the physical characteristics of fly ash from air and oxygen combustion with those from the in-furnace deSOx system, particles were sampled during different combustion conditions upstream of the dry ESP (sampling location A). The resistivity of the fly ash resulting from each combustion process was measured by Lodge-Cottrell, Inc., in accordance with IEEE-548, which provides the standard criteria for the laboratory measurement of fly ash resistivity (IEEE, 1984). The size distribution of the particles produced by the different combustion conditions was measured using both on- and off-site methods, i.e., a particle size analyzer with photon cross-correlation spectroscopy was used offsite (Nanophox, Sympatec GmbH, Germany), and on-site, an optical particle counter was used (Model 1.109, Grimm, Germany).

The particle removal performance of the ESPs in this study was expressed as the particle collection efficiency (η), which was obtained using the following equation:

$$\boldsymbol{\eta = \left(1 - \frac{C_{down}}{C_{up}}\right) \times 100}\ (\%) \quad (1)$$

where η is the collection efficiency, and C_{down} and C_{up} are the particle concentration downstream and upstream of the ESPs, respectively.

The initial purpose of the pilot test with the 0.7 MW boiler was to establish the design parameters of a dry ESP for Oxy-PC combustion. The performance of the dry ESP during air and oxygen combustion was compared, and the physical characteristics (e.g., size distribution and resistivity) of the particles produced were also compared. The pilot tests also confirmed the ability of the wet ESP with a thin water film to achieve a particle concentration of approximately 1 mg/Nm^3 by removing ultrafine particles.

4.2.3 Results and discussion

(1) Physical and chemical characteristics of fly ash produced under different combustion conditions

The experiments was conducted using Berau (sub-bituminous) coals with the highest heating value of 6,510 kcal/kg and a supply rate into the 0.7 MW_{th} boiler of 92.48 kg/hr. During oxy-firing, wet limestone ($CaCO_3$) for deSOx was sprayed directly into the boiler at a normalized stoichiometric ratio of [Ca]/[S] (NSR) 2.0.

Table 2. Summary of the chemical characteristics of the test coals and fly ash collected from the dry ESP in this study

Coal analysis (wt%)		Ash analysis (wt%)		
Proximate Analysis		Components	Ashes from coal analysis	Ashes from the dry ESP at the 0.7 MW_{th} Oxy-PC pilot
Moisture	2.35	SiO_2	47.14	29.9
Ash	8.00	Al_2O_3	17.50	14.9
Volatile Matter	40.12	Fe_2O_3	11.41	7.71
Fixed Carbon	49.53	MgO	2.57	3.04
Ultimate Analysis		K_2O	1.48	1.26
Moisture	2.35	BaO	0.14	0.13
Ash	8.00	Na_2O	3.18	3.01
Carbon	69.08	P_2O_5	0.44	0.40
Hydrogen	4.61	TiO_2	0.94	0.58
Nitrogen	1.49	CaO	6.84	23.2
Sulphur	0.94	SO_3	6.6	8.3
Oxygen	13.53	others	1.52	7.57

The basic characteristics of the coals used in this study and the resulting ashes are given in Table 2. The main chemical components of the ash produced from Berau coal, in order of quantity were SiO_2, Al_2O_3, Fe_2O_3, and CaO, which was considered typical. The main chemical components in the ash collected from the dry ESP at the 0.7 MWth Oxy-PC pilot plant, in order of quantity, were SiO_2, CaO, Al_2O_3, and Fe_2O_3. As expected, there was more CaO in the ash collected from the ESP due to the addition of $CaCO_3$ as a desulfurizing agent during oxy-firing.

Figure 2 shows a comparison of the size distributions of the fly ash produced during air combustion without spraying limestone and oxygen combustion with that resulting when limestone sprayed into the boiler at a NSR [Ca]/[S] of 2.0. The size distributions under the different combustion conditions, measured using off- and on-site measurement devices, were almost identical. The modal diameter at which the maximum concentration was observed was 2–4 μm regardless of the measurement method. This result was also observed in a previous study reported by the Alstom ESP research group at a 30 MW_{th} oxyfuel plant in Schwarze Pumpe, Germany (Bäck et al., 2011). There was no large increase in the particle concentration during oxygen combustion with limestone sprayed into the boiler at an NSR of 2.0 compared with air combustion, as the amount of wet limestone sprayed into the boiler was only approximately 2% of the total amount of coal supplied.

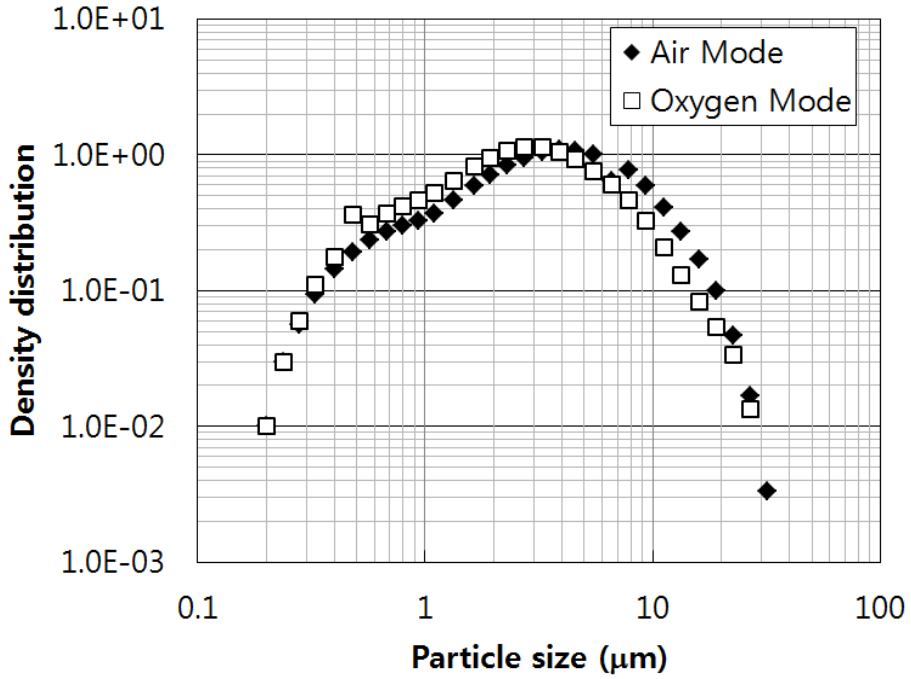

a) by off-site measurement

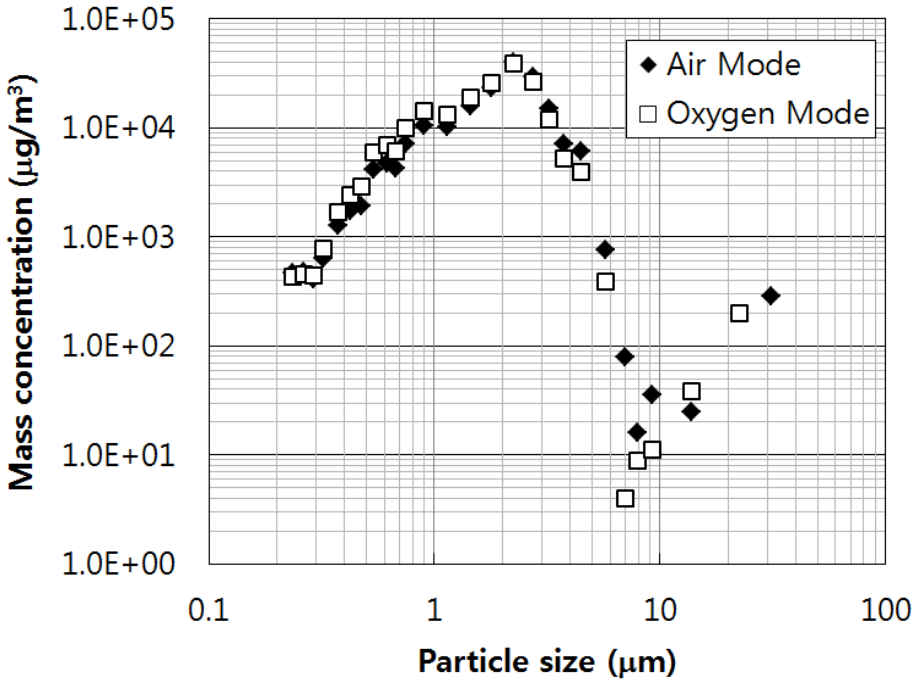

b) by on-site measurement

Figure. 2 Size distributions of fly ash collected before the dry ESP with air firing and oxy-firing with wet limestone sprayed at an NSR of 2 a) by off-site measurement and b) by on-site measurement

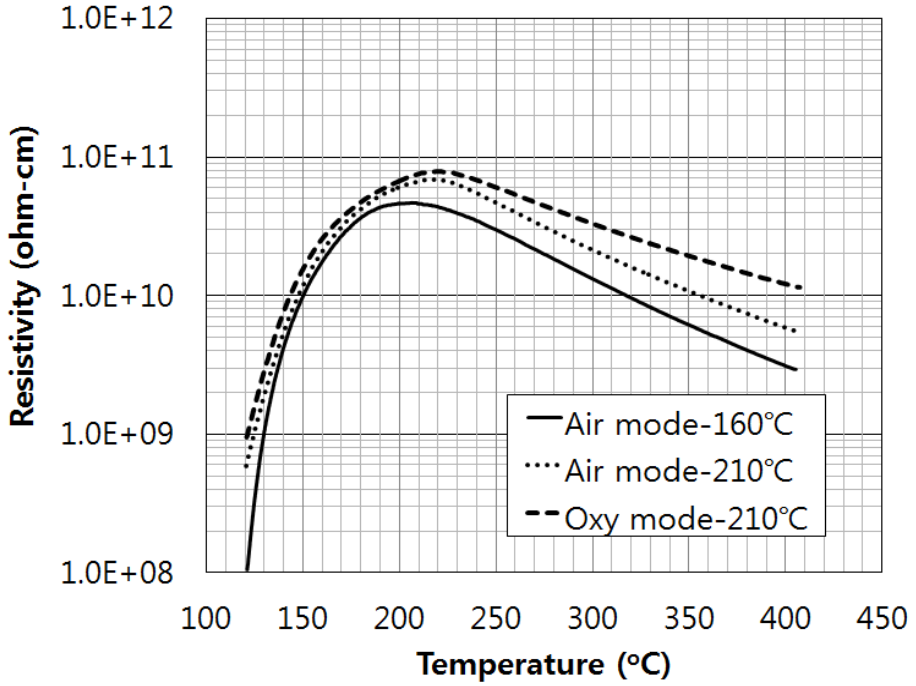

Figure. 3 Resistivity of fly ash collected before the dry ESP with air firing and oxy-firing with wet limestone sprayed at an NSR of 2.

Figure 3 shows a comparison of the resistivity of the fly ash produced under the three

different combustion conditions according to temperature. Two dust samples were sampled from the inlet of the dry ESP at 160℃ and 210℃ during the air-firing mode, and one at 210℃ during oxy-firing with the in-furnace deSOx system. The fly ash produced from all samples ranged in resistivity from 1E8 ohm·cm at low temperatures to 4–7E10 ohm·cm at the resistivity peak, which occurred at 190–220℃. The resistivity of the ash sampled at 160℃ was also lower than that of ash sampled at higher temperatures, which is typical. The difference in the resistivity between the air and oxy-firing conditions was negligible at around 190–230℃, which was the operating temperature of the dry ESP in this study, because the back corona is prevalent when the resistivity is high, i.e., above 2E11 ohm·cm (EPA, 2003). It was found that even if the ratios of the quantity of major chemical components between combustion processes was slightly different, the physical properties of the particles from oxy-PC combustion with in-furnace deSOx were not significantly different to those from air-PC combustion in terms of particle size and resistivity, which are important design parameters for a dry ESP.

(2) Electrical characteristics of dry and wet ESPs under different combustion conditions

Figure 4 shows the variation in current against the voltages applied to the dry ESP under the different combustion conditions investigated in this study. During the oxygen firing, a limestone solution with NSR of 2 was sprayed directly into the boiler as a deSOx technique. The corona current increased with increasing gas temperature at the same applied voltage due to the increased mobility of the ions generated at 200℃ (Noll, 2002). The corona current decreased significantly for the same applied voltage during oxygen combustion when the CO_2 fraction in the flue gas was high due to two occurrences of flue gas recirculation, shown in Figure 1. This has also been observed in previous studies (McDonald et al., 2009; Han et al., 2010) and can be explained by the lower electrical mobility of the ions when the CO_2 concentration in the flue gas is high. Despite the similarity in the properties of particles produced by air and oxy-firing, which were related to the ESP design, it is likely that when the same voltage applied to the ESP during oxygen combustion was applied during air combustion, lower collection efficiency resulted due to the lower corona currents generated for the same applied voltage.

Figure 5 shows the current variation against the voltages applied to the wet ESP for the different combustion modes. The gas temperature was approximately 50℃, and the current was lower than that used with the dry ESP because the specific collection area of the wet ESP was smaller than for the dry ESP by 4/60. As with the results for the dry ESP, the corona currents in the

wet ESP with oxy-PC combustion were also lower than those with air-PC combustion for the same applied voltage due to the high concentration of CO_2 in the flue gas. The corona discharge characteristics of ESPs with and without water films were also almost identical due to the uniformly thin water layer that formed on the collection plates of the ESP, with a low water consumption of only 4 L/min/2.4 m^2.

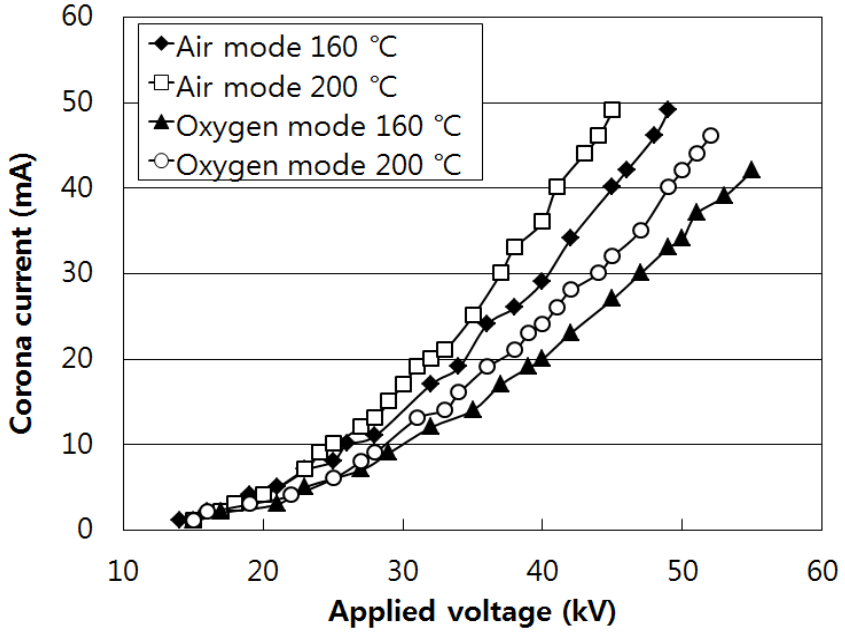

Figure. 4 Voltage-current curves of the dry ESP with different combustion modes and gas temperatures.

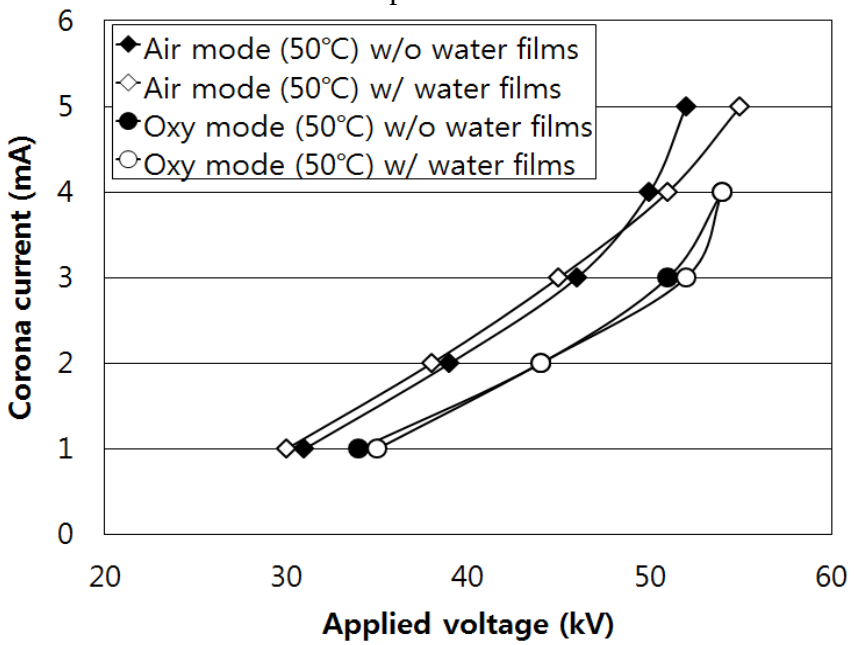

Figure. 5 Voltage-current curves of the wet ESP with different combustion modes.

(3) Particle collection characteristics of the dry ESP

In this study, I used Chochet's charging and Deutsch's collection equations for theoretical analysis because these are used many previous studies (Parker, 1997; Park and Chen, 2002; Xiangron et al., 2002) for the particles ranged from 0.1 to 10 μm. The calculation methods were described in Chapter II with equation (1) to (4). Also in this study, the collection efficiency of an ESP for different combustion conditions, such as oxygen and air firing, can vary with changes in the physical properties of the flue gas flowing into the ESP. The parameters that vary include the viscosity and mean free path of the flue gas, which affect the Cunningham factor, particle charge, and thus the migration velocity. In this study, the viscosity and mean free path of exhaust gases from different combustions were calculated using reference values for the gases (Wikipedia, 2014; NIST, 2014) and formulas used by previous researchers (Sutherland, 1893; Jennings, 1988), which are as follows:

$$\mu = \mu_0 \frac{T_0 + C}{T + C}\left(\frac{T}{T_0}\right)^{3/2} \quad (2)$$

$$\lambda = \frac{2\mu}{P\left(\frac{8M}{\pi RT}\right)^{1/2}} \quad (3)$$

where μ is the dynamic viscosity at a certain temperature (T), C is Sutherland's constant, μ_0 and T_0 are the reference viscosity and temperature, respectively, P is pressure, M is molar mass, and R is the gas constant (8.134 J/mol·K). The viscosity and mean free path of mixed gases from air and oxygen combustion were then obtained by the arithmetic mean of the free path and viscosity of each gas component at a certain temperature.

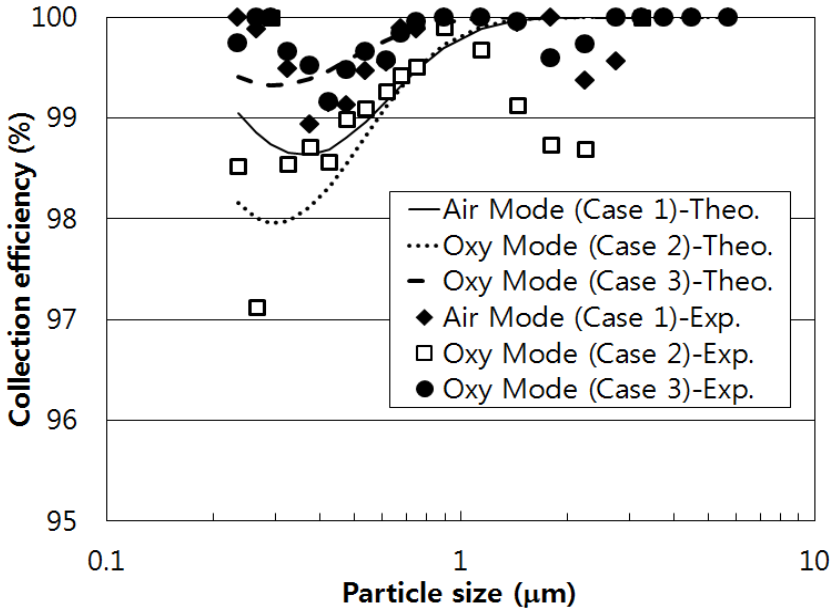

Figure 6. Comparison of the collection efficiency as a function of particle size as observed in this

study and theoretically predicted for the different combustion and voltage conditions.

Table 3. Test conditions for the comparison between experimental and theoretical analysis

Conditions		Case 1	Case 2	Case 3
Combustion type		Air	Oxygen	Oxygen
Gas temperature (℃)		200	200	200
Applied voltage (kV)		45	45	51
Corona current (mA)		49	32	44
Corona power (W)		2205	1440	2244
Gas composition at a dry ESP (%)	CO_2	16.7	67	67
	O_2	4	5.5	5.5
	H_2O	10	20	20
	N_2	69.3	7.5	7.5
Gas properties from theoretical calculation	μ (Pa·sec)	2.393E-5	2.217E-5	2.217E-5
	λ (μm)	0.1082	0.0899	0.0899
Particle property (at 0.3-0.5 μm)	$Q_{p,\infty}$ (×1.6E-19As)	2.43	2.24	2.54
	Cu	1.8	1.65	1.65
	W_{th} (m/s)	0.0241	0.0223	0.0286

Figure 6 shows a comparison of the collection efficiency of a dry ESP as a function of particle size as found in this study and the efficiency predicted by a theoretical analysis, which was mentioned above. The collection area of the dry ESP was 60 m^2, and the gas flow rate was 1,200 m^3/h. The other experimental and theoretical parameters are summarized in Table 3. Experimental collection efficiencies were similar to those predicted by Deutsch's ESP collection theory and Cochet's charging theory, particularly for Cases 2 and 3 with particles larger than 0.4 μm. Also, the lowest collection efficiencies for both cases were observed between 0.3 and 0.5 μm, which is typical for dry ESPs (Parker, 1997). Even though the theoretical collection efficiency of Case 3 (51 kV/44 mA and 2200 W) was higher than that of Case 1 (45 kV/49 mA and 2200 W) during air combustion, the experimental efficiencies of Cases 1 and 3 were similar. This could be explained by the strong theoretical dependence of the particle charge on the applied voltage with the assumption of sufficient ion density and charging time (Hinds, 1999); thus, the particle charge in Case 3 was higher than that in Case 1. However, the ion density in Case 3 during oxygen firing, which was related to the corona current, could become lower than that in Case 1. The effects of both the increased applied voltage

and the decreased corona current in Case 3 could result in almost the same collection performance as in Case 1.

Figure 7 shows the variation in experimental collection efficiency in terms of the gravimetric concentration plotted against the calculated collection efficiency based on the fact that in an ESP, the collection efficiency is exponentially expressed by the amount of power supplied by the corona divided by the gas flow rate (Electrostatic Precipitator Knowledgebase, 2014). The average mass concentration before the dry ESP was 11.1 g/m^3, and the average flow rate was approximately 1,200 m^3/hr. The collection efficiencies were exponentially dependent on the values calculated according to power consumption and flow rate regardless of the type of combustion. The results shown in Figures 6 and 7 indicate that the reduction in the efficiency of an ESP by the corona current decrease during oxygen firing compared with air firing could be recovered by increasing the applied voltage to make the power consumption the same as that for air firing.

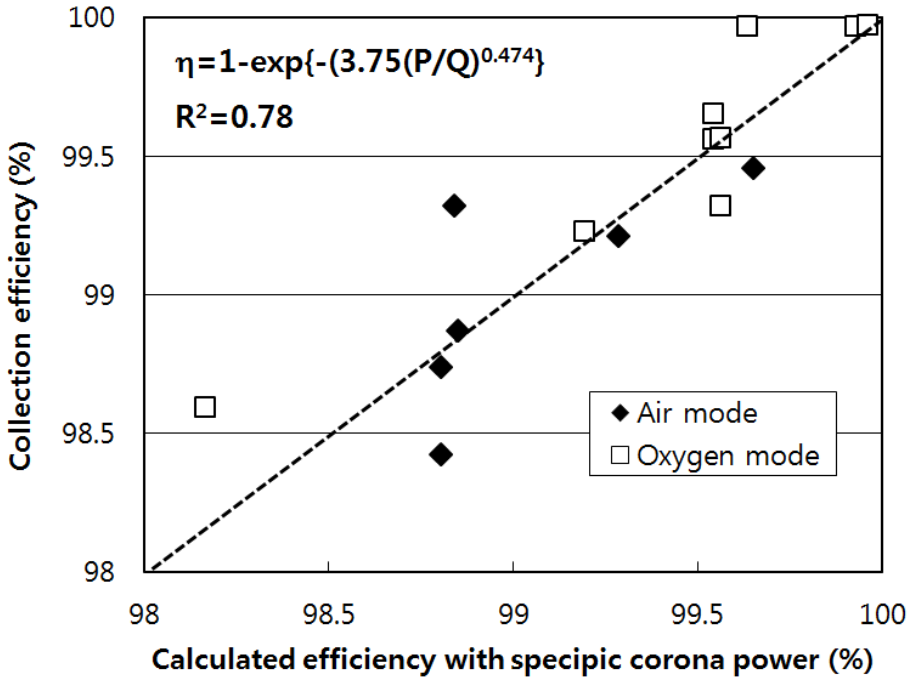

Figure. 7 Gravimetric measurements of the particle collection efficiency of the dry ESP against the collection efficiency calculated using specific corona power [corona power (P)/flow rate(Q)].

(4) Particle collection characteristics of the wet ESP

The particle number and volume concentrations upstream and downstream of the wet ESP were measured by an optical particle counter connected to an ejector-type dilutor with a dilution ratio

of 1:1900, which was carefully measured with ambient air before the experiment. Water with a neutral pH was supplied at a rate of 4 L/min to form a thin water film on each of four collection plates in the wet ESP at an SCA of 2.4 m^2 /400 Nm^3/h.

Figure 8 shows the variation in the size distributions of particles upstream of the wet ESP based on particle number and volume. Unlike the size distribution before the dry ESP shown in Figure 2, the mode diameters at which the highest particle concentrations were observed based on particle number and volume were located at 0.3 and 0.5 μm, submicrometer size ranges that are difficult to remove.

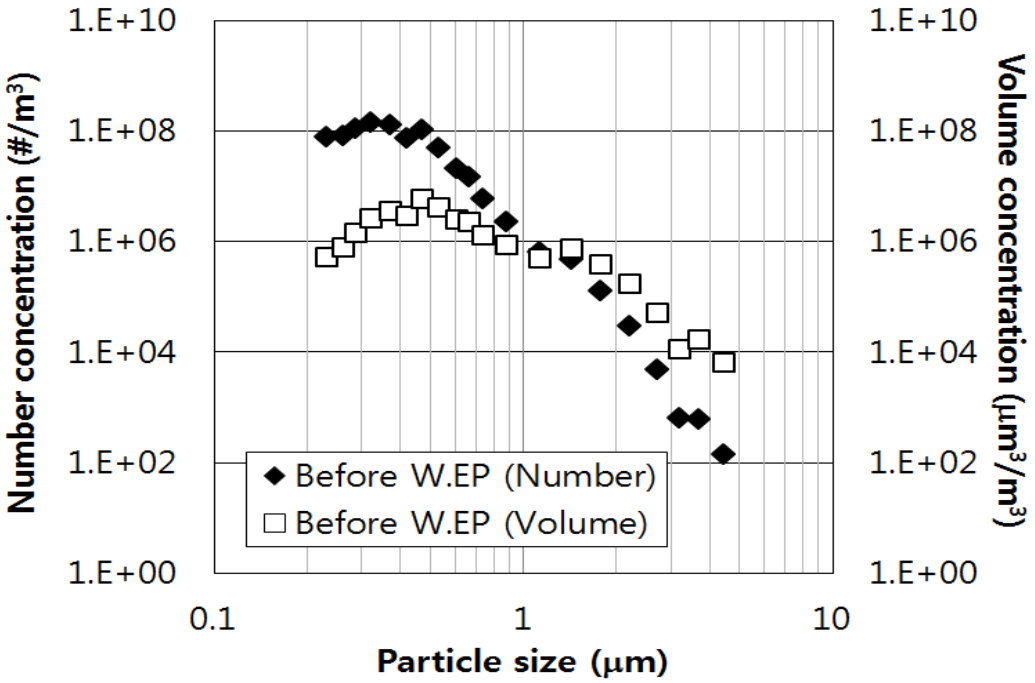

Figure 8. Variation in the size distribution of the particles upstream of the wet ESP based on particle number and volume.

Figure 9 shows the variation in collection efficiency plotted against particle size for different voltages applied to the wet ESP. The collection efficiency was calculated for particles before and after the ESP with the applied voltage increasing up to 60 kV. The collection efficiencies increased as particle size and applied voltage increased; however, the lowest collection efficiency was not observed at a specific size range because the optical particle counter measured particles from 0.25 to 30 μm. Even if the majority of the particles shown in Figure 8 were in the size range of 0.25–1 μm, more than 80% of all the particles were efficiently collected in the wet ESP with a minimum voltage and current combination of 50 kV/ 3 mA. The collection efficiency was over 90% at an applied voltage of 60 kV for 0.3 μm particles.

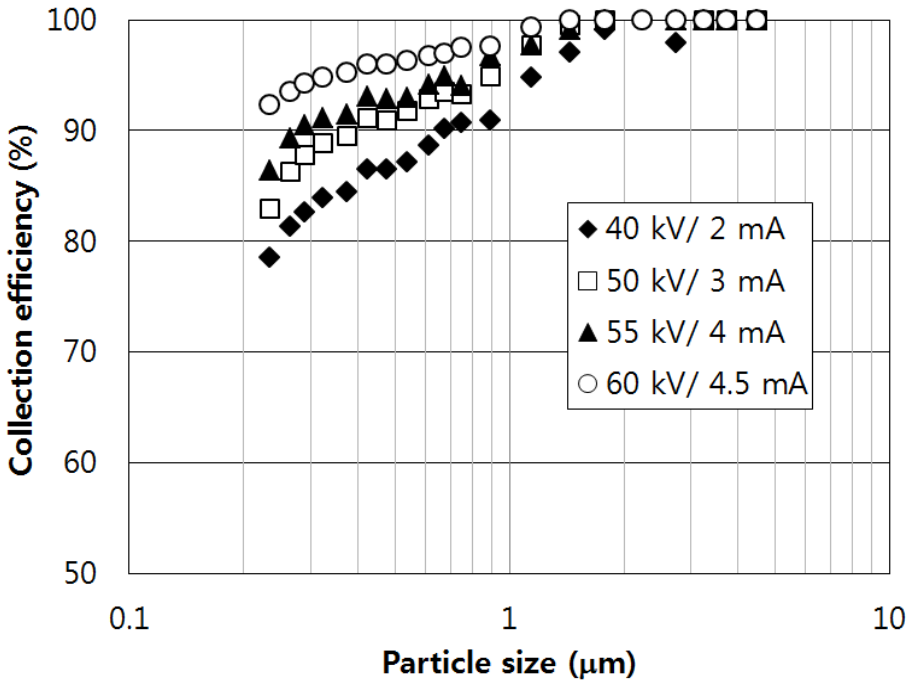

Figure 9. Variation in the collection efficiency plotted against particle size for different voltages applied to the wet ESP.

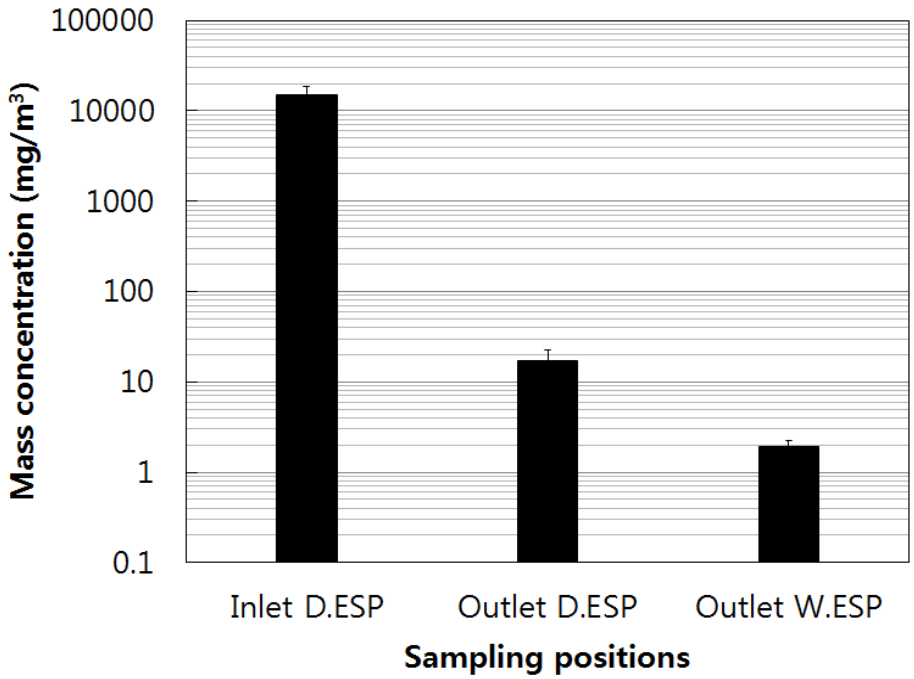

a) PM removal

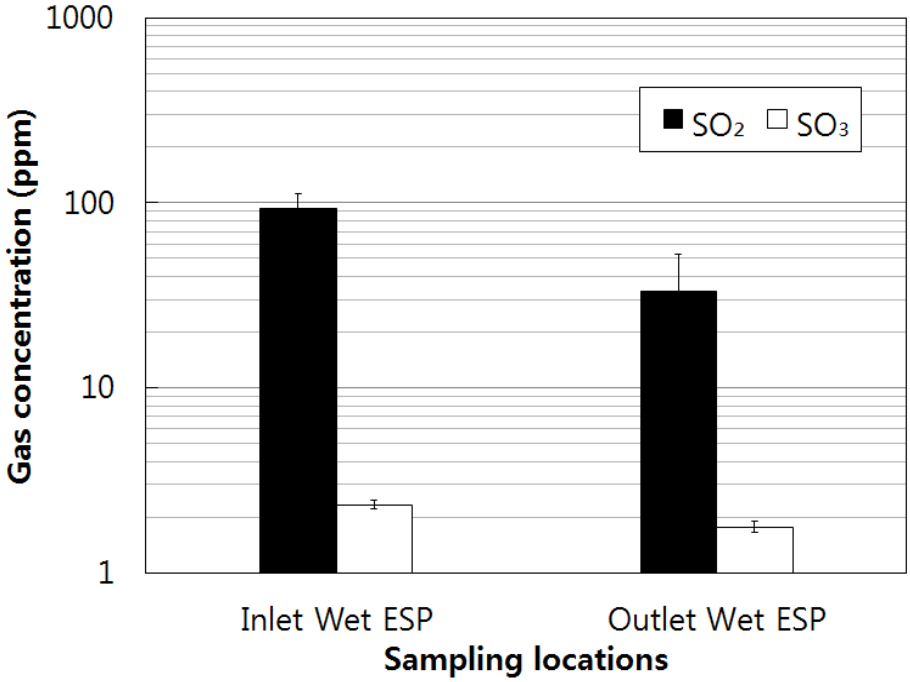

b) SOx removal

Figure 10. Particle and SOx concentrations at different sampling locations in this study. a) PM removal; b) SOx removal

Figure 10 shows the particle and SOx concentrations simultaneously measured by the EPA methods 5 and 8 (EPA, 1996a; 996b) at different sampling locations. The voltages applied to the dry and wet ESPs were kept at their maximums of approximately 60 kV/ 60 mA and 60 kV/ 4.5 mA, respectively. Figure 10 (a) shows the average particle concentrations from seven measurements during the third test campaign. The average gravimetric concentrations downstream of the wet ESP were only 1.8 mg/m^3 due to the additional reduction in small particles in the wet ESP, and those upstream and downstream of the dry ESP were 11.1 g/m^3 and 19.0 mg/m^3, respectively. Moreover, the concentrations of SO_2 and SO_3 decreased from 93.4 and 2.34 ppm to 33.2 and 1.8 ppm, respectively. This was attributable to the fact that the wet ESP removed the mists that were generated by the condensation of the gases passing through the FGC and the wet ESP.

4.2.4 Conclusion

I investigated variations in the performance of dry and wet ESPs for different combustion conditions and ESP operating parameters at a 0.7 MW oxy-PC combustion pilot plant that utilized an in-furnace deSOx process and CCS. A novel water film was applied to the ESP, which consumed

only 1.7 L/min/m^2 during the final gas cleaning stage to achieve very low particle emissions of approximately 1 mg/m^3. The dry and wet ESPs had single-field geometry with a plate spacing of 30 mm and SCAs of 60 m^2/1,200 m^3/hr and 2.4 m^2/400 m^3/hr, respectively. We also compared the experimental results with theoretical predictions using the Deutsch equation and Cochet's charging model, with the physical and chemical properties of exhaust gases changing due to the different types of combustion.

The experimental results showed that the size distributions of particles emitted from the different combustion conditions were almost identical, and the mode diameter at which the maximum concentration was measured was located at 2–4 μm. This size range also produced the largest particle resistivity for an operational temperature of around 200℃. However, the corona current decreased significantly with the same applied voltage during oxygen firing when the CO_2 concentration in the flue gas was high, which resulted in low collection efficiency compared with the results at the same applied voltage with air firing. This decrease was also found in the theoretical analysis. The decrease in the particle collection efficiencies was overcome by increasing the voltage to the dry ESP, so that the same corona power was applied as during the air firing because the collection efficiencies were exponentially dependent on the power consumption divided by gas flow rate regardless of the type of combustion.

Unlike with the dry ESP, the mode diameters of particles flowing into the water film ESP in this study were located at 0.3 and 0.5 μm based on particle number and volume, and the corona characteristics of the wet ESP with and without water films were almost identical. In particular, the collection efficiency of the wet ESP was higher than 90% even against fine particles including mists, resulting in a total particle collection efficiency of the gas cleaning system for the 0.7 MW pilot plant of 99.98% (corresponding to the total particle gravimetric concentration of only 1.8 mg/m^3) at the inlet of the CCS facility when the wet and dry ESPs were used simultaneously. The use of the wet ESP also led to the additional removal of SO_2 and SO_3 by 64.5 ± 19.4% and 23.1 ± 6.9%, respectively, due to the thin water film on the collection plates.

4.2.5 References

Bäck, A., Grubbström, J., Ecke, H., Strand, M., and Pettersson, J. (2011). Operation of an electrostatic precipitator at a 30 MWth oxyfuel plant. Proceeding of the 12th International Conference on Electrostatic Precipitation, May 9–13, Nuremberg, Germany.

Burchhardt, U. (2009). Experiences from commissioning and test operation of Vattenfall's oxyfuel

pilot plant. Proceeding of the 1st International Oxyfuel Combustion Conference, Sep 7-11, Cottbus, Germany.

Chen, C., and Zhao, C. (2006), Mechanism of highly efficient in-furnace desulfurization by limestone under O_2/CO_2 coal combustion atmosphere. International & Engineering Chemistry Research, 45(14), 5078-5085.

Chen, J., Yao, H., Zhang, P., Xiao, L., Luo, G., and Xu, M. (2011). Control of PM1 by kaolin or limestone during O_2/CO_2 pulverized coal combustion. Proceedings of the Combustion Institute, 33, 2837-2843.

Czakiert, T., Sztekler, K., Karski, S., Markiewicz, D., and Nowak, W. (2010). Oxy-fuel circulating fluidized bed combustion in a small pilot-scale test rig. Fuel Processing Technology, 91, 1617-1623.

Electrostatic precipitator knowledgebase. ESP Design parameters and their effects on collection efficiency. Neundorfer, Inc., Chapter 3, pp. 1–34. Last visited [online] http://www.neundorfer.com/FileUploads/CMSFiles/ESP%20Design%20Parameters[0].pdf, Jan. 23, 2014.

EPA. Air pollution control technology fact sheet. US Environmental Protection Agency, EPA-452/F-03-027. Issued 07/08/2003.

EPA. Method 5 (1996). Determination of particulate matter emissions from stationary sources. US Environmental Protection Agency. Issued 08/16/1996.

EPA. Method 8 (1996). Determination of sulphuric acid and sulphur dioxide emissions from stationary sources. US Environmental Protection Agency. Issued at 10/29/1996.

Han, B., Kim, H.J., and Kim, Y.J. (2010). Fine particle collection of an electrostatic precipitator in CO2-rich gas conditions for oxy-fuel combustion. Science of the Total Environment, 408(21), 5158-5164.

Hinds, W.C. (1999). Aerosol Technology: properties, behaviour, and measurement of airborne particles. New York: John Wiley & Sons, Inc., (Chapter 15).

IEEE. IEEE Std 548-1984 (1984). IEEE Standard Criteria and Guidelines for the Laboratory Measurement and Reporting of Fly Ash Resistivity. The Institute of Electrical and Electronics Engineers, Inc., Issued 12/21/1984.

Jennings, S. G. (1988). The mean free path in air. Journal of Aerosol Science, 19(2), 159-166.

Kim, H.J., Han, B., and Kim, Y.J. (2012) Electrostatic precipitator using precipitation plates. Patent No. KR101173496 B1.

Kim, H.J., Han, B., Kim, Y.J., Hwang, K.D., Oh, W.S., Yoo, S.Y., and Oda, T. (2011). Fine particle removal performance of a two-stage wet electrostatic precipitator using a non-metallic pre-charger. Journal of the Air & Waste Management Association, 61 (12), 1334-1343.

Levasseur, A.A., Chapman, P.J., Nsakala, Y.N., and Kluger, F. (2009). Alstom's oxy-firing technology development and demonstration—near-term CO_2 solutions. In Proceedings of the 34th International Technical Conference on Clean Coal & Fuel Systems, May 31–June 4, Clearwater, FL, USA.

Lin, G.Y., Tsai, C.J., Chen, S.C., Chen, T.M., and Li, S.N. (2010). An efficient single-stage wet electrostatic precipitator for fine and nanosized particle control. Aerosol Science and Technology, 44, 38–45.

McCauley, K.J., Farzan, H., Alexander, K.C., McDonald, D.K., Varagani, R., Prabhakar, R., Tranier, J-P., and Perrin, N. (2009). Commercialization of oxy-coal combustion: applying results of a large 30 MWth pilot project. Energy Procedia, 1, 439-446.

McDonald, D.K., Farzan, H., Varagani, R., Docquier, N., and Perrin, N. (2009). Evaluation of oxy-coal combustion at a 30 MW_{th} pilot. Proceeding of the 1st International Oxyfuel Combustion Conference, Sep 7–11, Cottbus, Germany.

NIST Chemistry WebBook. Fluid Properties. National Institute of Standards and Technology, Last visited [online] http://webbook.nist.gov/cgi/cbook.cgi?Name=H2O&Units=SI Jan. 23, 2014.

Noll, C. G. (2002). Temperature dependence of dc corona and charge-carrier entrainment in a gas flow channel. Journal of Electrostatics, 54, 245-270.

Park, J.H., and Chen, C.H. (2002). An improved modeling for prediction of grade efficiency of electrostatic precipitators with negative corona. Journal of Aerosol Science, 3, 673-694.

Parker, K.R. (1997). Applied Electrostatic Precipitation. London: Blackie Academic & Professional, (Chapter 3).

Stanger, R., and Wall, T. (2011). Sulphur impacts during pulverised coal combustion in oxy-fuel technology for carbon capture and storage. Progress in Energy and Combustion Science, 37, 69-88.

Suriyawong, A., J. Hogan Jr., C., Jiang, J., and Biswas, P. (2008). Charged fraction and electrostatic collection of ultrafine and submicrometer particles formed during O_2–CO_2 coal combustion. Fuel, 87, 673-682.

Sutherland, W. (1893). The viscosity of gases and molecular force. Philosophical Magazine, S. 5, 36, 507-531.

Wall, T.F. (2007). Combustion process for carbon capture. Proceedings of the Combustion Institute, 31, 31-47.

Wikipedia. Viscosity. Wikimedia Foundation, Inc., Last visited [online] http://en.wikipedia.org/wiki/Viscosity Jan. 23, 2014.

Xiangron, Z., Lianze, W., and Keqin, Z. (2002). An analysis of a wire-plate electrostatic precipitator. Journal of Aerosol Science, 33, 1595-1600.

Chapter V

Combination of ESP and metallic filter for submicron particles in high temperature gases from diesel engines

5.1 Development of electrostatic diesel particulate matter filtration systems combined with a metallic flow through filter and electrostatic methods

5.1.1 Introduction

Diesel engines have been widely used for on- and off-road vehicles and machinery due to their advantages of superior fuel efficiency and durability compared to gasoline engines (Monaghan, 2000; Karra and Kong, 2010; Maricq, 2007). Furthermore, with increasing oil prices, the development of post-treatment technologies such as DPF and DeNOx catalysts, and the increasing world-wide demand for tighter controls on CO_2 emissions in order to tackle global warming, diesel-driven cars have become a viable alternative to gasoline-powered personal automobiles in many countries. Despite of their lower fuel consumption, longer durability, and lower CO_2 emissions compared with gasoline-driven cars, it is well known that diesel engines emit significant amounts of Particulate Matters (PMs) and Nitrogen Oxides (NO_x), and thus contribute to the overall PM and NO_x pollution of the outdoor environment (Yoon and Cho, 2009; An et al., 2006; Jacobs et al., 2006; Jeong et al., 2008). In particular, off-road diesel engines contribute approximately 50% of the total particulate emissions from combustion engines (Burtscher, 2005). Due to these environmental concerns, regulations on PM emission from diesel engines for on- and off-road use (Euro V, VI and Tier III, IV standards) are becoming more stringent. Also, the scope of these regulations has also broadened from passenger vehicles to construction, agricultural, and marine equipment (Burtsher, 2005; Johnson, 2006; Johnson, 2008; Fukuoka et al., 2009).

Furthermore, all diesel engines, even newly-developed ones, produce similar amounts of ultrafine particles, and it is the presence of these that largely determines the number concentration of PM in diesel exhaust. Harmful effect of diesel particles on human beings is known to be related to particle size, and the presence of smaller particles may be linked with more serious respiratory or

cardiovascular diseases (HEI, 2002). Therefore, regulations on total particle mass concentration for PM emission from diesel vehicles are now based on both particle mass and number concentration, and this reflects a concern regarding the impact of diesel nanoparticle emission on human health, e.g. as the European Union adopts the Euro V and VI emission standards (Ristovski et al., 2006; Wallace et al., 2007; Myung et al., 2011).

In order to reduce both the mass and number concentrations of PM in the exhaust gases of diesel vehicles, post-treatment systems using ceramic Diesel Particulate Matter (DPF) filters have been commercialized for the retrofit of selected vehicles, and are on commercialization in light and heavy duty diesel automobiles as well. Wall-flow type ceramic filters, coated using metal catalysts, have shown over 90% in filtration efficiency with the diesel particulates. However, the diesel ceramic filters still have problems such as insufficient reliability and excessively high pressure drop because of clogging by solid particles under lower exhaust temperature conditions (Saito et al., 2010; Hayashi et al., 2009). Furthermore, excessive heat release and an unbalanced thermal gradient throughout the filter during filter regeneration cause mechanical cracking and failure of the ceramic filter (Saiyasitpanich et al., 2007).

The development of alternative of ceramic DPF designs has generated considerable research interest. In particular, PM control devices manufactured using metallic materials, have shown considerable promise in PM emission control technology, because these devices can exhibit a relatively low pressure drop and avoid the numerous problems and complex structure of DPFs. As a result of these benefits, many researchers have investigated the development of a PM filtration system using metallic filters (Yoon and Cho, 2009; Brück et al., 2001; Müller-Haas et al., 2007). Yoon and Cho (2009) and An et al. (2006) studied the design of metallic foam filter and analyzed its aerodynamic performance, differential pressure drop, and filtration efficiency. Their experimental results showed that the filter removed more than 50% of the diesel PM, based on mass. Other several researchers (Brück et al., 2001; Majewski, 2008; Park et al., 2006) applied a filtration system with metallic Flow-Through Filters (FTFs) to heavy duty diesel vehicles and investigated their efficiency for removing diesel PM and gaseous compounds. The experimental results from these studies showed that mass concentrations of diesel PM were decreased by 50 - 70% using the FTF, but number concentrations were decreased by less than 50%. These metallic filters have open flow-through passages that permit exhaust gases to pass, when their PM holding capacity is exceeded. Thus the pressure drop is not dramatically increased, but their efficiency for removing PM based on

number concentration is low, compared with that of DPFs.

In order to compensate for the low performance of metallic filters for the removal of PM, Park et al. (2007) applied a corona charger upstream of a metallic foam filter and thus increased their PM collection efficiency by 10 - 20% above that of the filter itself. To date, however, few studies have been conducted on the application of electrostatic charging and precipitation to metallic FTF even though these devices have become fully commercialized in Korea and several European countries. In the study reported herein, newly-designed electrostatic filtration systems consisting of electrostatic devices and commercial FTFs were developed in order to achieve PM removal performances as high as those of commercial DPFs, by making use of particle charging and additional electrostatic force on the FTF in order to enhance the collection efficiency of the standalone filter. The pressure drop and PM collection performance of the combined systems were investigated and compared with those of a commercially available ceramic DPF under a variety of operating conditions using a diesel engine attached to a dynamo.

5.1.2 Experimental set up

Figure 1 shows the schematic representations of the Electrostatic Diesel Particulate filtration Systems (EDPSs) used in the study. Figure 1 a) shows the two constituent parts of EDPS 1, namely the electrode, which generates unipolar ions and simultaneously applies an electrostatic force to the front of the flow-through filter, and the filter itself. The edge-type electrode (an astral shape with eight legs) of the first section was aligned parallel to the front section of the FTF. The length of the section that generated the ions was 60 mm, the length and diameter of the FTF were 105 mm and 130 mm, respectively. Figure 1 b) shows EDPS 2, which is also composed of a section that generates unipolar ions and imposes an additional electrostatic force, and the FTF. In contrast to EDPS 1, the edge-type electrode (the rod with edges) to which the perforated plate was attached in order to impose the electrostatic force on the filter, was positioned perpendicular to the face of the FTF. The total length of the electrode was 205 mm and the length of the FTF was the same as that of the filter in EDPS 1. EDPS 3, which was designed in order to increase PM collection efficiency, was a two stage set up consisting of the same unit as the EDPS 2 but manufactured with two filters, each of which was half the size of the FTF of EDPS 1 or EDPS 2. The total length of this system was 515 mm. The EDPS devices were connected to the exhaust of a 3000 cc diesel engine with an engine dynamo. The characteristics of the devices were investigated by varying the engine operating

conditions and comparing their performance with the DPF under the same experimental conditions.

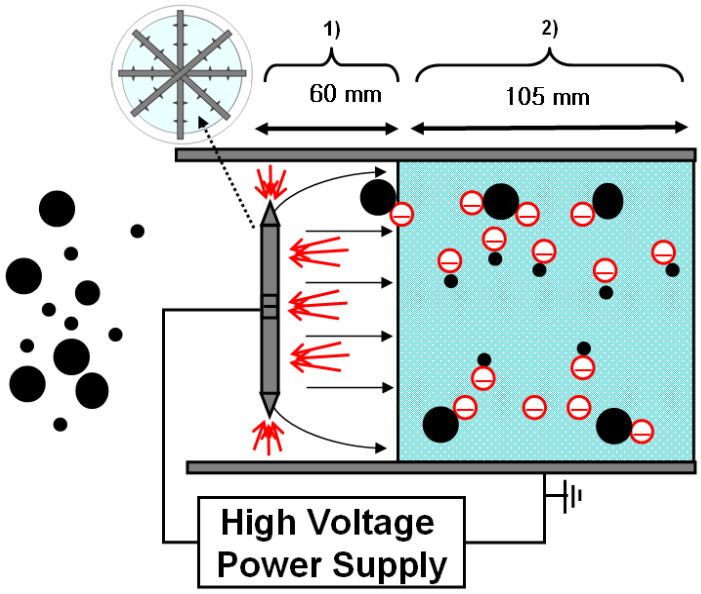

(a) EDPS 1 (Parallel type)

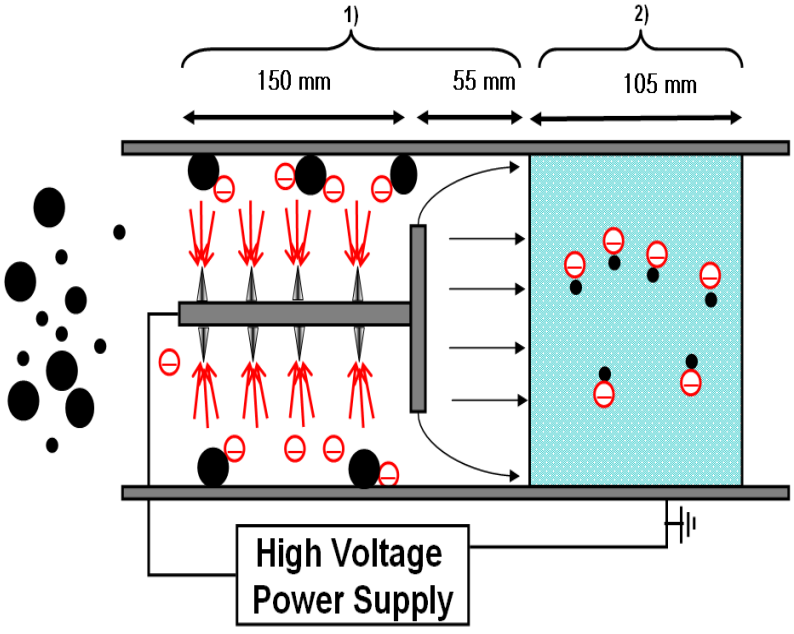

(b) EDPS 2 (Perpendicular type)

Figure 1. Schematic representation of the electrostatic EDPSs showing: 1) the sections which generate unipolar ions and applying an electrostatic force on the flow-through filter, 2) a flow-through filter coated with catalysts.

The test engine that I used was the a 3000 cc diesel engine (Model Frontier, Hyundai Motors, Korea) with a maximum torque and speed of 17 kg·m and 4000 rpm, respectively. The engine speed was set at idle and 2000 rpm with no load and 2000 rpm with loads of 20% and 50%. The experimental set up is shown in Figure 2 and Figure 3, and specification of the test diesel engine is summarized in Table 1. The high power supply (Max. -30 kV/ 10 mA) was connected to devices installed at the center of the exhaust line and the sampling probes were inserted just before and after the EDPSs, in order to measure their PM collection efficiency.

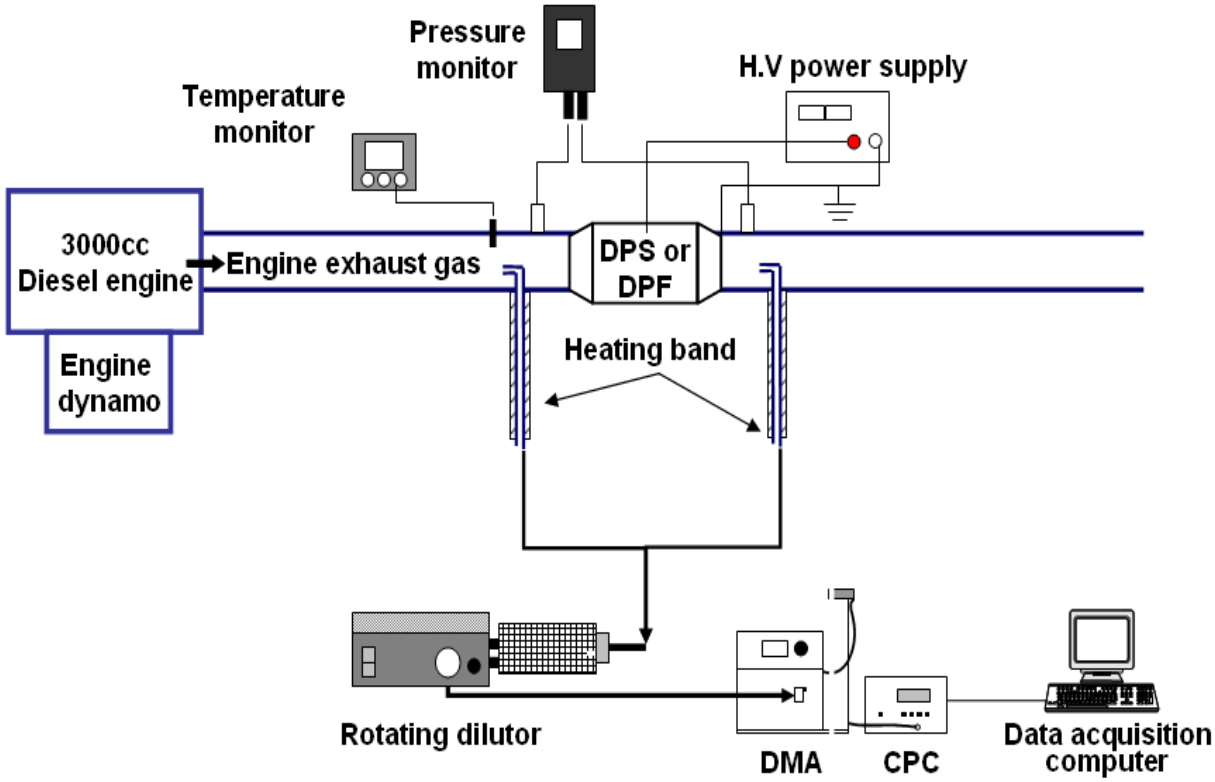

Figure 2. Experimental setup of the performance tests using the EDPSs and the commercially-available DPF.

In order to minimize variations in the concentrations of the diesel PM caused by gaseous compounds, all the sampling lines connected to the rotating dilutor (Model MD-19, Matt Engineering, Switzerland) were electrically heated to 200 ℃, and the sampled gases were mixed with air at a dilution ratio of 1:1200. A DMA (Differential Mobility Analyzer, Model 3080, TSI, USA) and a CPC (Condensation Particle Counter, Model 3076, TSI, USA) were used to measure the number concentration and size distribution of the diesel particles before and after the operation of the

filtration systems under test.

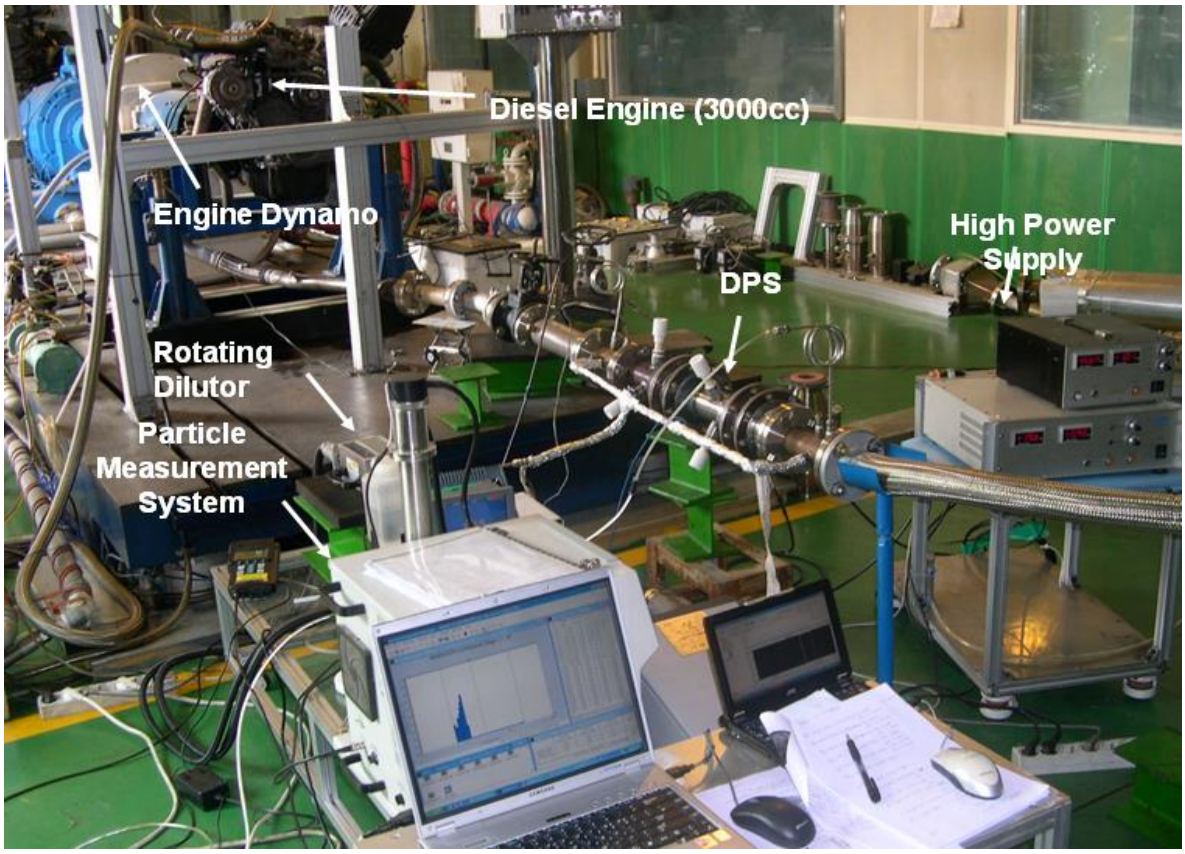

Figure 3. Photograph showing the experimental set up.

Table 1. Specification of the test diesel engine

Engine type	Model	Displacement	Max. Torque	Max. Speed
Diesel engine	Frontier	2957 cc	17 kg·m	4000 rpm

The PM collection efficiency was calculated using following formula,

$$\eta = \left(1 - \frac{C_{out}}{C_{in}}\right) \times 100 \quad (1)$$

where :

η : collection efficiency, %

C_{out} : outlet concentration of particles, /cc

C_{in} : inlet concentration of particles, /cc

In addition, a device for measuring pressure (Testo 350-M/XL*testo 454, Testo, Germany) was connected to tabs located at the inlet and outlet of the EDPSs, and a thermocouple linked to a temperature monitoring system (Model V18, SDD, Korea) was also inserted into the line upstream of the filtration systems in order to measure the pressure drop and the inlet temperature.

5.1.3 Results and discussion

(1) Performance test results of the two types of electrostatic EDPS

Figure 4 shows the distributions of number concentration as a function of particle diameter for the different engine operating conditions used. The number concentration of the diesel particles was increased, and their size distribution shifted to the right, as the engine speed and load were increased. Most of the particles from the engine exhaust were found in nuclei and accumulation modes less than 100 nm in diameter. The mean diameter of the particles was in the range of 30 - 50 nm.

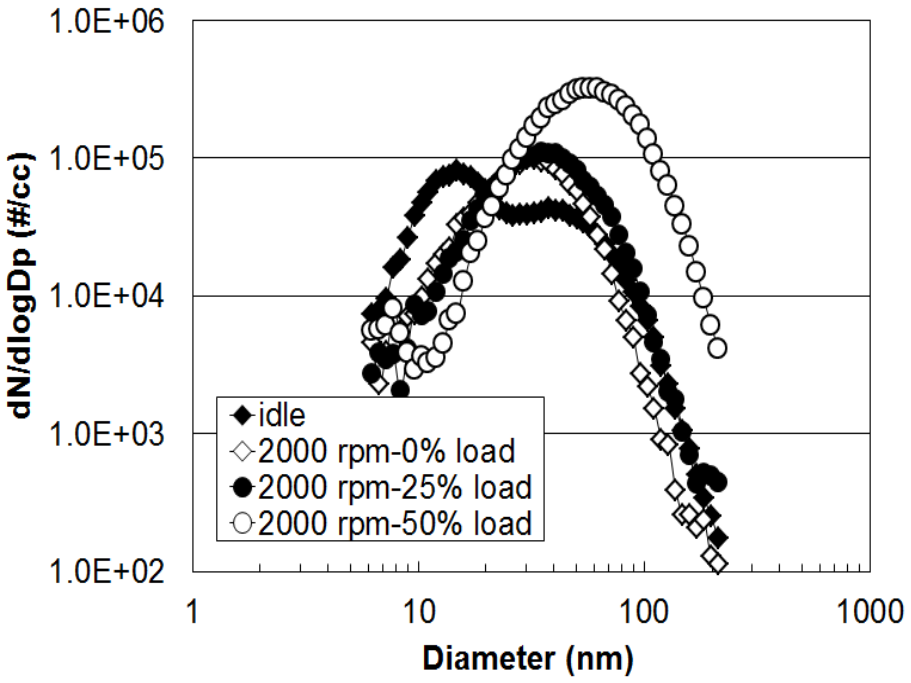

Figure 4. Size distributions of the diesel PM in the engine exhaust for various speed/load combinations.

Figure 5 shows the curves of corona voltage against current at different engine speeds and loads, which were compared for each EDPS in order to investigate the electrical characteristics of the respective systems.

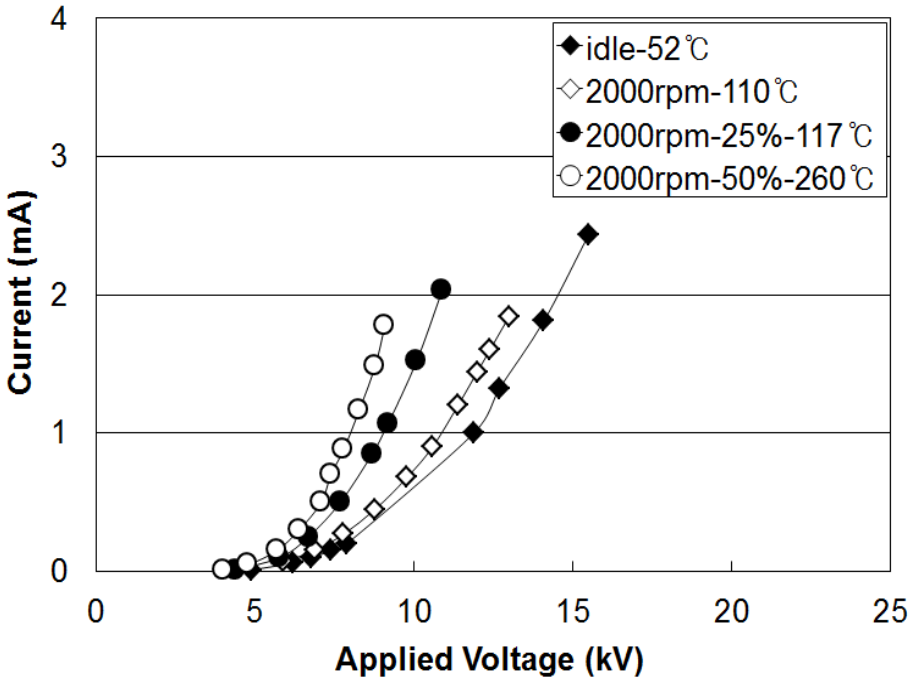

a) EDPS 1

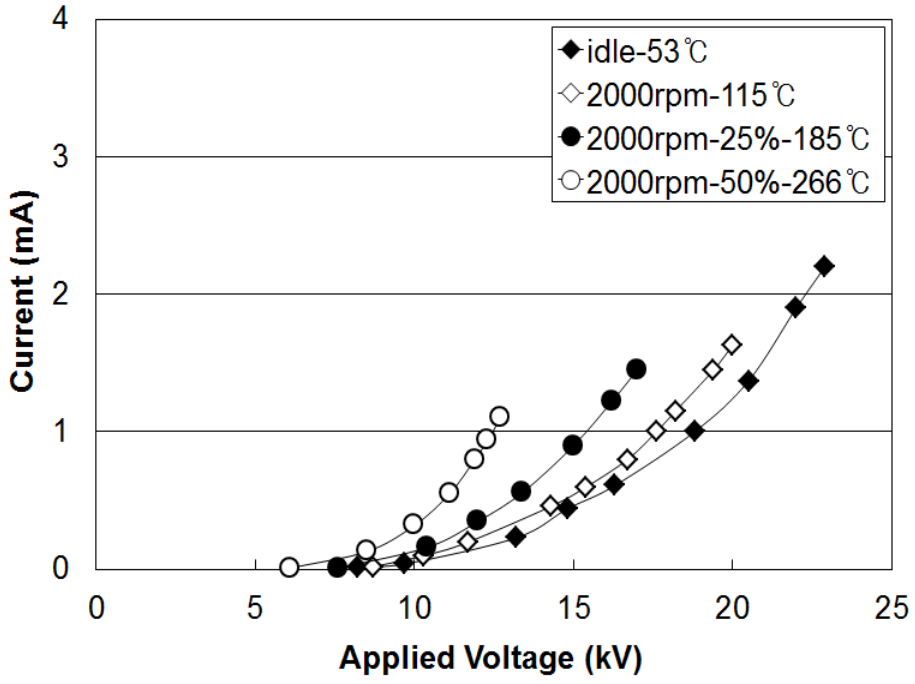

b) EDPS 2

Figure 5. Corona current against applied voltage for various speed/load combinations.

The curves for both EDPSs were moved to the left, and the corona current was higher for the same applied voltage, when the engine speed and load were increased. In particular, 'sparkover' in the EDPSs, which indicated the start of the unstable corona discharge, was observed at lower applied voltages when the speed and load were increased. This occurred mainly as a result of the increased temperature of the exhaust gas. In the case of the negative corona discharge, as the temperature of the gas is increased, the mean free path between the gas molecules is increased, and the frequency of the collisions between electrons and the gas molecules becomes significantly lower. Consequently, those electrons that do not collide with the gas molecules are electrically forced to the grounded side. Thus, temperature leads to unstable corona discharge (Kim et al., 2001). In the case of EDPS 2, the initial voltage was higher than that of EDPS 1 (Figure 5). Since the distance between the sharp edges of the electrode and the grounded side in EDPS 2 (see Figure 1 b)) was wider than that in EDPS 1 (Figure 1 a)), the corona in EDPS 2 was initiated at higher voltages than in EDPS 1 (Hinds, 1999).

Figures 6 and 7 show the PM collection efficiency of EDPS 1 against mean PM diameter for various applied voltage/current combinations at different engine speeds and loads.

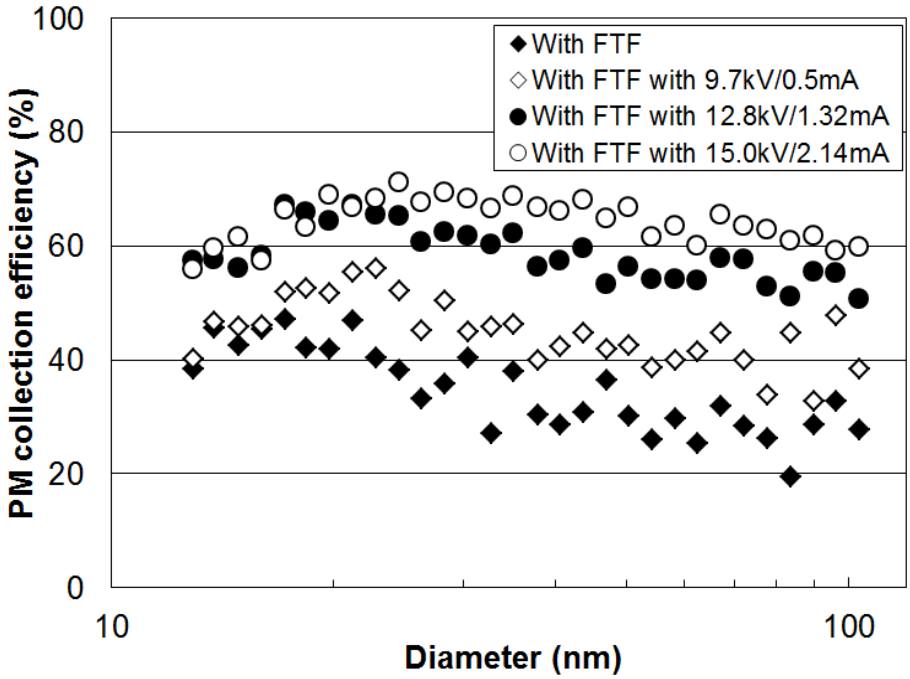

a) idle

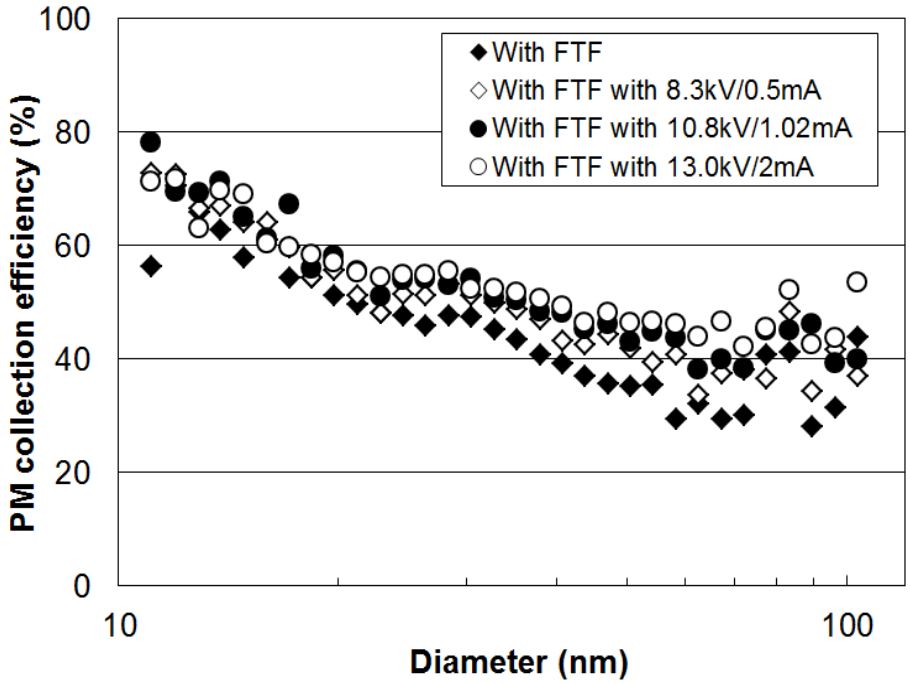

b) 2000 rpm with no load

Figure 6. PM collection efficiency against PM diameter for various applied voltage/current combinations at different engine speeds – EDPS 1.

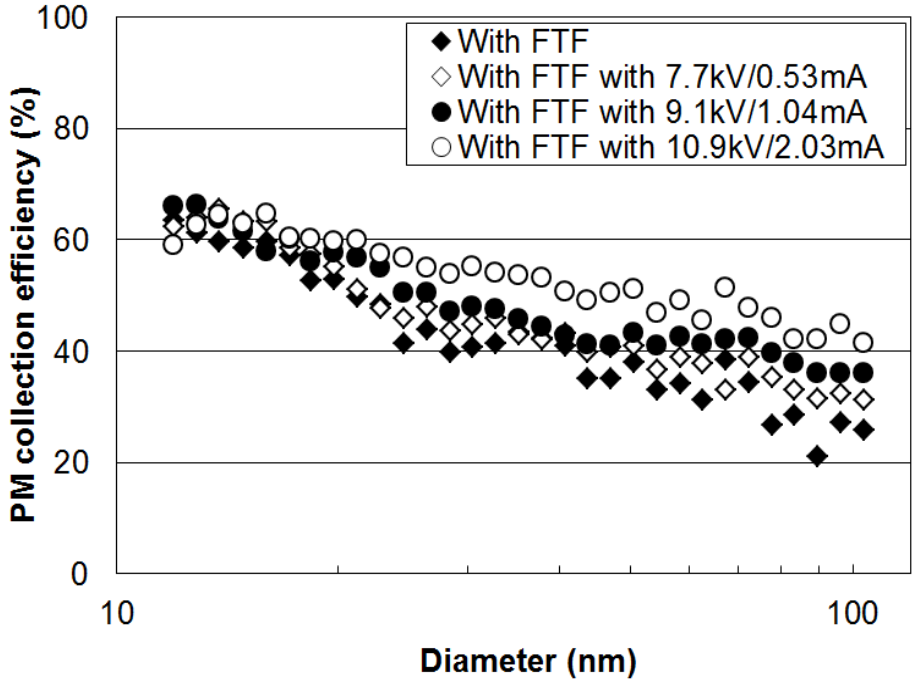

a) 2000 rpm with a 25% load

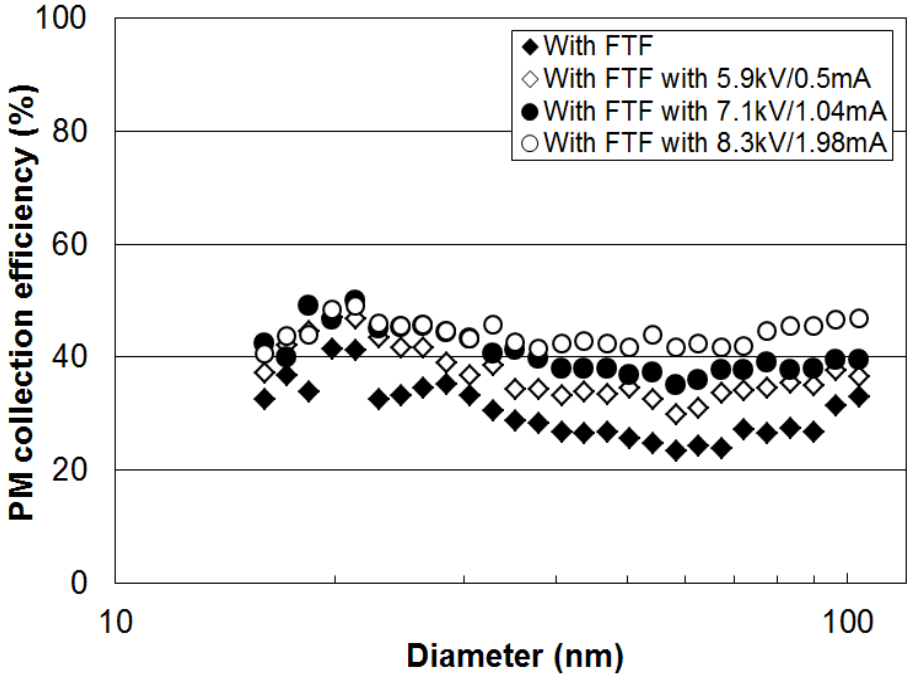

b) 2000 rpm with a 50% load

Figure 7. PM collection efficiency against particle diameter for various applied voltage/current combinations at different engine loads – EDPS 1.

The efficiency of EDPS 1 with the FTF was 30 - 80%, which is higher than that of the standalone filter, whose efficiency was 25 - 50% at idle, 2000 rpm without load, and at 2000 rpm with loads of 25% and 50%. Since both the charging efficiency of the diesel particles and the electrostatic force on FTF were increased as the voltage applied to EDPS 1 is increased, the efficiency with which the diesel particles were removed was higher than that of the FTF itself. Furthermore, at low speed/load combinations, when the temperature of the exhaust gas was low, the particle collection efficiency was higher than that observed under the higher speed/load combinations, because of higher applied voltages and longer residence times at the low combinations.

Figures 8 and 9 show the PM collection efficiency of EDPS 2 against mean PM diameter for various applied voltage/current combinations for each of the engine speeds and loads. In contrast with EDPS 1, the efficiency with which the diesel particles were removed in EDPS 2 was 30 - 50% higher than that of the standalone filter, and the collection efficiency was over 85% at temperatures over 250℃, and more than 95% at temperatures less than 200℃, which was similar to the efficiency of the commercial DPF.

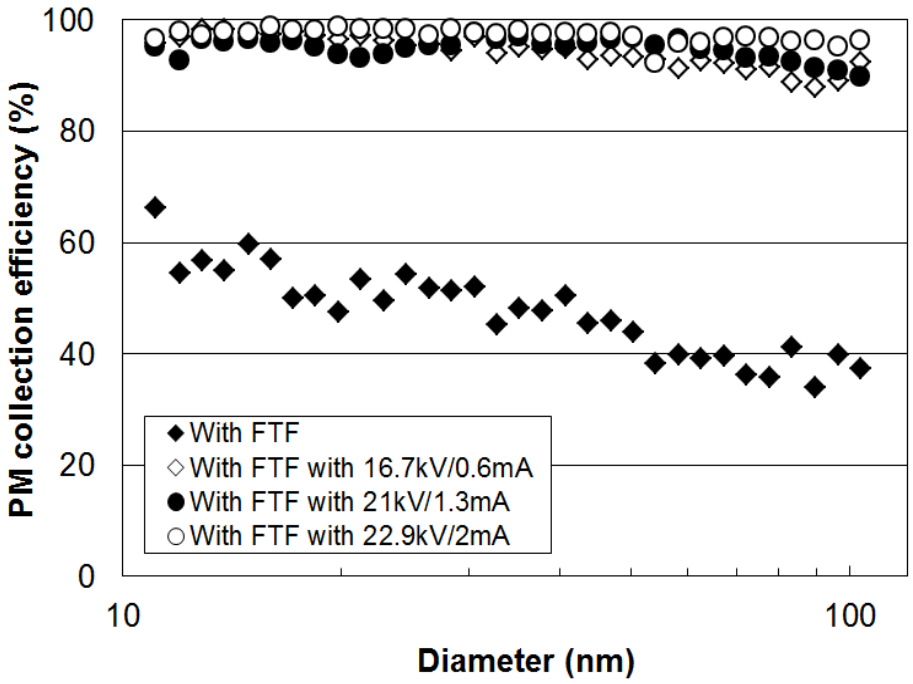

a) idle

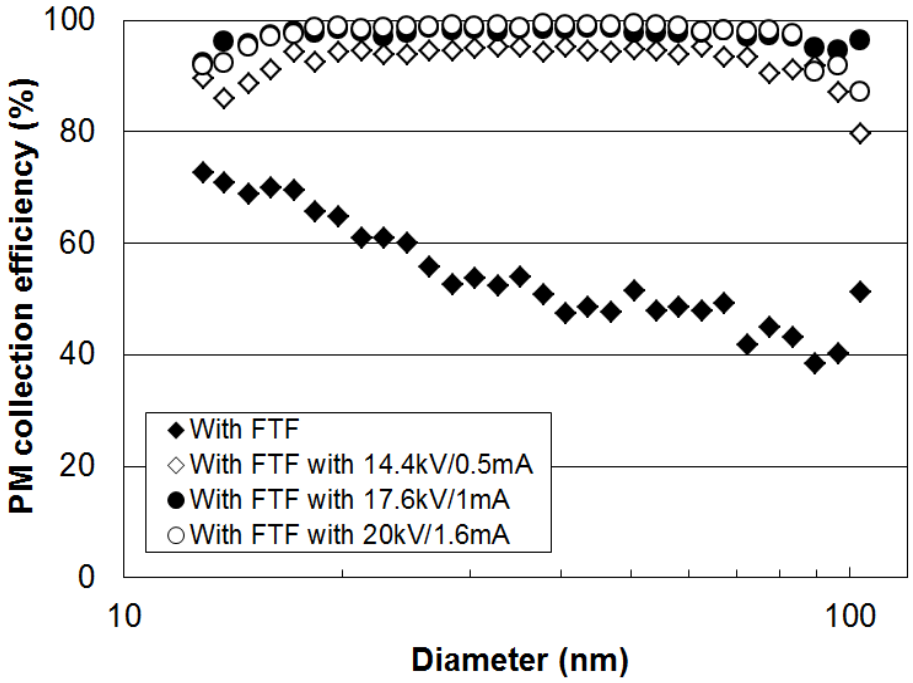

b) 2000 rpm with no load

Figure 8. Collection efficiency at various different engine speeds as a function of changing particle diameter for various applied voltage/current combinations – EDPS 2.

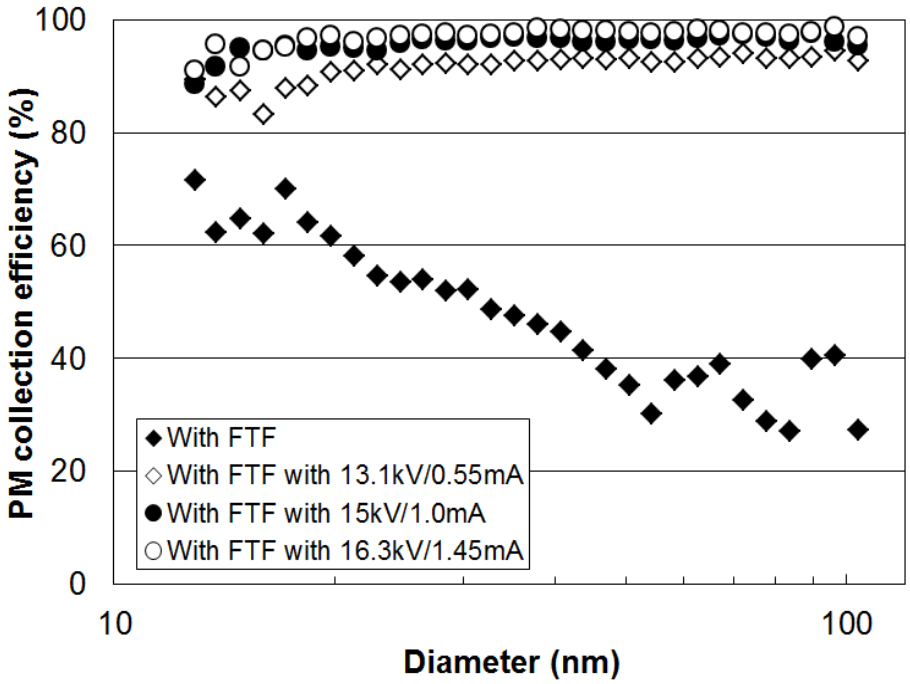

a) 2000 rpm with a 25% load

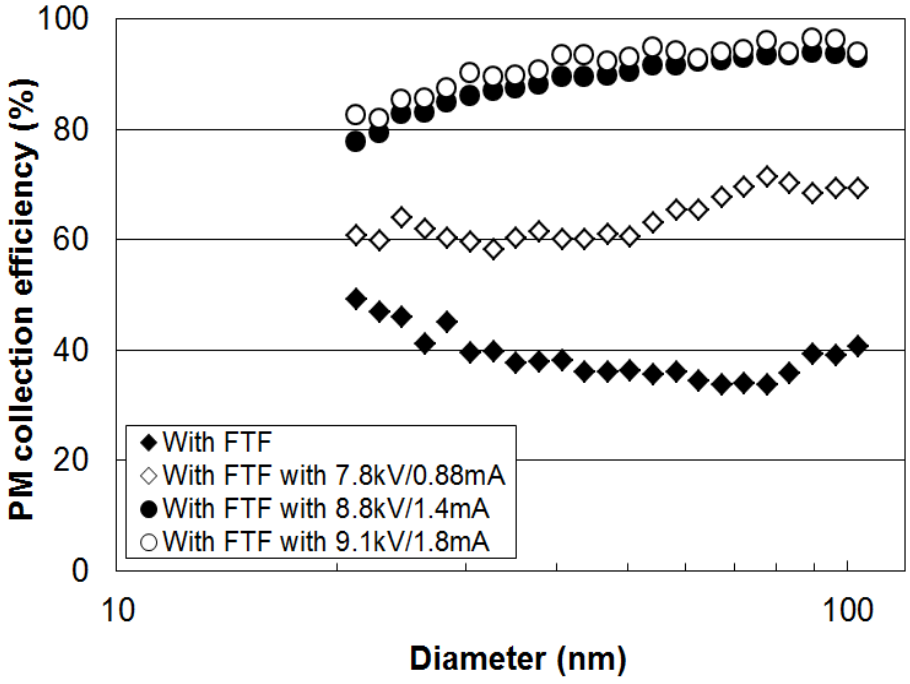

b) 2000 rpm with a 50% load

Figure 9. Collection efficiency for various different engine loads at 2000 rpm as a function of particle diameter for various applied voltage/current combinations – EDPS 2.

Shown in Figure 1, since the direction of the corona discharge of the ionizer in EDPS 1 was parallel to the direction of the exhaust flow, and the residence times of the particles and unipolar ions in the charging region were shorter while the direction of the corona discharge in EDPS 2 was perpendicular to the direction of flow and the charging region wider than that of EDPS 1. For the reasons, the charging rate of the particles in EDPS 2 was expected to be higher than that in EDPS 1, which would explain why the efficiency of the DPF 2 exceeded that of EDPS 1.

(2) Comparison between the electrostatic EDPSs and the commercially-available DPF

The performance of the EDPS 2 that showed greater PM collection efficiency than EDPS 1 was compared with that of the commercially-available DPF under the same experimental conditions, namely at 2000 rpm under loads of 25% load and 50 %. To improve the collection efficiency of EDPS 2 at 2000 rpm with 50% load, EDPS 3 was designed by serial combination of EDPS 2s and then its performance was also compared with that of the commercialized DPF.

The ceramic DPF used in this study had a diameter of 142 mm and a length of 154 mm. The PM collection efficiency was calculated for the peak particle diameter of 40 nm.

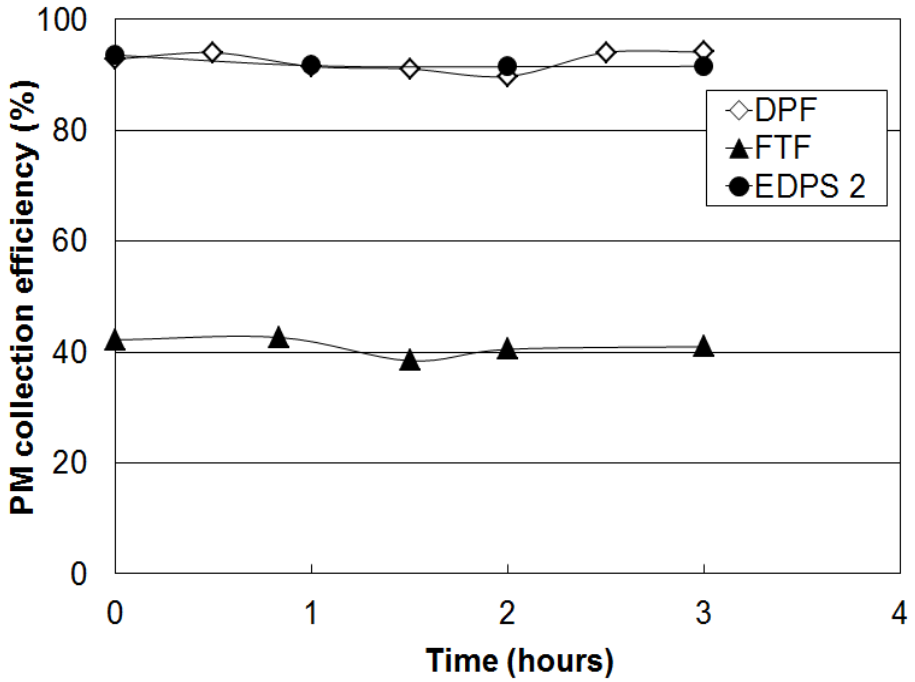

Figure 10. Comparison of the PM collection efficiency at mode diameter, 40 nm, among the FTF, the EDPS 2 and the DPF at 2000 rpm with a 25 % load applied for 3 hours.

Figures 10 and 11 show the performance of the three filtration systems, namely the FTF, EDPS 2, and the DPF, in terms of their PM collection and observed pressure drop, respectively. The temperature of the exhaust gas at 2000 rpm and 25% load was 180℃. The efficiency of EDPS 2 when the high voltage/current (14.3 kV/1 mA) was applied was over 90%, which was similar to that of the DPF and significantly higher than that of the standalone FTF. Furthermore, the observed pressure drop of EDPS 2 was 200 mmH_2O, which was significantly lower than the 800 mmH_2O of the DPF and which did not increase even during the 3 hours of the test.

Figures 12 and 13 show the variation in the performance of EDPS 3 and the DPF over 8 hours of the test at 2000 rpm under 50% load. The temperature of the exhaust gas was over 260℃, and the applied voltages and currents in the first and second stages were 13.4 kV/1 mA and 11.5 kV/2 mA, respectively.

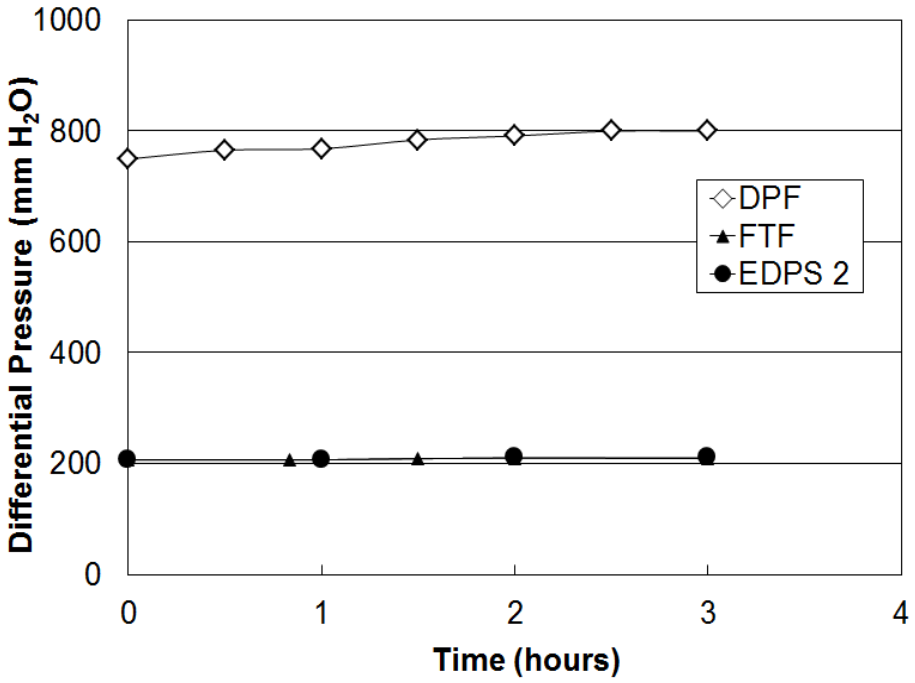

Figure 11. Comparison of the differential pressure among the FTF, EDPS 2 and the DPF at 2000 rpm with a 25 % load applied for 3 hours.

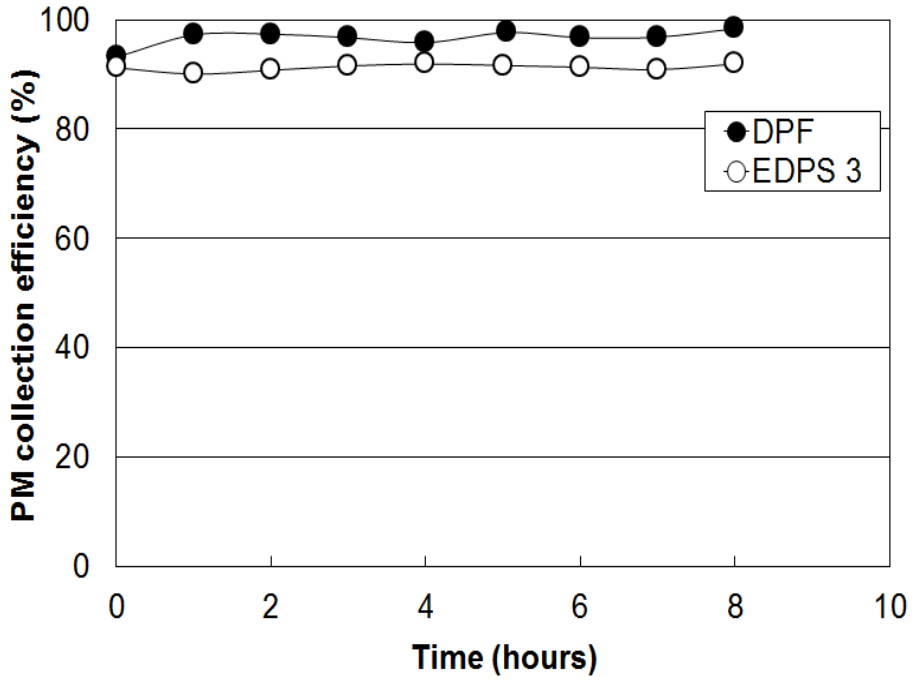

Figure 12. Comparison of the PM collection efficiency at mode diameter, 40 nm, between the EDPS 3 and the DPF at 2000 rpm with a 50 % load applied for 8 hours.

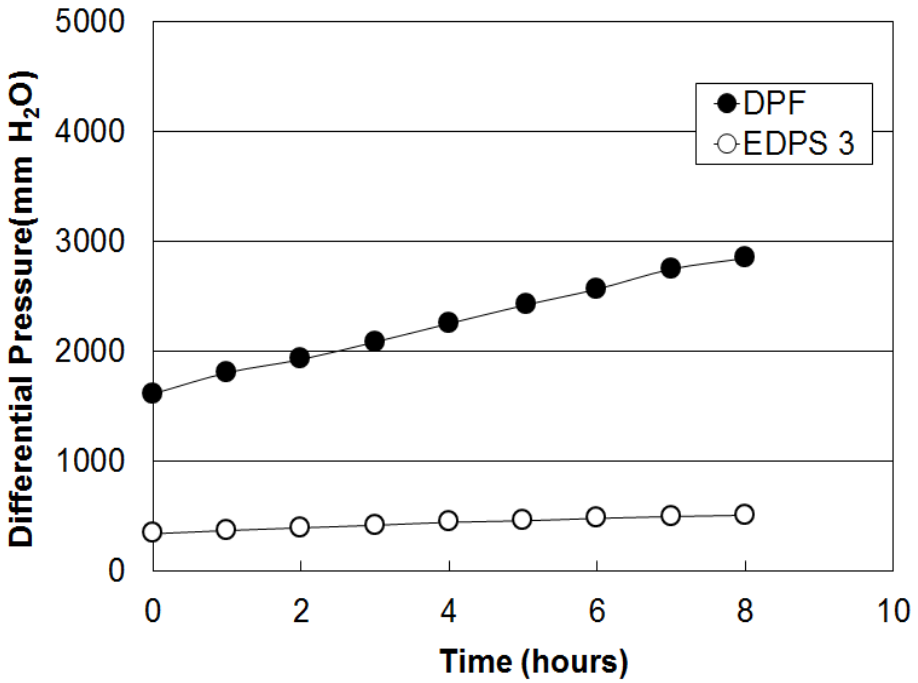

Figure 13. Comparison between the differential pressure between the EDPS 3 and the DPF at 2000 rpm with a 50 % load applied for 8 hours.

As shown in Figure 12, the particle collection efficiency was over 90% for the whole 8 hours, and the pressure drop (343 mm H_2O, Figure 13) was significantly lower than that of the DPF. Furthermore, it did not increase over time, in comparison with the DPF whose initial pressure drop (1700 mmH_2O) increased dramatically to 3000 mmH_2O after 8 hours operation.

5.1.4 Conclusion

I developed electrostatic EDPSs that achieve performance with respect to PM collection and pressure drop, which is similar to that of commercially-available DPFs. The EDPSs were designed using a commercial FTF combined with an additional electrostatic particle removal technique. I conducted performance tests on each system and made comparisons between them and a commercially-available DPF. Our major findings may be summarized as follows:

(1) The EDPSs were tested at constant engine speeds of idle and 2000 rpm, and loads of 25 and 50% at 2000 rpm by using 3000cc diesel engine. The PM collection efficiency of the FTF was improved from 20 - 60% to 40 - 95% at the engine operation conditions using an electrostatic precipitation method.

(2) The EDPS 2 set up was used in the study achieved a PM collection efficiency of over 90% at an exhaust temperature of less than 170℃, and showed a PM collection of more than 80%, even at the exhaust temperatures exceeding 260℃

(3) The one-stage (EDPS 2) and two-stage (EDPS 3) filtration systems showed similar PM collection to the commercially-available DPF over 3 and 8 hours' engine operations at 2000 rpm at loads of 25% and 50%, while their pressure drops were only 200 and 343 mmH_2O, compared to 800 and 1700 - 3000 mmH_2O of the DPF at the same operation conditions.

(4) An electrostatic technique that generates unipolar ions and imposes strong electrostatic force on the FTF could compensate for the low PM collection performance of the FTF while maintaining the required low pressure drop.

5.1.5 References

An, S., Cho, G., Choi, H., Jeong, Y., Lee, E., Oh, K., Han, S., Kim, K. and Park, S. (2006). A study on the PM reduction of catalytic metal foam filter, KSAE paper No. 06-F0055, 366-370.

Brück, R., Hirth, P., Reizig, M., Treiber, P., and Breuer, J. (2001). Metal supported flow-through particulate trap; a non-blocking solution, SAE Paper No.2001-01-1950.

Burtscher, H. (2005). Physical characterization of particulate emissions from diesel engines: a review, Aerosol Science, 36, 896-932.

Fukuoka, Y., Hatanaka, Y., and Takashima, H.K.K. (2009). Development of a marine diesel particulate filter (M-DPF) applied for high frequency induction heating, Paper presented at the 13th European Conference on Power Electronics and Applications, 8-10 Sept., Barcelona, Spain.

Hayashi, H., Takasaki, Y., Kawahara, K., Takenaka, T., Takashima, K., Mizuno, A., and Chang, M. B. (2009). Electrostatic charging and precipitation of diesel soot, Paper presented at Industry Applications Society Annual Meeting, 4-8 Oct., Houston, TX.

HEI (2002). Understanding the health Effects of components of the particulate matter mix: Process and Next Steps, HEI Perspectives,

[Online] Health Effects Institute, Boston, MA, Available at

http://www.healtheffects.org/Pubs/Perspectives-2.pdf

Hinds, W. C. (1999). Aerosol technology 2nd Edition, 15, 331-341. U.S.A.

Jacobs, T., Chatterjee, S., Conway, R., Walter, A., Kramer, J. and Mueller-Hass, K. (2006). Development of partial filter technology for HDD retrofit, SAE Paper No.010213.

Jeong, S. J., Kang, J. H., Kim, T. M. and Lee, H.S. (2008). A study on the uniform PM deposition and improvement of regeneration performance of PDPF of heavy duty diesel engine, KSAE paper No. 08-S0042, 256-262.

Johnson, T.V. (2006). Diesel emission control in review, SAE Paper No.2006-01-0030.

Johnson, T. (2008). Diesel engine emissions and their control, Platinum Metals Rev., 52, 1, 23-37.

Karra, P.K. and Kong, S.C. (2010). Experimental study on effects of nozzle hole geometry on achieving low diesel engine emissions, Journal of Engineering for Gas Turbine and Power, 132, 022802-1-022802-10.

Kim, Y. J., Hwang, T. K. and Yoo, J. S. (2001). A study on the collection characteristics of submicron particles in an electrostatic precipitator-I. Electrical Characteristics, Korean Journal of Air-

Conditioing and Refrigeration Engineering, 7, 7, 572-578.

Majewski, W.A. (2008). Flow-through filters, DieselNet Technology Guide, [Online]Ecopoint Inc. Available at http://www.dieselnet.com/tech/cat_ftf.html[Accessed 03 December 2008].

Maricq, M. M. (2007). Chemical characterization of particulate emissions from diesel engines: a review, Aerosol Science, 38, 1079-1118.

Monaghan, M. L (2000). Future gasoline and diesel engines-review, Int. J. Automotive Technology., 1, 1, 1-8.

Müller-Haas, K., Rice, M., Dean, R., Olsen, R., Adams, J., Manasse, L., and Church, M. (2007). Development of advanced metallic substrate design for close coupled converter application, SAE Paper No.2007-01-1262.

Myung, C.L., Kim, J., Kwon, S., Choi, K., Ko, A., and Park, S. (2011). Nano-particle emission characteristics of European and Worldwide Harmonized test cycles for heavy-duty diesel engines, 12, 3, 331-337.

Park, S. J., Lee, D. G., Kim, J., Cho, G., Kim, H. and Jeong, Y. (2007). Filtration characteristics of metal foam filters for DPF combined with electrostatic precipitation mechanism, Transactions of KSAE., 15, 2, 151-158.

Park, Y., Choi, Y., Jung, H., Kim, N. and Lee, J. (2006). A study on the emission reduction performance of a partial flow diesel particulate filter, KSAE paper No. 06-F0037, 248-253.

Ristovski, Z.D., Jayaratne, E.R., Lim, M., Ayoko, G.A., and Morawska, L. (2006). Influence of diesel fuel sulfur on nanoparticle emissions from city buses, Environ. Sci. Technol., 40, 1314-1320.

Saito, M., Hoshino, H., Furuhata, T., and Arai, M. (2010). Continuous regeneration of an electrically heated diesel particulate trap: mechanism of particulate matter trapping and improvement of trapping efficiency, Int. J. Engine Res., 11, 127-136.

Saiyasitpanich, P., Keener, T. C., Khang, S. J., and Lu, M. (2007). Removal of diesel particulate matter (DPM) in a tubular wet electrostatic precipitator, Journal of Electrostatics, 65, 618-624.

Wallace, W.E., Keane, M.J., Murray, D.K., Chisholm, W.P., Maynard, A.D., and Ong, T. (2007). Phospholipid lung surfactant and nanoparticle surface toxicity: lessons from diesel soots and silicate dusts, Journal of Nanoparticle Research, 9, 23-38.

Yoon, C. S. and Cho, G. (2009). Study of design and CFD analysis for partial DPF utilizing metal foam, Transactions of KSAE., 17, 1, 24-34.

5.2 Collection performance of an electrostatic filtration system combined with a metallic flow-through filter for ultrafine diesel particulate matter

5.2.1 Introduction

The main purpose of this study to combine electrostatic precipitation method to metallic filters such as FTFs is to develop a metallic PM filtration device with low pressure drop for heavy-duty diesel engines and off-road diesel engines such as construction vehicles and marines which exhaust high volumetric gas because commercialized ceramic DPFs for diesel vehicles could not be solution for removal of ultrafine particles from the high volume diesel engines due to high pressure drop caused by the closed structure of the filters

With this reason, in the previous study (Kim et al., 2010), the three newly-developed Electrostatic Diesel Particulate matter filtration Systems (EDPS 1,2,3) were evaluated under four steady-state engine operating conditions such as idle, 2000 rpm with no load, and 2000 rpm under 25 % and 50% load. Of the two developed alternatives, EDPS 1 and EDPS 2, the EDPS 2 consisting of an ionization section, electrostatic field additional section and Flow-Through Filter (FTF) achieved almost 90% collection of particulate matter (PM) under the engine's operating conditions, with the efficiency of the FTF being maintained at 20 - 50%, based on particle number. Results comparing the long-term performance of EDPS 2 and EDPS 3 (effectively a serial combination of two EDPS 2s) with a commercially-available Diesel Particulate Filter (DPF), showed that EDPS 2 and EDPS 3 achieved almost the same efficiency for removing PM as the DPF, but showed as significantly improved (75 - 90% lower) differential pressure drop.

However, the study was done primarily to evaluate the applicability of the combination systems for diesel engines under the specific engine operating conditions of the steady states at low speed (~2500 rpm) and load (~50%). Also, the electrical insulation of the EDPS at engine conditions with high speeds and loads when particle number and temperature were high was needed to improve by preventing particle contamination on the holder of the high voltage electrodes in the EDPS.

Therefore, I modified the previous system (Kim et al., 2010) with a novel air insulation device in order to evaluate the electrostatic diesel particulate matter filtration system (EDPS) for industrial applications at high speeds and loads when PM with high concentration and high temperature over 300℃ are exhausted from diesel engines and flow into the filtration system. The PM collection performance of the modified system was investigated under various operating

conditions, from idle to full rpm and with 0 to 60% load in order to find out relationship among key design parameters (flow rate, applied power consumption, collection efficiency etc) of the EDPS for a scale up. The system was also compared with a commercialized ceramic DPF in terms of PM collection and pressure drop, using a standard test mode for diesel vehicles, i.e. the European Stationary Cycle (ESC) 13, from zero to full speed and loads when the exhaust gas temperature changed from 100 to 600℃.

5.2.2 Experimental set up

Figure 1 shows the schematic and specifications of the EDPS used in this study. The EDPS was composed of a sharp-edge electrode-to-cylinder-type charging stage (150 × 75 mm), round plates (1 mm) having many sharp edges that generated negative ions and charged the diesel PMs, an electrostatic field imposing stage (55 × 140 mm) having a 3-mm-perforated round plate that was directly connected to a high-voltage electrode to impose the additional electrostatic force onto the FTF, and the FTF (51 × 140 mm), which was a half-sized commercially-available FTF.

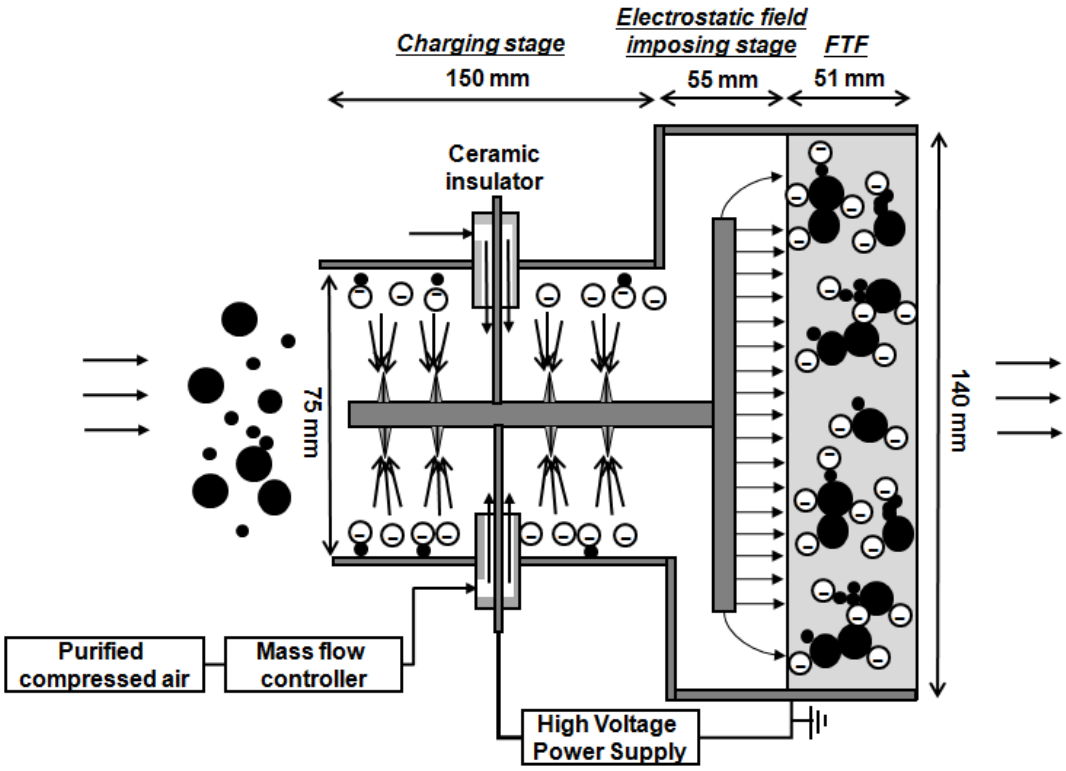

Figure 1. Schematic and specifications of the EDPS.

I needed to generate a stable corona and minimise deposition of diesel particulates on the surface of the electrical insulator of the system at high speeds and loads when the exhaust gas temperature was over 300℃. Under these conditions, the concentration of diesel PM is much higher than that at low speeds and loads. To do this, purified compressed air was supplied to the slit surrounding the supporting rod in the insulation device, and the flow rate through the air slit was controlled by a mass-flow controller from 20 to 100 L/min depending on the engine exhaust conditions. The edge-type electrode (rod with edges), to which a perforated plate was attached to impose the electrostatic force onto the FTF, was perpendicular to the face of the FTF. A power supply (max. –30 kV/10 mA, Korea Switching, Seoul, Korea) was connected to the filtration system. Figure 2 shows the EDPS with the air insulation modification used in this study.

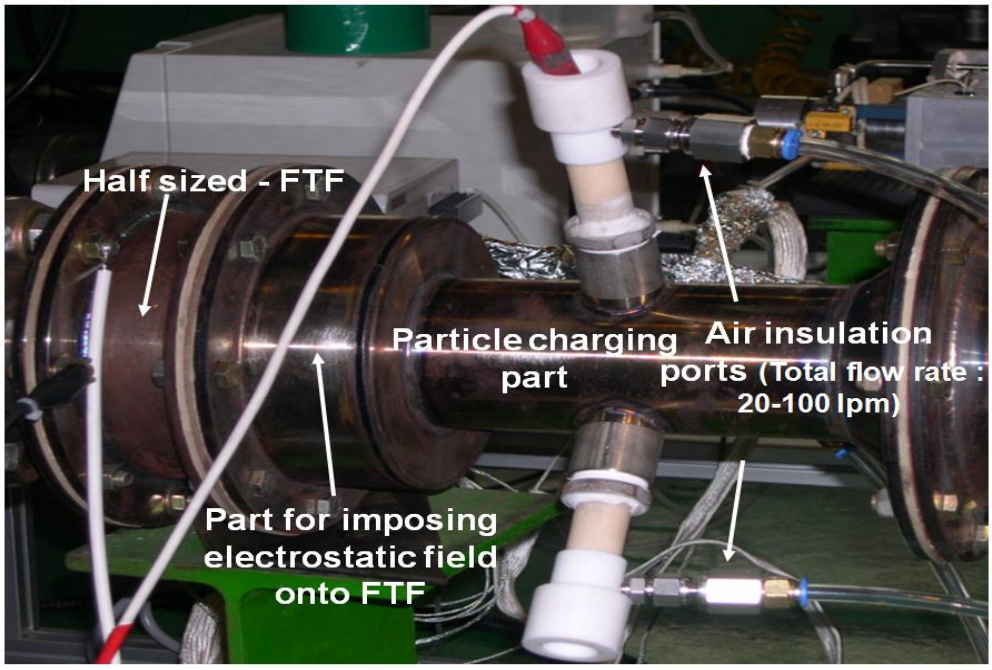

Figure 2. Photograph of the EDPS with the air insulation.

Figure 3 shows the experimental setup for the performance tests using the newly- developed filtration system and a commercially-available DPF. The two test engines were 3000 cc diesel engines with maximum torques of 167 and 334 Nm and a maximum speed of 4000 rpm. One engine (model Frontier, Hyundai Motors, Korea) was used to test a filtration system under steady-state operating conditions (idle, 2000 rpm with no load, 2000 rpm with loads of 25% and 50%, 3000 rpm

with a load of 50%, and 3500 rpm with a load of 60%) in order to understand effect of some operation parameters such as applied voltage, flow rate, rpm, and load on the PM collection performance of the EDPS. The second engine (model Carnival, Hyundai Motors, Korea) was used for a comparison test with the EDPS, FTF, and DPF using the standard test mode (ESC 13 mode) because the engine was equipped with automatically controlled dynamo system, real-time temperature and pressure measurement system, and air conditioning system which was used to keep the specific test condition of temperature and humidity of 25℃ and 50% in the test room. The specifications of the test diesel engines are summarised in Table 1. Filtration systems were installed at the centre of the exhaust line from the diesel engine with an engine dynamo. Two stainless steel sampling probes were inserted just before and after the filtration systems. To minimise variation in the concentrations of the diesel PM, all the sampling lines connected to the rotating dilutor (model MD-19, Matt Engineering, Switzerland) were electrically heated to 200℃, and the temperatures of the first and the second dilution stages of the rotating dilutor were set at 150℃ and 300℃, respectively. The dilution ratio was maintained at 1:1500.

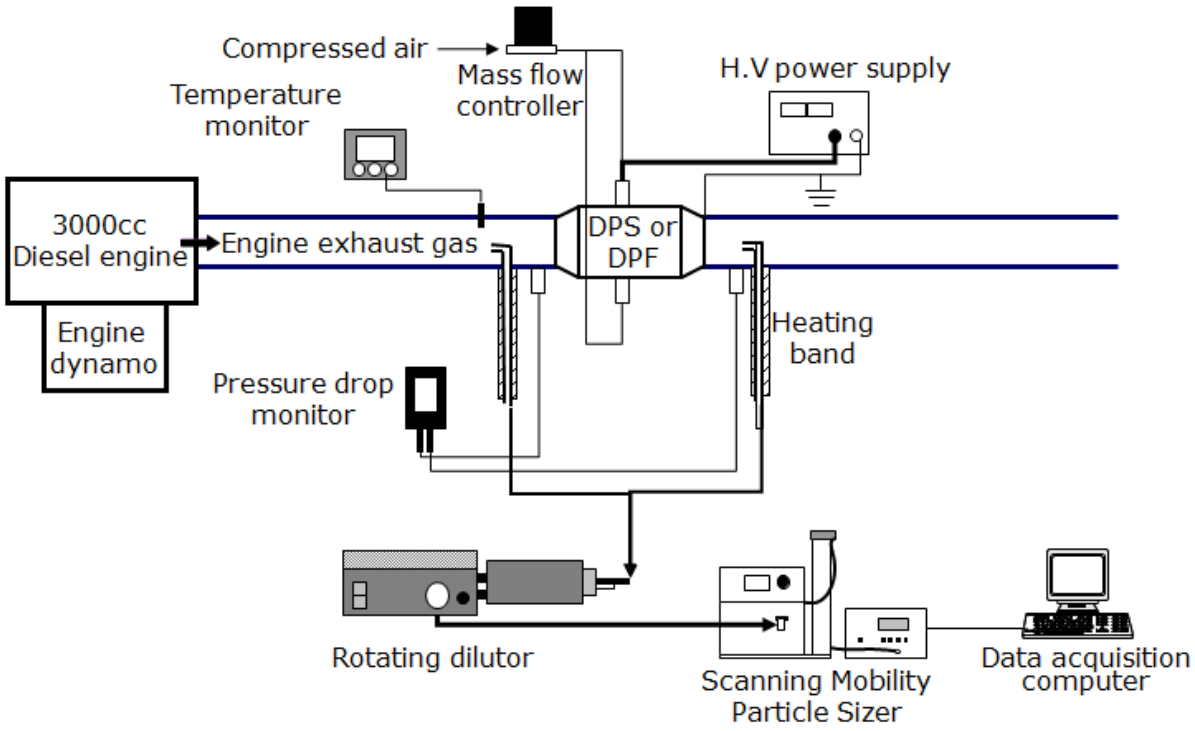

Figure 3. Experimental setup of the performance tests using the EDPS and the commercially-available DPF.

A differential mobility analyzer (DMA, model 3080, TSI, USA) and a condensation particle counter (CPC, model 3076, TSI, USA) were used to measure the number concentration and size distribution of the diesel particles before and after operation of the filtration systems under steady-state conditions. Additionally, a device for measuring pressure (Testo 350-M/XL*testo 454, Testo, Germany) was connected to tabs located at the inlet and outlet of the filtration systems. A thermocouple linked to a temperature monitoring system (model V18, SDD, Korea) was also inserted into the line upstream of the filtration systems. These two devices tracked the pressure drop and the inlet temperature.

Table 1. Specifications of the tested diesel engines.

Engine type	Model	Maker	Displacement (cm^3)	Max. Torque (Nm)	Max. Speed (rpm)	Peak Particle size (nm)	Test condition
Diesel engine	Frontier	Hyundai Motors	3,000	167	4,000	50	Steady state test
Diesel engine	Carnival	Hyundai Motors	3,000	345	4,000	100	ESC 13 mode test

The EDPS in this study was also evaluated under an international standard test cycle mode, ESC 13 mode, which is steady-state cycle for emission certification of heavy-duty diesel engines such as truck and bus engines, and compared with a commercially-available DPF (diameter 142 mm, length 154 mm). To compare the EDPS and the DPF based on their particle collection efficiencies, the particle collection performance under ESC 13 mode was evaluated by measuring the number concentration of the diesel PM for 100-nm particulates. This was the mode diameter of the diesel PMs from the test engine at which the highest number concentration was measured. The temperature and pressure before and after the filtration devices were also monitored. Table 2 summarises the experimental conditions for the performance testing of the filtration systems.

The PM collection efficiency and pressure drop were calculated using Equations 1 and 2:

$$\boldsymbol{\eta = \left(1 - \frac{C_a}{C_b}\right) \times 100} \qquad (1)$$

where

η: collection efficiency, %

C_a: PM concentration after or within test units, #/cm_3

C_b: PM concentration before or outside test units, #/cm^3

$$P_{diff} = P_a - P_b \quad (2)$$

where

P_{diff}: pressure drop, mbar

P_a: pressure at the inlet of the test unit, mbar

P_b: pressure at the outlet of the test unit, mbar

Table 2. Experimental conditions for the performance tests of the filtration systems for the diesel engines.

Test condition	Speed (rpm)	Load (%)	Test units	Calculation formula	Particle size for Eff.	Measure-ment	Tempera-ture (℃)
Steady state	Idle	0	DPSs	1- C_{out}/C_{in}	All	Eff.	60
	2000	0	DPSs		All	Eff.	120
	2000	25	DPS/FTF		All	Eff.	170
	2000	50	DPS/FTF		All	Eff.	250
	3000	50	DPS/FTF		All	Eff.	300
	3500	60	DPS/FTF		All	Eff.	400
Standard mode (ESC 13)	Idle -3750	0-100	DPS/FTF/DPF	1- $C_{w/\ unit}/C_{w/o\ unit}$	100 nm	Eff., P_{diff}	100-600

* Eff. : efficiency, P_{diff} : Differential pressure (pressure drop)

5.2.3 Results and discussion

(1) Electrical and particle collection performance under steady-state engine operation.

Figure 4 shows the curves of corona voltage as a function of current at different engine speeds and loads. The curves for the EDPS are shifted to the left, i.e. the corona current was higher at the same applied voltage when the engine speed and load were increased. ‘Sparkover’ in the EDPS, which indicated the start of unstable corona discharge, was observed at lower applied voltages when the speed and load were increased. The corona current increased with gas temperature for the same

applied voltage because of the increased electrical mobility of the generated ions and the contaminated insulation (Kim et al., 2001; Rinar et al., 1987; Han et al., 2010). However, as the temperature of the exhaust exceeded 250℃, e.g. at 2000 rpm with a load of 50%, the corona current dramatically increased, even at less than 1 kV, due to severe contamination by diesel particles of the insulation device that supported the high- voltage electrode. The draining of the electrical field due to coating of the ceramic insulator with a layer of conductive particles is the one of the major challenges in applying an electrostatic charging process within a diesel exhaust gas stream (Kukla, 2003). To maintain the electrostatic potential in the presence of conductive carbon particle deposits, I designed a novel insulation device using air-slit injection.

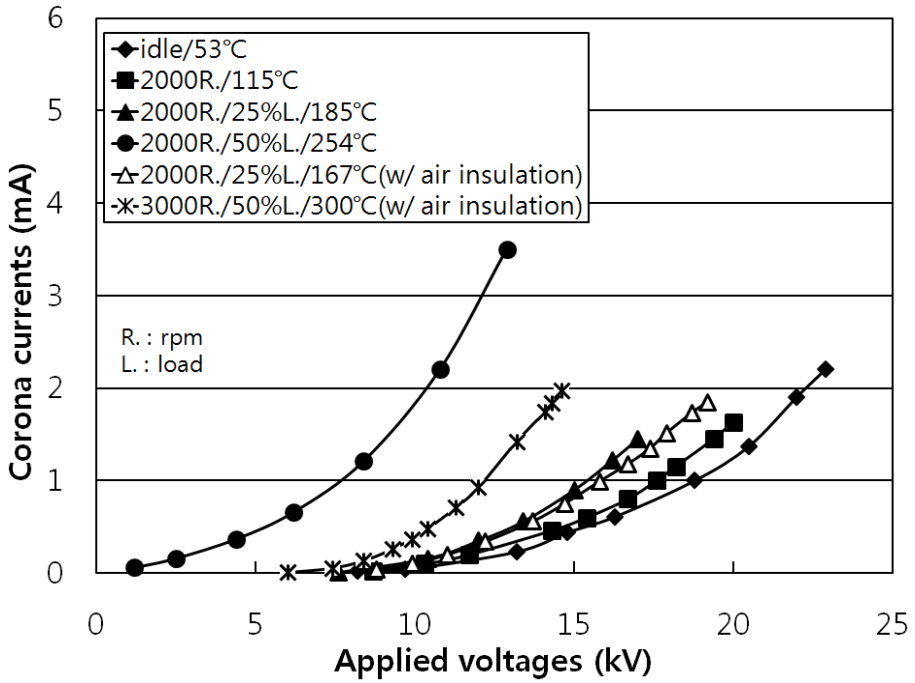

Figure 4. Changes in the curves of corona voltage as a function of current at different engine speeds and loads with and without air insulation.

As shown in Figure 1, I supplied air at velocity of 7 m/s through a slit between the supporting rod of the high-voltage electrode and the ceramic insulator so that the surface around the electrode was kept free of particle deposits. As shown in Figure 4, the high electrical potential was maintained at a voltage and current up to 15 kV and 2 mA due to the air-slit insulation, even when the engine speed and load were increased to 3000 rpm and 50%, when the temperature was higher than 300℃.

Figure 5 shows the PM collection efficiency of the stand-alone FTF, without applying high

voltage to the charger, as a function of particle size for different engine speeds and loads. The temperature of the exhaust gas increased from 60 to 250℃ with increasing speed and load of the engine. The particle number collection efficiency for just the FTF ranged from 25 to 70%, depending on the particle size. The average collection efficiency was 44.8%, which is significantly lower than 95% efficiency of the DPF (Myung et al., 2011; Zarvalis et al., 2007). The main particle trap mechanisms of an FTF are diffusion and impaction or interception (Hinds, 1999). I found that the minimum collection efficiency occurred for 100-nm particles, a size that is too large for diffusion to be effective yet too small for impaction or interception to be effective. Relative to the no-load at 2000 rpm condition, the average overall collection efficiency of the FTF decreased from 52.9 to 35.9% with increasing engine load at the same engine speed. This was because of the faster (by 36%) flow rate and hence lower residence time in the filtration zone and higher (by 17%) total number concentration of the diesel PM.

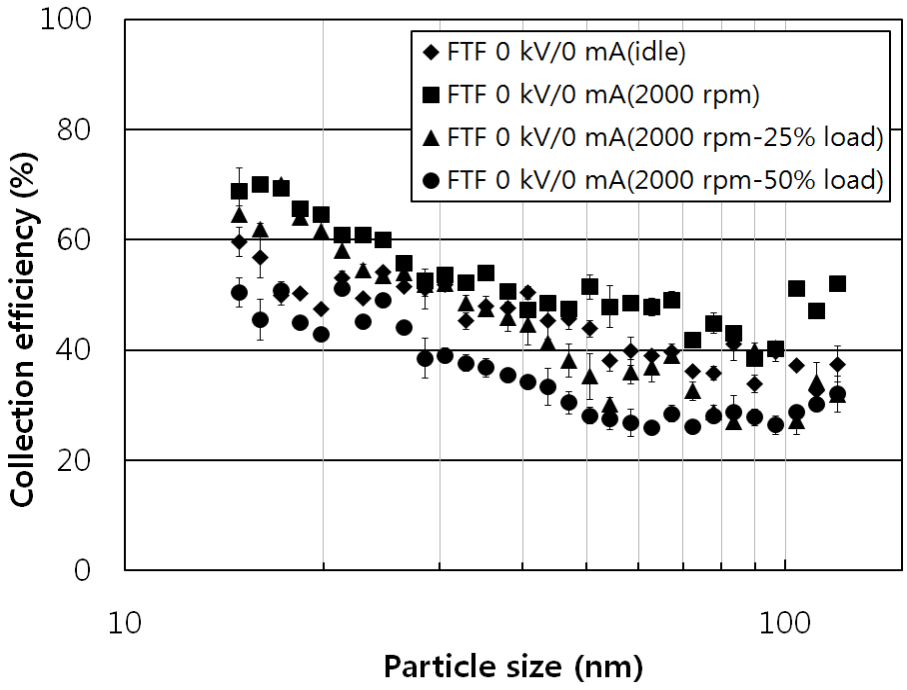

Figure 5. PM collection efficiencies of the stand-alone FTF without applying high voltage to the charger as a function of particle size for different engine speeds and loads.

Figure 6 shows the PM collection efficiency of the EDPS without air insulation as a function of diesel PM size for the combination of maximum applied voltage and current for each engine speed and load. Compared to the results in Figure 5, the efficiency with which the diesel particles were

removed by the EDPS was 30–50% higher than that by the FTF (the EDPS without applied voltage). In particular, the collection efficiencies with electrostatic charging and collection exceeded 95%, regardless of particle size, until the exhaust temperature was lower than 250℃ under the speed and load combination of 2000 rpm and 25%. Because both the charge of the diesel particles and the electrostatic force on the FTF increased as the voltage applied to the EDPS increased, the collection efficiency was much higher than that of the FTF itself (Han et al., 2010; Kim et al., 2010). Furthermore, at those low speed and load combinations when the temperature of the exhaust gas was low, the particle collection efficiency was higher than that observed under the higher speed and load combinations because of higher corona power (applied voltage × corona current) and longer residence times (lower flow rate) with the less intensive combinations. However, the efficiency of the EDPS at 2000 rpm with a load of 50% decreased significantly to 60–70% because of a low electrical potential caused by the contamination of the electrodes by particles.

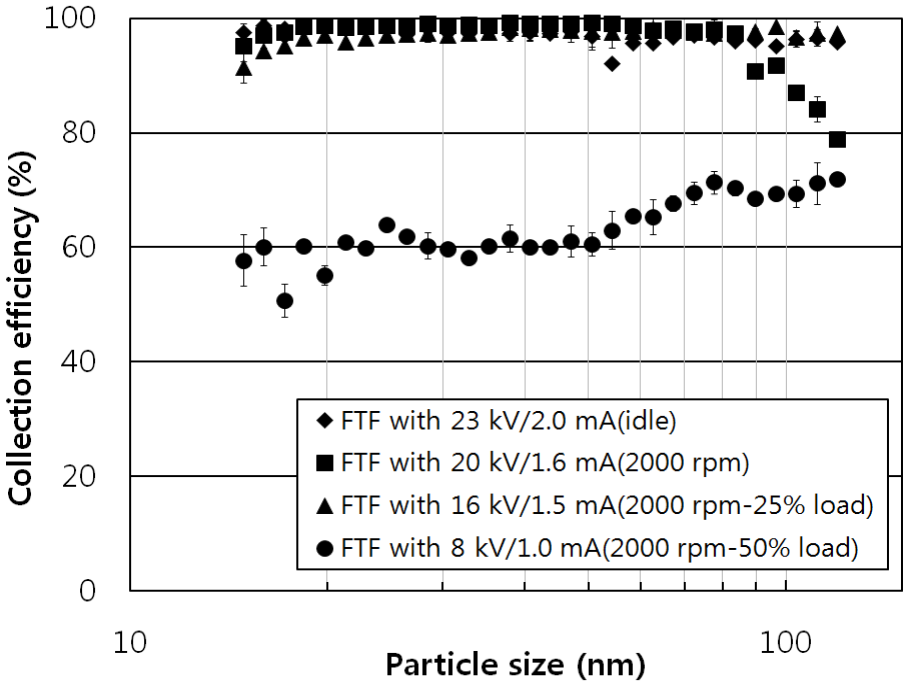

Figure 6. PM collection efficiencies of the EDPS without air insulation as a function of diesel PM size for the maximum applied voltage and current combination for each engine speed and load.

Figure 7 shows the variation in the distributions of the number concentrations of the diesel PM at 3000 rpm with 50% and 3500 rpm with 60% load for operating conditions, before and after passing the PM through the EDPS whose high-voltage supporting rod was protected by air insulation. The temperature of the exhaust gas at the inlet of the EDPS at 3000 rpm with 50% load and 3500

rpm with 60% load was 300 and 400℃, respectively. I chose applied voltages for the experiments of size dependent particle collection by the EDPS as 11-14 kV in order to maintain stable corona discharge at the EDPS even with exhaust temperature over 300°C, shown in Figure 7. The number concentration of the PM was unimodal, and the maximum size of the particles was about 50 nm in each case. The total concentration of particles in the entire size range for both cases reduced significantly from 1.4×10^5 and 1.78×10^5 #/cm^3 to 2.5×10^4 and 3.21×10^4 #/cm^3, respectively, when 13.2 kV and 11 kV were applied to the EDPS. The number concentrations of the PM in all size ranges decreased slightly to 1.1×10^5 and 1.6×10^5 #/cm^3 after they passed through the stand-alone FTF without applying high voltage to the EDPS.

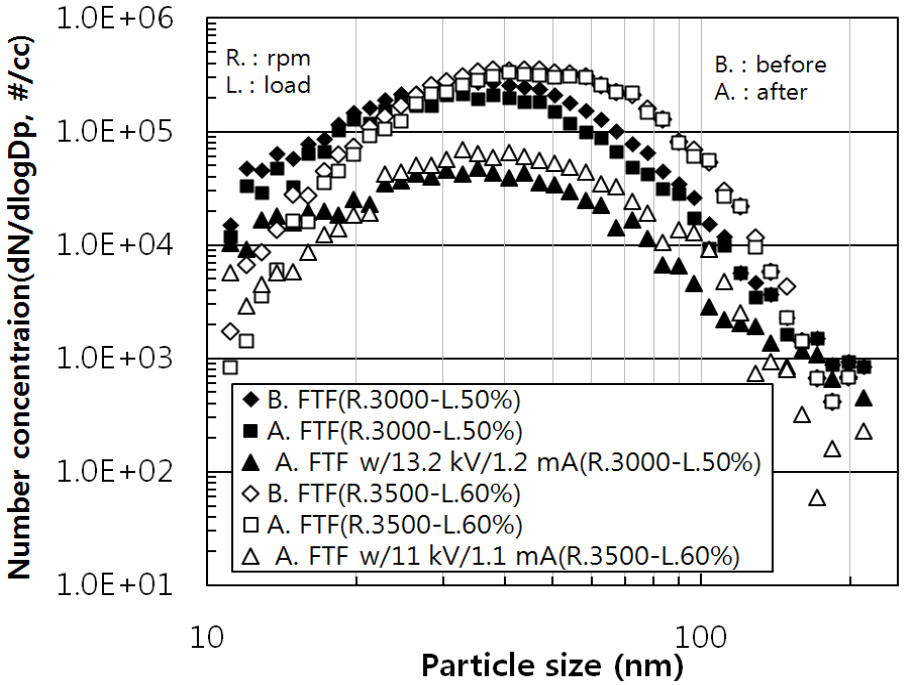

Figure 7. Variation in the distributions of the number concentrations of the diesel PM at 3000 rpm with 50% load and 3500 rpm with 60% load of engine operation, before and after passing the PM through the EDPS

Figure 8 shows the variation in collection efficiency as a function of particle size with and without the application of high voltage to the EDPS. The operating conditions were 3000 rpm with 50% load and 3500 rpm with 60% load, when the temperature was over 300℃.

The average collection efficiency with the FTF alone was 18% at 3000 rpm with 50% load and 26% at 3500 rpm with 60% load, respectively. When 13.2 kV and 11 kV were applied to the EDPS at 50% and 60% loads, respectively, the average collection efficiency increased from 18% to 81.4% and 26%

to 79.0%, while efficiencies decreased to averages of 67.7% and 64.0% for particles smaller than 20 nm for each engine operating condition. This was because of the partial charging effect in that size range, as observed in previous studies (Yoo et al., 1997; Li and Christofides, 2006; Huang and Chen, 2002; Zhuang et al., 2000; Kim et al., 2011). However, the efficiency exceeded 80% for diesel particles larger than 20 nm when high voltage was applied to the EDPS and even 85% for particles at the peak size of the number concentration distribution, which was 50 nm.

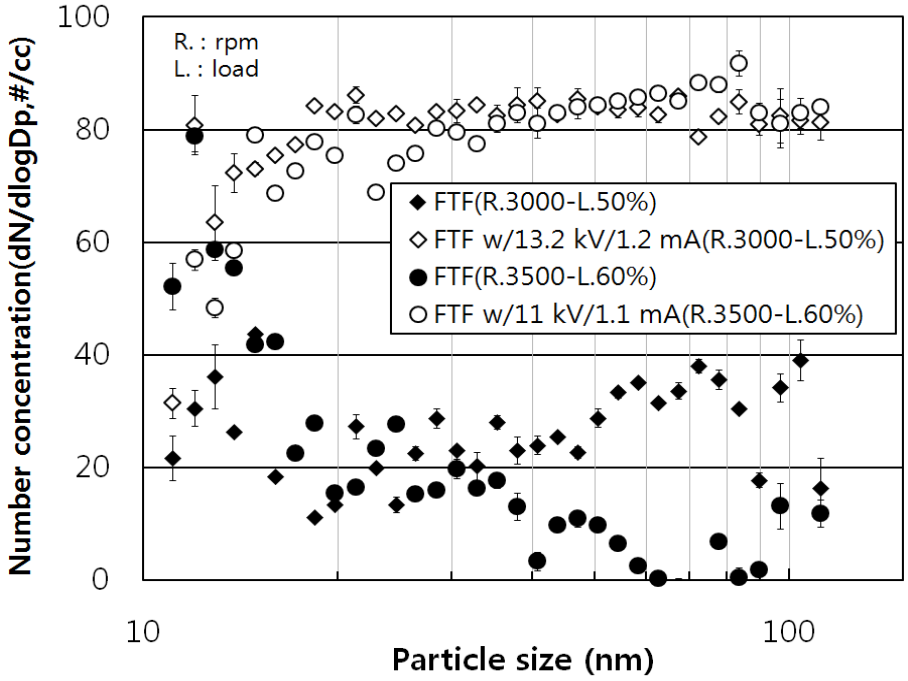

Figure 8. Variation in collection efficiencies as a function of particle size with and without applying high voltage to the EDPS at 3000 rpm with 50% load and 3500 rpm with 60% load.

Figure 9 shows the variation in the concentration and collection efficiency of the EDPS for the 50-nm diesel PM in the exhaust over almost 4 hours of continuous operation. Operating conditions were 3000 rpm with 50% load and 3500 rpm with 60% load, when the gas temperature was over 300℃. I also chosen applied voltages to the EDPS as 11-14 kV to make sure stable corona discharge at the EDPS for 4 hour continuous operation even with exhaust temperature over 300oC, shown in Figure 9, and the applied voltages was the same as those in Figure 8. The initial concentrations of the particles were 2.6×10^5 and 3.4×10^5 #/cm^3, respectively. These concentrations decreased dramatically to 5.0×10^4 and 6.2×10^4 #/cm^3, which corresponded to collection efficiencies of 80.9% and 81.4%. It is noteworthy that the collection efficiency remained steady during the test.

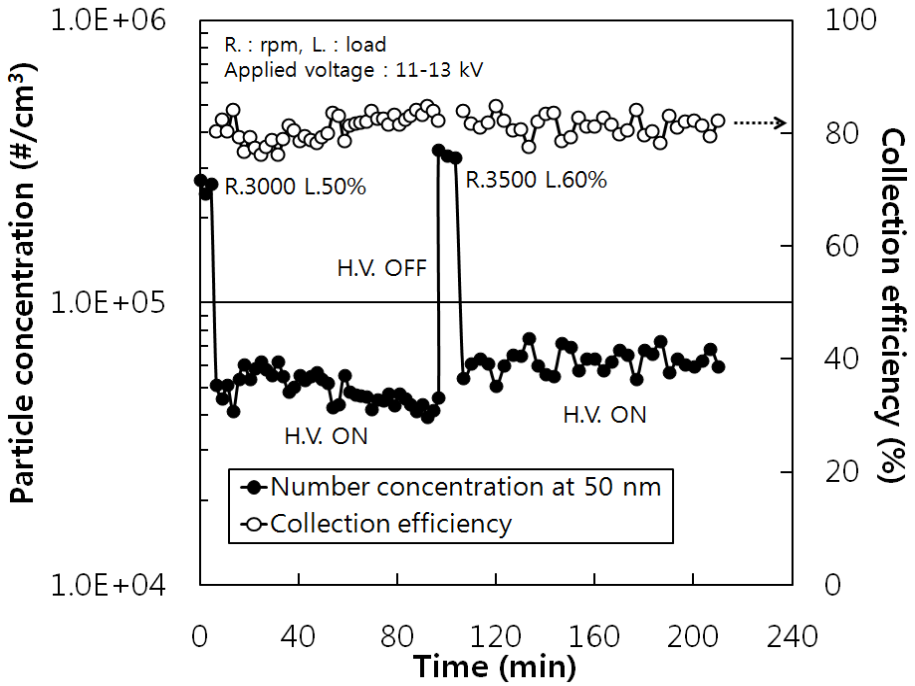

Figure 9. Variation in the concentration and collection efficiency of the EDPS for the 50-nm diesel PM in the exhaust over almost 4 hours of continuous operation of the EDPS at 3000 rpm with 50% load and 3500 rpm with 60% load.

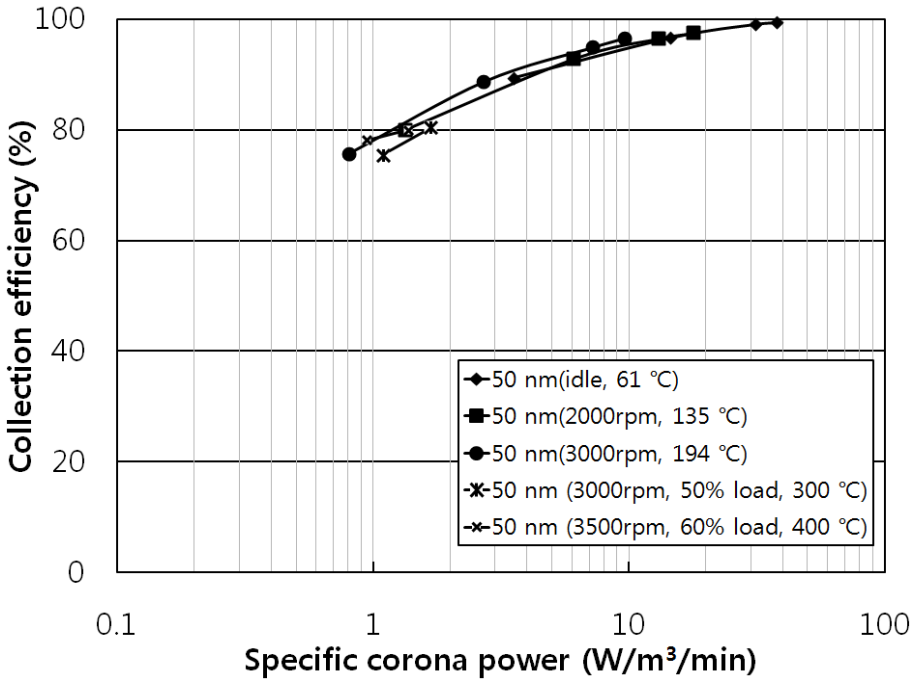

Figure 10. The collection efficiency of 50-nm particles in the EDPS as a function of the specific corona power applied to the EDPS for different engine operating conditions and temperatures.

Figure 10 shows the collection efficiency of 50-nm particles in the EDPS as a function of the specific corona power applied to the EDPS for different engine operation conditions and temperatures. The collection efficiency of the system increased with the log of the specific power input (Han et al., 2010; Kim et al., 2010). For specific corona powers from 1 to 30 W/(m^3/min), the EDPS had a high collection efficiency, over 80%, based on the number of particulates. Furthermore, the efficiencies correlated with specific corona power, which was determined by the applied voltage, corona current, temperature, and flow rate, for any combination of engine speed and load.

(2) Particle collection and pressure drop performance during the ESC 13 mode test.

Figure 11 shows the operating conditions for the ESC 13 mode used to evaluate the particle collection and pressure drop performance of the EDPS with and without applied voltage, compared to a commercially-available DPF. The speed of the engine was increased from 854 to 3750 rpm and the torque increased from 0 to 345 Nm.

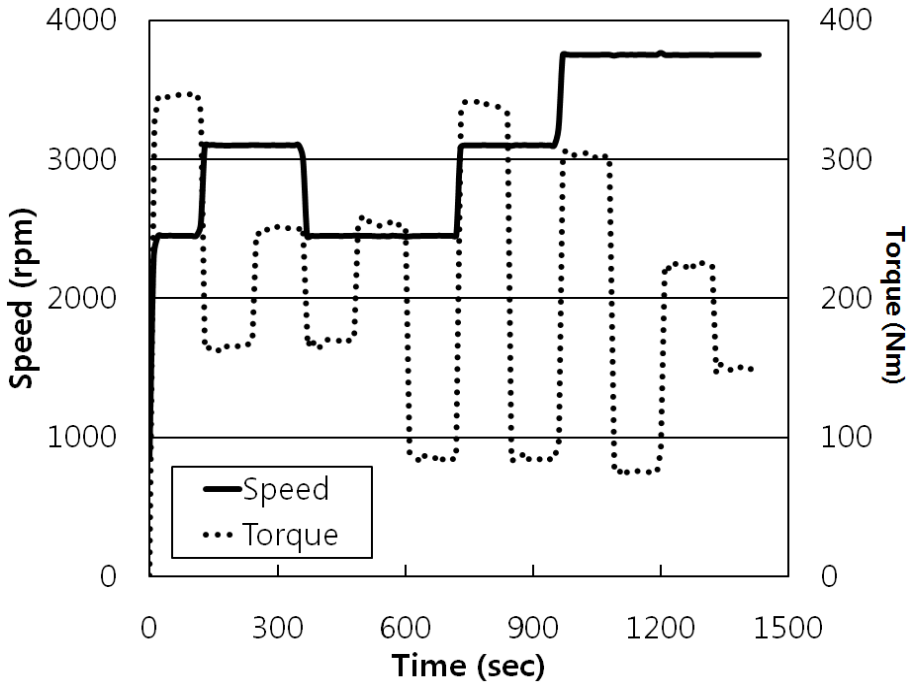

Figure 11. The operating conditions of the ESC 13 mode for diesel vehicles.

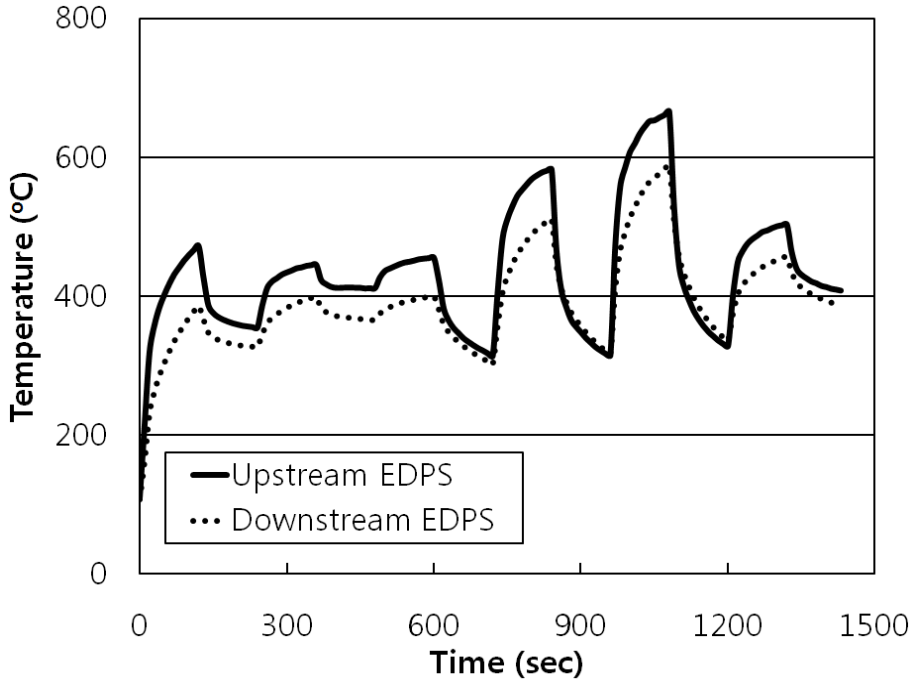

Figure 12. Variation in the temperature upstream and downstream of the EDPS during the mode test.

As shown in Figure 12, the temperature changed from 100 to 700℃ and 100 to 600℃ upstream and downstream of the EDPS, respectively, during the test. Only one engine (model Canival, 3000 cc, Hyundai Motors, Korea) was used for this mode test; its specifications are shown in Table 1.

The PM collection efficiency was calculated for 100-nm particles; this was the maximum size of the PM from the diesel engine used. The pressure drops before and after the filtration systems were measured concurrently.

Figures 13 and 14 compare the particle collection and pressure drop performances for the FTF , the EDPS, and the DPF. The applied voltage and current to the EDPS was controlled at 11–20 kV/1–2 mA during the test. As shown Figure 13, the collection efficiency of the DPF was the highest, approximately 99%, and that of the FTF with no applied voltage was the lowest, approximately 50%. Even though the collection efficiency of the EDPS dropped to 50% at 3000 rpm with a load of 100%, the average collection efficiency of the EDPS during the entire ESC 13 mode test was 89%. This was only 10% less than that of the DPF. The collection efficiency of the EDPS ranged from 95 to 99% for the test conditions having an exhaust gas temperature below 400℃. As shown in Figure 14, the pressure drop of the EDPS during the ESC 13 mode test increased from 30 to 150 mbar, while that of the DPF increased from 130 to 560 mbar. Notably, the average pressure drop of the EDPS during the mode test was 83 mbar, which was only 27% of that of the DPF.

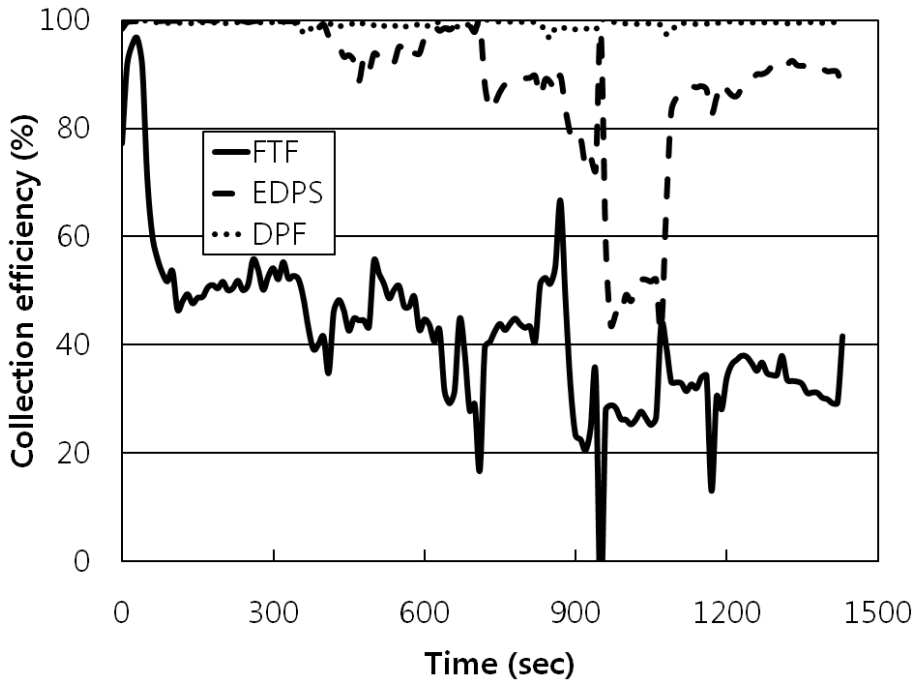

Figure 13. Comparison of the particle collection performances among the FTF, the EDPS, and the DPF during the ESC 13 mode test.

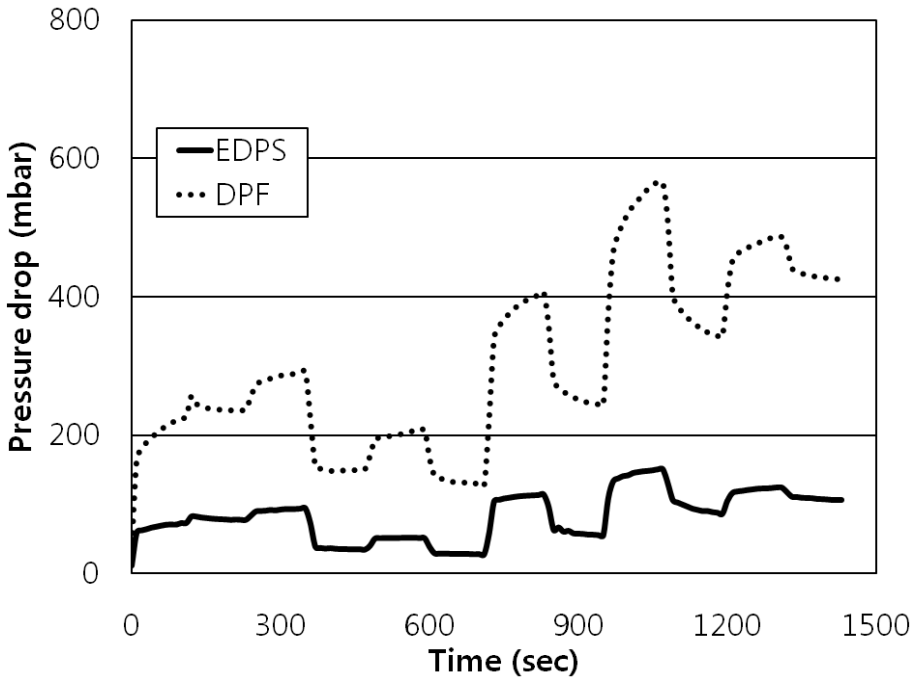

Figure 14. Comparison of the pressure drop performances among the FTF, the EDPS, and the DPF during the ESC 13 mode test.

5.2.4 Conclusion

An EDPS was developed with a novel air insulation technique, combined it with a commercially-available FTF, and evaluated the performance of the combined system and a commercially-available DPF under steady-state conditions. These conditions included exhaust gas temperatures over 300℃ as well as the standard ESC 13 mode that generated a temperature profile from 100 to 600℃. Our major findings from the experiments are as follows:

1) Using an air-slit insulation device enabled stable corona discharge in the EDPS even for temperatures over 300℃.

2) The efficiency with which the diesel particles were collected in the EDPS was over 95% at exhaust gas temperatures less than 250℃. This was 30–50% higher than that for the FTF.

3) The average efficiency of the EDPS was 80% at exhaust gas temperatures over 300℃. This efficiency, maintained over 4 hours of continuous operation, was 40–60% higher than that of the FTF using the novel air insulation.

4) With a specific corona power between 1 and 30 W/(m^3/min), the EDPS achieved a high collection efficiency – over 80% – based on the number of particulates. Moreover, the collection efficiency of the system correlated with specific corona power, which was determined by the applied voltage, corona current, temperature, and flow rate. This correlation could be used for an electrical and physical design of an EDPS for other diesel engines having different flow rates.

5) The ESC 13 mode test results demonstrated that the EDPS had a 47% higher collection performance than the FTF and 10% lower performance than the DPF. This was achieved at a significantly lower pressure drop (82 mbar), which was only 27% of that for the DPF.

5.2.5 References

Han, B., Kim, H. J., and Kim, Y. J., Fine particle collection of an electrostatic precipitator in CO_2-rich gas conditions for oxy-fuel combustion, Science of the Total Environment, 2010, 408, 5158-5164.

Huang, S. H. and Chen, C. C., Ultrafine aerosol penetration through electrostatic precipitators; Environ. Sci. Technol. 2002, 36, 4625-4632.

Hinds, W. C., Aerosol Technology: Properties, Behavior, and Measurement of Airborne Particles, 1999 (John Wiley & Sons, Inc., New York).

Kim, H. J., Han, B., Hong, W. S., Shin, W. H., Cho, G. B., Lee, Y. K., and Kim, Y. J., Development of electrostatic diesel particulate matter filtration systems combined with a metallic flow through filter and electrostatic methods, International of Journal of Automotive Technology, 2010, 11, 4, 447-453.

Kim, H. J., Han, B., Kim, Y. J., and Yoa, S. J., Characteristics of an electrostatic precipitator for submicron particles using non-metallic electrodes and collection plates, Journal of Aerosol Science, 2010, 41, 987-997.

Kim, H. J., Han, B., Kim, Y. J., Hwang, K. D., Oh, W. S., Yoo, S. Y., and Oda, T., Fine particle collection performance of a two-stage wet electrostatic precipitator using a nonmetallic pre-charger, Journal of the Air & Waste Management Association, 2011, 61, 1334-1343.

Kim, Y. J., Hwang, T. K., and Yoo, J. S., A study on the collection characteristics of submicron particles in an electrostatic precipitator-I. Electrical Characteristics, Korean Journal of Air-Conditioning and Refrigeration Engineering, 2001, 7, 7, 572-578.

Kukla, P., Electrostatic diesel particulate trap from Per-Tec, DieselNet Technology Guide (2003)
[Online] http://www.dieselnet.com/news/2003/05pertec.php

Li, M. and D. Christofides, P., Collection efficiency of nanosize particles in a two-stage electrostatic precipitator; Ind. Eng. Chem. Res., 2006, 45, 8484-8491.

Myung, C.L., Kim, J., Kwon, S., Choi, K., Ko, A., and Park, S., Nano-particle emission characteristics of European and Worldwide Harmonized test cycles for heavy-duty diesel engines, 2011, 12, 3, 331-337.

Rinar, G., Rugg, D. E., and Yamamoto, T., High-temperature high-pressure electrostatic precipitator electrical characterization and collection efficiency, IEEE Transactions on industry applications, 1987, 1A-23, 1, 114-119.

Yoo, K. H., Lee, J. S., and Oh, M. D., Charging and collection of submicron particles in two-stage parallel-plate electrostatic precipitators, Aerosol. Sci. Tech., 1997, 27, 308-323.

Zarvalis, D., Dolios, I., Papaioannou, E., Vlachos, N., and Konstandopoulos, A. G., Collection efficiency of diesel particulate filters: multi-instrumental assessment, paper presented at 3rd European Combustion Meeting ECM 2007, 11-13 April, Crete, Greece, 2007.

Zhuang, Y., Kim, Y. J., Lee, T. G., and Biswas, P., Experimental and theoretical studies of ultra-fine particle behavior in electrostatic precipitators; J. Electrostat. 2000, 48, 245-260.

Chapter VI

ESP type air cleaner with low ozone generation

6.1 Submicron particle removal indoors by a novel ESP with a high clean air delivery rate, low ozone emission, and carbon fiber ionizer

6.1.1 Introduction

The most efficient method of cleaning indoor air is to use air cleaners, which remove airborne contaminants relatively quickly by several different processes of varying effectiveness, such as filtration, capture on activated carbon, ionization, and photo-catalytic oxidation. The methods for removing contaminants vary, depending on the phase of the contaminant and the design of the air cleaner (Shaughness and Sextro, 2006). Common types of air cleaners include high-efficiency particulate air (HEPA) filters, ozone generators, electrostatic precipitators, and negative ion generators (Berry et al., 2007; Sultan et al., 2011). Currently, most of the air cleaners used in residences is the HEPA-filter type. These devices can remove a variety of contaminants including ultrafine particles and bioaerosols (e.g., allergens and fungi) with high efficiency (>90%) and do not emit harmful byproducts such as ozone, which is generated by air cleaning devices fitted with ozone and negative-ion generators (California EPA, 2008). In the filtration method, dense nanometer fibers remove particles by interception, inertial impaction, and diffusion, generating a pressure drop through the filter media, which allows for high-efficiency particle removal (Hinds, 1999).

Air cleaners based on electrostatic precipitation have been widely applied to remove ultrafine particles and enhance IAQ. Many different designs of air cleaners utilizing electrostatic precipitation have been developed and tested in terms of single-pass collection efficiency, pressure drop, and CADR (Botvinnik et al., 2008; Mizuno et al., 1999; Morawska et al., 2002). Electrostatic precipitators (ESP) can be classified by the number of stages used to charge and collect particles of a pollutant gas. Single-stage ESPs apply a high voltage to charge particles and subsequently collect them within the same chamber on surfaces of opposite charge, and are most commonly used to reduce coarse dusts from boilers and other industrial processes. Two-stage ESPs consist of a charging stage, utilizing thin wires equally spaced from the parallel or cylindrical grounded plates or tubes, and a collection stage involving separate parallel metal plates that collect negatively (positively)

charged particles on positively (negatively) charged plates. The two-stage ESPs were originally designed for air purification in conjunction with air conditioning systems to improve IAQ (Electrostatic Precipitator Knowledge, 2012). Botvinnik et al. (2008) developed novel two-stage ESP air cleaners with two types of wire-plate geometries. ESPs with a length of 74 cm have high collection efficiencies of almost 100 to 50% at air velocities of 1 to 2 m/s and a maximum CADR of 5 m^3/min with a 2.43 kV/ mm electric field of the collection region. However, ozone produced by the air cleaners consuming corona current of several hundred microamperes was removed by an additional chemical ozone filter. Ozone is normally generated as a by-product of the corona discharge in an ESP and in the indoor environment can damage respiratory organs and degrade materials used in furnishing. Consequently, the daily 8-hr maximum ozone concentration has been set at less than 60–80 ppb by environmental regulatory agencies such as the World Health Organization (WHO), U.S. Environmental Protection Agency, and the European Commission (Liu et al., 2000; Bell et al., 2006). Ozone production by particle charging in the metallic corona pre-charger (thin wires or sharp sparks) of an ESP depends on a number of factors including the flow rate, relative humidity, material used in the ESP, diameter or thickness of the high-voltage electrode, operational voltage and current, and polarity of the corona discharge (Yehia et al., 2000; Cardello et al., 2002; Goheen et al., 1984). Different thicknesses of the corona discharge electrode for a given discharge current can affect ozone generation from the charger because the area available for ionization and dissociation of oxygen molecules decreases as the thickness of the discharge electrode in the precharger decreases (Yasumoto et al., 2008).

Carbon fiber ionizers are made of graphite and can be utilized easily and inexpensively by applying a voltage of a few kilovolts to a bundle of approximately 300 carbon fibers (each a few micrometers in diameter) to generate ions (Peterson et al., 2005). These ionizers can produce high concentrations of stable unipolar ions, while generating negligible amounts of ozone owing to the fine diameters of the carbon fibers (Han et al., 2008a, 2008b, 2009a, 2009b; Kim et al., 2011). Consequently, carbon fibers have been used as an alternative to avoid the corona discharge from thin metallic wires and spikes. In previous studies, I successfully developed an ESP with carbon fiber ionizers and non-metallic collection plates for the treatment of fine and ultrafine particles and mists in corrosive gases released during the manufacture of semiconductors (Kim et al., 2010, 2012). Park et al. (2011) and Noh et al. (2011) also developed air cleaners using fibrous and electret filters, which were electrostatically assisted by carbon fiber ionizers. The particle removal efficiency of the air cleaner developed by Park et al. (2011) was only 20% for 100-300 nm particles at the relatively low

air velocity of 0.4 m/s, whereas the air cleaner developed by Noh et al. (2011) had an efficiency of 80% at 0.8 m/s. In the latter case, particle removal was enhanced by an electret filter, but the collection efficiency of the electret filter was only 60%, even when using four carbon fiber ionizers. This low enhancement of the electret filter, even with multiple carbon fiber ionizers, may be attributable to low charging efficiency because the ionizer geometry was arranged without electrostatic separation of each carbon fiber ionizer. Electrostatic separation was found to be important to charging efficiency in our previous studies (Kim et al., 2010, 2012). I am unaware of any previously developed air cleaner that utilizes a two-stage ESP method with carbon fiber ionizers and metallic parallel collection plates.

Figure 1 and Table 1 present a summary of indoor air cleaners certified by the Korea Air Cleaning Association (KACA) and Association of the Home Appliance Manufacturers (AHAM) (KACA, 2011; AMAH, 2011). The majority of the certified air cleaners have a CADR lower than 5 m^3/min, with only 11 (5.1%) of the air cleaners having a CADR larger than 10 m^3/min. According to the 2011 directories, air cleaners that have a high CADR over 12 m^3/min are only 2.6% of 195 models in US and 4.1% of 73 models in Korea, respectively, and all of the high CADR air cleaners are equipped with HEPA filters for particle removal.

Table 1. The number and percentage of room air cleaners in terms of filtration types and clean air delivery rates as certified by the Korea Air Cleaning Association and Association of the Home Appliance Manufacturers.

Conditions		Korea Air Cleaning Association - number (%)	Association of Home Appliance Manufacturers - number (%)
Total certified A.Cs		73 (100.0)	195 (100.0)
Filtration type	HEPA Filter	59 (80.8)	-
	HEPA filter and ion emission	14 (19.2)	-
CADR values	~ 5 m^3/min	46 (63.0)	131 (67.2)
	5 ~ 10 m^3/min	19 (26.0)	54 (27.7)
	10 m^3/min ~	8 (11.0)	10 (5.1)

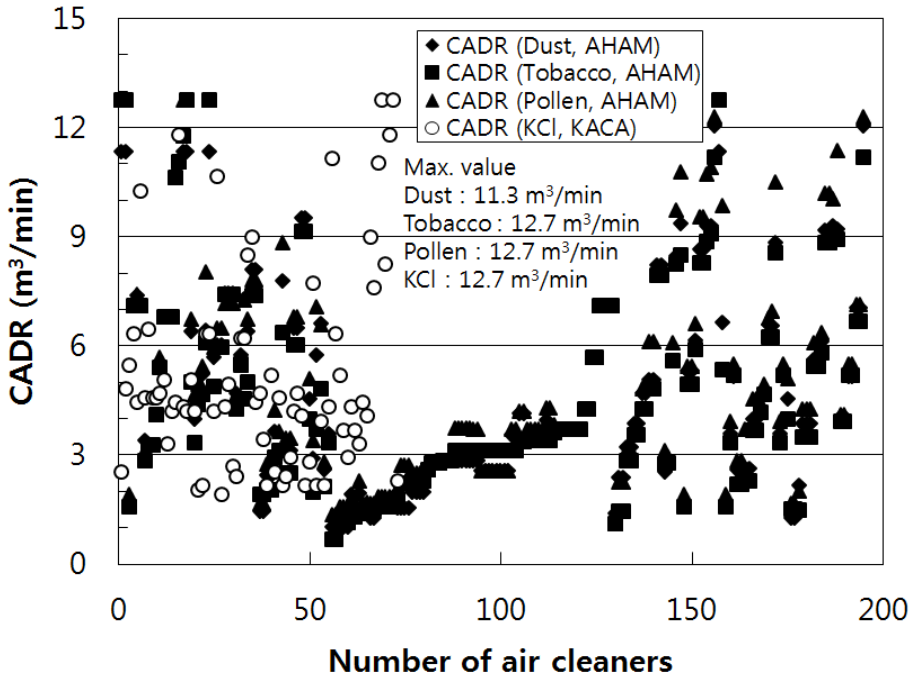

Figure 1. Distributions of CADRs for room air cleaners certified by the Korea Air Cleaning Association and Association of the Home Appliance Manufacturers.

In this study, to achieve a high CADR (>12 m^3/min) with negligible ozone production in a standard test chamber less than 10 ppb, I developed a novel two-stage ESP air cleaner with an ionizer composed of separate cells and carbon fibers that was located at the center of the each cell and with parallel metallic collection plates, which were covered by non-metallic insulating materials around the edges. To achieve ozone emissions much lower than the current regulation limit of 50 ppb, I used positive polarity for particle charging. In this study, I evaluated the particle removal efficiency of the air cleaner by changing several parameters in the ionizer and collection plates. Ozone emissions were also measured under the maximum operating conditions. Finally, experimentally acquired CADRs for the air cleaner were compared with those obtained from a theoretical analysis using the Deutsch equation and established diffusion and field-charging theories. Finally, I compared the CADR and pressure drop of the ESP air cleaner to those of an air cleaner with the same HEPA filter that is used for a commercially available air cleaner with a high CADR over 12 m^3/min which was certified by AHAM and KACA.

6.1.2 Experimental set up

Figure 2 is a schematic diagram of the two-stage ESP air cleaner used in this study, consisting of separate rectangular channel ionization and parallel plate collection stages, a main body, and a fan. Particles in the air drawn into the device by the fan receive a unipolar charge in the ionization stage at the inlet of the air cleaner. They then flow uniformly into the collection stage after passing through the perforated plate in the main body and are collected on the opposite polarity collection plates. The ionization stage (400 x 400 x 140 mm^3) was made of unipolar carbon brush chargers located at the center of 16 isolated channels that were equally spaced (50 mm) from the grounded walls of the channels. The chargers were connected to a high-voltage power supply, and the channels were electrically grounded. The collection stage (400 x 400 x 210 mm^3) consisted of 51 parallel metallic plates, 7 mm apart with dimensions of 400 mm (length), 210 mm (width), and 3 mm (thickness). The holes into which each plate was inserted were positioned at the edge of the collection stage. The collection plates were alternately connected to the high-voltage power supply and grounded. The fan was located at the outlet of the air cleaner and its flow rate was controlled with an electrical inverter.

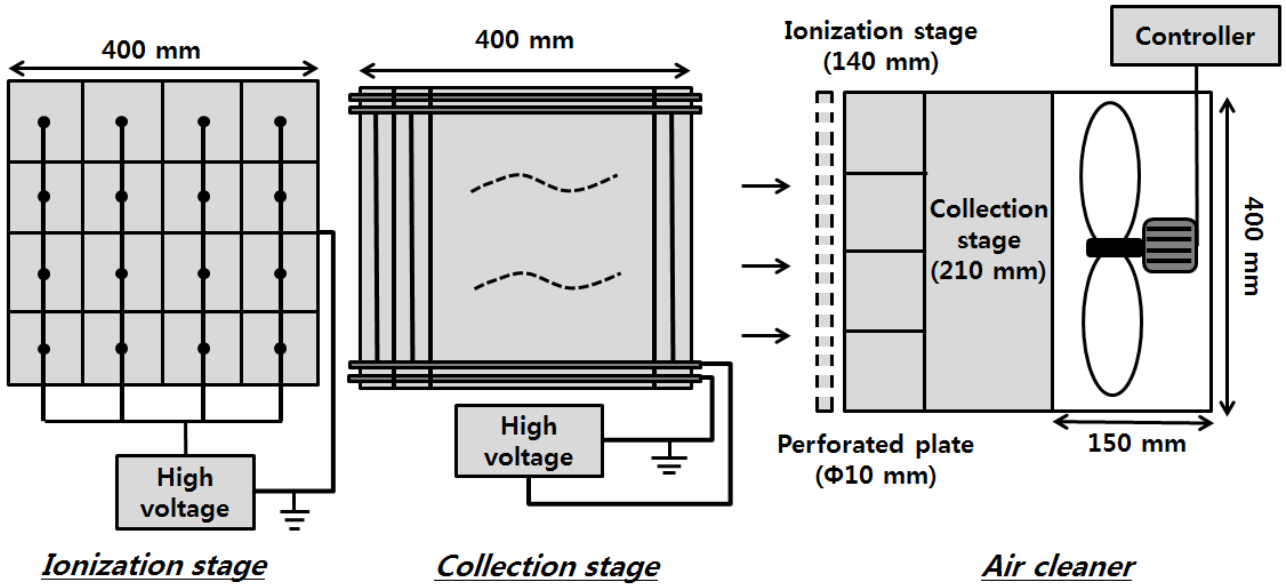

Figure 2. The structure of the ESP air cleaner developed in this study.

Figure 3 shows the experimental setup for the single-pass collection efficiency test for particles in the size range from 0.25 to 0.35 μm, which includes the particle size, 0.3 μm, used as the Korean and Japanese test standard for air cleaners (KACA, 2006; JEMA, 1995), and is also the most

penetrating particle size range for the ESP that measured in our previous study using particles with the size range from 0.03 to 10 μm (Kim et al., 2012). The procedure used was a Korean standard test method for an air cleaner, SPS-KACA-002-132 (KACA, 2006). Potassium chloride (KCl) aerosol particles, with diameters in the range 0.01~0.5 μm, were generated by nebulizing a solution of KCl (w/w 0.05% in water) using an atomizer with a constant output (Model 3076: TSI Inc., Shoreview, MN., USA) and passing them through a Kr-85 neutralizer and finally a diffusion dryer. The charged fractions of the test particles were removed using a plate condenser (to which a high voltage of -10 kV was applied), and uncharged particles were then introduced upstream of the test duct (600 x 600 mm). Clean air filtered by a HEPA filter was introduced and the particles then passed through the perforated plates and flowed uniformly into the air cleaner. The initial concentration of particles upstream of the ESP air cleaner was maintained at approximately 10^8-10^9 #/m^3. The ESP air cleaner was inserted into the test duct with the inlet and outlet of the air cleaner separated by sealant tape and a plate specifically designed to ensure that no test particles were able to leak downstream of the air cleaner without filtration.

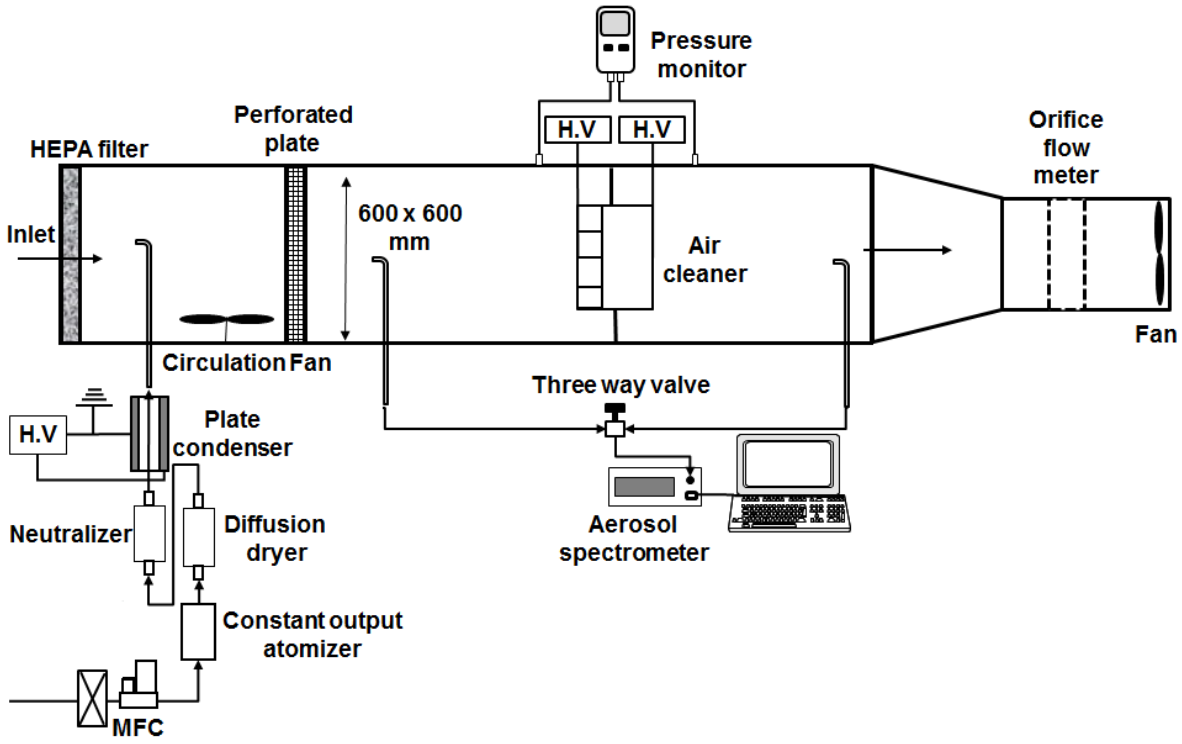

Figure 3. Experimental arrangement for the single-pass collection efficiency test.

By using the fan, the air flow rate of the air cleaner was varied from 10 m^3/min to 20 m^3/min, which corresponded to approximately 1 m/s and 2 m/s through the ionization and collection stage. Two

high-voltage power supplies (Max +/- 30 kV/ 10 mA, Korea Switching, Korea) were connected to the ionization stage and the collection stage. The applied voltages and corona currents were measured using digital multimeters (Model 286, Fluke Corporation, Japan). The number concentrations of the KCl particles upstream and downstream of the ESP air cleaner were repeatedly measured using a three-way valve and an optical particle counter (Model 1.109: Grimm Aerosol Technik GmbH, Germany). The pressure drop through the ESP air cleaner was measured at inlet and outlet of the ESP using a pressure monitor (350-M/XL-454: TESTO AG, Germany).

The performance of the ESP used in this study was expressed in terms of the single-pass particle collection efficiency (η), which was obtained by the following equation:

$$\boldsymbol{\eta = \left(1 - \frac{C_2}{C_1}\right) \times 100} \qquad (1)$$

where η is the single-pass collection efficiency, C_1 is the number concentration of particles downstream of the ESP with voltage applied only to the collection plates, and C_2 is the number concentration of the particles downstream of the ESP with voltages applied to both the chargers and collection plates. This minimized the impact of particles, which were charged during particle generation on the collection efficiency of the ESP air cleaner. To fully understand the effect of varying the operating parameters on particle single-pass collection efficiency of the air cleaner, the efficiency was measured after changing both the flow rate and the voltage applied to ionizers and collection plates.

The AHAM established decay-measured CADR as a performance metric based on an air cleaner's ability to reduce airborne particles in a closed chamber (AHAM, 2006). This study measured the particle-removal efficiency of a room air cleaner (i.e., the CADR) with variations in the same parameters used for single-pass collection efficiency tests.

The experimental arrangements for the decay-measured CADR measurements are shown in Figure 4. The ESP air cleaner was placed in a closed chamber (30.4 m^3), and an optical particle counter (Model 1.109: Grimm Aerosol Technik GmbH, Germany) was used to measure the particle concentrations in the chamber. The natural decay of a known particle concentration (approximately 3 x 10^8 particles/m^3) indicated no decrease in the initial concentration over a 1-hour period. Therefore, particle loss on the wall of the test chamber was considered to be negligible during the test.

A blower which was connected to the HEPA filtration system was operated until the concentration of residual particles in the test chamber had decreased to less than 10^5 #/m^3. When the background level of particles in the test chamber fell below this limit, a circulation fan was operated to ensure particle mixing. Uncharged KCl particles generated from a constant output atomizer (Model 3076: TSI Inc.)

were introduced to the chamber with clean compressed air at a rate of 2 L/min until the initial concentration of the test particles ranged between 10^8 and 10^9 #/m^3. When the required concentration was reached, the circulation fan was turned off, the air cleaner was turned on, and particle concentrations were recorded at 1-min intervals for a 30 min period.

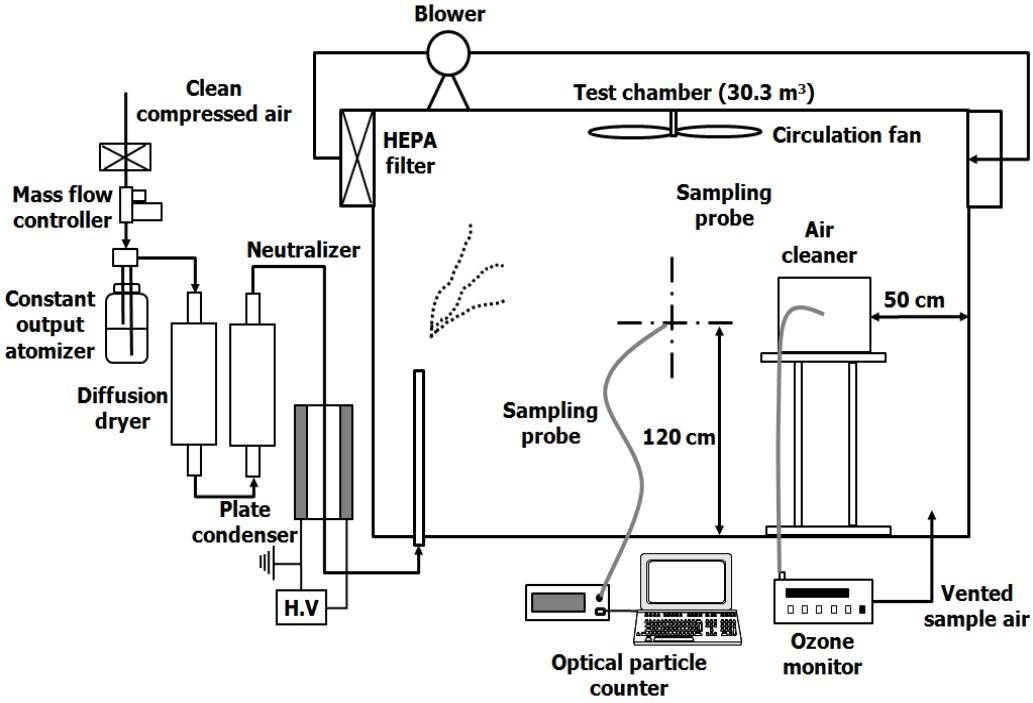

Figure 4. Experimental arrangement for the decay-measured CADR and ozone concentration tests in a test chamber.

The decay-measured CADRs of the ESP air cleaner under different operating conditions were calculated using the AHAM method (AHAM, 2006).

Theoretically, the regression of particle concentration follows a first-order decay model:

$$C_t = C_0 e^{-kt} \quad (2)$$

where

C_t = concentration at time t (#/m^3)

C_0 = initial concentration at t = 0 (#/m^3)

k = decay constant (t^{-1})

t = time (min)

The time-resolved decay constant k is calculated statistically by a linear regression of $\ln C_{ti}$ and t_i using the following formula:

$$\mathbf{k} = \left[\frac{S_{XY}}{S_{XX}}\right] \quad (3)$$

where

$$\mathbf{S_{XY}} = \sum_{i=1}^{n} \mathbf{t_i ln C_{t_i}} - \frac{1}{n}\left(\sum_{i=1}^{n} \mathbf{t_i}\right)\left(\sum_{i=1}^{n} \mathbf{ln C_{t_i}}\right)$$

$$\mathbf{S_{XX}} = \sum_{i=1}^{n} (\mathbf{t_i})^2 - \frac{1}{n}\left(\sum_{i=1}^{n} \mathbf{t_i}\right)^2$$

Using equations (2) and (3), the AHAM method for calculating CADR is

$$\text{CADR} = V (k_e - k_n) \quad (4)$$

where

CADR = clean air delivery rate (m^3/min)

V = volume of test chamber (m^3)

k_e = total decay rate (min^{-1})

k_n = natural decay rate (min^{-1})

In this study, the natural decay (k_n) was measured with the same test procedure used for the measurement of the total decay rate, where the air cleaner was operated with a high voltage applied to only the collection plates. Any decay in particle concentration prior to the operation of the air cleaner was negligible because there was no leakage or diffusion loss of particles in the test chamber during the 30-min test period. The CADRs of the air cleaner were also measured in the test chamber with both different flow rates and voltages applied to the ionizers and collection plates.

Previous studies (Ginestet et al., 2008; Waring et al., 2008) showed that if the air flow rate and single-pass removal efficiency are known, a single-pass CADR can be estimated using the following formula:

$$\text{CADR} = \eta \times Q \times E \quad (5)$$

where

η : single-pass collection efficiency of the ESP air cleaner

Q: air flow rate of an air cleaner

E: short-circuit factor (E = 1 under well-mixed conditions)

From equation (5), I calculated the single-pass CADR with Q and η values, which were obtained from the single-pass particle collection efficiency test under set test conditions.

Ozone, which is normally generated as a by-product from ESPs with edge or wire-to-plate ionizers, was measured using an ozone monitor (API 100E: Teledyne Technologies Inc. Thousand Oaks, CA, USA) when a set voltage was applied, with positive or negative polarity to the carbon fiber ionizers of the ESP air cleaner. The ozone monitor was calibrated against ozone standards of 0, 100, and 300 ppb. By measuring the ozone emission with a variety of voltages applied to the ionization stage of the air cleaner, I was able to determine conditions emitting less than 10 ppb ozone during 12 hours of continuous operation in a test chamber.

Table 2. Parameters for the theoretical calculation of CADRs for the ESP air cleaner used in this study.

Collection efficiency		**Charges by diffusion charging**		**Charges by field charging**	
d_p (μm)	0.3	d_p (μm)	0.3	d_p (μm)	0.3
E_c (V/m)	714,000~1,000,000	T (K)	273	ε	4.6
L (m)	0.21 m	t (sec)	0.067~0.134	t (sec)	0.067~0.134
v (m/s)	1.04-2.08	N_i (ions/m^3)	10^{14}	E (V/m)	116,000
s (m)	0.007			N_i (ions/m^3)	10^{14}

6.1.3 Theoretical calculation of the CADR of the ESP air cleaner

The theoretical CADRs of the ESP air cleaner for these particles were compared with CADRs measured in this study. To determine the theoretical CADR, I used equation (5) in this study, and the theoretical single-pass collection efficiency was calculated with the Deutsch model, which has been widely used in previous studies of the efficiency of two-stage ESPs (e.g., Yoo et al., 1997; Kim et al., 2011, 2012). In particular, in this study I assumed that the particle charge (n_e) is a function of time calculated by summing diffusion charging (n_1) and field charging (n_2) theory results because the particle size range that I chose in this study was only from 0.25 to 0.35 μm in which both of the two mechanisms are operating and the charging phenomenon is much more complicated. In particular, particle charges using this summation assumption among various charging theories

showed a fairly good agreement with experimental results for size-dependent particle charges in the previous study (Long and Yao, 2010). The calculation methods were expressed in detain with equation (1), (2), (15), and (16) in Chapter II.

Table 2 shows the parameters for collection efficiency and charge acquisition by diffusion and field charging that were used in our theoretical CADR calculations. I also used the same value of permittivity of KCl (4.6) as used by Park et al (2011). The N_i generated from the carbon fiber ionizers was measured using an ion counter (Ionometer IM806: Umweltanalytik Holbach GmbH, Wadern, Germany).

6.1.4 Results and discussion

Figure 5 shows the variation in current against the voltages applied to the carbon brush chargers with different polarity and flow rates. At the same applied voltage from 5 to 10 kV, a positive corona led to 45 to 70% lower corona currents than with a negative corona. For a given voltage, no significant changes were observed by increasing the flow rate of the test air, regardless of the polarity. The positive corona current at 8 kV to 16 carbon brush chargers was average 87 μA which was significantly lower than several hundred microamperes that consumed in the EPS air developed by the previous research (Botvinnik et al., 2008).

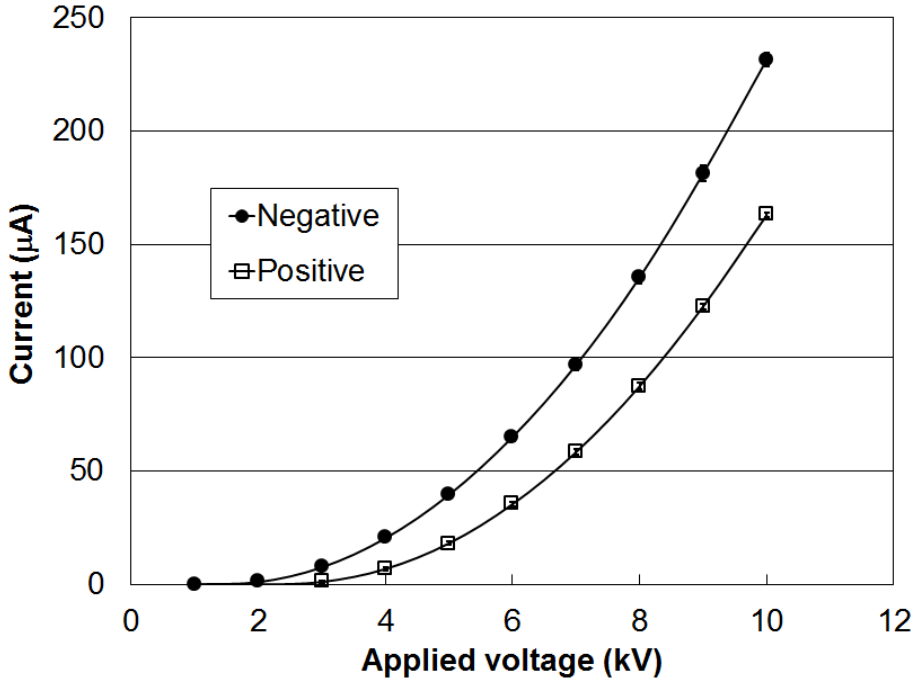

Figure 5. Voltage and current curves for different voltages applied to the carbon fiber ionizers at different polarities and flow rates.

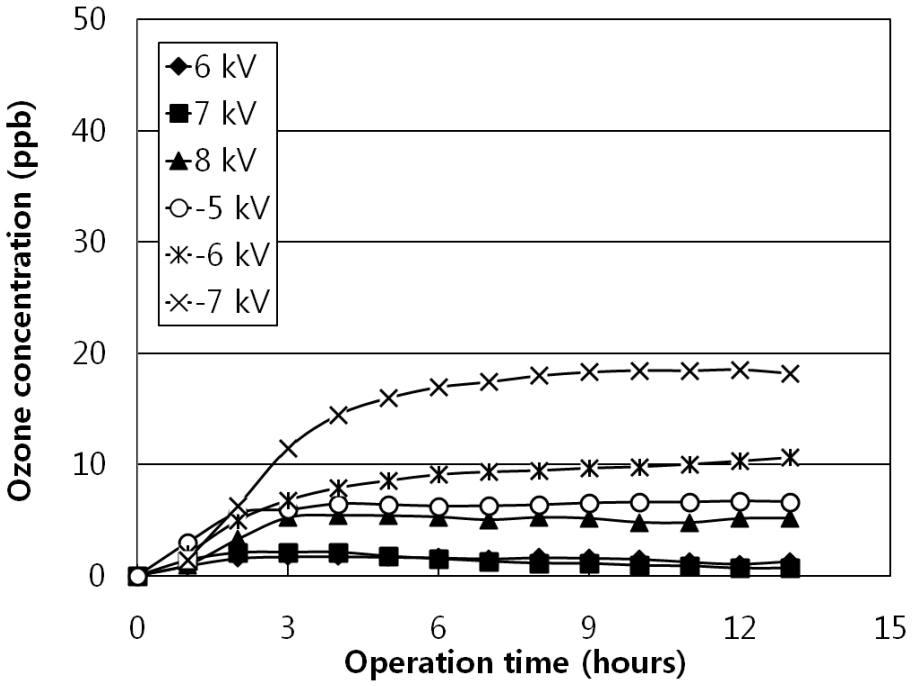

a) Different applied voltages and polarities

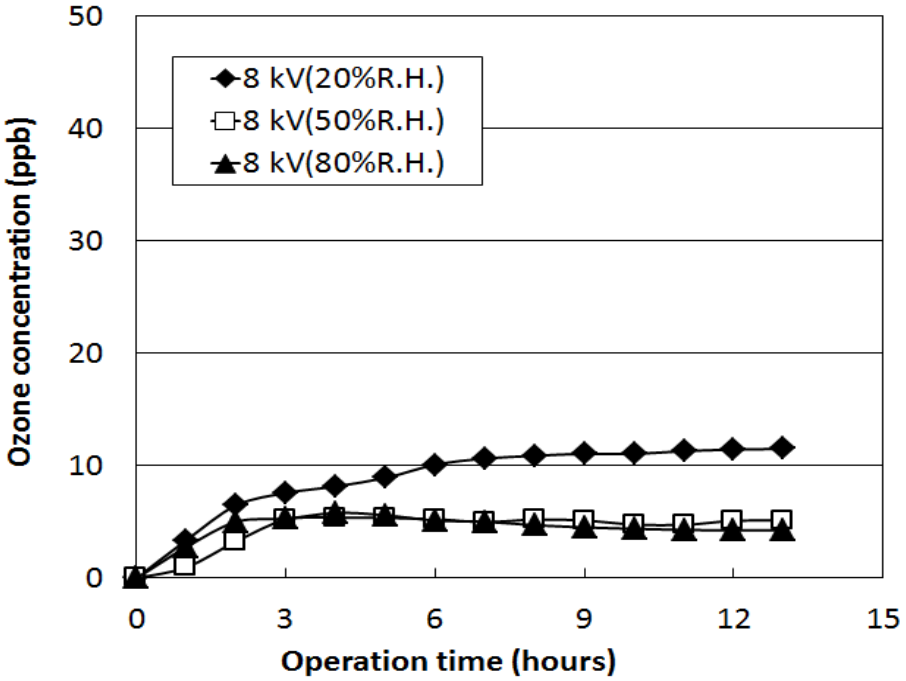

b) Different humidity

Figure 6. Ozone concentrations resulting from emissions of the ESP air cleaner over 12 hours of continuous operation for (a) different voltages applied to the carbon fiber ionization stage at negative and positive polarities and (b) for different relative humidity at positive polarities.

Figure 6 shows ozone emission from the ESP air cleaner over 12 hours of continuous operation for different voltages applied to the carbon fiber ionization stage: 6, 7, and 8 kV for positive polarity, and 5, 6, and 7 kV for negative polarity, respectively. The air cleaner was operated at 20 m^3/min with which the air cleaner achieved highest CADRs. The half-life time of ozone with approximate 20 ppb in the test chamber was approximately 32 minutes. Shown in Figure 6 a), ozone concentration with positive polarity in the test chamber was approximately only 25% of that with negative polarity at the same applied voltages. In particular, with positive polarity the maximum ozone concentrations were only from 2 to 6 ppb which was much lower than 50 ppb, the ozone concentration limit for 24-hour operation of ESP air cleaners set as the UL safety standard for electrostatic air cleaners, UL 867 (UL 867, 2004). The most likely reason for the low levels of ozone is that the diameter of the carbon brushes (several micrometers) used in this study is significantly smaller than the diameters (several hundred micrometers to millimeters) generally used in electrodes in ESPs. The ozone formation is reduced with a decrease in diameter and thickness of the high-voltage electrode of the ESP because the area available for ionization and dissociation of oxygen molecules decreases as the thickness of the discharge electrode in the precharger decreased (Boelter and Davidson, 1997; Yasumoto et al., 2008). Also, the electrical potential just around the thinner micrometer carbon brushes could be high enough for discharge, even though the electrical potential of 6 to 8 kV with about a 50 mm distance in the ionization stage of this study was much smaller than 12 to 13 kV with a distance between 25 and 51 mm in general two-stage ESPs (Electrostatic Precipitator Knowledge, 2012). Shown Figure 6 (b), the ozone emission of the ESP air cleaner with 8 kV of applied voltage increased with decrease of the relative humidity. This is the due to the destruction of ozone by water vapor in the inlet of air stream (Viner, 1992). Even though the ozone emission at 20 %R.H. of relative humidity was 11.5 ppb, higher than those at 50 and 80 %R.H, 5.1 and 4.3 ppb, respectively, the concentration was still much lower than 50 ppb.

Figure 7 shows the variation in single-pass collection efficiency of the particles at the different voltages applied to the carbon fiber ionization stage of the ESP air cleaner for different flow rates. The voltage applied to the collection plates was maintained at 7 kV, while the voltage applied to the ionization stage was varied from 6 to 8 and the flow rate varied from 10 to 20 m^3/min (CMM: cubic meters per minute)) corresponding to face velocities of approximately 1 to 2 m/s through the air cleaner. The single-pass collection efficiency of the particles increased linearly with the increase in voltage applied to carbon fiber ionizers.

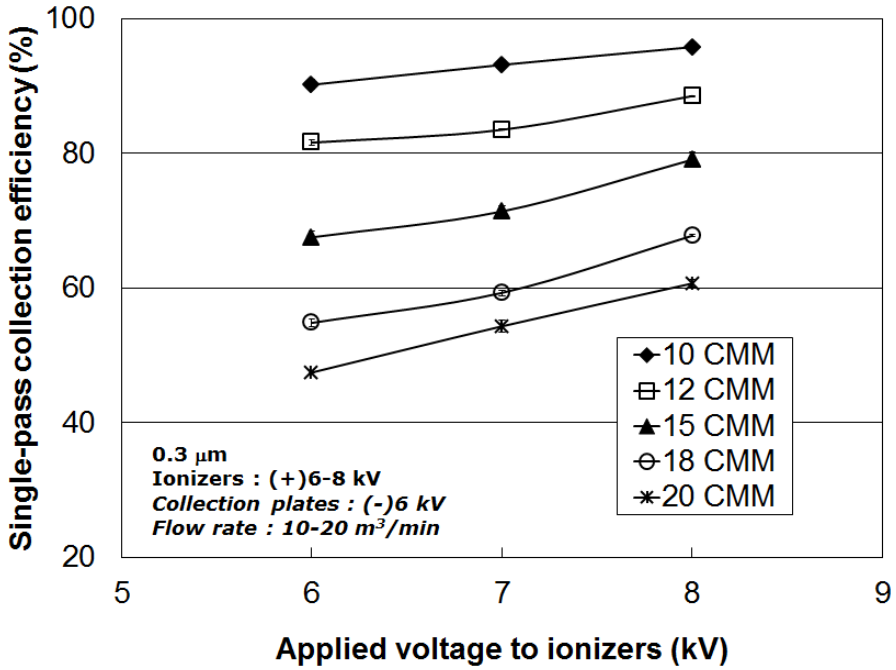

Figure 7. Variation in single-pass collection efficiency of the particles for different voltages applied to the carbon fiber ionization stage of the ESP air cleaner at different flow rates.

This result is consistent with the findings of Han et al. (2010), who examined a high-voltage electrode of the metallic triangle-edge type that is commonly used in ESPs for industrial applications. Constants of proportionality were dependent on flow rates and increased from 2.8 to 6.6 as the flow rate increased from 10 to 20 m^3/min. In particular, with a voltage applied to the collection plates of -6 kV and a voltage higher than 7 kV applied to the ionizers at flow rates less than 15 m^3/min, the single-pass collection efficiency of the air cleaner in this study was over 70%, which is the minimum single-pass collection efficiency required for certification by the KACA (KACA, 2006).

Figure 8 shows the variation in single-pass collection efficiency for these particles with different voltages applied to the collection stage of the ESP air cleaner at different flow rates. The voltages applied to the collection stage varied from -5 to -7 kV, and flow rates ranged between 10 and 20 m^3/min, while the voltage applied to the ionizers was maintained at 7 kV. Like for the results with ionizers shown in Fig. 7, the single-pass collection efficiency for the particles also increased linearly with an increase in voltage applied to the collection plates under the same experimental conditions, owing to the higher electrical field strength (Kim et al., 2010). With a voltage applied to the carbon fiber ionizers of 7 kV and a voltage higher than -6 kV applied to the collection plates at flow rates below 15 m^3/min, the single-pass collection efficiency of the air cleaner was also over 70%.

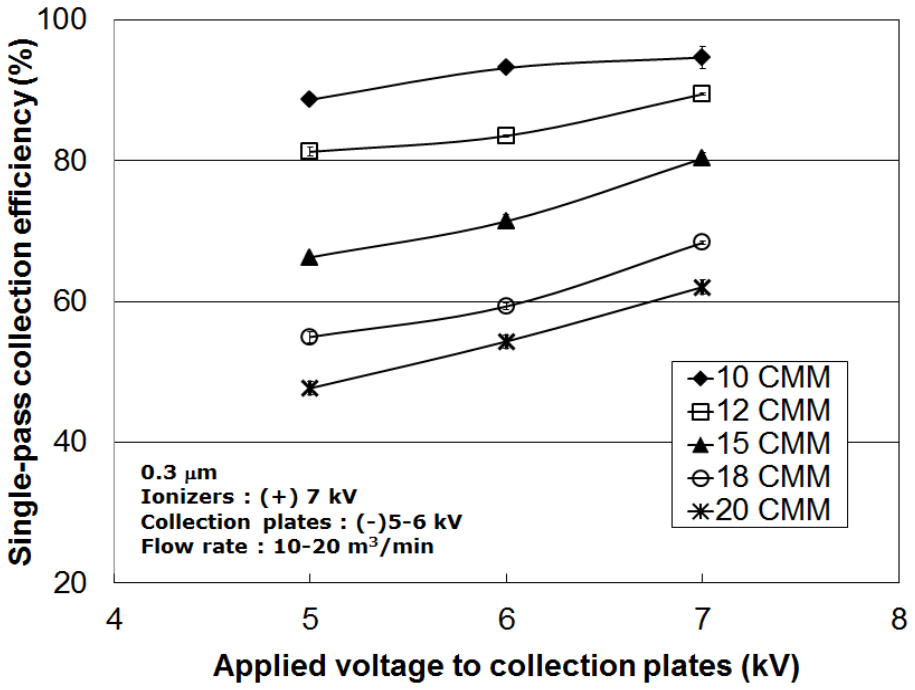

Figure 8. Variation in single-pass collection efficiency of particles for different voltages applied to the collection stage of the ESP air cleaner at different flow rates.

The results of this study suggest that certain collection efficiency is possible with a voltage applied to the ionizers over 8 kV and a voltage applied to the collection plates over 7 kV, and this could be used to select the voltage needed to achieve a set collection efficiency of an ESP air cleaner.

Figure 9 shows the variation in single-pass collection efficiency of the particles with different flow rates through the ESP air cleaner with different voltages applied to the chargers and collection plates. The flow rate ranged between 10 and 20 m^3/min. The single-pass collection efficiency of the particles decreased linearly with an increase in the air flow rate of the air cleaner under the same experimental conditions because of a decrease in the residence time in both the ionization and collection regions. Constants of proportionality for different applied voltages to ionizers and collection plates were similar: -4.15 %/m^3/min with a standard deviation of 0.798 %/m^3/min and -4.68 %/m^3/min with a standard deviation of 1.59 %/m^3/min. This result suggests that a decrease in the collection efficiency at higher flow rates should be expected, but can be avoided by increasing the voltages applied to ionizers and collection plates to achieve set collection efficiency for the ESP air cleaner. Ozone emissions will need to be evaluated from the ESP air cleaner after increasing the voltage applied to the ionization stage to over 9 kV to achieve high

single-pass collection efficiency.

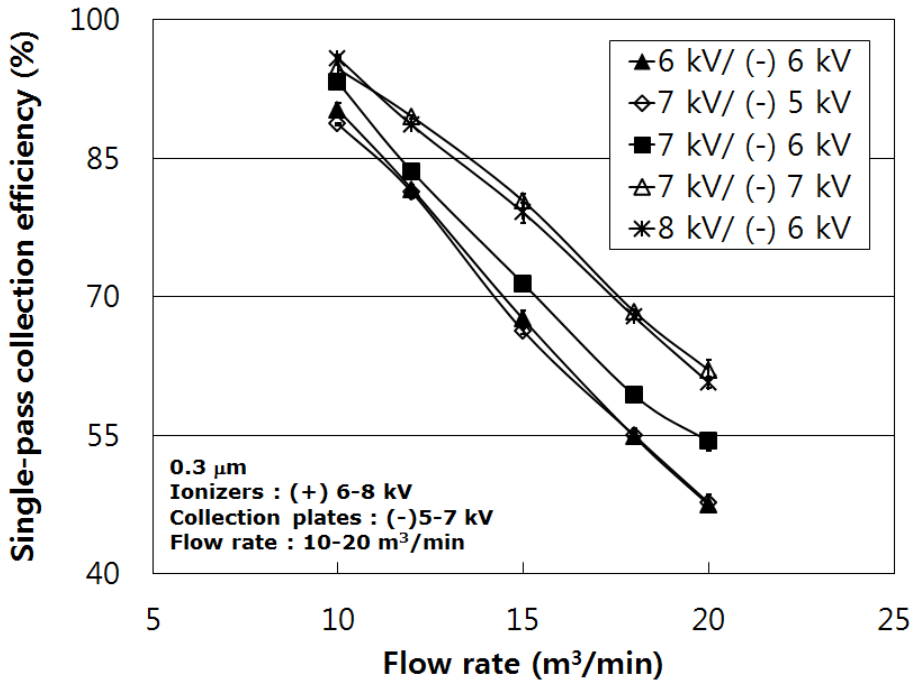

Figure 9. Variation in single-pass collection efficiency of particles for different flow rates through the ESP air cleaner at set voltages applied to the chargers and collection plates.

Figure 10 shows the variation in the single-pass CADRs of the ESP air cleaner for the particles at different voltages applied to the carbon fiber ionization stage and to the collection stage at different flow rates. The CADRs were calculated from equation (5) using the single-pass removal efficiencies shown in Figures 7 and 8. Unlike the collection efficiencies determined previously, the single-pass CADRs (a function of the product of flow rate and single-pass collection efficiency) were not linearly dependent on flow rates because collection efficiency decreased as flow rate increased. The single-pass CADRs increased at flow rates up to 15 m^3/min when lower voltages were applied to the ionizers (6 kV) and collection plates (- 5 kV), while the CADRs increased at flow rate up to 18 m^3/min when voltages above 7 kV were applied to the ionizers and voltages above -6 kV were applied to the collection plates.

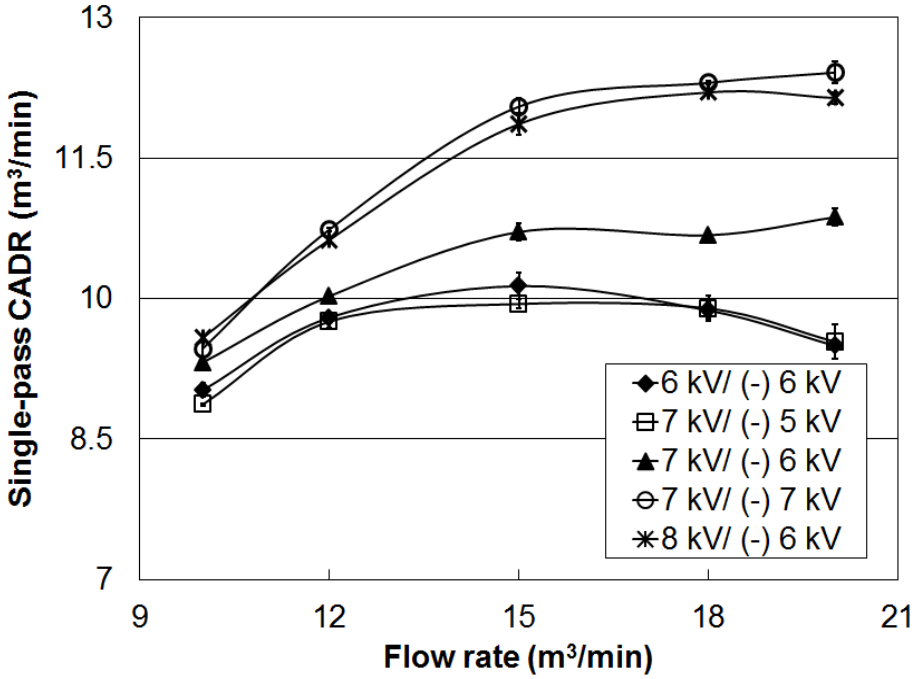

Figure 10. Variation in CADRs of the ESP air cleaner for particles at different voltages applied to the carbon fiber ionization stage and to the collection stage at different flow rates.

Figure 11 also shows the variation in decay-measured CADRs of the ESP air cleaner for the particles, measured with the CADR certification test methods used by the KACA and AHAM (KACA, 2006; AHAM, 2006). The voltages applied to the carbon fiber ionization stage and the collection stage, and the flow rate were maintained at the same test conditions as shown in Figure 10. As with the single-pass CADRs in Figure 11, the decay-measured CADRs with different voltages applied to the ESP air cleaner showed a small increase as flow rate increased because of the negative proportionality of the collection efficiency to the flow rate shown in Figure 9. The CADRs at flow rates over 15 m^3/min exceeded 10.5 m^3/min with voltages applied to the ionizers and collection plates over 7 kV and -6 kV, respectively. These were the voltages applied to the ESP air cleaner to obtain a single-pass collection efficiency higher than 70%. The CADRs of the air cleaner at flow rates over 18 m^3/min, and the voltages applied to the ionizers and collection plates over 7 and -6 kV, respectively, reached 12 m^3/min. This is one of the highest CADR values reported by the KACA and the AHAM, using an ionization stage with dimensions of 0.4 x 0.4 x 0.14 m^3 and a collection stage with dimensions of 0.4 x 0.4 x 0.21 m^2.

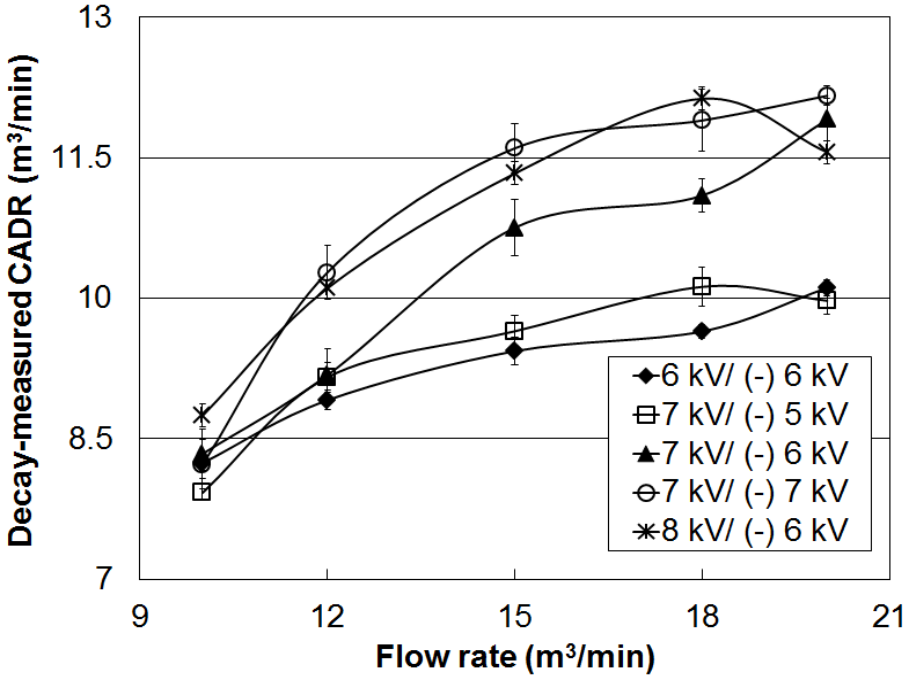

Figure 11. Variation in CADRs of the ESP air cleaner for particles, measured with the CADR certification test methods used by KACA and AHAM.

Figure 12 (a) shows the relationship of the single-pass CADRs obtained from equation (5) and the decay-measured CADRs using the KACA and AHAM test methods performed from March 2003 to December 2010, for 244 air cleaners commercially available in Korea, Japan, and the USA. Of these air cleaners, 98.8% were based on HEPA filters. The decay-measured CADRs were linearly proportional to the single-pass CADRs with a constant of 0.87, which is the short-circuit factor of the test chamber for these tests. Using this linear relationship, the CADR of a HEPA-filter air cleaner can be estimated from a simple calculation of the product of 0.87, single-pass efficiency, and flow rate, without the need for experimental determination.

Figure 12 (b) also shows the relationship of the single-pass and decay-measured CADRs for the carbon fiber ESP air cleaner used in this study. Both CADRs were also linearly proportional to each other with a short-circuit factor of 0.97, which indicates that the test particles were well mixed during the tests with the air cleaner in the same test chamber owing to the relatively high air flow rate. These results showed that the required CADR for the ESP air cleaner developed in this study can be determined by simply measuring the single-pass collection efficiency and the flow rate.

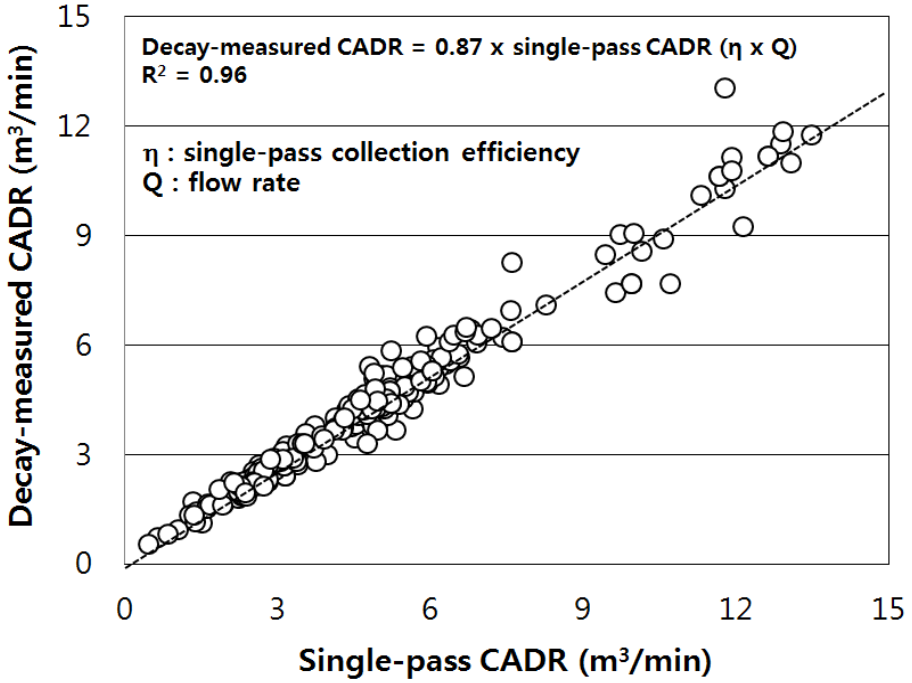

(a) For 244 HEPA-filter-type air cleaners commercially available in Korea, Japan, and America.

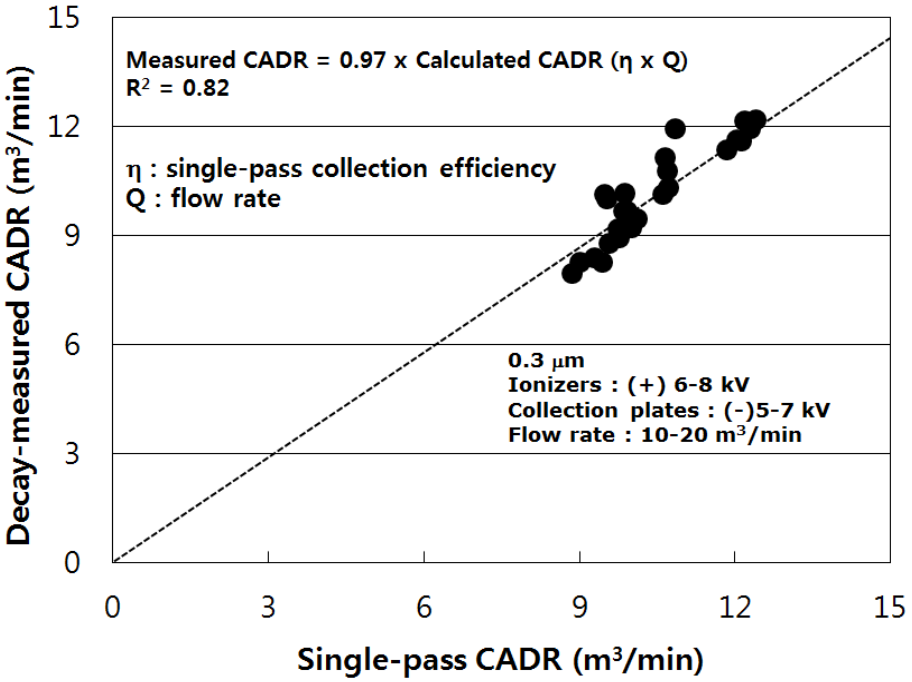

(b) For the ESP-type air cleaner used in this study.

Figure 12. Relationship between the single-pass CADRs and the decay-measured CADRs

Figure 13 shows CADRs as a function of flow rate and compares the decay-measured CADRs in this study with the CADRs predicted by diffusion and field-charging theories and the Deutsch collection efficiency model in Chapter II. The flow Reynolds number of this study was

27,000 to 53,000. The decay-measured CADRs agreed well with the predictions. The results shown in Figures 12 and 13 indicate that a simple product of single-pass collection efficiency predicted by the Deutsch equation, charging theories, and flow rate could be used to estimate the particle removal efficiency (i.e., CADR) in a closed room for ESP air cleaners without any experimental work.

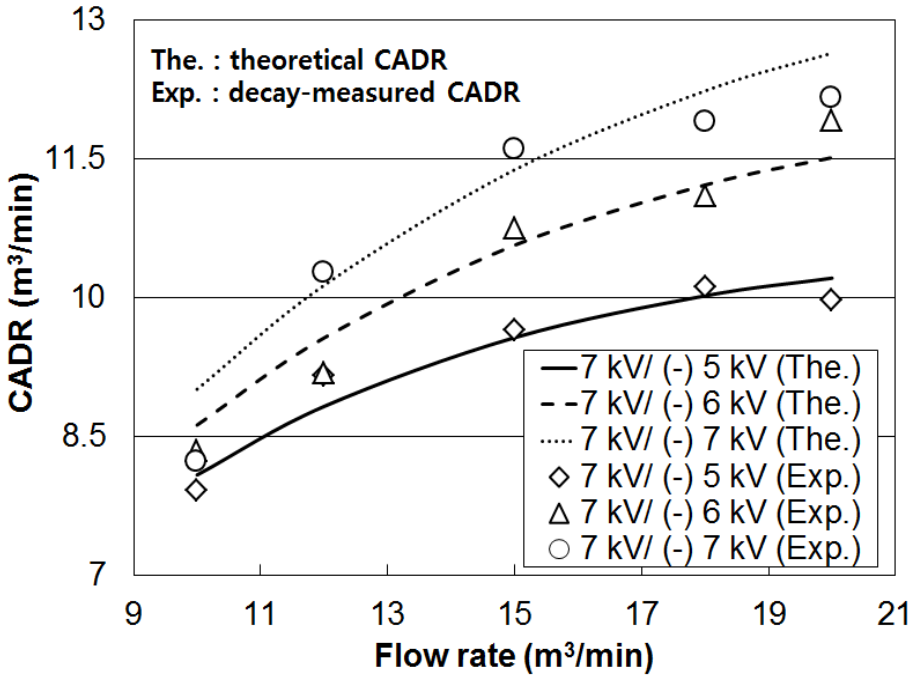

Figure 13. Comparison of CADRs as a function of flow rate (as measured in this study) and the CADRs predicted by diffusion and field-charging theories and the Deutsch collection efficiency model.

Figure 14 shows the comparison of performances between using the ESP in this study and using a HEPA filter (0.5 x 0.56 x 0.045 m^3) used in a commercial air cleaner which showed the CADR of 12.7 m^3/min at the flow rate of 16.1 m^3/min with using 0.3-μm KCl particles. The performance was evaluated with a pressure drop divided by a single-pass CADR at certain flow rate. The performance value with the HEPA filter increased with increase of flow rate because the pressure drop increased from 9.7 to 24.1 Pa while the single-pass CADR did from 9.8 to 19.1 m^3/min. However, the value with the ESP decreased as the flow rate increased because the pressure drop was maintained at average 4.6 Pa while the single-pass CADR increased. The average performance value with the ESP was 0.4 Pa/m^3/min which is only 36% of that with the HEPA filter. This results indicate that the air cleaner with the ESP in this study could achieve a high CADR performance with

significantly lower pressure drop than that of an air cleaner with a HEPA filter, and thus this technology could be very useful especially for air conditioning devices indoors which need to clean high volumetric air flow rate.

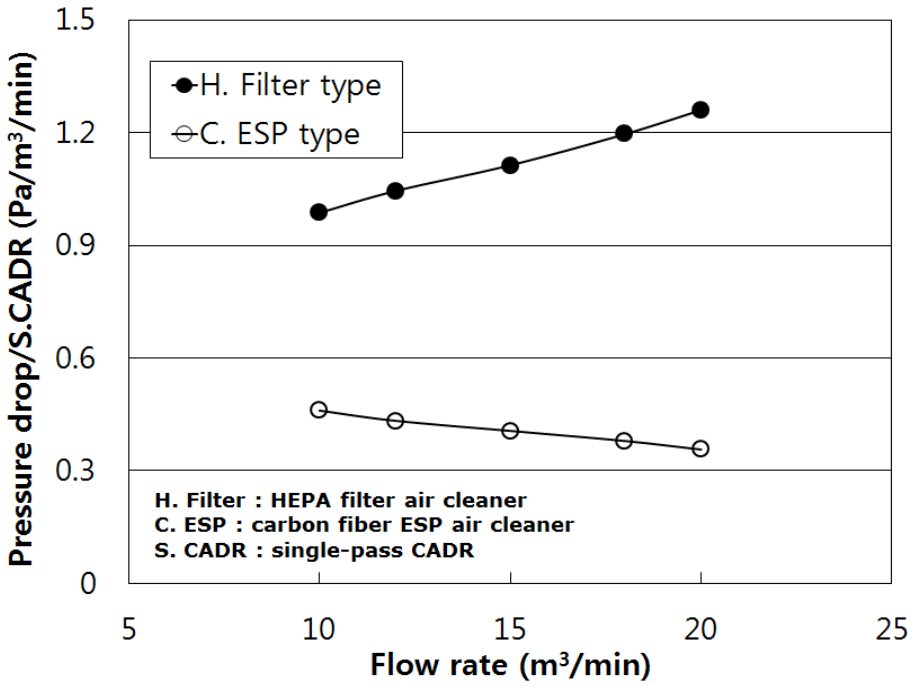

Figure 14. Comparison of the performance values of pressure drop divided by single-pass CADR at different flow rates between using the ESP in this study and using a HEPA used in a commercial air cleaner.

6.1.5 Conclusions

I developed a novel air cleaner based on electrostatic precipitation, which was composed of a perforated plate for uniform flow distribution, a channeled ionization stage (dimensions: 0.4 x 0.4 x 0.14 m^3) with 16 carbon fiber ionizers, and a collection stage (dimensions: 0.4 x 0.4 x 0.21 m^3) with parallel metallic plates with edges covered by nonmetallic insulators and a fan. The particle collection efficiency of the ESP air cleaner was evaluated for particles ranged between 0.25 and 0.35 μm, which are difficult to collect with the ESP, and the voltage applied to the ionization and collection stages and the flow rates were varied.

The test results indicated that emissions from the ESP air cleaner resulted in ozone levels lower than 10 ppb, which is just 1/5 of the current ozone regulations for a room air cleaner in a closed chamber. The ESP also achieved a high clean air delivery rate (>12 m^3/min). This is one of the

highest CADRs reported by the KACA and AHAM, with a voltage higher than 7 kV applied to the ionization stage and a voltage higher than -6 kV applied to the collection stage at flow rates faster than 15 m^3/min. It was also determined that the collection efficiency varied from 50 to 95% and was linearly proportional to both the voltages applied to the ionization and collection stages, and flow rates. The CADR varied between 7.9 and 12.1 m^3/min. The simple product of the single-pass collection efficiency and flow rate with experimental tests or a theoretical calculation can be used to determine the CADR of the ESP air cleaner in this study, eliminating the need to measure CADR. This simple determination of CADR could also aid in designing some operational parameters of air cleaners such as the voltages and flow rates required to achieve a certain collection efficiency or CADR. Finally, the average performance value (single-pass CADR/pressure drop in this study) with the ESP was 0.4 Pa/m^3/min which is only 36% of that with the HEPA filter. This results indicate that the air cleaner with the ESP in this study could achieve a high CADR performance with significantly lower pressure drop than that of an air cleaner with a HEPA filter.

Therefore, the ESP air cleaner described here is a promising device with an extremely high CADR for ultrafine particles coupled with low ozone emissions. It is particularly applicable for indoor environments with high air volumes.

6.1.5 References

AHAM (2006): Method for Measuring Performance of Portable Household Electric Room Air Cleaners, Washington, D.C., Association of Home Appliance Manufacturers (ANSI/AHAM AC-1-2006).

Association of Home Appliance Manufacturers (2011) 2011 Directory of certified portable electric room air cleaners. Edition No-4-October, Washington, DC, USA.

Bell, M.L., Peng, R.D. and Dominici, F. (2006). The exposure-response curve for ozone and risk of mortality and the adequacy of current ozone regulations, Environ. Health. Persp., 114(4), 532-536.

Berry, D., Mainelis, G. and Fennell, D. (2007). Effective of an ionic air cleaner on indoor/outdoor particle ratios in a residential environment, Aerosol. Sci. Tech., 41(3), 315-328.

Boelter, K.J. and Davidson, J.H. (1997). Ozone generation by indoor, electrostatic air cleaners, Aerosol. Sci. Tech., 27 (6), 689-708.

Botvinnik, I., Taylor, C.E. and Snyder, G. (2008). High-efficiency portable electrostatic air cleaner with insulated electrodes, IEEE. T. Ind. Appl., 44 (2), 512-516.

California Environmental Protection Agency (2008). Evaluation of ozone emissions from portable indoor air cleaners: electrostatic precipitators and ionizers, California EPA, Air Resources Board.

Cardello, N., Volckens, J., Tolocka, M. P., Wiener, R. and Buckley, T. J. (2002). Performance of a personal electrostatic precipitator particle sampler, Aerosol Sci. Technol., 36, 162-165.

Electrostatic Precipitator Knowledgebase. ESP Operation; Neundorfer, Inc.: Willoughby, OH, 2007; http://www.neundorfer.com/FileUploads/CMSFiles/ESP%20Operation[0].pdf

(Accessed October 2, 2012).

Ginestet, A., Blondeau, P., Frochot, D., Kaluzny, P., Lefévre, M.G., Ott, M., Blay, F., Pepin, L., Pugnet, D., Ribot, B. and Squinazi, F. (2008). A new test method for indoor air cleaner efficiency determination and harmlessness assessment, In: proceedings of Indoor Air 2008, Paper ID :154.

Goheen, S. C., Larkin, E. C. and Bissell, M. G. (1984). Ozone produced by corona discharge in the presence of water, Int. J. Biometeorol., 28, 157-161.

Han, B., Hudda, N., Ning, Z., Kim Y.J. and Sioutas, C. (2008). Enhanced unipolar charging of concentration-enriched particles using water-based condensational growth, J. Aerosol. Sci., 39, 770-784.

Han, B., Kim, H.J., Kim, Y.J. and Sioutas, C.(2008). Unipolar charging of fine and ultra-fine particles using carbon fiber ionizers, Aerosol. Sci. Tech., 42, 793-800.

Han, B., Hudda, N., Ning, Z., Kim, H.J., Kim, Y.J. and Sioutas, C. (2009). A novel bipolar charger for submicron aerosol particles using carbon fiber ionizers, J. Aerosol. Sci., 40, 285-294.

Han, B., Hudda, N., Ning, Z., Kim, Y.J. and Sioutas, C. (2009). Efficient collection of atmospheric aerosols with a particle concentrator-electrostatic precipitator sampler, Aerosol. Sci. Tech., 43, 757-766.

Han, B., Kim, H.J. and Kim, Y.J. (2010). Fine particle collection of an electrostatic precipitator in CO_2-rich gas conditions for oxy-fuel combustion, Sci. Total. Environ., 408, 5158-5164.

Hinds, W.C. (1999) Aerosol Technology: properties, behavior, and measurement of airborne particles, New York, John Wiley & Sons, Inc.

JEMA (1995). The household air cleaner, Tokyo, Japan, Japan Electrical Manufacturers' Association (JEM 1467).

KACA (2006) Room air cleaner standard, Seoul, Korea, Korea Air Cleaning Association (SPS-KACA002-132).

Kim, H.J., Han, B., Kim, Y.J., Hwang, K.D., Oh, W.S., Yoo, S.Y. and Oda, T. (2011). Fine particle removal performance of a two-stage wet electrostatic precipitator using a nonmetallic pre-charger, J. Air. Waste. Manage., 61(12), 1334-1343.

Kim, H.J., Han, B., Kim, Y.J. and Yoa, S.J. (2010). Characteristics of an electrostatic precipitator for submicron particles using non-metallic electrodes and collection plates, J. Aerosol. Sci., 41, 987-997.

Kim, H.J., Han, B., Kim, Y.J., Yoa, S.J. and Oda, T. (2012). Integration of a nonmetallic electrostatic precipitator and a wet scrubber for improved removal of particles and corrosive gas cleaning in semiconductor manufacturing industries, J. Air. Waste. Manage., 62(8), 905-915.

Korea Air Cleaning Association (2011) Directory of certified air cleaners. To September of 2011, Seoul, Korea.

Liu, L., Guo, J., Li, J. and Sheng, L. (2000). The effect of wire heating and configuration on ozone emission in a negative ion generator, J. Electrostat., 45, 81-91.

Long, Z. and Yao, Q. (2010). Evaluation of various particle charging models for simulating particle dynamics in electrostatic precipitators, J. Aerosol. Sci., 41, 702-718.

Mizuno, A., Kisanuki, Y., Noguchi, M., Katsura, S., Lee, S.H., Hong, Y.K., Shin, S.Y. and Kang, J.H. (1999). Indoor air cleaning using a pulsed discharge plasma, IEEE. T. Ind. Appl., 35 (6), 1284-1288.

Morawska, L., Agranovski, V., Ristovski, Z., Jamriska, M. (2002). Effect of face velocity and the nature of aerosol on the collection of submicrometer particles by electrostatic precipitator, Indoor Air, 12(2), 129-137.

Noh, K.C., Lee, J.H., Kim, C., Yi, S., Hwang, J. and Yoon, Y.H. (2011). Filtration of submicron aerosol particles using a carbon fiber ionizer-assisted electret filter, Aerosol. Air. Qual. Res., 11, 811-821.

Park, J.H., Yoon, K.Y. and Hwang, J. (2011). Removal of submicron particles using a carbon fiber ionizer-assisted medium air filter in a heating, ventilation, and air-conditioning (HVAC) system, Build. Environ., 46, 1699-1708.

Peterson, M.S., Zhang, W., Fisher, T.S. and Garimella, S.V. (2005). Low-voltage ionization of air with carbon-based materials, Plasma. Sources. Sci. T., 14, 654-660.

UL (2004) UL standard for Safety for electrostatic air cleaners, Northbrook, IL, Underwriters Laboratories Inc (UL 867).

Shaughnessy, R. J. and Sextro, R. G. (2006). What is an effective portable air cleaning device? A

review, J. Occup. Envion. Hyg., 3 (4), 169-181.

Sultan, Z.M., Nilsson, G.J. and Magee, R.J. (2011). Removal of ultrafine particles indoor air: Performance of various portable air cleaner technologies, HVAC & R. Res., 17 (4), 513-525.

Viner, A.S., Lawless, P.A., Ensor, D.S. and Sparks, L.E. (1992). Ozone generation in DC-energized electrostatic precipitators, IEEE Trans. Ind. Applicat., 28, 504-512.

Waring, M.S., Siegel, J.A. and Corsi, R.L. (2008). Ultrafine particle removal and generation by portable air cleaners, Atmos. Environ., 42, 5003-5014.

Yasumoto, K., Zukeran, A., Takagi, Y., Ehara, Y., Takahashi, T. and Yamamoto, T. (2008). Effect of electrode thickness for reducing ozone generation in electrostatic precipitator, Denki Gakkai Ronbunshi., 128-A (11), 689-694.

Yehia, A., Abdel-Salam, M. and Mizuno, A. (2000). On assessment of ozone generation in dc Coronas, J. Phys. D. Appl. Phys., 33, 831-835.

Yoo, K.H., Lee, J.S., Oh, M.D. (1997). Charging and collection of submicron particles in two-stage parallel-plate electrostatic precipitators, Aerosol. Sci. Tech., 27, 308-323.

Chapter VII

Size-dependent allergen particle removal by indoor air cleaning devices

7.1 A simple and efficient method for evaluating air-cleaning performance against airborne allergen particles

7.1.1 Introduction

Indoor air quality has received increasing attention in recent years with the global increase in allergic diseases. Exposure to indoor allergens is probably more important than exposure to outdoor allergens because we spend most of our time indoors. Indoor exposure is also perennial and often involves high concentrations, and the level of exposure increases with modernization in housing design (Tovey and Marks, 1999). In particular, exposure to allergens derived from house dust mites (HDM) causes bronchoconstriction in asthma patients and induces an inflammatory response in the lungs due to the release of cytokines, chemokines, and additional mediators (Kauffman et al, 2006). Also, HDM allergens, including Der P 1, a major group 1 allergen, are the most common cause of allergic diseases worldwide (Custovic et al., 1996; Sporik et al., 1990). Exposures to dog and cat allergens are also believed to play important roles in the etiology of asthma. Almost 40% of children with asthma are sensitive to cat allergens, and these allergens are a significant risk factor for acute asthma in patients seeking treatment in emergency rooms; even slight exposure to cats can precipitate severe asthma symptoms in susceptible individuals (Gelber et al., 1993; Custovic et al., 1998). The single major cat allergen (Fel d 1) is responsible for a large proportion of cat-specific IgE in patients who are allergic to cats (Ohman, 1978).

Different allergens are carried by particles with a range of shapes and sizes, which affects their behavior when they are disturbed and airborne. Using an aerosol sampler that collected airborne particles larger than 5 μm and an optical microscope, Lucaa et al. (1999) investigated the physical characteristics of Der P 1 in a house and found that 80% of detectable Der P 1 aerosols were associated with particles larger than 10 μm and that a small portion was associated with particles smaller than 5 μm. However, particles with aerodynamic diameters less than 10 μm increased the likelihood of lung deposition. Custovic et al. (1998) also investigated the size distribution of airborne

Fel d 1 particles using an aerosol sampler and the ELISA method based on allergen mass and found that 49% of the total allergens were larger than 9 μm, and almost 23% of the airborne Fel d 1 was carried on small particles (<4.7 μm) that could remain airborne for several days. However, these studies were only conducted using sampled allergen particles and were only based on allergen mass.

The use of electrical devices, such as air-cleaning devices, to reduce airborne house dust mite and cat allergens indoors may be of clinical benefit for allergen-sensitized respiratory patients (Pauli et al., 2000; Eggleston and Bush, 2001; O'Connor, 2005; Eggleston, 2005). Several researchers have studied the effects of filtration devices on the removal of allergen particles indoors (Green et al., 1999; Gore et al., 2003; Francis et al., 2003; van Strien et al., 2004). However, most of these studies were conducted using only measurements based on the time-consuming ELISA (two-site enzyme-linked immunosorbent assay) method, which cannot analyze the real-time size-dependent aerodynamic properties of removal devices.

The size- and time-dependent aerodynamic behaviors of airborne influenza particles were evaluated with various kinds of air cleaners in a closed chamber using in-situ optical particle sizers, while using NaCl particles, not real airborne influenza particles (Zurami et al., 2011).

In this study, the size and time-dependent aerodynamic behaviors of airborne allergen particles in a 30-m^3 chamber, both with and without the operation of air-cleaning devices, were evaluated by taking in-situ real time measurements using an optical particle counter. I also compared the particle-counter results to those from the ELISA method and suggested a new simple method that can predict air-cleaning performance against airborne allergen particles.

7.1.2 Experimental set up

Figure 1 shows photographs of the test powders that were used in this study. To prepare test powders that contained house dust mite and cat allergens, 30 g of culture medium containing house dust mite allergen (Der P 1) and cat allergen (Fel d 1) was cultured at a temperature of 25 ± 3℃ and a relative humidity of 75 ± 2%. The culture medium was then dried for 24 hours in an electric dryer. The cultured medium was carefully ground with a stirred ball mill for 10 minutes, and the mass concentration of the allergen proteins in the ground powder was 10% of the total mass.

Figure 2 shows the size distribution of the test powers based on numeric and volumetric concentrations when 0.2–0.25 g of powder was pulverized in a closed chamber. Based on the volume of airborne particles, the peak concentration of particles with diameters of 3.7–6.7 μm was continuously observed. There were no significant differences in the size distribution of airborne

allergen particles during five repeated measurements.

Figure 1. Photograph of test powder containing house dust mite and cat allergens at a concentration of 10% of the total mass.

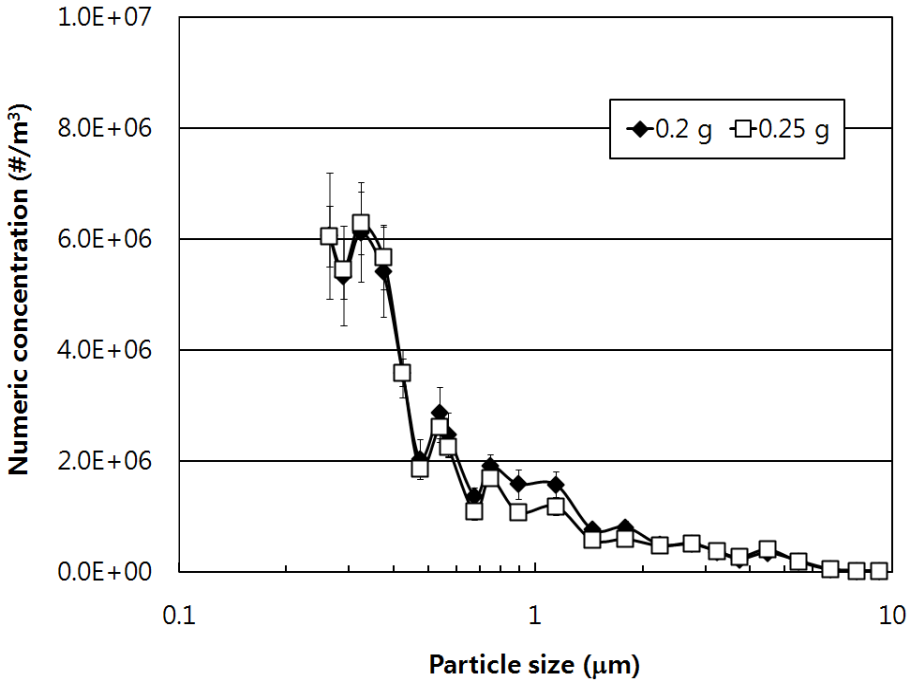

(a) numeric

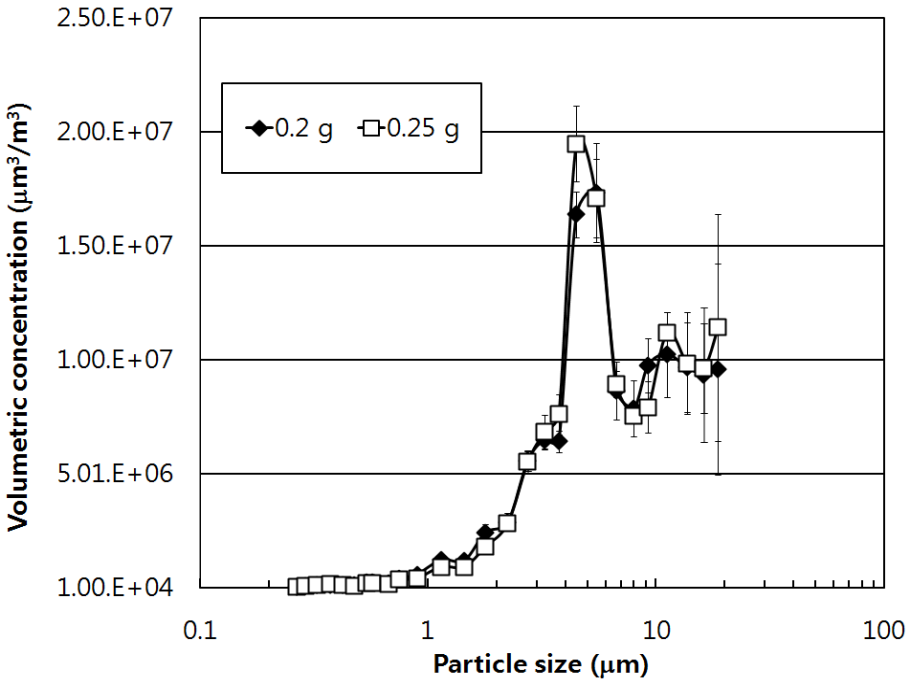

(b) Volumetric

Figure 2. Size distributions of airborne allergen powders based on numeric and volumetric concentrations in a 30-m3 closed test chamber: (a) numeric and (b) volumetric.

The experimental set-up for measurements of CADR (clean-air delivery rate) and the removal efficiency of air-cleaning devices for airborne allergen particles are shown in Figure 3. A dehumidifier, an air conditioner with a pre-filter, an air cleaner with a HEPA filter, and an ESP type air cleaner studied in Chapter 6 were tested in a closed test chamber with the room temperature and relative humidity of 23±5℃ and 55±15%, and the other functions of the devices to remove water vapor and to reduce temperature in a test chamber were not operated during tests for allergen removal performance because the functions could affect the test conditions of the chamber. The specifications of the test equipment, which were commercially available in Korea, are summarized in Table 1. A closed stainless steel chamber (4 x 3 x 2.5 m^3) was used in this study. Particle leakage of the test chamber was negligible during the test. When I checked the natural decay after one hour with a known particle concentration of approximately 3 x 10^8 particles/m^3 of 0.3 μm KCl (Potassium chloride) particles, there was decrease less than 3 % in the initial concentration, which is the test chamber condition of air cleaners for one hour, recommended by the Association of Home Appliance Manufacturers (AHAM) (AHAM, 2006).

Until residual particles in the test chamber decreased to less than 10^4 particles/m^3, a blower

connected to a HEPA filtration system was operated. When the background level of particles that were approximately 0.3 μm in diameter fell below the limit in the test chamber, a circulation fan turned on, and 0.2–0.25 g of allergen powders generated in a powder dispersion device was introduced to the test chamber with clean compressed air at a rate of 30 L/min. The direction of the spraying nozzle was symmetrically toward below the circulation fan in the chamber. When the concentration of airborne allergen particles reached its maximum, the circulation fan was turned off, the air-cleaning device, which was located 10 cm away from the wall of the chamber, was turned on, and particle concentration data were acquired at 1-minute intervals for 60 min.

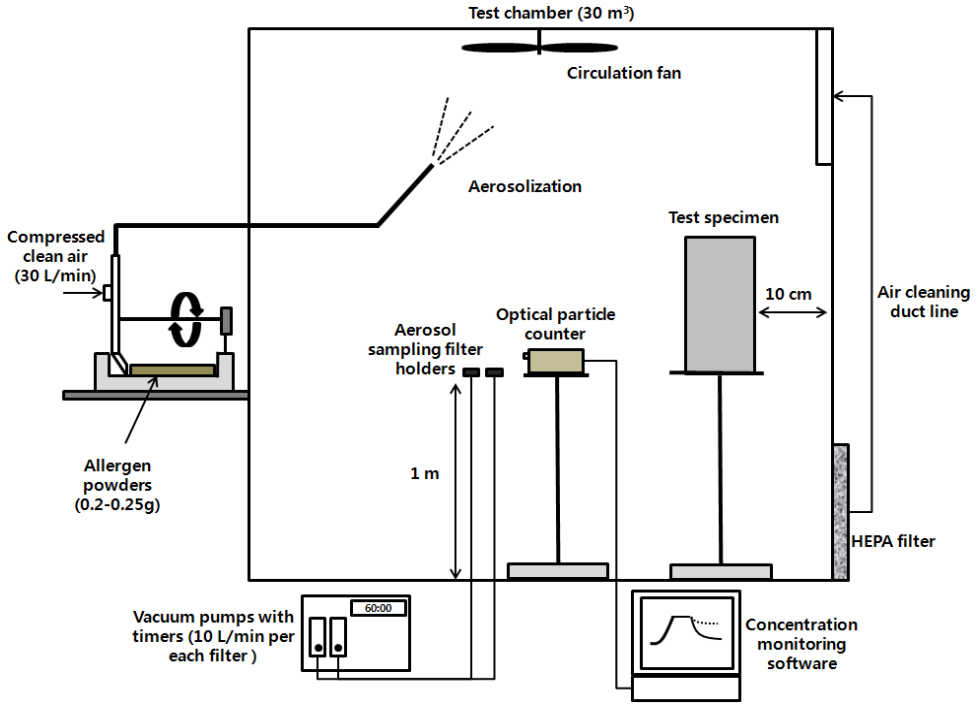

Figure 3. Experimental setup for the CADR and removal efficiency tests of air-cleaning devices against airborne allergen particles

Table 1. Descriptions of the air-cleaning devices tested in this study.

Type	Manufacturer	Model	Flow rate	Type of a filter
Dehumidifier	LG electronics	LG 45Pt	3.4 m^3/min	Mesh type pre-filter
Air conditioner	LG electronics	SRAC 12,000 Btu/h	8.6 m^3/min	Mesh type pre-filter
Air cleaner	Woongjin	AP-3008FH	16.1 m^3/min	HEPA filter
Air cleaner	Studied in Chapter 6	-	20.0 m^3/min	ESP

The particle concentration of the airborne particles during each experiment was measured, using a particle-sampling probe that was installed 1 m above the chamber floor at the center of the chamber and an optical particle counter (Portable Aerosol Spectrometer, Model 1.109, Grimm Aerosol Technik, Ainsring, Germany). The measurement of the concentration was started after 3 to 5 minutes of turning the air cleaner on when there was no change of the initial concentration of 0.3 μm airborne particles, which might be caused by unexpected leakage in the test chamber or malfunction of the air-cleaning device etc. Particle concentrations were also measured as above but without an operating air-cleaning device in the test chamber to examine the decrease in the number of airborne allergen particles due to natural gravitational settling including unexpected particle loss in the test chamber such as wall loss.

To compare the performance of test results measured by an optical particle counter with results from a two-site ELISA, airborne particle sampling for ELISA was performed at the same time and at the same position as the optical particle-counter measurements. Airborne particles in the closed chamber were collected on four glass fiber filters (Model GF/C ϕ 47 mm, pore size 1.6 mm, Whatman International Ltd, Maidstone, UK) using vacuum pumps at a flow rate of 10 L/min for 60 minutes after the concentration of allergen particles in the chamber reached its maximum. In this study, I did not consider a particle decrease by the suction sampling for 60 minutes in the test chamber because the volume of the sampling was only 2% of the total volume of the chamber.

House dust mite and cat allergens (Der p 1 and Fel d 1) were extracted from the glass filters using borate buffered saline (BBS) (170 mM boric acid, 125 mM NaCl, pH 7.0) for 18 hours at room temperature with gentle shaking. Der P 1 and Fel d 1 concentrations in each extracted solution were measured by two-site ELISA (Indoor Biotechnologies, Manchester, UK) following the manufacturer's recommendations (Indoor Biotechnologies, 2012a, 2012b).

The airborne allergen-particle removal performance of each air-cleaning device, as measured by the optical particle counter, was expressed as a universal air-cleaning performance metric, a CADR, which is based on the time-dependent particle reduction of an air-cleaning device in a closed chamber. This metric was established by the AHAM.

Theoretically, the regression of the particle concentration follows a first-order decay model:

$$C_t = C_0 e^{-kt} \quad (1)$$

where

C_t = concentration at time t (particles/m^3)

C_0 = initial concentration at t = 0 (particles/m^3)

k = decay constant (t^{-1})

t = time (min)

The time-resolved decay constant k is calculated statistically using a linear regression of ln C_{ti} and t_i using the following formula:

$$k = \frac{\sum_i (t_i \cdot \ln \frac{C_0}{C_{t_i}})}{\left(\sum_i t_i^2\right)} \qquad (2)$$

The CADR in the AHAM method is calculated using the following formulas:

$$CADR_t = V \times k_t \qquad (3)$$

$$CADR_n = V \times k_n \qquad (4)$$

$$CADR = CADR_t - CADR_n \qquad (5)$$

where

$CADR_t$ = the clean-air delivery rate with an operating air-cleaning device and gravitational settling (m^3/min)

$CADR_n$ = the clean-air delivery rate with only gravitational settling and without an operating air-cleaning device (m^3/min)

CADR = clean air-delivery rate (m^3/min)

V = volume of test chamber (m^3)

k_t = total decay rate (min^{-1})

k_n = natural decay rate (min^{-1})

The airborne allergen particle-removal performance of each air-cleaning device was also expressed as removal efficiency, calculated using the following formula:

$$\eta_t = \left(1 - \frac{C_{t,t}}{C_{t,n}}\right) \times 100 \qquad (6)$$

where

η_t : removal efficiency of an air-cleaning device at time (t)

$C_{t,t}$: numeric or volumetric concentration of allergen particles in the chamber at time (t) with an

operating air-cleaning device and gravitational settling

$C_{t,n}$: numeric or volumetric concentration of allergen particles in the chamber at time (t) with only gravitational settling and without an operating air-cleaning device

The airborne allergen particle-removal performance of each electrical device as measured by the ELISA method was calculated using Eq. (6), with the mass concentrations of the proteins Del p 1 and Fel d 1, which were sampled for 60 minutes with and without an operating air-cleaning device.

7.1.3 Results and discussion

Figure 4 shows numeric concentrations over time for airborne allergen particles of different particle sizes both with and without an operating dehumidifier. The initial numeric concentrations of the allergen particles were 10^5 to 10^7 particles/m^3 depending on the particle size, and the decay in the concentration of airborne particles was size dependent in both cases. Figure 4 a) shows that without the operation of a dehumidifier, when decay in the concentration of airborne particles was only due to gravitational settling, the numeric concentrations of the allergen particles larger than 1 μm decreased from 6.41 x 10^5 and 2.31 x 10^5 particles/m^3 to 3.58 x 10^5 and 4.6 x 10^4 particles/m^3 for particles with diameters of 2.24 μm and 5.7 μm, respectively, whereas the particles smaller than 1 μm were maintained at their initial concentration. The decay lines for the particles smaller than 2.24 μm did not fit well with the first-order model explained in Eq. (1) because the concentrations of these particles decreased very little within 60 minutes when only exposed to natural gravitational force. In contrast, the numeric concentrations of the particles of all sizes decreased when the dehumidifier was operating, and in particular, the concentration of the particles smaller than 1 μm decreased from 5.84 and 2.76 x 10^6 particles/m^3 to 2.83 and 1.66 x 10^6 particles/m^3 for 0.32 and 0.54 μm particles after the dehumidifier had operated for 60 minutes. All of the decay lines for the airborne allergen particles with the operation of the dehumidifier fitted very well to the first-order model in Eq. (1).

As is shown in Figure 5, CADRs were calculated with the decay constants that were obtained using Eq. (2)-(4), both with and without an operating air-cleaning device, according to the size of the airborne particles. The log of CADR curves for all conditions were proportional to the log of particle sizes, which had also been observed during previous research in our group that was conducted using an air cleaner with electrostatic precipitation (Agrawal et al., 2010).

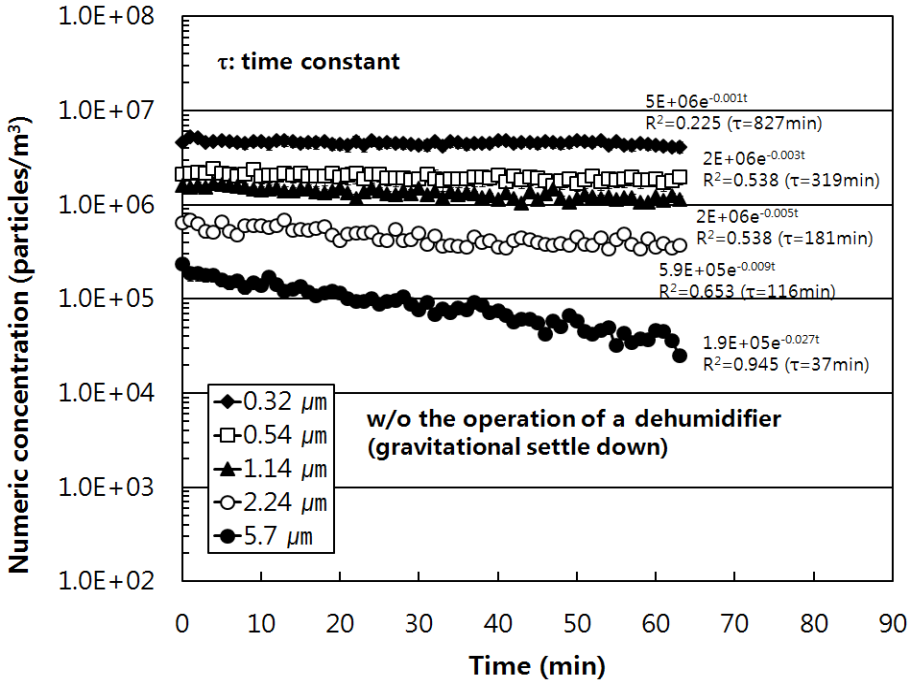

(a) w/o the operation of a dehumidifier

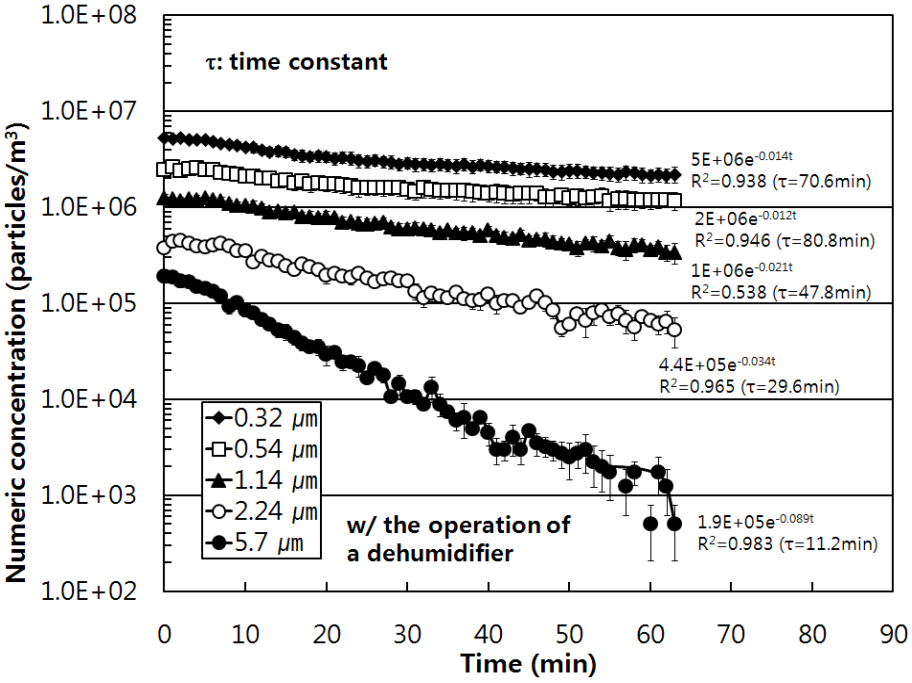

(b) w/ the operation of a dehumidifier

Figure 4. Numeric concentrations over time of airborne allergen particles with various particle sizes both with and without an operating dehumidifier: (a) w/o the operation of a dehumidifier and (b) w/ the operation of a dehumidifier. (τ: time constant, a time when a concentration reached approximately 37% of its initial concentration)

The CADRs by air cleaners which were equipped with a HEPA filter and an ESP were much higher than those by gravitational settling, an operating dehumidifier, and an operating air conditioner.

In particular, the removal of airborne allergen particles for submicrometer size range was enhanced significantly with the air cleaners, and the performance of the different air-cleaning devices was clearly discriminated by the CADRs with an order of the air cleaners, the air conditioner, and the dehumidifier.

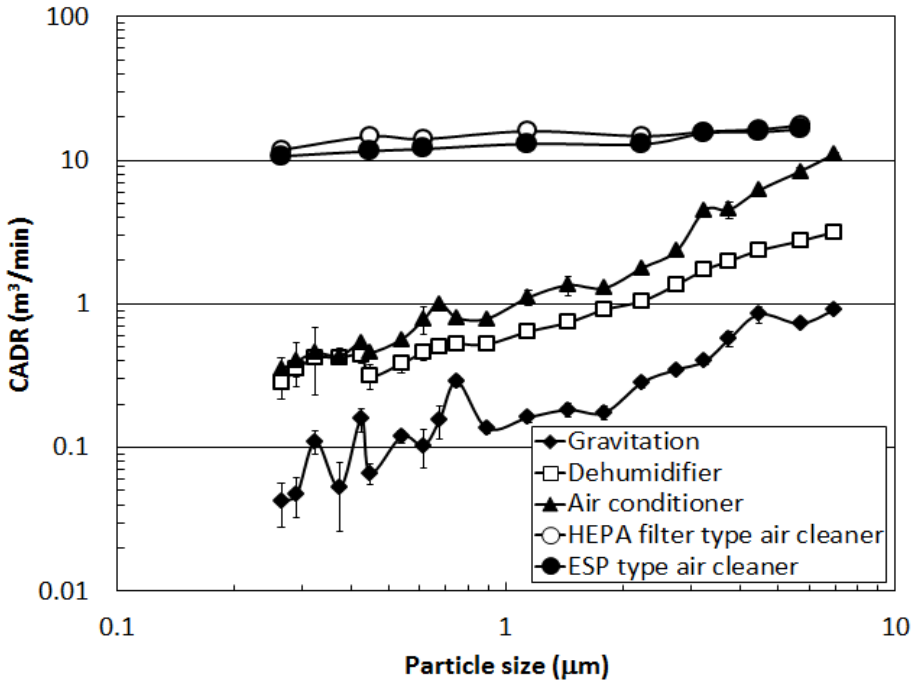

Figure 5. CADRs with and without an operating air cleaning devices

In previous studies (Waring et al., 2008; Novoselac and Siegel, 2009; Kim et al., 2012), if the air flow rate and the single-pass removal efficiency were known, a CADR could be obtained using the flowing formula:

$$CADR = \eta \times Q \times E \quad (7)$$

where

η : single-pass removal efficiency of an air-cleaning device

Q : airflow rate of an air-cleaning device

E : short-circuit factor (E = 1 under well-mixed conditions)

As is shown in Table 1, the dehumidifier and the air conditioner used the same type of pre-filter; therefore, the single-pass removal efficiency of the air-cleaning devices could have been similar. However, the flow rate of the air conditioner (8.6 m^3/min) was 2.5 times higher than that of the dehumidifier (3.4 m^3/min); therefore, the CADR of the air conditioner was larger than that of the dehumidifier. In particular, the CADRs of the air cleaners were approximately 40 times was larger than those of the dehumidifier and the air conditioner because the flow rate of the air cleaners was approximately 5 and 2 times higher than that of the humidifier and air conditioner, and also the collection efficiency of an ESP and HEPA filter was much higher (over 60% for 0.3 μm particles in Chapter 6 than the efficiencies of pre-filters which might be less than 10 % in general. With experimental results, operation of air cleaning devices with a high CADR performance is necessary to remove fine airborne allergen particles efficiently within a short period of time, and the air cleaner with the ESP developed in Chapter 6 could be an efficient method for allergen removal.

Figure 6 shows log-normalized concentrations of particles measured under three different cases: with gravitational settling, with an operating dehumidifier, and with an operating air conditioner. The concentration of particles at time *t* was divided by its initial concentration at time = 0, when the allergen particle concentration in the test chamber reached the maximum value. Total volumetric concentrations of the particles were also calculated by summing the total volumes of all of the particle size classes, which were obtained by multiplying the numeric concentration of a certain particle size by the volume of the particle. As is shown in Figure 6a, the particles smaller than 1 μm showed very little settling due to their low settling velocity, which is proportional to the square of particle size, whereas 90% of airborne 5.7-μm allergen particles were removed after 60 minutes simply because of their relatively high gravitational force (Hinds, 1998). In particular, the regression of the total volumetric concentration of particles was very similar to the numeric concentration of 5.7-μm particles, which was the modal size of airborne allergen particles when the peak concentration was observed, based on volume (Figure 2b).

In contrast to simple gravitational settling, the airborne allergen particles of all size classes decreased during the operation of air-cleaning devices (Figures 6b and 6c). In particular, the numeric concentration of the particles smaller than 1 μm decreased to 50 and 30% of the initial concentration when a dehumidifier and an air conditioner were in operation, respectively. Moreover, the concentration of 5.7-μm particles decreased to 9 and 0.3% of the initial concentration after only 30 minute of operation of a dehumidifier and an air conditioner, respectively. When the two air-cleaning devices were used, the regression of the total volumetric concentration of particles was similar to the

numeric concentration of 5.7-μm particles.

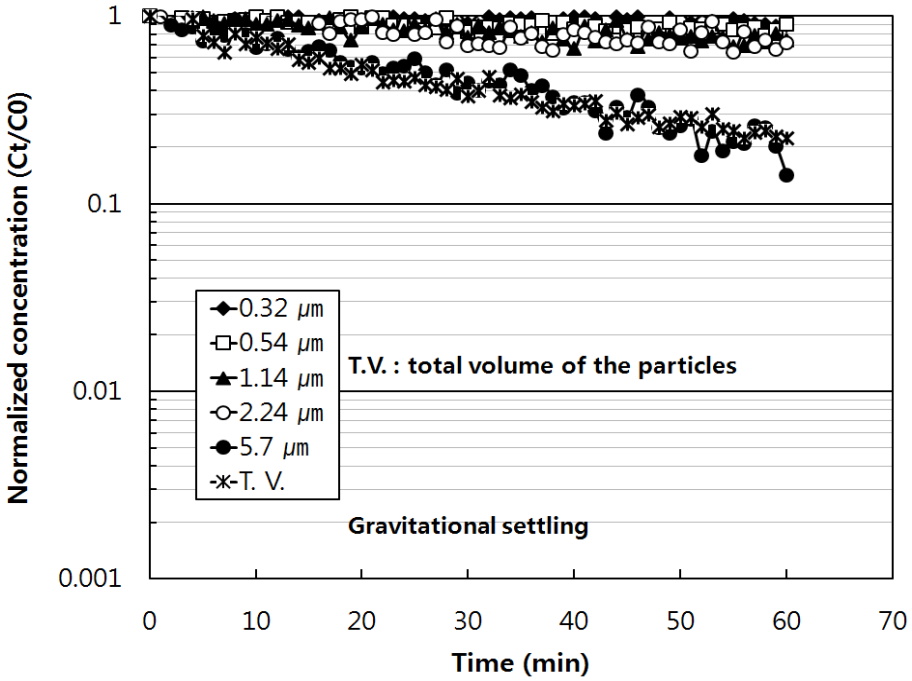

(a) gravitational settling

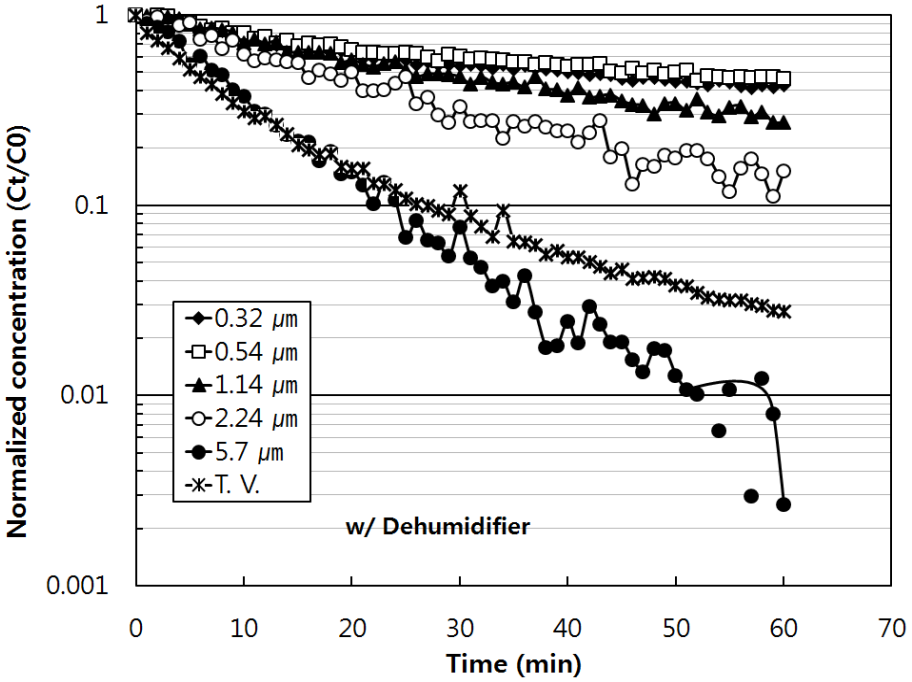

(b) dehumidifier operation

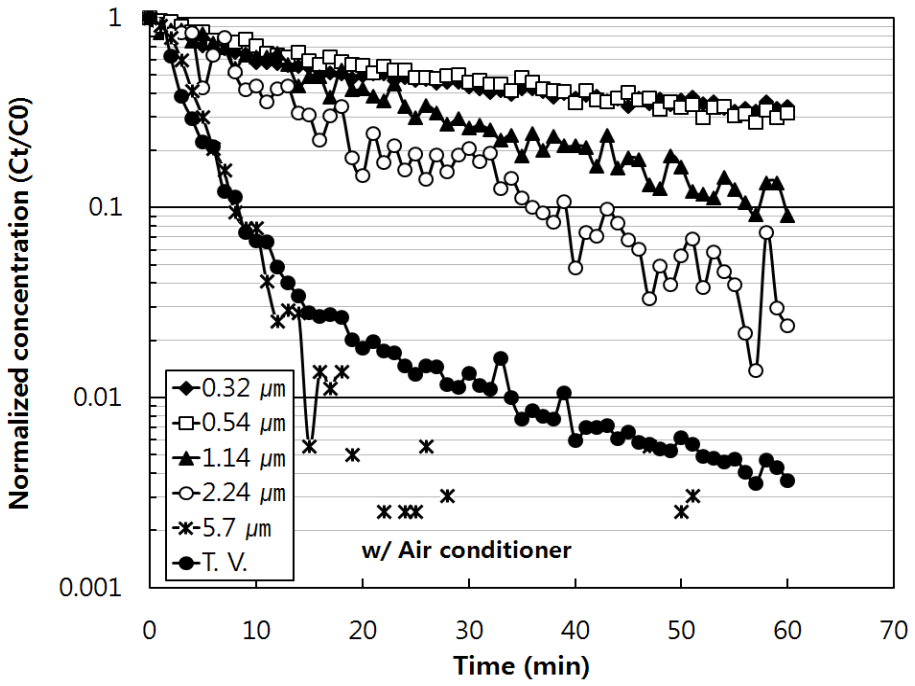

(c) air conditioner operation

Figure 6. Log-normalized concentration of airborne allergen particles with gravitational settling, dehumidifier operation, and air-conditioner operation: (a) gravitational settling, (b) dehumidifier operation, and (c) air conditioner operation.

Figure 7 shows removal efficiencies that were obtained using Eq. (6) over time with the numeric concentrations of five different particle sizes and the total volume of particles for the dehumidifier and air-conditioner treatments. The removal efficiencies of the test particles were smaller at the beginning of running the air-cleaning devices, and these results were also observed in the previous researches (Novoselac and Siegel, 2009; Shiue and Hu, 2011). This could be explained by the fact that there is time necessary to reach a well-mixed condition in the test chamber when the air cleaners showed their maximum removal performance because the time-dependent particle removal is significantly affected by the mixing condition in the test chamber shown in Eq. (7) (Shaughnessy and Sextro, 2006). Shown in Figure 7a, After 60 minutes of dehumidifier operation, the removal efficiency for the particles smaller than 1 μm was approximately 50%, whereas the removal efficiencies for 1.14-, 2.24-, and 5.7-μm particles were 63.4, 78.9, and 98.1%, respectively; the removal efficiency for the total volume of particles was 87.5%.

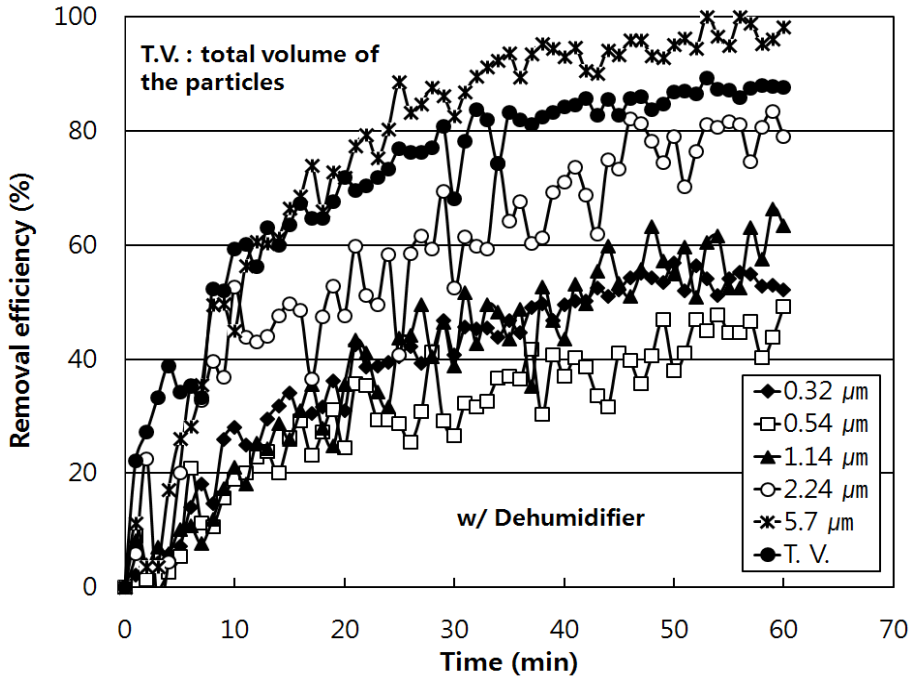

(a) dehumidifier

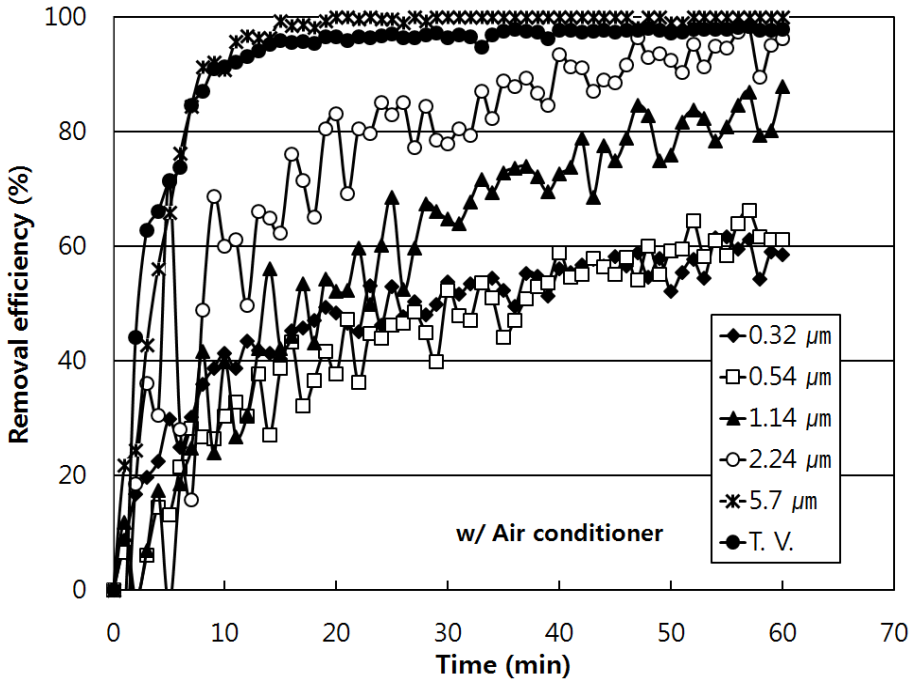

(b) air conditioner

Figure 7. Removal efficiencies over time, calculated as numeric concentrations of five different particle sizes and the total volume of particles for the dehumidifier and air conditioner: (a) dehumidifier and (b) air conditioner.

The air conditioner with a flow rate of 8.6 m^3/min removed the particles of all sizes more swiftly than did the dehumidifier, which had a flow rate of 3.4 m^3/min. Shown in Figure 7b, after 60 minutes of air-conditioner operation, the removal efficiency for the particles smaller than 1 μm was 60%, whereas the efficiency for 1.14-, 2.24-, and 5.7-μm particles were 87.9, 96.2, and 99.9%, respectively, and the removal efficiency for the total volume of particles was 97.9%. The volume of polluted air that was treated by the air conditioner in the test chamber was 2.5 times larger than the volume treated by the dehumidifier, which could explain the difference in removal performance between the two devices.

Figure 8 shows the removal efficiencies of the two air-cleaning devices obtained using Eq. (6) and total mass concentrations of allergen protein that was collected on sampling filters over 60 minutes and then measured by the ELISA method. The mass concentrations of Del P 1 and Fel d 1 without an operating dehumidifier were 0.181 ± 0.076 and 0.996 ± 0.239 μg/mL, respectively. The average removal efficiency of the dehumidifier, measured by ELISA, was 89.4% for the mite allergen and 83.2% for the cat allergen. The mass concentrations of Del P 1 and Fel d 1 without the operation of an air conditioner were 0.137 ± 0.071 and 1.691 ± 0.230 μg/mL, respectively. The average removal efficiency of the air conditioner, measured by ELISA, was 88.0% for the mite allergen and 95.4% for the cat allergen.

Figure 9 shows a comparison of removal efficiencies between the dehumidifier and the air conditioner using values that were calculated with total mass estimates and ELISA and with numeric concentrations and total volumes obtained from the size distribution of the allergen particles as measured by a particle counter. The average removal efficiency of the dehumidifier for both allergens as measured by ELISA was 86.3 ±3.14%, and the efficiencies for total volume of airborne allergen particles and for number of 5.7-μm particles were 85.97 ± 0.38% and 95.2 ± 0.58%, respectively. The removal efficiency of the air conditioner for the allergens was 91.7 ± 3.70%, and the efficiencies for total volume and number of 5.7-μm particles were 97.7 ± 0.06% and 99.8 ± 0.11%, respectively. Additionally, the efficiency values for the air conditioner obtained by ELISA and by the optical particle counter based on particle number in the peak particle size and on total volume were 1.06, 1.14, and 1.05 times greater than similar efficiency values for the dehumidifier. Also, the differences in the removal efficiencies of the air-cleaning devices for allergen particles as calculated using total mass measurements by ELISA and total volume measurements by an optical particle counter were 0.32% for the dehumidifier and 5.97% for the air conditioner.

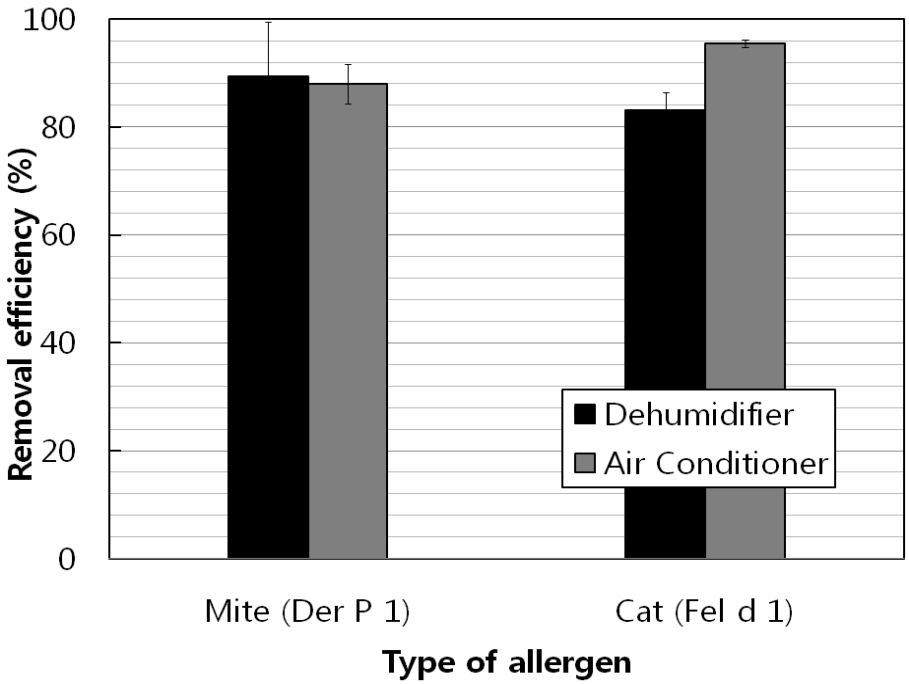

Figure 8. Removal efficiencies of the air-cleaning devices calculated using mass concentrations by the ELISA method.

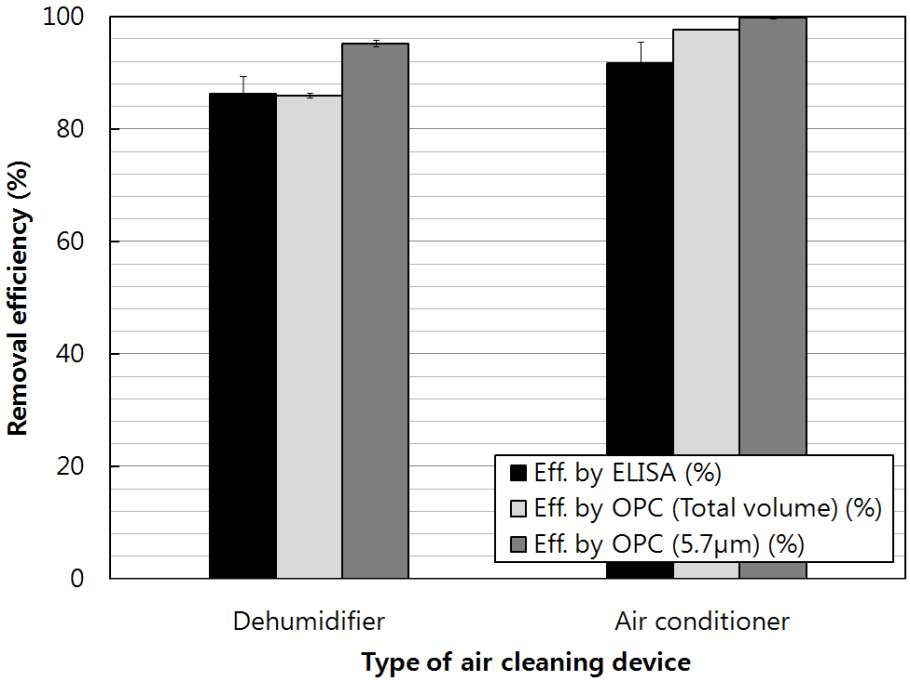

Figure 9. Comparison of the removal efficiencies of the dehumidifier and air conditioner calculated using mass by the ELISA, numeric concentration of 5.7-μm particles, and the total volumetric concentration by an optical particle counter.

7.1.4 Conclusion

In this study, I evaluated the aerodynamic characteristics of airborne allergen particles both with and without air-cleaning devices, i.e., a dehumidifier, an air conditioner, and air cleaners, using artificially created allergen powders that contained the proteins Del p 1 and Fel d 1. Measurements were taken using a real-time optical particle counter and a closed chamber (30 m^3). The CADR was measured both with and without operating air-cleaning devices for a variety of particle sizes. Time- and size-dependent particle-removal performance was evaluated using an optical particle counter, and the results were compared with measurements taken using the ELISA method. The CADRs were linearly proportional to particle size, and the removal of airborne allergen particles in submicrometer size range was significantly enhanced by the operation of HEPA filter and ESP type air cleaners. The time-dependent allergen particle removal performances of various air cleaning devices in a room were clearly discriminated by CADRs measured with a real-time particle counting method. The removal efficiency of the air conditioner obtained by ELISA and the optical particle counter based on particle number in the peak size and on total volume were 1.06, 1.14, and 1.05 times higher than comparable values for the dehumidifier. Also, the difference between the removal efficiencies of the air-cleaning devices for allergen particles calculated from total mass measured by ELISA and from total volume measured by an optical particle counter were 0.32% for the dehumidifier and 5.97% for the air conditioner. These results indicate that our simple measurement method, which used an in-situ optical particle counter, could easily predict values of air-cleaning performance against airborne allergens that were obtained by the time-consuming ELISA method. Also, the performance of the test for air-cleaning devices using these in-situ measurements is more realistic because airborne allergen particles cause allergic diseases via respiratory organs, such as the nose. This method is a promising tool for measuring air-cleaning performance for airborne allergen particles in indoor environments.

7.1.5 References

Agrawal SR, Kim HJ, Lee YW, Sohn JH, Lee JH, Kim YJ, Lee SH, Hong CS, Park JW. Effect of an air cleaner with electrostatic filter on the removal of airborne house dust mite allergens. Yonsei Med J 2010; 51(6): 918-923.

AHAM (Association of Home Appliance Manufacturers). ANSI/AHAM AC-1-2006. Method for measuring performance of portable household electric room air cleaners; 2006.

Custovic A, Taggart SCO, Francis HC, Chapman MD, Woodcock A. Exposure to house dust mite allergens and the clinical activity of asthma. J Allergy Clin Immunol 1996; 98(1): 64-72.

Custovic A, Simpson A, Pahdi H, Green RM, Chapman MD, Woodcock A. Thorax 1998; 53: 33-38.

De Lucca S, Sporik R, J. O'Meara T, Tovey ER. Mite allergen (Der p 1) is not only carried on mite feces. J Allergy Clin Immunol 1999; 103: 174-175.

Eggleston PA, Bush RK. Environmental allergen avoidance: an overview. J Allergy Clin Immunol 2001; 107: S403-405.

Eggleston PA. Improving indoor environments: Reducing allergen exposures. J Allergy Clin Immunol 2005; 116(1): 122-125.

Francis H, Fletcher G, Anthony C, Pickering C, Oldham L, Hadley E, Custovic A, Niven R. Clinical effects of air filters in homes of asthmatic adults sensitized and exposed to pet allergens. Clin Exp Allergy 2003; 33: 101-105.

Gelber LE, Seltzer LH, Bouzoukis JK, Pollart SM, Chapman MD, Platts-Mills TAE. Sensitisation and exposure to indoor allergens as risk factor for asthma among patients presenting to hospital. Am Rev Repir Dis 1993; 147: 573-578.

Green R, Simpson A, Custovic A, Faragher B, Chapman M, Woodcock A. The effect of air filtration on airborne dog allergen. Allergy 1999; 54: 484-488.

Gore RB, Bishop S, Durrell B, Curbishley L, Woodcock A, Custovic A. Air-filtration units in homes with cats: can they reduce personal exposure to cat allergen? Clin Exp Allergy 2003; 33: 765-769.

Hinds WC. Aerosol technology: properties, behaviors, and measurement of airborne particles. New York: Wiley-Interscience Publication; 1998.

Indoor Biotechnologies. ELISA Protocols – EL-DP1: Mite (Dermatophagoides) Der p 1 allergen: http://www.inbio.com/US/images/pdfs/EL-DP1_CoA.pdf, last accessed at 24 October 2012.

Indoor Biotechnologies. ELISA Protocols – EL-FD1: Cat (F. domesticus) allergen, Fel d 1: http://www.inbio.com/US/images/pdfs/EL-FD1_CoA.pdf, last accessed at 24 October 2012.

Kim HJ, Han B, Kim YJ, Yoon YH, Oda T. Efficient test method for evaluation gas removal performance of room air cleaners using FTIR measurement and CADR calculation. Build Environ 2012; 47: 385-393.

Kauffman H, Tamm M, B Timmerman JA, Borger P. House dust mite major allergens Der p 1 and Der p 5 activate human airway-derived epithelial cells by protesase-dependent and protease-independent mechanisms. Clinical and Molecular Allergy 2006; 4(5): 1-8.

Novoselac A, Siegel JA. Impact of placement of portable air cleaning devices in multizone residential environments. Build Environ 2009; 44: 2438-2356.

Ohman JL. Allergy in man caused by exposure to mammals. J Am Vet Med Assoc 1978; 172: 1403-1406.

O'Connor TG. Allergen avoidance in asthma: What do we do now? J Allergy Clin Immunol 2005; 116(1): 26-30.

Pauli G, de Blay F, Bessot JC. Indoor allergens: identification and environmental control. Rev Fr Allergol Immunol Clin 2000; 40: 222-229.

Shiue A, Hu SC. Contaminant particles removal by negative air ionic cleaner in industrial minienvironment for IC manufacturing processes. Build Environ 2011; 46: 1537-1544.

Shaughnessy RJ, Sextro RG. What is an effective portable air cleaning device? A review. J Occup Environ Hyg 2006; 3(4): 169-181.

Sporik R, T. Holgate S, Platts-Mills TAE, J. Cogswell J. Exposure to house-dust mite allergen (Der p 1) and the development of asthma in childhood. New Engl J Med 1990; 323(8): 502-507.

Tovey E, Marks G. Methods and effectiveness of environmental control. J Allergy Clin Immunol 1999 ; 103 (2-1): 179-191.

van Strien RT, Driessen MNBM, Oldenwening M, Doekes G, Brunekreef B. Do central vacuum cleaners produce less indoor airborne dust or airborne cat allergen, during and after vacuuming, compared with regular vacuum cleaners? Indoor Air 2004; 14: 174-177.

Waring MS, Siegen JA, Corsi RL. Ultrafine particle removal and generation by portable air cleaners. Atmospheric Environment 2008; 42: 5003-5014.

Zuraimi MS, Nilsson GJ, Magee RJ. Removing indoor particles using portable air cleaners: Implications for residential infection transmission. Build Environ 2011; 46: 2512-2519.

Chapter VIII

Conclusions

Adverse health effects seem to be linked with smaller particles, probably largely because of the increase in the number of particles and particle surface area per unit mass with decreasing particle size, among various factors. Because of the relationships of adverse health effects and fine particles, current pollution standards are mass-based such that as particles become finer, regulation by number or area will increase in the near future. Considering these small-particle regulation trends, current particle collection methods should be upgraded and newly developed to achieve extremely high-removal efficiency for particles. Among various air-cleaning methods such as filters, cyclones, and scrubbers, ESPs are the only electrical method. As noted in the technical and historical background in the chapter I and II, dry ESP technology has been already well-developed for conventional industries. Thus, in this study I focused mostly on new application fields such as IT manufacturing, new thermal power generation, diesel engines, and IAQ that currently concern about high efficiency against fine particles. Also, I used novel ESP technologies such as a non-metallic ESP, a thin water film ESP and a combined ESP with metallic filters etc., and compared the research results with theoretical analyses basically using the Deutsch's collection efficiency equation and the Cochet's charging theory, however specially using diffusion charging theories for particles in submicrometer size range or those smaller than 0.1 μm which have been rarely used for industrial scale ESP analyses. The major findings in this study are summarized as follows:

(1) I have developed a novel non-metallic, two-stage ESP composed of separate non-metallic charging and collection stages. This ESP uses carbon brush chargers at the center of the grounded channels of carbon fiber-reinforced polymer for the particle charging stage and PVC collection plates into which metallic films are inserted for the particle collection stage. The electrical and collection performances of the carbon brush charger were not changed with different materials (stainless steel, CFRP) that were used for gounded plates. The experimental efficiencies of the non-metallic ESP were compared with those from the Deutch collection theory, based on the Cochet's charging model, and the efficiencies from the experiments could be predicted with the same design and operation parameters of the ESP.

(2) Demonstration research with the non-metallic ESP for removal of particles and mists in

exhaust gases from a semiconductor manufacturing company at a flow rate of approximately 1,200 Nm^3/h (0.4 m x 0.4 m x 2 m/s) was conducted for 1 month, and the ESP had average collection efficiencies of 97% based on particle numbers of 0.3, 0.5, and 1 μm and 92% based on total particle mass; these collection efficiencies were achieved with a much smaller specific corona power of 0.028 $W/m^3/hr$(100 J/m^3) compared with the 0.05 to 0.3 $W/m^3/hr$ of conventional ESPs.

(3) I have developed a novel two-stage wet ESP that uses a carbon brush pre-charger and collection plates with a thin water film. The performance of the ESP was evaluated experimentally for ultrafine particles in the size range of 0.01~0.5 μm. To enhance the hydrophilicity of the collection plates, which increases the water film uniformity and minimizes water consumption, the collection surfaces of the plates were first sand-blasted and then coated with an alcohol solution in which approximately 5~10 nm nanoparticles were dispersed. The carbon brush pre-charger emitted low ozone compared to general pre-chargers not because of material but thin diameter of the brush tips. In particular, the ESP achieved a high collection performance, averaging 90% with negative voltage and 80% with positive voltage, for ultrafine particles based on number concentration. Also, for particles larger than 0.05 μm, the experimental collection efficiencies were similar to those predicted by the Deutsch ESP collection theory, based on the Cochet's charging theory. However, the differences between the results and those predicted by the Cochet's theory increased as particle sizes decreased to smaller than 0.05 μm because the charging for the particles in the size range is significantly related to diffusion charging. In this study, the theoretical collection efficiency for the particles smaller than 0.05 μm was successfully predicted, using the Fuchs' limiting sphere theory.

(4) Low ozone emission performance of a carbon brush charger was experimentally investigated by comparing to the emission performances of general chargers with different materials and diameters of high voltage electrodes, and the results showed that the low ozone was possible not by material but by sharpness of the high voltage electrode.

(5) In particular, the wet ESP with thin water film on the collection plates was applied to the final gas cleaning facility at the downstream of an dry ESP for 0.7 MW Oxy-PC combustion and CCS pilot plant, and achieved gravimetric concentration of particles near 1 mg/m^3, only consuming a water of 1.7 $L/min/m^2$.

(6) An electrostatic diesel PM filtration system (EDPS) was developed using a metallic filter combined with electrostatic charging and collection. Using an air-slit insulation device for the high voltage electrode of the filtration system enabled stable corona discharge in the EDPS even for temperatures over 300℃. The efficiency with which the diesel particles were collected in the EDPS was over 95% at exhaust gas temperatures less than 250℃. This was 30-50% higher than that for the metallic filter (FTF, flow through filter in this study). With a specific corona power between 1 and 30 W/(m^3/min), the EDPS achieved a high collection efficiency over 80%, based on the number of particulates. Moreover, the collection efficiency of the system correlated with specific corona power, which was determined by the applied voltage, corona current, temperature, and flow rate. This correlation could be used for an electrical and physical design of an EDPS for other diesel engines having different flow rates. In particular, the European standard mode test results demonstrated that the EDPS had a 47% higher collection performance than the FTF and 10% lower performance than the DPF (diesel particulate matter filter). This was achieved at a significantly lower pressure drop (82 mbar), which was only 27% of that for the DPF.

(7) I developed a novel air cleaner based on electrostatic precipitation, which was composed of a perforated plate for uniform flow distribution, a channeled ionization stage with 16 carbon brush chargers, and a collection stage with parallel metallic plates with edges covered by nonmetallic insulators and a fan. The particle collection efficiency of the ESP air cleaner was evaluated for particles ranged between 0.25 and 0.35 μm. The test results indicated that emissions from the ESP air cleaner resulted in ozone levels lower than 10 ppb, and The ESP also achieved a high clean air delivery rate (>12 m^3/min) which is one of the highest CADRs (clean air delivery rates) reported by the KACA and AHAM. In particular, the average performance value (single-pass CADR/pressure drop in this study) with the ESP air cleaner was 0.4 Pa/m^3/min which is only 36% of that with the HEPA filter. Also, the theoretical analysis for an ESP type air cleaner indoors was possible with a simple product of single-pass collection efficiency predicted by the Deutsch equation and charging theories, and flow rate, and thus it could be used to estimate the time-dependent particle removal performance (i.e., CADR) in a closed room for ESP air cleaners without any experimental work.

(8) I evaluated the aerodynamic characteristics of airborne allergen particles ranged

between 0.1 and 10 μm both with and without air-cleaning devices, i.e., a dehumidifier an air conditioner, an ESP air cleaner developed in this study, and a HEPA filter type air cleaner, using artificially created allergen powders that contained the proteins Del p 1 and Fel d 1. Time- and size-dependent particle-removal performance in a closed chamber (30 m^3) was evaluated using an optical particle counter, and the results were compared with measurements taken using the ELISA method which is not only time-consuming off-site analysis method but also can't analyze time-dependent performance of air-cleaning devices against airborne allergen particles. The time-dependent CADR was linearly proportional to particle size, and the removal of airborne allergen particles was significantly enhanced by the operation of air cleaning devices. The size-dependent performance of air cleaning devices for airborne allergen particles was perfectly discriminated with their CADRs. Also, the difference between the removal efficiencies of the air-cleaning devices for allergen particles calculated from total mass measured by ELISA and from total volume measured by an optical particle counter were only 0.32% for the dehumidifier and 5.97% for the air conditioner.

With these various researches on particle removal by the novel ESPs especially against fine particles, I would like to emphasize the possibility and importance of the electrostatic precipitation technologies in this study for cleaner and better air quality in atmospheric and indoor environment where conventional ESPs have not been applied until now because of high corrosive gas, particle loading, and temperature conditions as well as ozone limitation. Also, the theoretical analyses of the particle removal performance of the ESPs for particles in various outdoor and indoor environments even including ultrafine size level could be very useful for ESP developers and researchers in the future who want to expect collection performance without time-consuming experiments.

Supplementary

International Journal Papers

1. H.J. Kim, J.H. Kim, H.C. Oh, J.B. Chu, and S.S. Kim (2006). Generation of model diesel particles by spark discharge and hydrocarbon condensation, *Journal of Mechanical Science and Technology (KSME Int. J.)*, Vol. 20, No. 11, pp. 1972-1979.

2. H.J. Kim, B. Han, W.S. Hong, J. R. Ryu, and Y.J. Kim (2009). A new combination system using biotrickling filtration and nonthermal plasma for the treatment of volatile organic compounds, *Environmental Engineering Science*, Vol. 26, No. 8, pp. 1289-1297, 2009.

3. H.J. Kim, B. Han, W.S. Hong, G. B. Cho, Y. K. Lee, and Y.J. Kim (2010). Development of electrostatic diesel particulate matter filtration systems combined with a metallic flow-through filter and electrostatic methods, *International Journal of Automotive Technology*, Vol. 11, No. 4, pp. 447-453.

4. H.J. Kim, B. Han, Y.J., Kim, and S.Y. Yoa (2010). Characteristics of an electrostatic precipitator for submicron particles using non-metallic electrodes and collection plates, *Journal of Aerosol Science*, Vol. 41, pp. 987-997.

5. H.J. Kim, S.R. Agrawal, Y.W. Lee, J.H. Sohn, J.H. Lee, Y.J. Kim, S.H. Lee, C.S. Hong, and J.W. Park (2010). Effect of an air cleaner with electrostatic filter on the removal airborne house dust mite allergens, *Yonsei Med J*, Vol.51, No. 6, pp. 918-923.

6. H.J. Kim, B. Han, Y.J. Kim, K.D. Hwang, W.S., Oh, S.Y. Yoo, and T. Oda (2011). Fine particle removal performance of a two-stage wet electrostatic precipitator using a non-metallic pre-charger, *Journal of Air & Waste Management Association*, Vol. 61, No. 12, pp. 1334-1343.

7. H.J. Kim, B. Han, Y.J. Kim, S.J. Yoa, and T. Oda (2012). Integration of a non-metallic electrostatic precipitator and a wet scrubber for improved removal of particles and corrosive gas cleaning in semiconductor manufacturing industries, *Journal of Air & Waste Management Association*, Vol. 62, No. 8, pp. 905-915.

8. H.J. Kim, B. Han, Y.J. Kim, Y. H. Yoon, and T. Oda (2012). Efficient test method for evaluating gas removal performance of room air cleaners using FTIR measurement and CADR calculation, Building and Environment, Vol. 47, pp. 385-393.

9. H.J. Kim, B. Han, Y.J. Kim, C.S. Jeong, and S.H. Lee (2013). A simple and efficient method for evaluating air-cleaning performance against airborne allergen particles, *Building and Environment*, Vol. 60, pp. 272-279.

10. H.J. Kim, B. Han, G.B. Cho, Y.J. Kim, J.S. Yoo, and T. Oda (2013). Collection performance of an electrostatic filtration system combined with a metallic flow-through filter for ultrafine diesel particulate matter, *International Journal of Automotive Technology*, Vol 14, No. 3, pp. 489-497.

11. H.J. Kim, B. Han, Y.J. Kim, H. Won, and T. Oda (2013). Submicrometer particle removal indoors by a novel electrostatic precipitator with high clean air delivery rate, low ozone emissions, and carbon fiber ionizer, *Indoor Air*, Vol. 23, pp. 369-378.

12. H.J. Kim, B. Han, C. Woo, Y.J. Kim, R. Ono and T. Oda (2014). Performance characteristics of a dry and wet electrostatic precipitator with water films used in oxygen-pulverized coal combustion with a CO_2 capture and storage system, under review, submitted to *Journal of Aerosol Science*.

International conference papers

1. H.J. Kim, Y.J. Kim, J. H. Kim, Y.J. Choi, H.C. Oh, J.B. Choo, S.S. Kim. Generation of model diesel particles by spark discharge and condensation with diesel hydrocarbons: ozone effect on model diesel particles, Proc. of 7th International Aerosol Conference, pp. 645, Sept. 11-15, 2006, St. Paul, Minnesota USA.

2. H.J. Kim, B.Han, Y.B. Kim, Y.J. Kim. Ozone Effect on Artificial Exhaust Particles, Proc. of 5th Asian Aerosol Conference, pp. A1-2, Aug. 26-29, 2007, Kaohsiung, Taiwan,

3. H.J. Kim, B. Han, Y.J. Kim. Removal of volatile organic compounds using a plasma-assisted biofiltration system, Proc. of 18th International Symposium on Transport Phenomena, Paper No. ISTP12-359., Aug. 27-30, 2007, Daejeon, Korea.

4. H.J. Kim, D.K. Song, B. Han, W.S. Hong, S.H. Jeong, Y.J. Kim. Removal of submicron particles by high temperature electrostatic precipitators, Proc. of European Aerosol Conference 2008, Paper No. T07A011P, Aug. 24-29, 2008, Thessaloniki, Greece.

5. H.J. Kim, B. Han, Y.J. Kim, S.H. Lee, Y.Y. Lee, J.W. Park, Removal of airborne mite allergen particle by the air cleaners equipped with a fine mesh mechanical pre-filter and an electrostatic filter, Proc. of 28th American Association for Aerosol Research, Paper No. #1138,Oct. 26-30, 2009, Minneapolis, Minnesota, USA.

6. H.J. Kim, B. Han, D.K. Song, W.H. Shin, W.S. Hong, S.H. Jeong, S.H. Shim, Y.J. Kim. Development of a test method for evaluating performances of indoor air cleaners by applying clean air delivery rate measurement, Proc. of 6th Asian Aerosol Conference, Paper No. 20091130195419, Nov. 24-27, 2009, Bangkok, Thailand.

7. H.J. Kim, B. Han, D.K. Song, W.H. Shin, W.S. Hong, S.H. Jeong, Y.J. Kim. Diesel PM collection performance of a combined system with an electrostatic device and a partial-flow diesel particulate filter, Proc. of European Aerosol Conference 2009, Paper No. T083A06, Sep. 6-11, 2009, Karlsruhe,

Germany.

8. H.J. Kim, B. Han, W.S. Oh, T. Oda, Y.J. Kim. Development of a novel electrostatic precipitator using carbon fiber unipolar ionizers and dielectric collection plates and its removal of ultrafine particles, Proc. of Clean Technology Conference & EXPO, Paper No. 588, Jun. 21-24, 2009, Anaheim, CA, USA.

9. H.J. Kim, B. Han, S.J. Kim, Y.J. Kim. Removal performance of toluene, p-xylene and ethylene using a plasma-pretreated biotrickling system, Proc. of 7th International Symposium on Non-Thermal/Thermal Plasma Pollution Control Technology & Sustainable Energy, Paper No. VII-9, Jun. 21-25, 2010, St. John's Newfoundland, Canada.

10. H.J. Kim, B. Han, Y.J. Kim, T. Oda. Ultrafine particle collection performance of an electrostatic precipitator for semiconductor manufacturing industry using non-metallic electrodes and collection plates, 第 34 回 静電気学会講演論文集'10, pp.47-50, Sep. 14-15, 2010, 鳥取, 日本.

11. H.J. Kim, B. Han, W.H. Shin, W.S. Hong, S.H. Jeong, S.S. Shim, Y.J. Kim. Evaluation for gas removal performance of room air cleaners using CADR calculation method, Proc. of International Symposium of Contamination Control 2010, pp. 178-183, Oct. 5-9, Tokyo, Japan.

12. H.J. Kim, B. Han, G.B. Cho, W.S. Hong, Y.J. Kim, T. Oda. Ultrafine particle removal of diesel particulate matter filtration system combined with a metallic flow-through filter, パルスパワー/放電合同研究会論文集, pp. 17-22, Oct. 21-22, 2010, 大分, 日本.

13. H.J. Kim, B. Han, W.H. Shin, W.S. Hong, S.H. Jeong, S.S. Shim, Y.J. Kim. Comparison between dry and wet electrostatic precipitators for particle removal for Oxy-PC plant, Proc. of International Symposium on Low Carbon & Renewable Energy Technology, pp. 373, Nov. 15-18, 2010, Jeju, Korea.

14. H.J. Kim, B. Han, W.H. Shin, W.S. Hong, S.H. Jeong, S.S. Shim, Y.J. Kim. The Ultra-fine particle removal performance of a wet electrostatic precipitator for oxy-fuel combustion, Proc. of 29th American Association for Aerosol Research, Paper No. 8J8,Oct. 25-29, 2010, Portland, Oregon,

USA.

15. H.J. Kim, B. Han, T. Oda, Y.J. Kim. Fine particle removal of two-stage ESP using water film collection plates and non-metallic charger, Proc. of XII International Conference of Electrostatic Precipitation, Paper No. 61, May. 9-13, 2011, Nuremberg, Germany.

16. H.J. Kim, B. Han, Y.J. Kim, S.H. Lee, J.W. Park, Closed-chamber test of airborne allergen removal by an electrical air cleaner, Proc. of 12th International Society of Indoor Air Quality and Climate, Paper No. a710_2, Jun. 5-10, 2011, Austin, Texas, USA.

17. H.J. Kim, B. Han, Y.J. Kim, G.B. Cho, S.H. Jeong , S.S. Shim, W.S. Hong, W.H. Shin, T. Oda, Submicron diesel PM removal performance of an electrostatic filtration device combined with a metallic foam filter, Proc. of 7th Asian Aerosol Conference, pp. 1106, Aug. 17-20, 2011, Xian, China.

18. H.J. Kim, B. Han, Y.J. Kim. Comparison between dust removal performances of dry and wet ESPs for CCS of Oxy-PC combustion, Proc. of 30th American Association for Aerosol Research, Paper No. 2L.11,Oct. 3-7, 2011, Orlando, FL, USA.

19. H.J. Kim, B. Han, Y.J. Kim. Gas cooling performance of flu-gas condensers for oxy-pc combustion, Proc. of 1st Asian-Pacific Forum on Renewable Energy, Paper No. P-LCT-002, Nov. 16-19, Busan, Korea.

20. H.J. Kim, B. Han, Y.J. Kim, S. H. Lee. An efficient performance test method for air cleaning devices against airborne allergen particles, Proc. of 5th International Conference on Nano/Molecular Medicine and Engineering, Paper No. IP7-01, Nov. 9-12, 2011, Jeju, Korea.

21. H.J. Kim, B. Han, Y.J. Kim, T. Oda. Pilot tests with a non-metallic ESP for removing particles and mists in corrosive gases from semiconductor manufacturing industry in Korea, Proc. of 7th International Conference on Combustion, Incineration/Pyrolysis, Emission and Climate Change, pp.144, Sep.4-7, 2012, Ilsan, Korea.

22. H.J. Kim, B. Han, C.B. Cho, Y.J. Kim, T. Oda. Particle collection of metallic diesel particulate

filter combined with an electrostatic charger and a novel air insulation, Proc. of 7th International Conference on Combustion, Incineration/Pyrolysis, Emission and Climate Change, pp.151, Sep.4-7, 2012, Ilsan, Korea.

23. H.J. Kim, B. Han, Y.J. Kim. Submicron particle collection at high gas velocity of 12 m/s by metallic foam filter with electrostatic charger and electrostatic force enhancer, Proc. of 2st Asian-Pacific Forum on Renewable Energy, Paper No. O-LCT-001, Nov. 26-29, Jeju, Korea.

24. H.J. Kim, B. Han, Y.J. Kim. Gas cleaning performance of a wet electrostatic precipitator with a continuous thin wter film on collection plates using 1.5 L/min/m^2, Proc. of 2st Asian-Pacific Forum on Renewable Energy, Paper No. O-LCT-004, Nov. 26-29, Jeju, Korea.

25. H.J. Kim, B. Han, Y.J. Kim. Comparison of diesel pm removal performance of metallic flow-through filter and electrostatically assisted metallic foam filter, Proc. of 2st Asian-Pacific Forum on Renewable Energy, Paper No. O-LCT-019, Nov. 26-29, Jeju, Korea.

26. H.J. Kim, B. Han, Y.J. Kim, S.I, Gil, J.H. Yoon, T.H Kim, J.H. Jeong. The Electrical and particle removal performance of dry and wet electrostatic precipitators at a 0.7 MW-oxygen pulverized coal combustion pilot plant, Proc. of 31st American Association for Aerosol Research, Paper No. 2CH.4,Oct. 8-12, 2012, Minneapolis, Minnesota, USA.

27. H.J. Kim, B. Han, Y.J. Kim. Aerodynamic characteristics of fugitive dusts by the types of animal feed stuffs duing gravitational settle down, Proc. of 31st American Association for Aerosol Research, Paper No. 8RA.5, Oct. 8-12, 2012, Minneapolis, Minnesota, USA.

28. H.J. Kim, B. Han, Y.J. Kim, J.H. Jeong, K.N. Gwon, T. Oda. Particle removal near to 1 mg/Nm^3 by electrostatic precipitations for oxygen-pulverized coal combustion, 第 36 回 静電気学会講演論文集'12, pp.199-202, Sep. 13-14, 2012 , 八戸, 日本.

29. H.J. Kim, B. Han, Y.J. Kim, T. Oda. Particle removal of a non-metallic ESP for particles and mist in corrosive gases from semiconductor manufacturing industries, 第 36 回 静電気学会講演論文

集’12, pp.203-206, Sep. 13-14, 2012 , 八戸, 日本.

30. H.J. Kim, B. Han, G.B. Cho, Y.J. Kim. Enhancement of the filtration performance of metallic foam filter for diesel particulates by electrostatic charging and collection, Proc. of European Aerosol Conference 2012, Paper No. C-WG11S1P15, Sep. 2-7, 2012, Granada, Spain.

31. H.J. Kim, B. Han, G.B. Cho, Y.J. Kim. Removal performance of an electrostatic precipitator with edge to plate geometry for particulates in combustion gases for marines, Proc. of European Aerosol Conference 2012, Paper No. C-WG11S1P14, Sep. 2-7, 2012, Granada, Spain.

32. H.J. Kim. Fine particle removal by an ESP type air cleaner using carbon fiber ionizer for a high clean air delivery rate and low ozone emission performance, Proc. of 1st Joint Symposium on Plasma and Electrostatic Technologies for Environmental Applications, Paper No. M20-03, May. 19-21, 2012, Gero, Japan.

33. H.J. Kim, B. Han, Y.J. Kim, K.T. Park. Particle collection performance of oil mist eliminators for manufacturing industries, Proc. of International Symposium on Green Manufacturing and Applications 2013, Paper No. P-O-01, Jun. 25-29, 2013, Hawaii, USA.

34. H.J. Kim, B. Han, Y.J. Kim. Evaluation on removal performance of air cleaning devices against airborne allergen particles using an optical particle counter and ELISA method, Proc. of European Aerosol Conference 2013, Paper No. C140, Sep. 1-6, 2012, Prague, Czech.

35. H.J. Kim, B. Han, Y.J. Kim. Fine Particle and Mist Removal by a Wet ESP using 1.5 L/min/m^2 for Oxygen-Pulverized Coal Combustion, Proc. of 3rd Oxyfuel Combustion Conference, Sep. 9-13, 2013, Ponferrada, Spain.

36. H.J. Kim, B. Han, Y.J. Kim, H.S. Kim, T. Oda. PM removal of an electrostatic filtration device combined with a metallic foam filter under high velocity and temperature conditions for large volumetric diesel engines, 第 37 回 静電気学会講演論文集’13, pp.191-192, Sep. 10-11, 2013, 千葉, 日本.

37. H.J. Kim, B. Han, Y.J. Kim, T. Oda. High cleaner air delivery rate performance of an two-stage ESP air cleaenr for Indoor Air Quality with negligible ozone emission by carbon fiber ionizers, 第 37 回 静電気学会講演論文集'13, pp.203-204, Sep. 10-11, 2013, 千葉, 日本.

Acknowledgments

I would like to express my special appreciation and thanks to my advisor Professor Tetsuji Oda, you have been a tremendous mentor for me. I would like to thank Professor Ryo Ono and his students in Oda & Ono's laboratory who also gave me a great hospitality for three years and an half. I would also like to thank my committee members, professor Akira Mizuno, professor Kunihiko Hidaka, professor Yasushi Ono, and professor Akiko Kumada for serving as my committee members for letting my defense be an enjoyable moment, and for your brilliant comments and suggestions.

I would especially like to thank Dr. Yong-Jin Kim at Korea Institute of Machinery and Materials for letting me a valuable chance to study in the University of Tokyo, and also to thank my colleague Dr. Bangwoo Han and Dr. Chang-Gyu Woo. All of you have been there to support me when I performed experiments and analyzed data for my Ph.D. thesis. I also would like to thank all my colleagues in KIMM, especially Dr. Seok-Joon Kim who introduced me professor Oda. Furthermore I would like to thank professor Sang Soo Kim in Korea Advanced Institute of Science and Technology who was my supervisor for the master thesis and also helped me to be selected by Japan Society for the Promotion of Science. I would also like to thank all of juniors and seniors in KAIST and University of Tokyo who always supported me.

A special thanks to my family. Words cannot express how grateful I am to my parents and my mother-in law for all of the sacrifices that you've made on my behalf. Also, I would like to thank my lovely first baby to be born healthily. Your birth was a miracle to me. At the end I would like express appreciation to my beloved wife Hyo-hyen Park who was always my support in the moments when there was no one to answer my queries.